Australian Government
Geoscience Australia

pmd*CRC

Predictive Mineral Discovery Cooperative Research Centre

Extended Abstracts from the June 2004 Conference

A.C. Barnicoat and R.J. Korsch (Editors)

Record
2004/09

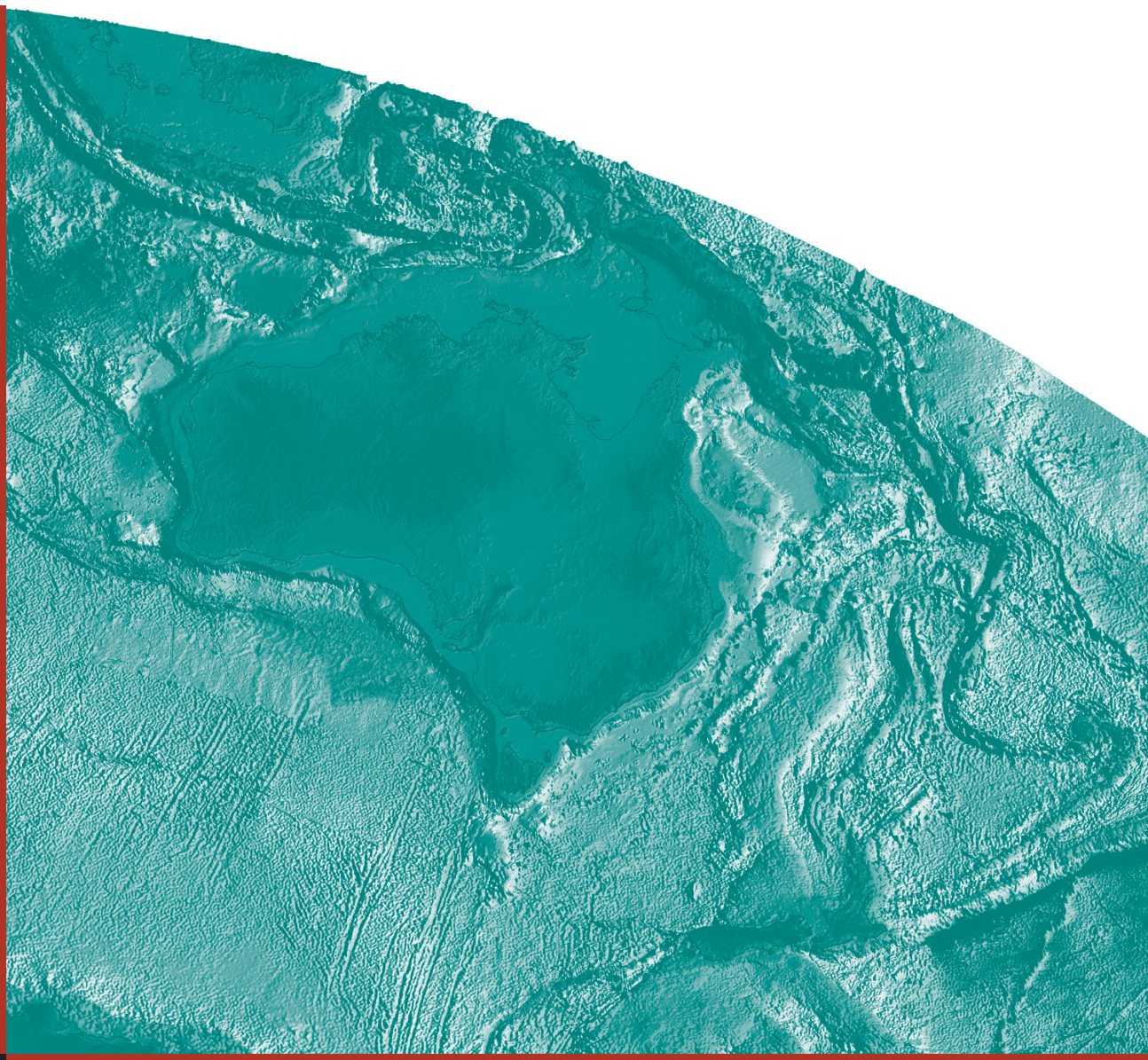

GEOSCIENCE AUSTRALIA RECORD 2004/09

PREDICTIVE MINERAL DISCOVERY COOPERATIVE RESEARCH CENTRE - EXTENDED ABSTRACTS FROM THE JUNE 2004 CONFERENCE

A.C. BARNICOAT AND R.J. KORSCH (EDITORS)
PREDICTIVE MINERAL DISCOVERY COOPERATIVE RESEARCH CENTRE

Department of Industry, Tourism & Resources

Minister for Industry, Tourism & Resources: The Hon. Ian Macfarlane, MP
Parliamentary Secretary: The Hon. Warren Entsch, MP
Secretary: Mark Paterson

Geoscience Australia

Chief Executive Officer: Dr Neil Williams

ISSN: 1448-2177
ISBN: 1 920871 03 9 (Hardcopy)
ISBN: 1 920871 44 6 (Online)

GeoCat no. 61180

Bibliographic reference: Barnicoat, A.C. and Korsch, R.J. editors, 2004. Predictive Mineral Discovery Cooperative Research Centre – Extended Abstracts from the June 2004 Conference. Geoscience Australia, Record 2004/09.

Abstracts were solicited by the Organising Committee and have been independently reviewed by at least two reviewers. However, any analyses or scientific opinions expressed in this volume are the sole responsibility of the authors.

Contents

PREFACE

The Predictive Mineral Discovery Cooperative Research Centre (pmd*CRC) was established under the auspices of the Commonwealth Government's Cooperative Research Centres Program in 2001. The purpose of the pmd*CRC is to generate a fundamental shift in mineral exploration practice and cost-effectiveness by developing a vastly improved understanding of mineralising processes and a four dimensional understanding of the evolution of the geology of mineralised terranes.

Specific objectives of the pmd*CRC are to:

- Contribute to the resolution of the key areas of uncertainty in current models for the formation of major economic mineral deposit types within mineralised terranes that have a high exploration priority.
- Build 3D and 4D images and histories of well known mineralised systems.
- Create a computational environment to simulate the 4D evolution of mineral systems with the goal of developing predictive capabilities for the location and quality of superior ore deposits.
- Transfer these concepts, skills and technologies into the mineral exploration industry to assure a long-term competitive advantage to the industry.

The partners in the pmd*CRC are

- CSIRO Division of Exploration and Mining
- Geoscience Australia
- James Cook University
- Monash University
- University of Melbourne, and
- University of Western Australia.

The pmd*CRC is currently sponsored by 17 mineral exploration companies and state geological surveys.

This volume contains extended abstracts for talk and poster presentations at the pmd*CRC's conference 'Focus on Science' held on 1-3 June 2004.

For further information on the pmd*CRC, visit the website at www.pmdcrc.com.au.

Digging deeper with worms: Finding structure in geophysics, Mount Isa Eastern Succession

J.R. Austin

*pmd*CRC, School of Earth Sciences, James Cook University, Townsville, QLD 4811*

James.Austin1@jcu.edu.au

Great Source of Ore, Source of Great Confusion

The Eastern Succession or Eastern Fold Belt (EFB) of the Mount Isa Inlier is a richly mineralised base metal province, containing world class Fe-oxide-Cu-Au (IOCG) and Ag-Pb-Zn deposits. The Isan Orogeny which occurred from ~1620 to ~1500 Ma left a record of complex deformation and a range of mineral deposits that may have been controlled by a combination of structure and syntectonic mafic and felsic intrusion.

Mineral deposits were discovered in the Mt Isa Inlier over 70 years ago, however the tectonic history remains hotly debated as different authors try to solve the same problem, using different methods. Observations made in a single field area can often become assumptions about the whole inlier and vice versa. O'Dea and Lister (1995) suggest one possible reason that variations in structural history reflect different mechanical responses to the same deformation event. Another source of confusion is the widely adopted, D1, D2, deformation nomenclature. The terminology is applied to different events, variant versions of it are used and new "D" sequences are proposed for recent or localised observations. Indeed there is still no conclusive evidence that deformation is consistent throughout the whole inlier. A major problem with many tectonic models put forward is that they do not correspond to better known tectonic analogues, but perhaps an integral piece of the puzzle has been overlooked.

What can "Worms" dig out of the EFB?

The magnetic worms derived from magnetic data provided by Xstrata Copper Australia reveal several, deep crustal structures, of which one is a 200km anomaly referred to as the Cloncurry Lineament (CL). The CL has a remarkable geophysical signature, yet it is unmapped and unknown geologically. It could be a crustal suture, a terrain bounding normal fault, a strike-slip fault or all three. It is a major contrast in magnetic potential. The paucity of ground control in 1:100 k geological mapping necessitates detailed investigation of its surface expression, which is an unmapped belt of mylonites. Worm interpretation will add a third dimension to the crustal structure, thus giving powerful insight into the tectonic evolution of the EFB. Understanding the role of the CL may be the missing link to a comprehensive understanding of the crustal evolution and mineralisation in the Mt Isa Inlier.

A major task for understanding the evolution of the EFB is to decipher the geological importance of the CL and its relationship to the Cloncurry Fault (CF) immediately to the west. Several authors note the CF as a major candidate for fluid migration and mineralisation, which appears to be associated with faulting and ~1500 Ma granitic and doleritic intrusions. But what role does the Cloncurry Lineament play? Initial work shows that the Marramungee Granite possibly intruded through the Cloncurry Lineament, questioning the role of 1550-1530 Ma granitic intrusions and suggesting a pre ~1550 Ma fault age. Large (e.g. Cannington, Ernest Henry) and several lesser deposits proximal to the Cloncurry Lineament highlight its potential

importance as a mineral-bearing fluid conduit. All early indications suggest the CL played a major role in tectonism and mineralisation of the EFB. The findings of this project will have major implications for mineral prospectivity and will be extrapolated to geology of the Eastern Succession that is under cover.

Reference

O'Dea, M.G. and Lister G.S, 1995. The role of ductility contrast and basement architecture in the structural evolution of the Crystal Creek Block, Mount Isa Inlier, NW Queensland, Australia. Journal of Structural Geology,17, 949-960.

Late Archaean arc and seamount volcanism in the Kurnalpi Terrane, Eastern Yilgarn Craton, Western Australia

M.E. Barley[1], M.G. Doyle[2], N. Kositcin[1], B. Krapez[1], K.F. Cassidy[3], and D.C. Champion[3]

*[1]pmd*CRC, School of Earth and Geographical Sciences, University of Western Australia, Crawley, WA 6009*
[2]Geological Survey of Western Australia, 100 Plain Street, East Perth, WA 6907
*[3]pmd*CRC, Geoscience Australia, GPO Box 378, Canberra, ACT 2601*

mbarley@segs.uwa.edu.au

The Eastern Yilgarn

The eastern Yilgarn Craton of Western Australia is one of the most intensely mineralized Late Archaean (2.8 to 2.6 Ga) granite-greenstone terranes. It contains world-class lode-gold and komatiite-hosted nickel sulphide deposits as well as minor volcanic hosted massive base metal sulphide deposits. Greenstone belts in the eastern Yilgarn contain tectonostratigraphic terranes (Figure 1) that range in age from 2665 Ma to ~2820 Ma (Myers, 1997; Swager 1997; Barley et al., 1998a; 2002). Each terrane has been defined on the basis of distinctive volcanic facies and geochemistry and age of felsic volcanism (age ranges in parentheses are felsic volcanic ages, and exclude the late stage siliciclastic units). The terranes are listed below:

Kalgoorlie Terrane (2707 – 2666 Ma); Extensive tholeiite and komatiite successions (Kambalda Sequence) interlayered with and overlain by a complex felsic volcaniclastic succession with TTD geochemistry (including the Spargoville and Kalgoorlie Sequences; "*Black Flag Beds*") intruded by mafic to ultramafic sills. The Kalgoorlie Terrane extends north to include TTD felsic rocks in the Agnew-Wiluna and Yandal Belts, and mafic-ultramafic successions near Lawlers.

Enclaves or domains of older (>2750 Ma) greenstone occur within the Kalgoorlie Terrane (the Norseman Terrane, Leonora, Kathleen Valley, and Wiluna Domains).

The Kalgoorlie Terrane itself therefore represents an amalgamation of young (<2710 Ma) and old (>2750 Ma) terranes.

Gindalbe Terrane (2694 – 2676 Ma), Bimodal HFSE-enriched rhyolite-basalt (e.g. Melita, Teutonic Bore), and intermediate to felsic calc-alkaline complexes (e.g. Spring Well), overlie older tholeiite-komatiite succession.

Kurnalpi Terrane (2715 – 2698 Ma); Tholeiitic and komatiitic basalt lavas, intermediate calc-alkaline complexes, feldspathic sedimentary rocks, and mafic to ultramafic intrusive rocks.

Edjudina Domain (2715 – 2710? Ma); Andesite derived volcaniclastic rocks, and fine-grained sandstone-shale units (+BIF?).

Laverton Terrane (Maximum age: 2808 Ma); Tholeiitic and komatiitic successions, Banded Iron Formation, and fine-grained tuffaceous sediments.

Duketon-Burtville Terrane (>2720 Ma); Intermediate and felsic calc-alkaline volcanic rocks and associated mafic (± ultramafic) rocks in the central and eastern part of the Duketon Belt as well as domains east of Laverton; Burtville (basalt, intermediate volcanic rocks, fine-grained sedimentary rocks, shales, dolerite), Jasper Hills and Jubilee Hill Domains (dominated by mafic and ultramafic lavas).

The most likely tectonic history of the eastern Yilgarn involves multiple submarine extensional to transtensional basins in the Kalgoorlie Terrane that were probably situated behind obliquely convergent plate margin magmatic arcs characterised by different styles of felsic magmatism (Gindalbie and Kurnalpi Terranes and High-Ca granitoids). This paper reports initial results of a key study from the *pmd*CRC* Y1 project that describes the volcanology and geochemistry of mafic and ultramafic volcanic rocks in the Kurnalpi Terrane and examines their relationship to calc-alkaline volcanic centres and their geodynamic significance.

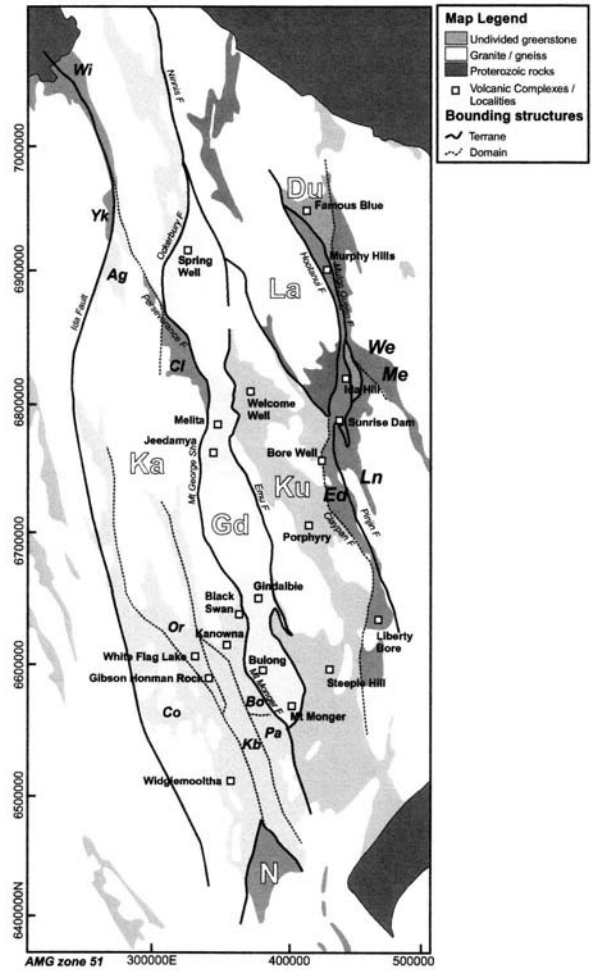

Figure 1 Simplified terrane map of the Eastern Yilgarn from Barley et al., (2002). K = Kalgoorlie, N = Norseman, Gd = Gindalbie, Ku = Kurnalpi, La = Laverton, D = Duketon-Burtville

The Kurnalpi Terrane

The Kurnalpi Terrane is characterized by 2704 to 2715 Ma calc-alkaline basaltic andesite to andesite volcanic complexes with minor dacite and rhyolite, (Kurnalpi Sequence). South of Laverton, the Kurnalpi Sequence overlies a succession of tholeiites, komatiites and banded iron formations (the Mt Margaret Sequence) with a maximum age of ~2.8 Ga including the Windarra komatiite-hosted nickel sulphide deposits. The Kurnalpi Sequence is intruded by mafic and ultramafic layered sills and overlain by 2698 to 2704 Ma tholeiites and komatiitic basalts (the Minerie Sequence). The volcanology and geochemistry of the Minerie Sequence have been studied in detail in the Minerie area.

Volcanology

The succession exposed in the Minerie area includes the interleaved products of proximal, medial, and distal felsic-ultramafic volcanism as well as synvolcanic intrusions. The succession consists of three principal volcanic facies associations, from stratigraphic lowest to highest respectively:

Association 1: Post-eruptive volcanogenic sedimentary deposits and andesitic-dacitic lavas (Welcome Well Complex, Kurnalpi Sequence). This association is dominated by polymictic andesitic conglomerate-sandstone-siltstone facies, intercalated with coherent andesite-dacite and associated autoclastic breccia (autobreccia, hyaloclastite). The poorly-sorted and diffusely bedded character of the conglomerate facies suggests rapid accumulation from gravity flows (principally debris flows), whereas sandstone-siltstone facies are mainly turbidites and suspension sedimentation deposits. Beds dominantly consist of rounded to angular, texturally variable, andesitic lithic clasts that range from weakly to strongly vesicular. Rounded to sub-angular clasts were

reworked in above-wave-base (fluvial, shoreline) environments prior to final deposition. Blocky clasts have phenocryst populations and shapes that suggest some were sourced from the autoclastic carapace of intrabasinal lavas by the parent sediment gravity flows. Bedforms are consistent with accumulation in a below-storm-wave-base environment, adjacent to an unpreserved, proximal-medial, emergent volcanic center.

Association 2: Komatiite and basaltic pillow lava-autoclastic breccia facies (Minerie Sequence). Although dominantly basaltic in composition, this association includes minor spinifex- and cumulate-textured komatiitic units. Basaltic intervals are characterised by lateral and vertical transitions between massive coherent facies, pillow lava and autoclastic facies. Flow interiors are commonly crystalline (doleritic), while flow tops are marked by intervals of in situ or clast-rotated hyaloclastite, autobreccia, and pillow-fragment breccia. Intercalated crystal-vitric sandstone-siltstone turbidites record extended breaks in eruptive activity and, combined with the widespread occurrence of pillow lava and associated breccia facies, suggest deposition in a relatively quiet, deep-submarine depositional environment.

Association 3: Komatiite and felsic syn- to post-eruptive facies (Minerie Sequence). This association includes intercalated komatiite and felsic pumice breccia-sandstone. The felsic deposits consist of 1-3 m thick, non-welded, normally graded pumice-crystal breccia beds, and planar- and cross-laminated ash sandstone-siltstone (low- and high-concentration turbidites, water-settled ash fall). Lithofacies character suggests subaqueous deposition (below storm wave base) during or soon after pyroclastic eruptions at medial to distal volcanic center(s). Lower contacts between komatiite flows and the felsic volcaniclastic substrate are typically planar, but locally comprise autobreccia, in situ hyaloclastite, and/or blocky peperite zones. Upper flow margins are coherent or incipiently fractured, and typically grade downward through a random spinifex-textured zone (A2 zone), into a zone of aligned (sheaf-like) pyroxene needles (A3 zone), and subsequent olivine cumulate B zone (peridoties and dunites).

Association 1 (the Kurnalpi Sequence) is interpreted as a calk-alkaline volcanic arc and Association 2 and 3 (the Minerie Sequence) initially interpreted as a mafic-ultramafic seamount possibly related to a mantle plume.

Geochemistry

The geochemistry of the Welcome Well Complex is dominated by subalkaline low- to medium-K andesite with subordinate basaltic andesite and dacite with a trend of Fe-depletion on an AFM diagram. Primordial mantle normalized trace element diagrams show enrichment in large ion lithophile elements LILE (Cs, Rb, K, Ba, and Sr) over high field strength elements HFSE (Nb, Zr, Hf and Ti) and moderate depletion of Ta and Nb, with fractionated light rare earth elements LREE and unfractionated heavy rare earth elements HREE. These characteristics are all typical of arc-related calc-alkaline magmas (Barley et al., 1998a; Brown et al., 2001) where melting of LILE-enriched mantle is triggered by dehydration of subducted oceanic crust. Resulting basaltic magmas undergo assimilation fractional crystallization (ACF) processes in the thickened arc crust to produce the full range of compositions. An enriched mantle source is favored by abundances of LILE in many of the intermediate rocks that are greater than would be produced by contamination of tholeiitic magmas by typical Archaean crustal rocks.

Basalts in the Minerie Sequence are typical High Ti Archaean tholeiites. Primordial mantle normalized trace element abundances are unfractionated with variable depletion in the LILE and LREE. The petrogenesis of these rocks most likely involves melting of depleted or undepleted mantle followed by fractional crystallization of olivine, pyroxene and plagioclase. These basalts are interlayed with and overlain by komatiitic basalts that are also the parent magmas to the Murin Murin Complex ultramafic cumulates. The komatiitic basalts are enriched in LILE and LREE relative to primordial mantle trace element abundances, and depleted in Nb, Ta and Ti. These major and trace element abundances are typical of Al-undepleted komatiitic basaltic

Geodynamic significance

The tectonostratigraphy of the Kurnalpi Terrane where plume-related tholeiitic and komatiitic magmatism follows calc-alkaline volcanism at ~2.7 Ga contrasts with that of the Kalgoorlie Terrane where pre 2.7 Ga komatiites and tholeiites are followed by repeated sequences of TTD felsic volcaniclastic rocks, and the Gindalbie Terrane where pre 2.7 Ga tholeiites and komatiittes are overlain by HFSE enriched basalts and rhyolites and calc-alkaline andesites and dacites. The tectonic histories of the three terranes reflect complex interactions between submarine tholeiitic magmatism, mantle plume related komatiites and convergent margin volcanic arcs (e.g. Barley et al., 1998b; Wyman, 1999) active between 2.66 and 2.8 Ga.

Acknowledgements

The sponsor companies of AMIRA projects P437, 437A, 624 and 763 are thanked for their continued support of our Yilgarn research.

References

Barley, M.E., Brown, S.J.A., Krapez, B., Hand J. and Cas, R.A.F.,1998a. Mineralised volcanic and sedimentary successions in the Eastern Goldfields Province, Western Australia, AMIRA Project P437 Final Report (unpublished).

Barley M.E., Krapez, B., Groves, D.I. and Kerrich. R, 1998b. The Late Archaean bonanza: metallogenic and environmental consequences of the interaction between mantle plumes, lithospheric tectonics and global cyclicity. Precambrian Research, 91, 65-90.

Barley, M.E., Brown, S.J.A., Krapez, B. and Cas, R.A.F., 2002. Tectonostratigraphic analysis of the Eastern Yilgarn Craton: an improved geological framework for exploration in Archaean terranes, AMIRA Project P437A Final Report (unpublished).

Brown, S.J.A., Krapez, B., Beresford, S.W., Cassidy, K.F., Champion, D.C., Barley, M.E. and Cas, R.A.F., 2001. Archaean volcanic and sedimentary environments of the Eastern Goldfields Province Western Australia- A field guide. GSWA Record 2001/13.

Myers, J.S., 1997. Preface: Archaean of the Eastern Goldfields of Western Australia- regional overview. Precambrian Research, 83, 1-10.

Swager, C.P., 1997. Tectono-stratigraphy of late Archaean greenstone terranes in the Southern Eastern Goldfields, Western Australia. Precambrian Research, 83, 11-42.

Wyman, D.A., 1999. A 2.7 Ga depleted tholeiite suite: evidence of plume-arc interaction in the Abitibi greenstone belt, Canada. Precambrian Research, 97, 27-42.

Geophysical modelling of the Palmerville Fault and other major structural components of the Broken River-Hodgkinson Provinces

M. Barlow[1], I. Vos[2] and F. Bierlein[2]

*[1]pmd*CRC, Geoscience Australia, GPO Box 378, Canberra ACT 2601*
*[2]pmd*CRC, School of Geosciences, Monash University, Melbourne VIC 3800*

michael.barlow@ga.gov.au

The Palmerville Fault represents a major Precambrian - Palaeozoic boundary in the Northern Tasmanides. Central to the "understanding of the tectonic evolution of the crust in Northern Queensland" (Shaw et, al., 1987), it constitutes a 'poorly-endowed' case-study for the A1 project in predicting mineral potential of major fault systems.

Almost as a consequence of lack of proven mineral potential, it is relatively poorly understood and surface and 3D datasets are sparse. From this perspective, the role of geophysics is instrumental in defining the structural form, depth extent, kinematic evolution and ultimately, factors leading to fluid pathways and mineral potential of the Palmerville Fault. Constraining this 1st-order structure also has major implications for our understanding of the tectonic evolution of the Northern Tasmanides during the Early Palaeozoic.

Armed with only regional databases: 200m line airborne magnetics, 10km spaced gravity and very limited petrophysics, potential field modelling has been driven by conceptual structural ideas, simplicity and minimisation of field annihilators. In contrast to the tectonic model of Shaw et,al. (1987), with multiple phases of west over east thrusting, a more elegant and straightforward model is proposed. Specifically, forward modelling of magnetic and gravity data supports normal movement on an easterly dipping Palmerville Fault, with minor later-stage back-thrusting associated with the Mitchell Fault Zone.

From a mineral potential viewpoint, the significance of this simple model fit is still to be investigated. However one possible repercussion is that while the fault may still have provided a fluid conduit, there are no compounding features and subsequent dilation zones to provide effective sites for mineralisation.

Potential-field studies are also redefining the significance of other tectonic elements in these Provinces, most notably the Alice Palmer Structure. Previous interpretations have the Palmerville overprinted or terminating at this major feature, but multi-scale edge analysis ('worming') suggests that they are both of similar timing and are bifurcated by an undefined east-west lineament. Detailed modelling will be undertaken to further study the relationship, and to continue the structural analyses into the Broken River Province.

Reference

Shaw, R.D., Fawckner, J.F. and Bultitude, R.J., 1987. The Palmerville fault system: A major imbricate thrust system in the Northern Tasmanides, North Queensland. Australian Journal of Earth Sciences, 34, 69-93.

Pb-Pb step-leaching: progress and future prospects for the direct dating of minerals

Kate Bassano, Janet Hergt, Roland Maas, Jon Woodhead

*pmd*CRC, School of Earth Sciences, The University of Melbourne, VIC, 3010*

k.bassano@pgrad.unimelb.edu.au

Background

Project aims

The ability to place metamorphic, deformation and mineralisation events into a temporal context is central to understanding the processes by which ore bodies form. The primary goal of the H2 project is to determine how robust the Pb-Pb step-leaching technique is in dating the growth or re-equilibration of individual mineral phases. Broadly, we aim to establish suitable analytical protocols for a range of minerals, determine the conditions or environments under which each mineral might be expected to generate meaningful results, evaluate the precision and reliability of the data generated by the technique, and examine the factors that contribute to the success or failure of these protocols. In this way we aim to provide a new dating tool, capable of resolving key areas of uncertainty in the geological histories of high priority mineralised terranes.

Pb-Pb step-leaching: the approach

In the traditional 'isochron' approach, the isotopic compositions of rocks or minerals known to have formed or equilibrated at a particular time are analysed, and the variations between them are employed to generate age information. In the case of metamorphic rocks, it is not necessarily true that all minerals within a particular sample were re-equilibrated during the metamorphic/deformation episode of interest. More disturbing is that some phases may remain unaffected by the event, with others completely or only partially reset. Thus, it is seldom possible to date metamorphism or deformation events using this multi-mineral approach.

In an analogous way, ores may be deposited via isotopically complex processes involving changes in fluid and/or host rock compositions. Although mixed assemblages in finely disseminated ores may share common initial Pb-isotope ratios, coarsely or sequentially deposited ores are less likely to fulfill this fundamental requirement of isochron construction. Again, the use of different minerals, selected to cover a range of parent/daughter ratios, to construct meaningful isochrons is fraught with difficulties.

One means around this impediment is to extract grains of a single phase known to have formed during the specific event of interest, and sequentially leach these with different acids following customised protocols, in order to 'unpack' the radiogenic and common Pb components. The mechanism of Pb-isotope unmixing in step-leaching was examined by Frei et al. (1997) who proposed two main processes: the surface/crystallographic site dependent hydrolysis of metal cations, and the progressive remobilisation of radiogenic Pb from the leached gel-like structure. Different rates of these processes during progressive leaching results in an effective separation of common and radiogenic Pb, producing generally linear unmixing arrays with age significance in $^{206}Pb/^{204}Pb$ v. $^{207}Pb/^{204}Pb$ diagrams.

Employing this approach, an isochron may be constructed from handpicked mineral separates of a single phase and thus concerns about whether or not other co-existing minerals were in isotopic equilibrium at the time this phase grew become irrelevant. Clearly, minerals that would lend themselves to this approach must contain sufficient U to generate radiogenic Pb, be robust to further disturbance (or record disturbances of interest faithfully), and be relatively commonly occurring if they are to attract broad use within the geological community. If proven to fulfill these requirements, minerals known to form part of the metamorphic or ore-forming assemblage could provide unambiguous age information regarding their formation (or resetting). This potentially sets the Pb-Pb step-leaching approach apart from other techniques that must

assume the accessory phase employed grew/was reset during the key event of interest (e.g., zircon).

Results

Garnet step-leaching

The H2 project commenced with a study of garnets sampled from different lithologies including metapelites and amphibolites (Tonelli, 2002). One pitfall in analysing porphyroblasts is their propensity to contain inclusions such as monazite and zircon as these may degrade the isochrons. Even careful handpicking cannot avoid micro-inclusions and an approach was developed in which the 3D visualisation of the Pb-isotope data makes it possible to identify and remove the effects of such inclusions prior to regression of the isochron (Figure 1).

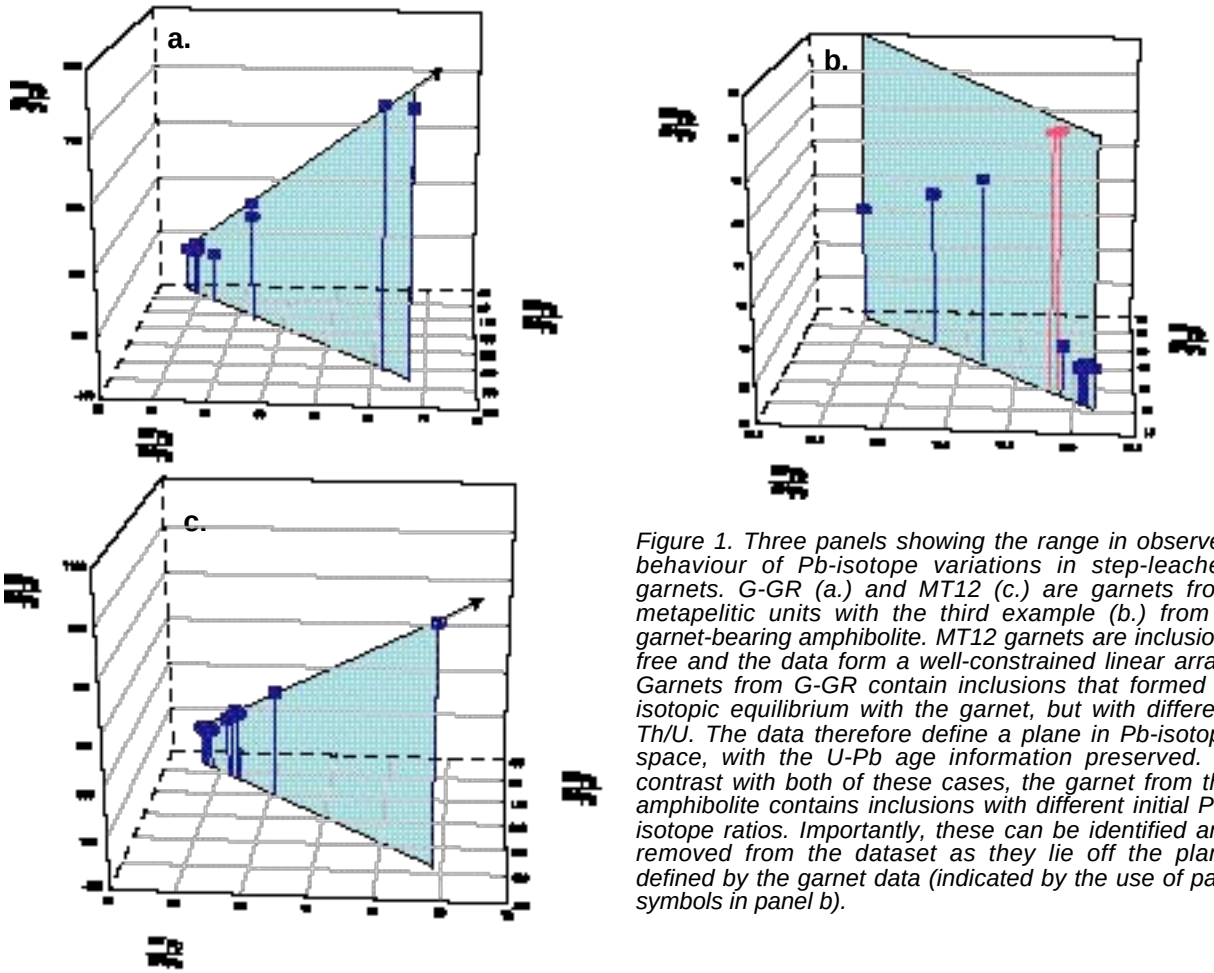

Figure 1. Three panels showing the range in observed behaviour of Pb-isotope variations in step-leached garnets. G-GR (a.) and MT12 (c.) are garnets from metapelitic units with the third example (b.) from a garnet-bearing amphibolite. MT12 garnets are inclusion-free and the data form a well-constrained linear array. Garnets from G-GR contain inclusions that formed in isotopic equilibrium with the garnet, but with different Th/U. The data therefore define a plane in Pb-isotope space, with the U-Pb age information preserved. In contrast with both of these cases, the garnet from the amphibolite contains inclusions with different initial Pb-isotope ratios. Importantly, these can be identified and removed from the dataset as they lie off the plane defined by the garnet data (indicated by the use of pale symbols in panel b).

The step-leaching approach was developed and applied to a small number of structurally well-constrained samples from the Southern Cross area of the Broken Hill Block. This area has undergone multiple episodes of amphibolite facies metamorphism and ages of 1602±30 Ma, 1599±1 Ma, 1594±7 Ma, 1592±16 Ma, 1556±10 Ma and 1481±44 Ma have been obtained from garnets extracted from six samples. The metapelitic units returned well-constrained ages (i.e., small uncertainties) consistent with other available data (e.g., U-Pb SHRIMP zircon ages). The success of these samples is linked to the large range in Pb-isotope ratios obtained by the leaching process. In contrast, garnets from the amphibolite only generated a narrow spread in ratios and consequently, the precision of the age is poor. The difference in these results is likely to reflect the lower U and Th contents of the garnets in the amphibolite compared with the metapelite. Garnets extracted from samples directly associated with ore from Broken Hill deposits failed owing to the presence of high common Pb, possibly involving galena inclusions, that dominated the Pb-isotope signal.

From the perspective of potential users within the *pmd**CRC, the most important result of this work has been to demonstrate that garnets, particularly those from metapelitic units, preserve age information consistent with independent geochronometers (e.g., SHRIMP U-Pb). Thus, in cases where suitable phases are unavailable (e.g., zircon growth zones are too small for analysis) the Pb-Pb step-leaching of garnet can provide a powerful alternative.

Extension of the technique to other silicates?

As part of the original garnet study, preliminary tests were also performed on other silicates. Ages of 1555±18 Ma, 1330±33 Ma and 876±71 Ma were obtained from different generations of staurolite and its inclusions, and an age of 1568±3 Ma was obtained from tourmaline. An experiment involving kyanite failed to produce any age information. The results of these pilot tests indicate that while not universally applicable, there is great potential for a wide number of phases to lend themselves to this step-leaching approach.

Extension of the technique to ore minerals?

On the basis of the results derived from silicate minerals, this part of the project aims to test the reliability of Pb-Pb step-leaching in directly dating ore minerals such as sulfides (chalcopyrite, pyrite) and oxides (magnetite), thereby obtaining the timing of mineralisation from a phase that is unambiguously linked to the ore-forming process. This exploits the often surprisingly high U contents and initial U/Pb ratios in some low-Pb sulfides. Although still in its early stages, the technique has already been applied to well-constrained samples from a number of Australian ore deposits covering a range of mineralisation types. These include the analysis of chalcopyrite and magnetite from Broken Hill (Copper Blow), Mt Isa, Ernest Henry and Osborne.

Initial studies were undertaken on chalcopyrite samples from Mount Isa, however, these have low Pb contents and leaching failed to create sufficient spread in isotopic ratios for the production of a meaningful isochron. In contrast, magnetite extracted from samples of the same region had high contents, but too much common Pb, shielding the radiogenic signal. Alternative samples from this area (geographically well-separated from galena) may prove more successful; in the meantime, experiments were conducted on materials from other deposits.

Preliminary studies of chalcopyrite from Copper Blow (Broken Hill) have yielded promising results. Lead isotope ratios obtained, particularly in the second leach step, indicate the presence of radiogenic Pb with $^{206}Pb/^{204}Pb$ ratios ranging up to ~57. As chalcopyrite at Copper Blow occurs with torbernite (U-rich), typical grains were interrogated using the SEM to confirm that the Pb compositions reflect those of the chalcopyrite and not inclusions. Results for magnetite from the same deposit display greater spread in the $^{206}Pb/^{204}Pb$ (~23 to 183). The age estimates obtained from these co-genetic minerals are the same, to within error, although the uncertainties are quite large (Figure 2). An interesting observation is that, unlike the $^{206}Pb/^{204}Pb$ and $^{207}Pb/^{204}Pb$ ratios, $^{208}Pb/^{204}Pb$ displays very little variation, retaining values typical of common lead (~37 to 38). This indicates that the mineralising fluid from which these phases grew carried U but not Th into the system. This is not true for other samples so far investigated.

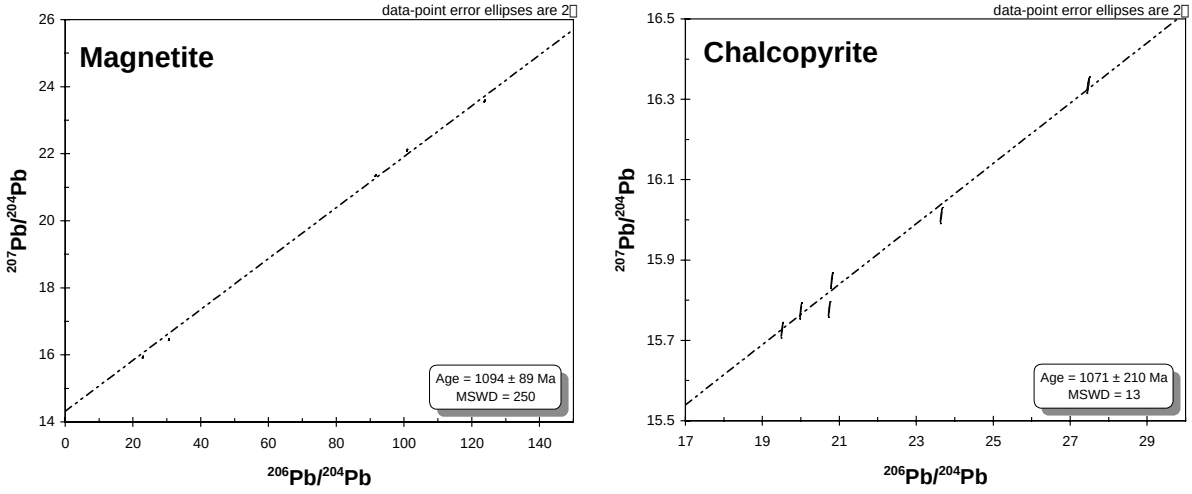

Figure 2. Preliminary 'isochron' diagrams for a sample from Copper Blow (Broken Hill) containing coexisting magnetite and chalcopyrite. Note the change in scales on both axes; magnetite generates variations in ratios more than three times greater than those observed in chalcopyrite from the same sample.

Both chalcopyrite and magnetite were also analysed from the Osborne deposit. The chalcopyrite displays radiogenic values ($^{206}Pb/^{204}Pb$ ~20 to 48) that generate an age estimate of 1252±190Ma. Although the Pb contents of magnetite leach steps were too low to yield viable results, preliminary data indicate the sample contains highly radiogenic Pb and a second experiment will be conducted employing more sample. The low concentration of Pb in the final step may be further attributed to problems associated with dissolving the sample.

Preliminary studies at Ernest Henry indicate the samples are also highly radiogenic. Chalcopyrite shows a large spread in $^{206}Pb/^{204}Pb$ (~18 to 257) generating an age estimate of 1666±120Ma. The variation in $^{206}Pb/^{204}Pb$ ratios displayed by the associated magnetite is even greater (~214 to 965) although the scatter is considerable. These data yield a poorly constrained age of 1044±450Ma because, although the range in ratios is considerable, 'gaps' in the array contribute to the large errors obtained as the isochrons become dominated by one or two points.

Future Directions

The goal in the short term will be on reducing the uncertainties on the 'ages' obtained in the magnetite and chalcopyrite samples already analysed. The specific focus will be on filling the 'gaps' in the data, achieved by further development of the leaching protocols. The intention is then to extend the work to include pyrite.

One preliminary observation that requires further examination is that, in cases of co-existing magnetite and chalcopyrite, the former appears to show a factor of three or more variation in Pb-isotope ratios. If proven to be systematic, it would suggest that in deposits where both phases occur, work should be focused on the magnetite as the ages are likely to be better constrained.

The presence or absence of variation in $^{208}Pb/^{204}Pb$ provides information on the role of Th in the mineralising system and hence the chemistry of the fluid. Although constraining the composition of the mineralising fluid is not an identified goal of this study, further investigations will be conducted into this as a by-product of the geochronological work.

ICPMS trace element analyses of samples will be utilised for two purposes. First, the compositions derived from bulk-separates will reveal any trace element control on the viability of samples from particular ore deposit types (e.g. to help explain cases in which the approach may fail to yield age information). The concentrations of trace elements in leachates from individual steps will also be investigated and compared with the bulk mineral concentrations. This will provide insights into the behaviour of different elements during the various stages of leaching and help identify what may be controlling the retention or release of radiogenic Pb. As with the garnet study, PIXE and TEM element mapping may also prove useful in understanding the leaching process.

Acknowledgements

The authors would like to thank the many members of the *pmd**CRC who have provided us with the well-constrained materials required for this study.

References

Frei, R., Villa, I.M., Nagler, Th. F., Kramers, J. D., Przybylowicz, W.J., Prozesky, V.M., Hofmann, B.A., and Kamber, B. S., 1997. Single mineral dating by the Pb-Pb step leaching method: Assessing the mechanisms. Geochimica et Cosmochimica Acta, 61, 393-414.

Tonelli, M., 2002. An evaluation of Pb step leaching geochronology as applied to high-grade metamorphic terranes, PhD Thesis, University of Melbourne, (unpublished).

The two-phase problem of modelling complex fluids

Evgeniy N Bastrakov [1] and Yuri V Shvarov [2]

*[1]pmd*CRC & Geoscience Australia, GPO Box 378, Canberra, ACT 2601*
*[2]pmd*CRC & Moscow State University, Moscow, 119899, Russia*
Evgeniy.Bastrakov@ga.gov.au

Introduction

One of the activities of the Fluids module of the *pmd**CRC is to improve calculation capabilities of the available geochemical packages to address the modelling problems pertinent to the specific *pmd**CRC goals. An example of such a problem is modelling of mobilization, transport, and deposition of metals in gas-rich (*e.g.,* X_{gas} > 5 mol%) water-salt fluids. This is especially important for understanding of the processes controlling the distribution of the Yilgarn lode gold deposits, as well as the distribution of ore at the deposit scale.

Overall, lode gold deposits were emplaced over a substantial range in pressure-temperature (PT) conditions (200 to > 600˚C, < 1 to 4 kbar). Despite this diversity, the ore-forming fluids exhibit similar characteristics: they are near neutral, low salinity (3 to 7 wt% NaCl equivalent) H_2O-CO_2±CH_4 fluids (5 to 25 mol% CO_2+CH_4), with redox conditions often near the aqueous CO_2/CH_4 buffer. Quite frequently, these fluids underwent separation of a generic supercritical H_2O-CO_2±CH_4-salt fluid into essentially aqueous phase and CO_2-rich gas.

The Problem

Two fundamental problems are associated with modelling fluids containing high concentrations of gas components: (1) changes in the solvent properties, e.g., the dielectric constant of the mixed water-gas fluids (Akinfiev and Zotov, 1999 and references therein), and (2) effects of fluid immiscibility (Bowers, 1991). Both effects will significantly affect solubilities of ore components, including gold (Akinfiev and Zotov, 1999; Bowers, 1991).

Despite the numerous equations-of-state (EOS) available in the geochemical literature (see Bakker, 2003 for a comprehensive list of references), there is no unified and numerically-effective approach that allows accurate simultaneous simulation of supercritical fluid densities, sub-critical immiscibility, and solubility of minerals in multi-component geochemical fluids. The problem with many EOS is that they are tuned for particular chemical systems, do not allow incorporation of additional chemical components, and are quite complicated in nature, containing numerous empirically-fitted cross-interaction parameters (e.g., Duan et al., 2003). This precludes their ready extension into multi-component systems and incorporation in popular codes for mass-transfer geochemical modelling. The main goal of the current sub-project is to develop numerical algorithms for calculation of activity coefficients of fluid components in supercritical and heterogeneous fluid mixtures for incorporation into one of the popular packages for geochemical modelling, HCh (Shvarov, 1999). Subsequently, they can be also incorporated into other modelling packages of the *pmd**CRC modelling framework.

Suggested approach

The main issue is the merger of the “symmetrical” description of the two-phase fluids (as provided by some gas EOS), with non-symmetrical description provided by conventional geochemical packages (i.e., essentially water-rich fluid with the dedicated precise EOS for water

v. the gas phase with a special “gas”-oriented EOS). The latter approach cannot adequately address the changes in the activity coefficients of the liquid water and the dissolved gases in a gas-rich liquid phase; this makes reproduction of the phase equilibria impossible in a significant area of the PTX compositional space even for simple systems.

A resolution of this problem was suggested by Bowers (1991) who suggested using a “gas” equation of state to calculate fluid densities and activity coefficients of “liquid” water and the dissolved gases in the mixed fluid; these activities then can be plugged back into the “liquid” phase defined according to the modified Helgeson-Kirkham-Flowers model. A number of authors (e.g., Bowers, 1991; Akinfiev and Zotov, 1999) used this approach for supercritical fluid mixtures applying modified versions of the Redlich-Kwong equation of state. However, they have not attempted to extend this approach to reproduce the phase immiscibility boundaries within their modelling software. For example, Bowers (1991) had to use empirical polynomial fitting of the H_2O-CO_2 solvus as a function of pressure in her version of EQ3/6 software.

In this study, we have attempted to assess the feasibility of the application of the improved Peng-Robinson equation of state (Stryjek and Vera, 1986) for the description of supercritical and two-phase fluids in the water-gas systems for geological problems. This equation is well known in chemical engineering and was developed specifically to reproduce liquid-gas equilibria. The Peng-Robinson-Stryjek-Vera EOS is attractive because it is simple, general, and provides a potential for incorporating new gas components with minimum knowledge of the gas cross-interaction parameters.

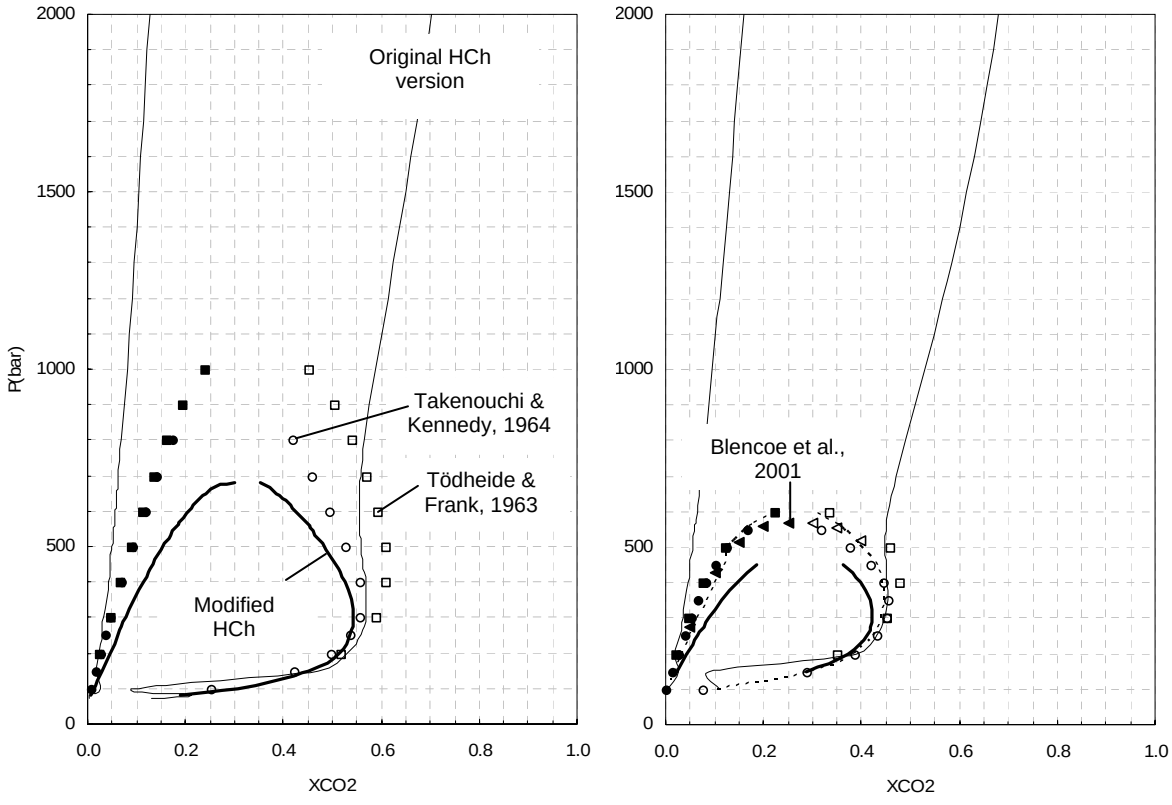

Figure 1. Isotherms showing the compositions of gas and liquid phases in the system H_2O-CO_2: calculated (lines) vs experimental (points) results. The filled symbols represent data for the “aqueous” liquid phase, and open symbols – data for the gas phase. (a) 275°C; (b) 300°C. The dotted line is calculated with a very comprehensive EOS of the program GEOFLUIDS (referenced in Duan et al., 2003)

Implementation

Most up-to-date versions of HCh allow users to create their own add-on dynamic link libraries (dll) for calculation of activity coefficients of components of the specified solution phases. Thus, we have developed a module that complements the free energy minimisation solver of HCh, Gibbs, and calculates the activity coefficients of the specified components of the liquid phase (e.g., H_2O(aq) and the dissolved gases such as CO_2(aq)) according to the Peng-Robinson-Stryjek-Vera EOS. The current version of the module utilizes only the cross-interaction parameters automatically calculated from the geometric mixing rules using data for pure gases, and does not include any empirical fitting parameters.

Current Results

The approach was tested against the available experimental data on the H_2O-CO_2 system (Figures 1-3).

As can be seen from the figures, we have managed to improve the performance of HCh in modelling water-gas mixtures, and reproduce the main features of the water-CO_2 diagram. Though not perfectly, the software now reproduces the H_2O-CO_2 *solvus* over a wide range of PT parameters. The current performance cannot match the accuracy of the published EOS *specifically* tuned for the H_2O-CO_2±CH_4±NaCl system, but demonstrates the validity of the suggested method. We expect that further improvements can be achieved via adding a few adjustable cross-interaction parameters for the components of the "PRSV sub-system" of aqueous species.

Further developments will include recalculation of the dielectric constant of the gas-rich aqueous phase to enable improved calculation of mineral solubilities in gas-rich fluids.

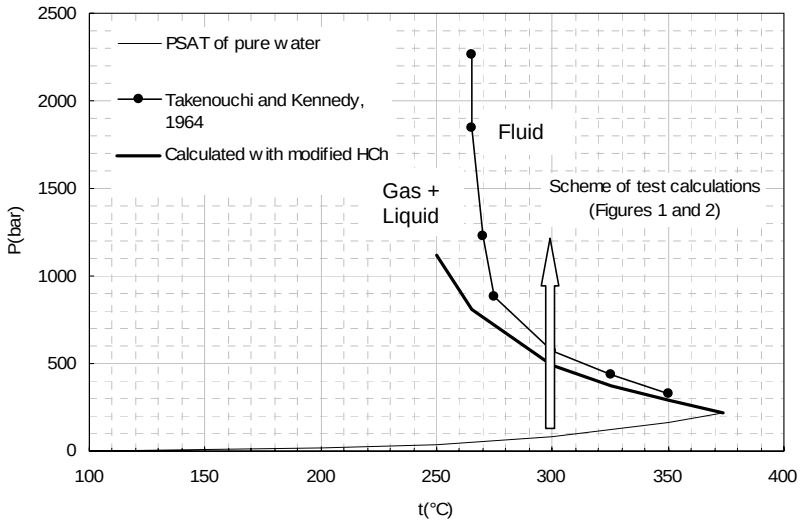

Figure 3. PT projection of the part of the critical curve of the system H_2O-CO_2 (calculated vs experimental results).

Conclusions

The implemented approach will provide us with a tool to model the broad range of processes that could have resulted in gold deposition in the orogenic lode gold deposits both at a regional scale (low-pressure crustal sections), and deposit scale (local PT variations). This will explicitly take into account the effects of phase separation.

References

Akinfiev, N. and Zotov, A., 1999. Thermodynamic description of equilibria in mixed fluids (H_2O-non-polar gas) over a wide range of temperature (25–700°C) and pressure (1–5000 bars). Geochimica et Cosmochimica Acta, 63, 2025-2041.

Bakker, R. J., 2003. Package FLUIDS 1. Computer programs for analysis of fluid inclusion data and for modelling bulk fluid properties. Chemical Geology, 194, 3-23.

Blencoe, J. G.,Naney, M. T. and Anovitz, M. L., 2001. The CO_2-H_2O system: III. A new experimental method for determining liquid-vapor equilibria at high subcritical temperatures. American Mineralogist, 86, 1100–1111.

Bowers, T. S., 1991. The deposition of gold and other metals: pressure-indiced fluid immiscibility and associated stable isotope signatures. Geochimica et Cosmochimica Acta, 55, 2417-2434.

Duan, Z., Moller, N. and Weare, J. H., 2003. Equations of state for the NaCl-H_2O-CH_4 system and the NaCl-H_2O-CO_2-CH_4 system; phase equilibria and volumetric properties above 573 K. Geochimica et Cosmochimica Acta, 67, 671-680.

Shvarov, Yu., 1999. Algorithmization of the numerical equilibrium modelling of dynamic geochemical processes. Geochemistry International, 37, 571-576.

Stryjek, R. and Vera, J. H., 1986. PRSV: An improved Peng-Robinson equation of state for pure compounds and mixtures. Canadian Journal of Chemical Engineering, 64, 323-333.

Takenouchi, S. and Kennedy, G. C., 1964. The binary system H_2O-CO_2 at high temperatures and pressures. American Journal of Science, 262, 1055–1074.

Tödheide, K. and Franck, E.U., 1963. Das Zweiphasengebiet und die kritische Kurve im System Kohlendioxyd-Wasser bis zu Drucken von 3500 bar. Zeitschrift für Physikalische Chemie Neue Folge, 37, 387–401.

Controls on ore deposition in Zn-Pb skarns: geochemical modeling and fluid inclusions constraints

M. Bertelli, T. Baker and J.S. Cleverley

*pmd*CRC, Economic Geology Research Unit, School of Earth Sciences, James Cook University, Townsville, QLD 4811*

martina.bertelli@jcu.edu.au

Abstract

Equilibrium geochemical modeling has been used to investigate possible ore deposition mechanisms that led to the genesis of the Bismark Zn-Pb skarn deposit (northern Chihuahua, Mexico). We have simulated several ore-forming processes potentially responsible for the ore deposition. The composition of the fluid used in the calculations was constrained by LA-ICP-MS analysis of fluid inclusion and phase equilibria relationships. The processes considered are: 1) temperature decrease, 2) reaction with the host rock 3) reaction with the host rock and simultaneous cooling. The results of the modeling indicate that the deposit may have formed by acid neutralization of the ore fluid as it reacts with the limestone dominant host rock. Temperature variations may have played a role in the ore deposition but was not the principal ore-forming mechanism.

Introduction

Metal deposition is the result of changes in the thermodynamic properties of ore transporting fluids. These changes are in turn the result of several processes including temperature variation, fluid mixing, host rock reaction and pressure variation. This study represents an attempt to clarify issues related to ore deposition using geochemical modeling to test ore forming processes and fluid inclusion microanalytical data as constraints. This methodology has been applied to the Bismark deposit, a stock-contact zinc-rich skarn sited in northern Chihuahua, Mexico. The availability of fluid inclusion data from microthermometry (Baker and Lang, 2003), proton-induced X-ray emission analysis (PIXE; Baker et al., 2004) and laser ablation–inductively coupled plasma–mass spectrometry analysis (LA-ICP-MS; unpublished) together with a well constrained geological setting make the Bismark deposit a good system to develop the microanalysis-modeling procedure. The mineralization at Bismark consists mainly of Zn (8%) with minor Pb (0.5%), Cu (0.2%) and Ag (50 g/t) (Baker and Lang, 2003; Haptonstall, 1994). Mineralization is associated with a quartz monzonite stock that has intruded a sequence of Cretaceous limestones with intercalated horizons of quartzite and shale. Fluid inclusion studies (Baker and Lang, 2003; Baker et al., 2004) have linked the formation of the Bismark deposit to an evolving magmatic system, in agreement with a model recently proposed for the formation of skarns (Meinert et al., 2003). The evolution of the system consists of early high temperature exsolution of immiscible brine (salinity ranges from 32 to 62 wt. % NaCl equiv) and vapor from the magma, followed by the formation of late low salinity fluid (10 wt. % NaCl equiv) in response to changes in temperature and pressure conditions. Samples of this late low salinity fluid were found in quartz veins associated with the mineralization suggesting that it is the ore-forming fluid (Baker and Lang, 2003).

The chemistry of these inclusions has been determined by LA-ICP-MS analysis and used in this study to test different depositional processes likely to have formed the Bismark deposit: 1) cooling, 2) host rock reaction, and 3) a combination of the previous two processes.

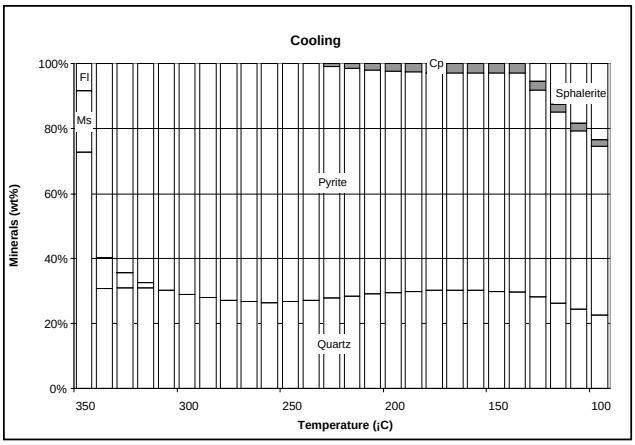

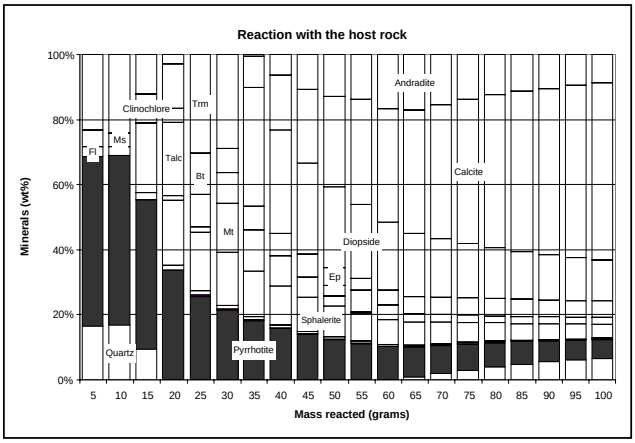

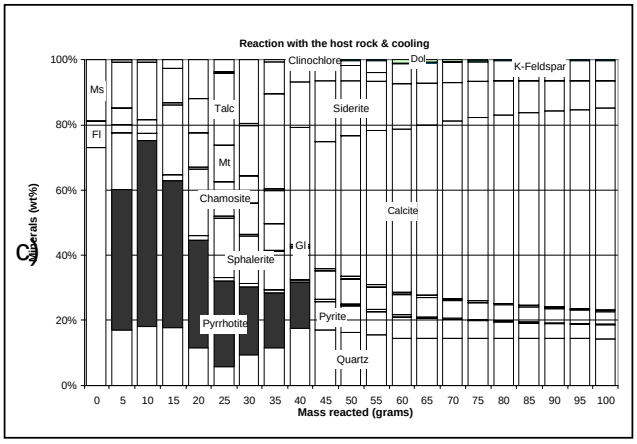

Fig. 1. Mineral assemblages resulting from simulations of different ore- forming processes: a) temperature decrease; b) host rock reaction; c) host rock reaction and simultaneous cooling. Precipitation of minerals is expressed in wt% temperature in °C and the amount of rock reacted in grams.

Methodology

All the thermodynamic calculations have been carried out using The Geochemist's Workbench software package (Bethke, 2002). The program React has been used for equilibrium calculations, polythermal and titration path modeling. The thermodynamic dataset employed was created using utilities developed within the pmd*CRC F1 project (Cleverley and Bastrakov, submitted). The fluid composition used in the simulations has been partly constrained by laser ablation analysis of the low salinity inclusions at Bismark (Table 1). The inclusion analysis selected has been chosen because of the good correlation displayed between the PIXE and LA-ICP-MS data. The missing components have been determined through phase equilibrium calculation using the pre-ore mineral assemblage. In particular we have used pyrite, quartz, fluorite, chalcopyrite and K-feldspar to constrain the amount of total sulphur, $SiO_2(aq)$, F^-, Cu^+ and Al^{3+} respectively. Temperature, pressure and Cl-content has been defined by microthermometric studies (Baker and Lang, 2003). CO_2 has been set equal to 0.01 molality unit, based on previous studies on similar geologic system (Changsheng Lu et al., 1992).The composition of the fluid obtained is shown in Table 2.

Results

The fluid obtained has been used to test different ore depositional processes including: 1) temperature decrease; 2) reaction with the host rock; 3) cooling of the ore fluid and reaction with the host rock.

Temperature decrease

We have simulated the cooling of the fluid from 350°C to 100°C (Fig. 1a). The predicted mineral assemblage includes three main stages: at higher temperature the system comprises quartz, pyrite, minor muscovite and fluorite, followed by a pyrite-quartz stage and finally at lower

temperature the mineral assemblages include sphalerite, pyrite, quartz with minor chalcopyrite. All these phases are present at the ore stage at Bismark.

Host rock reaction

We have simulated a fluid-rock interaction at constant temperature (350°C) (Fig. 1b). The host rock composition (Table 3) used for the calculation has been created to represent the real composition of the host rock at the Bismark deposit. The initial fluid-ratio is 1.3kg/100g. This ratio decreases with progress reaction as new rock mass is added to the fluid. For high fluid-rock ratio the resulting mineral assemblage is mainly composed of sulphide minerals (sphalerite and pyrrhotite) with quartz and lesser chlorite, fluorite, biotite, talc, muscovite, magnetite and tremolite (the last four are not present at Bismark). For lower fluid-rock ratios (when more than 35g of rock has reacted with the fluid) the produced minerals consist of sulphides (sphalerite, pyrrhotite and chalcopyrite) and the typical skarn assemblage (calcite, diopside, epidote, andradite,). All these latter minerals with the only exception of calcite are not present in the ore stage at Bismark. Furthermore, the model fails to produce galena and pyrite.

Elements	Concentration (ppm)
Na	37400
Mg	848
K	22997
Ca	21581
Mn	353
Fe	3269
Zn	2501
Ag	3
Pb	220

Table 1.Selected fluid inclusion composition of ore stage fluid inclusion from LA-ICP-MS analysis.

Temperature decrease and host rock reaction

Finally, we have tested a fluid-host rock reaction (initial fluid rock ratio 1.3kg/100g) allowing the system to cool from 350°C to 100°C. As in the previous case the initial mineral assemblage (Fig.1c) consists of quartz and sulphide minerals and lesser amount of fluorite, chlorite, muscovite, talc and magnetite. The sulphides predicted from the simulation are sphalerite, pyrite, pyrrhotite, chalcopyrite and galena and correspond to the ore mineral assemblage. For lower fluid-rock ratios and lower temperature the mineral assemblage includes sulphide minerals (pyrite, sphalerite, galena, and chalcopyrite) and calcite, quartz, chlorite, siderite and dolomite (the latter two are not observed at Bismark).

Elements	**Concentration (ppm)**
log fO2	*-31*
pH	*3.9*
Cl-	1.29E+05
H2S(aq)	*2953*
CO2(aq)	316.3
SiO2(aq)	*617.7*
Ca++	**2.17E+04**
Na+	**3.75E+04**
K+	**2.31E+04**
Al+++	*18.72*
Fe++	**4771**
Mg++	**851.2**
Mn++	**354.4**
Cu+	*34.84*
Pb++	**221.2**
Zn++	**2075**
Ag+	**3.279**
F-	*110.8*

Table 2: Composition of the fluid used for the simulations. Values in bold were derived form LA-ICP-MS analysis; values indicated in italic were calculated through phase equilibrium calculation using the pre-ore mineral assemblage.

Host rock composition	
Calcite	80
Shale	10
Quarzite	10
Shale composition	
Clay minerals	2.8
Quartz	5.3
Kfeld	0.4
Plagioclase	0.2
Calcite	0.3
Dolomite	0.8
Pyrite	0.2

Table 3: Composition of the host rock used for the simulations

Discussion and Conclusions

The results of the modeling indicate that a temperature decrease can produce part of the minerals assemblage observed at the Bismark deposit. However, the calculations fail to predict important phases, such as galena, pyrrhotite, and calcite. This is an indication that cooling alone was not responsible for sulphide deposition, but was probably a secondary factor in the formation of the Bismark deposit.

Simulation of fluid-rock interaction shows that there is a good but not an exact correspondence between the predicted mineral assemblages and the observed assemblages at Bismark and has produced part of the ore and gangue assemblage. During the first reaction steps the pH value rapidly increases from 3.9 to 5.2 as a result of the reaction with a rock dominantly composed of carbonate. This suggests that sulphide deposition was likely caused by neutralization of the ore fluid as it replaced the limestone.

Simulation of fluid-rock reaction with simultaneous cooling presents a good prediction of ore and gangue minerals for higher fluid-rock ratios. For lower fluid/rock the system contains minerals not observed at Bismark (siderite and dolomite). Sulphides precipitate during the first phases of the reaction when less than 25g of rock have reacted with the fluid. At this stage the temperature is still high (342°C), while pH values increase from 3.9 to 5.2. This is further evidence to suggest that the primary control on ore deposition was reaction with the carbonate host rock.

In conclusion, the modeling results indicate that the sulphide deposition was probably the result of fluid neutralization caused by the reaction with the host rock, which primarily consists of limestone. This is supported by the sudden increase of the pH value in the first steps of the reaction, when the sulphides precipitate. A temperature variation is likely to have contributed to ore deposition, though simple fluid cooling was not the main mechanism that leads to the formation of the Bismark deposit.

References

Baker, T. and Lang, J.R., 2003. Reconciling fluid inclusion types, fluid processes, and fluid sources in skarns: an example from the Bismark Deposit, Mexico. Mineralium Deposita, 38, 474-495.

Baker, T., van Achterberg, E., Ryan, C.G. and Lang, J.R., 2004. Composition and evolution of ore fluids in a magmatic-hydrothermal skarn deposit. Geology 32, 117-120.

Bethke, C.M., 2002. The Geochemist's Workbench: A User's Guide to Rxn, Act2, Tact, React, and Gtplot. University of Illinois, USA.

Changsheng Lu, Reed, M.H. and Misra, K.C., 1992. Zinc-lead skarn mineralization at Tin Creek, Alaska: Fluid inclusions and skarn-forming reactions. Geochimica et Cosmochimica Acta, 56, 109-119.

Cleverley, J.S. and Bastrakov, E.N., submitted. K2GWB: Utility for generating thermodynamic data files for The Geochemist's Workbench (R) at 0 - 1000'C and 1 - 5000 bars from UT2K and the UNITHERM database. Computers and Geosciences.

Haptonstall, J.C., 1994. Bismark; Mexico's new major zinc mine. Mining Engineering, 46, 295-302.

Meinert, L.D., Hedenquist, J.W., Satoh, H. and Matsuhisa, Y., 2003. Formation of anhydrous and hydrous skarn in Cu-Au ore deposits by magmatic fluids. Economic Geology, 98, 147-156.

The role of mafic rocks in the genesis of IOCG and Base Metal deposits, Mount Isa Eastern Succession, NW Queensland, Australia.

Kris Butera

*pmd*CRC, School of Earth Science, James Cook University, Townsville, QLD 4811*

kris.butera@jcu.edu.au

Introduction

Controls on the spatial distribution and genesis of Australian Proterozoic base metal and IOCG deposits are not well understood, and this is a major impediment to successful exploration. In the context of the Eastern Succession of the Mt Isa Inlier, one possible factor that has not been widely considered may be the presence of mafic intrusions, which have a history of emplacement extending throughout the period of Proterozoic base metal (Ag-Pb-Zn and Cu) and Fe-oxide-Cu-Au-U-REE mineralization. Mafic bodies may have been important as sources of metals, sulphur, or have provided rheological contrasts for fluid trapping leading to ore deposition.

This study is designed to integrate the results of Spatial Data and Fractal Analysis into the modelling of ore genesis processes involved in IOCG and Base Metal deposits.

Fractal Analysis

In this study, the spatial distribution of both base and precious metal deposits and of mafic rocks were analysed using binary images in the freeware program ImageJ. An image of the spatial distribution of deposits was produced, with each deposit occupying one pixel, and box counting of this image was compared to box counting of a binary image of the distribution of mafic rocks.

Box counting was performed over a range of box sizes from 0.34km to 34.2 km. These data showed typical patterns of roll-off at small box sizes. The range of box sizes over which the data were linear was 8.53 km to 34.2km. Regression over these limits was used to derive the fractal dimensions, standard errors of regression and correlation coefficients. The very similar fractal dimensions for the mafic intrusive rocks and the deposits demonstrates a fundamental similarity in their spatial distributions.

	Regression Limits (km)		Number (Deposits)	Fractal Dimension	Standard Error	Correlation Coefficient
	Min	Max	N	D	E	R
Mafics	8.53	34.2	-	**1.4345**	0.0357	0.997221
Deposits	8.53	34.2	240	**1.432**	0.0468	0.99523

Table 1. Results of Fractal Analysis of Mafics and Mineral Deposits, Eastern Succession

Weights of Evidence

The Weights of Evidence feature on the Mapinfo Add-in MI-SDM was used to measure the strength of the spatial relationships between various rock units and fault styles and mineral deposits. Spatial relationships were evaluated by the Contrast value, which compares the association between deposits and rock units or faults with that predicted by chance. Of particular interest, mafic intrusives over the study area were tested.

Mafic intrusives in the study area display a very strong spatial relationship with base metal and IOCG Deposits, but relatively weak associations with Au-only deposits. The greatest association between mafic bodies and deposits occurs at distances from 0-250m, and the implied importance of mafic bodies in the genesis of these deposits is comparable to that of major faults. In contrast, values for granite were lower than those of the mafics, with the exception of Au-only deposits. This work supports the results from fractal analysis of mafic rock distribution with respect to mineralisation.

Sulphur Availability

Mass fraction calculations for sulphur in all known deposits within the study area were compared to a number of calculations of sulphur sequestering from the mafics. The total amount of copper in the deposits was calculated to be ~3.34Mt, with ~6.5Mt sulphur necessary to form the ore. The total surface area of the mafics was measured to be ~98 km^2, with an assumed average density of 2.8t/m^3. The amount of sulphur available for ore genesis was calculated using a number of variables including initial concentration (ppm), the thickness of the unit that sulphur was extracted from, and efficiency of extraction of sulphur. For 1000m thickness, initial S concentration of 80ppm, and 30% extraction efficiency, ~6.8Mt of S would be supplied to the ore bodies. This is more than enough to account for all known mineralisation in the study area.

A more realistic estimate for the availability of sulphur, at initial S of 150ppm, and 50% extraction efficiency (as indicated by preliminary petrographic and geochemical studies) over 1000m depth would yield over 20Mt of sulphur – more than 3 times S than needed to supply known deposits! The depth from which we may reasonably extract sulphur would be the approximate thickness of the Soldiers Cap Group (~7500m), leading to a much higher sulphur budget for the study area (150Mt). This work has important implications for base metal and IOCG exploration, including exploration potential, target generation and ore genesis models for the Eastern Succession and other Proterozoic terranes. Petrographic and geochemical studies of the mobility of sulphur through these mafic bodies is currently underway.

Preliminary IOCG Deposit Model

The strength of the spatial relationships between mafic rocks and mineralisation determined by Weights of Evidence and Fractal Analysis implies that there is a genetic relationship between them. The two key possibilities in regards to the genetic link are: 1) that these Pre-D1 mafic intrusives were the source of sulphur (and possibly some metals), and 2) the mafics provided the rheological contrast necessary for structural entrapment of mineralising fluids. Due to the high Contrast values for mineralisation within or proximal to major and medium faults (the principal structural element for fluid entrapment), and the fact that Williams Batholith hydrothermal fluids were low in sulphate (from observations of barium in fluid inclusions), we postulate that the early Eastern Succession mafics were potentially the source of sulphur (and possibly some metals) for mineral deposits.

The preliminary model for IOCG genesis involves a fault driven Au-bearing fluid originating at depth from potentially the Wimberu, Mount Dore or Gin Creek Granites, interacting with a regionally extensive (and possibly Cu-bearing) brine that leached sulphur (and possibly Cu) from mafics just prior to ore deposition, proximal to (or within) major extensional (pre-D1) phase detatchment or D3 (syn-felsic magmatic) faults.

Depositional controls and alteration patterns within Myally Subgroup and Quilalar Formation, Western Succession, Mt Isa

Simon Debenham[1], Avon McIntyre[1], George Gibson[1], Paul Henson[1], Aleks Kalinowski[1], Alexis Lambeck[1] and Laurie Hutton[2]

*[1]pmd*CRC, Geoscience Australia, GPO Box 378, Canberra, ACT 2601*
[2]Queensland Department of Natural Resources, Mines and Energy, Block A, 80 Meiers Road, Indooroopilly, QLD 4068

Simon.Debenham@ga.gov.au

Introduction

Measured sections and map thickness information from the Leichhardt River Fault Trough have been used in the construction of 3-dimensional isopach maps for both the Myally Subgroup and Quilalar Formation. These 3-dimensional isopach maps were generated in an attempt to reconstruct basin shape for both sedimentary packages at their time of deposition, and provide a visual aid (in GOCAD) toward identifying possible structural controls on basin architecture (i.e. growth faults). Elucidation of the basin shape and position of local depocentres has increased understanding of basin geometry and active structures at the time of deposition, thereby giving a more complete picture of the early geodynamic evolution of this important mineral province/rift basin. In addition, alteration styles within the Myally Subgroup and Quilalar Formation have been observed and sampled in an effort to map out regional alteration patterns through remote sensing applications.

Previous Work

Work performed by NABRE in the Leichhardt River Fault Trough and Lawn Hill Platform has provided insight into the depositional controls and basin architecture of the Surprise Creek and Mount Isa-McNamara Groups, which occupy the upper stratigraphy of the Mt Isa Western Succession. This work proposed a strike-slip model for the Surprise Creek and Mount Isa-McNamara Group which were deposited in a largely south-east thickening basin, with the main depocentre occurring in the vicinity of the Mt Isa Valley (Southgate et al., 2000).

Myally Subgroup

The Myally Subgroup (ca 1760 Ma; Nijman et al., 1992) is the uppermost division of the Haslingden Group overlying the extensive Eastern Creek Volcanics in the Leichhardt River Fault Trough. The sedimentary package consists of quartzite and siltstone assemblages largely deposited in shallow near shore to terrestrial conditions (Nijman et al., 1992; Eriksson et al., 1993).

Previous research had differing views on the structural controls influencing basin architecture at the time of Myally Subgroup deposition. O'Dea et al. (1997) identified a N-S extension regime producing a series of E-W oriented half-graben growth faults. Conversely, Eriksson et al. (1993) interpreted the basin to have formed through E-W extension forming a longitudinal N-S oriented basin.

Analysis of a 3-dimensional isopach map (Figure 1a) together with measured sections through the Myally Subgroup across E-W structures (Figure 1b) indicate that an element of both structural styles (N-S and E-W extension) may have been contemporaneous in their influence over basin architecture, and sediment deposition at Myally Subgroup time.

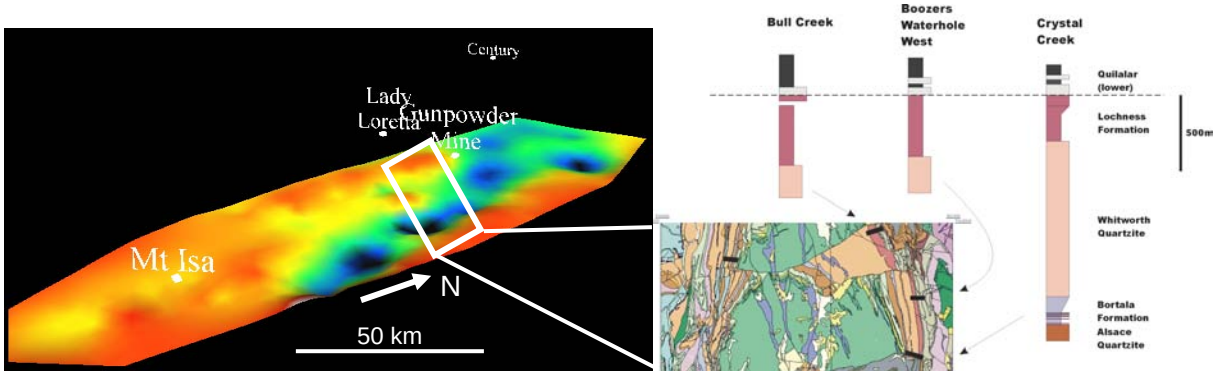

a) b)

Figure 1. a) 3-dimensional isopach map (2 x vertical exaggeration) of the Myally Subgroup showing a Northwards thickening basin shape with numerous local depocentres within the basin. Darker colours represent deeper parts of the basin (depocentres). Note: A major erosional surface is present on the western basin margin which is down-cutting into the upper Myally Subgroup and producing a shallow basin artifact. b) Measured section information from field traverses indicating a thickening of the upper Myally Subgroup (Lochness Formation) into a major E-W fault (Investigator Fault).

Figure 1a, in particular, indicates that in its present day outcrop pattern, the Myally Subgroup was deposited in a NW trending basin corridor within which the Myally Subgroup thickens northwards. The nature of the NW trending basin corridor suggests it was largely controlled by E-W oriented extension. However, numerous individual depocentres within this corridor coincide with E-W faults implying a component of N-S oriented extension acting at the time of deposition.

A major erosional surface cutting down into the top of the Myally Subgroup (Lochness Formation and Whitworth Quartzite) along the western margin of the basin makes the nature of the original basin shape uncertain. In an attempt to remove the influence of erosion and validate the Northerly thickening Myally Subgroup, a 3-dimensional isopach map of only the lowermost two formations (Alsace Quartzite and Bortala Formation) was generated to illustrate the initial basin shape at the onset of deposition (Figure 2).

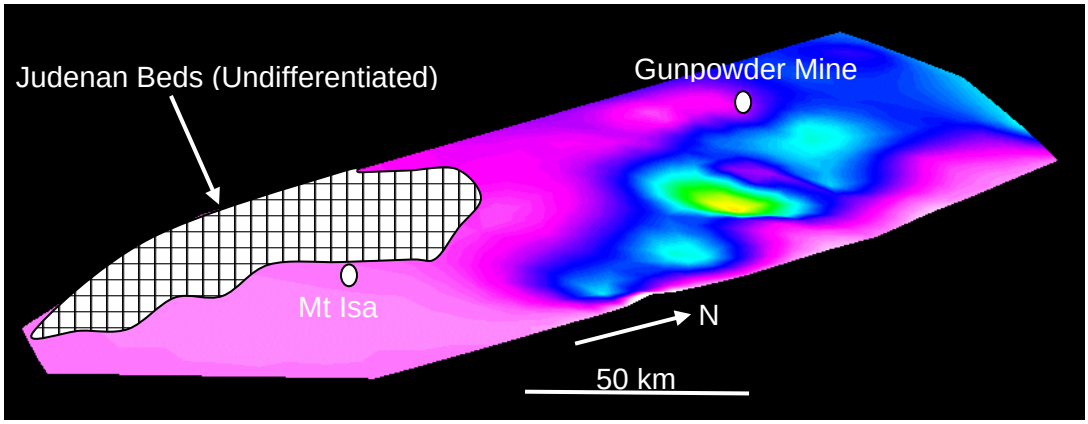

Figure 2. 3-dimensional isopach map (2 x vertical exaggeration) of the lowermost Myally Subgroup (Alsace Quartzite and Bortala Formation) showing a NW thickening isopachs indicating basin shape and position of local depocentres at the time of deposition. Darker colours represent deeper parts of the basin (depocentres). Note: The Judenan Beds (Myally Subgroup equivalents) which crop out near Mt Isa were omitted. A better understanding of how formations within the Judenan Beds correlate with the Myally Subgroup is required to provide a more complete picture of basin architecture.

Figure 2 shows a similar pattern of northwards thickening of the Myally Subgroup. Additionally, the presence of depocentres in the vicinity of EW faults again implies elements of both E-W and N-S extension influencing the basin architecture. The relationship between the Myally Subgroup and the Judenan Beds cropping out near Mount Isa is unknown. Therefore, a complete basin picture is still uncertain. A better understanding of how formations within the Judenan Beds correlate with those in the Myally Subgroup will improve understanding of the basin architecture at this time.

Quilalar Formation

The Quilalar Formation (*ca.*1740 Ma**;** Nijman et al., 1992) lies conformably or disconformably over the Myally Subgroup. It consists of quartzite, siltstone and carbonate units deposited in alternating terrestrial and shallow marine conditions (Jackson et al., 1990; Simpson & Eriksson, 1991). The formation is absent from the western Leichhardt River Fault Trough, which could be the result of either erosion or non deposition. Measured section and map thickness information was combined to construct a 3-dimensional isopach map illustrating the general basin shape at time of deposition (Figure 3)

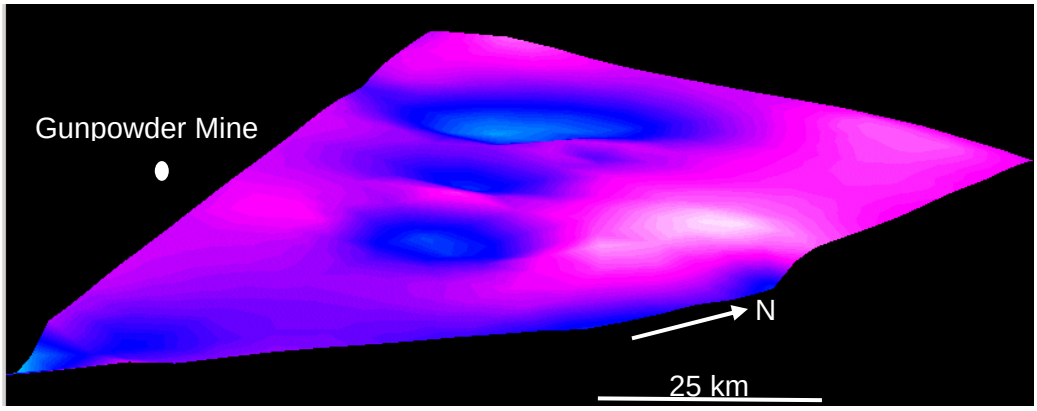

Figure 3. 3-dimensional isopach map (2 x vertical exaggeration) of the Quilalar Formation showing a NW trending corridor of deposition thickening to the SE.

The Quilalar Formation does not crop out as greatly as the Myally Subgroup in the Western Succession. However, the Corella Formation does crop out extensively in the Eastern Succession and is thought to be a correlative of the Quilalar Formation (Eriksson et al., 1993). Figure 3 indicates that while part of the Quilalar Formation was deposited in a NW trending corridor similar to that into which the Myally Subgroup was deposited, it thickens to the SE towards the Eastern Succession. This pattern supports the hypothesis that the Quilalar Formation is perhaps a correlative of the Corella Formation as suggested by Eriksson et al. (1993).

Alteration

In addition to mapping out the basin shape for the Myally Subgroup and the Quilalar Formation, field observations have also revealed K-feldspar and Fe alteration occurring within each sedimentary package respectively. Both styles of alteration are secondary features within the respective sedimentary packages. K-feldspar alteration is apparent within the finer grained units of the Myally Subgroup, namely the Bortala and Lochness Formations. Within the Bortala Formation, alteration occurs within en-echelon quartz veins sub-parallel to bedding (e.g. Esperanza Waterhole). K-feldspar alteration in the Lochness Formation occurs as a fluid replacement style alteration (e.g. Julius South). Similarly, alteration in the Quilalar Formation occurs as Fe replacement within the lower carbonate-dolomitic siltstone unit of the formation

(e.g. Bull Creek). Sampling of alteration minerals within the Myally Subgroup and Quilalar Formation was undertaken to assess spectral properties (PIMA) in an effort to map alteration patterns regionally through remote sensing applications to try and target areas of fluid flow as a vector to possible mineralisation.

Acknowledgements

Special mention must go to Peter Southgate for his help and advice in applying a sequence stratigraphic approach and facies interpretation to measured sections obtained from the I1 2003 field season.

References

Eriksson K. A., Simpson E.L. and Jackson M.J., 1993. Stratigraphical Evolution of a Proterozoic syn-rift to post-rift basin: constraints on the nature of lithospheric extension in the Mount Isa Inlier, Australia. In*:* Frostick L.E. and Steel R.J., eds., Tectonic Controls and Signatures in Sedimentary Successions. International Association of Sedimentologists Special Publication, 20, 203-221.

Jackson M.J., Simpson E.L. and Eriksson K. A., 1990. Facies and sequence stratigraphic analysis in an intracratonic, thermal relaxation basin: the Early Proterozoic, Lower Quilalar Formation and Ballara Quartzite, Mount Isa, Australia. Sedimentology, 37, 1053-1078.

Nijman W., Van Lochem J.H., Spliethoff H. and Feijth J., 1992. Deformation Model and sedimentation patterns of the Proterozoic of the Paroo Range, Mount Isa Inlier, Queensland, Australia. In: Stewart A.J. and Blake D.H., eds., Detailed Studies of the Mount Isa Inlier. Australian Geological Survey Organisation Bulletin, 243, 29-73.

O'Dea M.G., Lister G.S., Betts P.G. and Pound K.S., 1997. A shortened intraplate rift system in the Proterozoic Mt Isa terrane, NW Queensland, Australia. Tectonics, 16, 425-441.

Simpson E.L. and Eriksson K.A., 1991. Depositional facies and controls on parasequence development in siliciclastic tidal deposits from the Lower Proterozoic, upper Mount Guide Quartzite, Mount Isa Inlier, Australia. In*:* Smith D.G., Reinson G.E. and Rahmani R.A., eds., Clastic Tidal Sedimentology. Canadian Society of Petroleum Geologists Memoir, 16, 371-387.

Southgate P.N., Scott D. L., Sami T.T., Domagala J., Jackson M.J., James N.P. and Kyser T.K., 2000. Basin shape and sediment architecture in the Gun supersequence: a strike-slip model for Pb-Zn-Ag ore genesis at Mt Isa. Australian Journal of Earth Sciences, 47, 509-531.

Late Archaean mineralised high-field-strength-element (HFSE) enriched igneous rocks in the Gindalbie Terrane, Eastern Yilgarn Craton, Western Australia

C.A. Dickins[1], M.E. Barley[1] and K.F. Cassidy[2]

[1]pmd*CRC, Centre for Global Metallogeny, School of Earth and Geographical Sciences, University of Western Australia, Crawley, WA 6009

[2]pmd*CRC, Geoscience Australia, c/- GSWA, 100 Plain St, East Perth, WA 6004

dickic01@geol.uwa.edu.au

Introduction

The Eastern Yilgarn Craton is an intensely mineralised Late Archaean mainly low-grade granite-greenstone terrane (Myers, 1997). Consisting of five tectonostratigraphic terranes (Gindalbie, Kalgoorlie, Kurnalpi, Laverton and Duketon-Burtville (Figure 1) defined by their distinct geological characteristics (Myers, 1990; Swager, 1997; Barley et al., 2002) the Eastern Yilgarn Craton is a site of enormous economic significance. While individual terranes are well defined within the Eastern Yilgarn, the history of terrane accretion, deformation, volcanism, sedimentation and metamorphism, and ultimately the thermal history, is not so well understood. Barley et al., (2004, this volume) gives more detail on the terranes of the Eastern Yilgarn Craton.

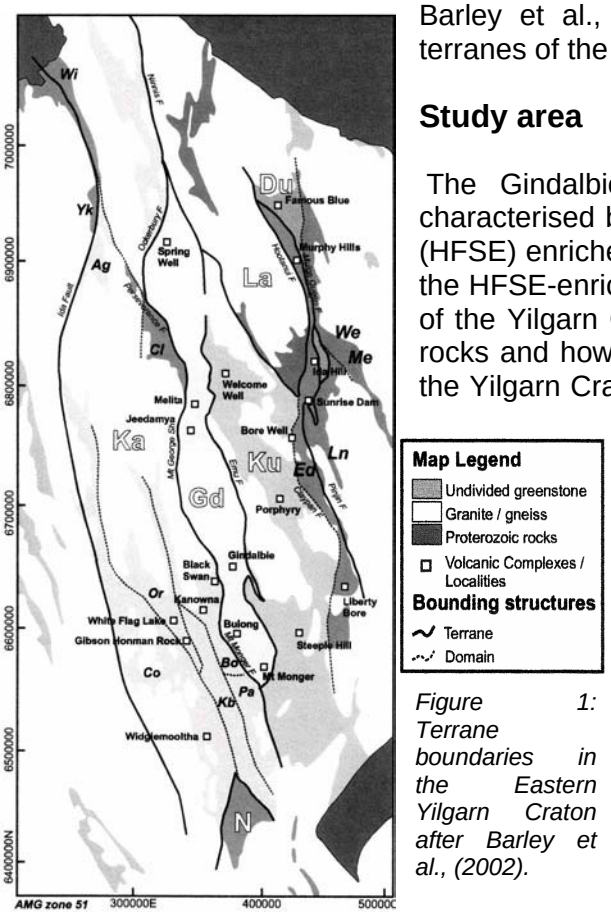

Figure 1: Terrane boundaries in the Eastern Yilgarn Craton after Barley et al., (2002).

Study area

The Gindalbie Terrane in the Eastern Yilgarn Craton is characterised by a suite of ~2.69Ga high-field-strength-element (HFSE) enriched plutonic and bi-modal volcanic rocks. Although the HFSE-enriched rocks have been included in general studies of the Yilgarn Craton, a petrogenetic history of these particular rocks and how they fit into the overall geodynamic evolution of the Yilgarn Craton has not been investigated thoroughly before. The Gindalbie Terrane locally hosts VHMS-mineralisation at Teutonic Bore and the recently discovered Jaguar deposit. A better understanding of the petrogenesis and tectonic setting of HFSE-enriched rocks in the Gindalbie Terrane is important to understanding relationships between terranes in the Eastern Yilgarn Craton and developing a better model for its overall geodynamic evolution; this will be important for understanding the regional mineralisation potential of the Eastern Yilgarn, and at a local scale evaluating which parts of the Eastern Yilgarn have the best VHMS potential.

Geochemistry

The Gindalbie Terrane consists of a series of volcanic successions consisting of mostly coarse quartz-bearing volcaniclastic breccias, rhyolitic lavas and sills, pillowed basalts and associated hyaloclastites, and fine-grained sediments which are geochemically similar to contemporaneous granitoid plutons, and are intruded by lamprophyre dikes, and thick dolerite and gabbro sills (Barley et al., 1998). A previous study at Melita shows that these rhyolites are typically high-silica rhyolites (SiO_2 >74%), which are highly enriched in all incompatible elements relative to other Eastern Goldfields felsic volcanic associations (Brown et al., 2002). MORB-normalised multi-element plots show enriched LILE, HFSE, and HREE, with slight to moderate negative Ta-Nb anomalies and strong negative Ti anomalies (Figure 2).

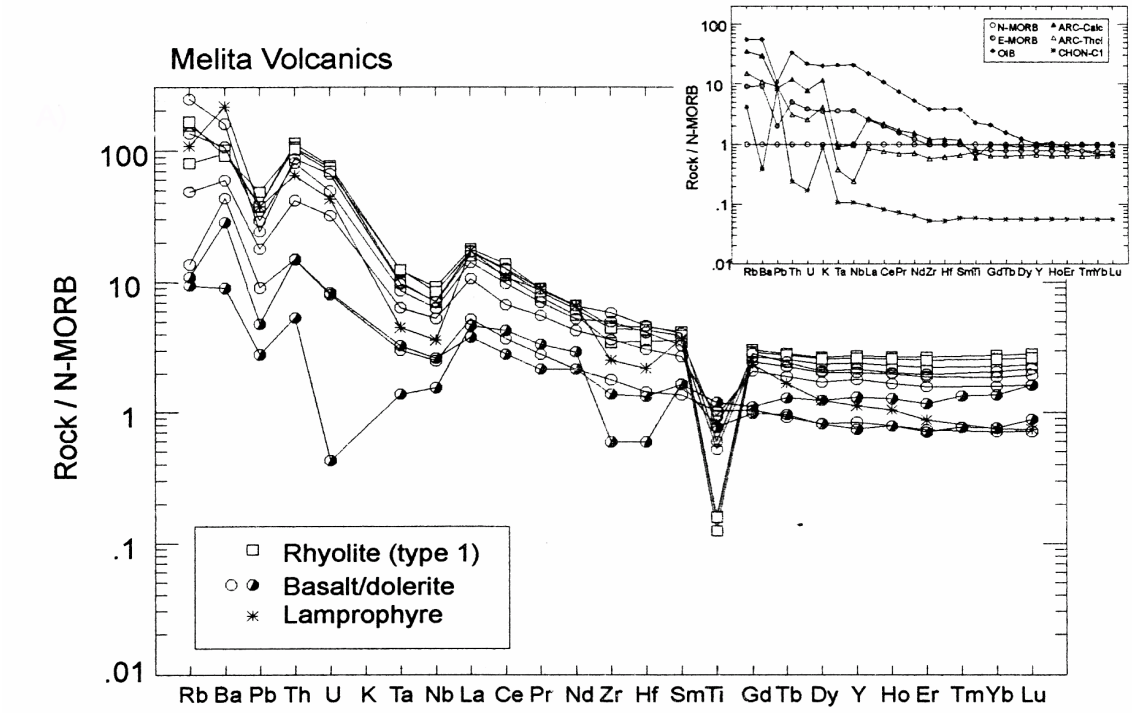

Figure 2: MORB-normalised spider plot for volcanic rocks from the Melita complex (after Barley et al., 1998).

Geodynamic significance

The Gindalbie Terrane occupies a key position between the Kalgoorlie (characterised by tonalite-trondjhemite-dacite TTD volcanism) and Kurnalpi (characterised by calc-alkaline volcanism) Terranes. While these terranes are interpreted as back arc and intra-arc volcanism respectively, the geodynamic setting of mineralised volcanic rocks in the Gindalbie Terrane is uncertain. Barley et al., (1998) suggested that the bimodal basalt-rhyolite volcanic association is most likely derived via decompression melting of subduction modified upper mantle with extensive crustal assimilation and fractional crystallisation processes producing dacites and rhyolites. In post-Archaean terranes bimodal tholeiitic to mildly per-alkaline, HFSE-enriched volcano-plutonic suites are typical of rifting of thickened magmatic arc crust. Geochemically similar volcanic complexes in the Abitibi belt studied by Barrie et al. (1993) have been interpreted to be the product of plume-arc interaction.

Arc rift or plume-arc interaction

Wyman (1999) conducted a study that established that the Kidd Creek giant massive sulphide deposit in the Abitibi, Canada, which is remarkably similar to the smaller Teutonic Bore massive sulphide deposit in the Gindalbie Terrane, occurs at a komatiite-to-arc-tholeiite transition (Wyman et al., 1999). This was further interpreted to reflect evolution from a proto-arc to an

evolved arc setting. The geodynamic history of the Southern Volcanic Zone in the Abitibi belt was then interpreted to be the result of plume ascent under and near an Abitibi arc, which generated a topographic and thermal high outboard. Subduction zone jamming and suture of plateau fragments caused stepback of subduction and formation of a proto arc, followed by rifting of juvenile arc along and near a significant break resulting in eruption of a tholeiitic group. In the study by Brown et al., (2002) of the Melita Volcanic Complex it was suggested that the compositional range, eruptive style, abundance of thick mass-flow deposits, and association with late mafic sill complexes demonstrated by the igneous rocks was typical of intra-arc-rift settings, such as the Sumisu Rift, Isu-Bonin arc, Japan, and the bimodal basalt-rhyolite volcanism was characteristic of active rifting in a marginal arc, like those demonstrated in the Taupo Volcanic Zone of New Zealand. The close proximity of the rocks at Teutonic Bore, and the similar style means that this geodynamic setting could also be a plausible model.

Due to the similar geochemistry of the Gindalbie Terrane HFSE-enriched igneous rocks to those at Kidd Creek in the Abitibi, this model could be used to explain the geodynamic evolution of the Gindalbie Terrane.

VHMS potential

Barrie et al. (1993) and Barrie (1995) reviewed the geochemistry of felsic volcanic rocks associated with Cu-Zn mineralisation in the Archaean Abitibi subprovince, which are geochemically similar to those in the Gindalbie Terrane. They showed that barren and mineralised successions can be separated on host-rock chemistry. Mineralised successions are characterised by bimodal basalt-andesite and high-silica rhyolite with elevated HFSE contents and flat to depleted LREE patterns with negative Eu anomalies. In contrast, barren successions consist of basaltic andesite to rhyodacite with low HFSE contents and relatively higher $(La/Yb)_{CN}$ ratios. Although VHMS deposits in the Gindalbie Terrane are much smaller than those in the Abitibi, the potential for VHMS discovery in the Gindalbie Terrane is high due to their elevated HFSE contents.

Barrie (1995) investigated zircon thermometry of high-temperature rhyolites in the Abitibi subprovince, and found that those rhyolites associated with VMS mineralisation had the highest zircon saturation temperatures (840-940°). Similar trends have been detected in preliminary work conducted by Brown and Barley (unpublished, Figure 3), and rocks from Teutonic Bore and Jaguar will be tested to see if they show similar high temperatures.

Understanding and unravelling the geological evolution of a particular mineralised rock association in an important terrane such as the Gindalbie Terrane will be imperative towards the discovery of VHMS deposits. VHMS mineralisation only occurs in one other terrane in the Yilgarn Craton at the Golden Grove-Scuddles deposit in the Murchison Terrane. Adding to our knowledge of terrane stratigraphy and the thermal history of the Yilgarn Craton will certainly aid in predictive mineral discovery.

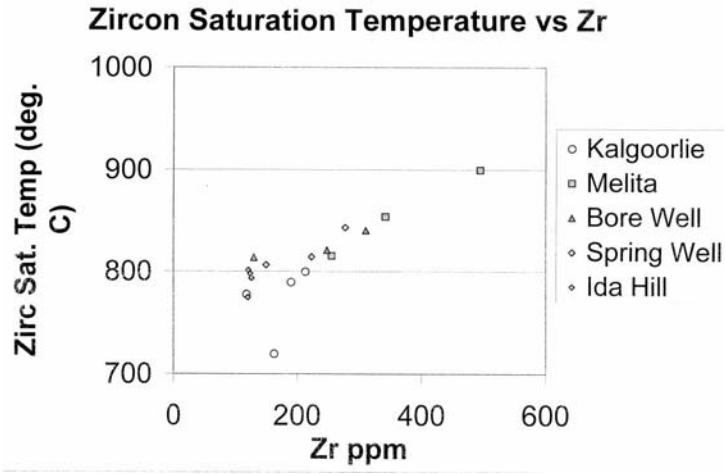

Figure 3: Zircon saturation temperatures for igneous rocks in the Eastern Yilgarn Craton. After Brown and Barley (unpublished).

References

Barley, M.E., Brown, S.J.A., Krapez, B. and Cas, R.A.F., 1998. Mineralised volcanic and sedimentary successions in the Eastern Goldfields Province, Western Australia. AMIRA Project P437 Final Report (unpublished).

Barley, M.E., Brown, S.J.A., Krapez, B. and Cas, R.A.F., 2002. Tectonostratigraphic analysis of the Eastern Yilgarn Craton: an improved geological framework for exploration in Archaean terranes. AMIRA Project P437A Final Report (inpublished).

Barrie, C.T., Ludden, J.H. and Green, T.H., 1993. Geochemistry of volcanic rocks associated with Cu-Zn and Ni-Cu deposits in the Abitibi Subprovince. Economic Geology, 88, 1341-1358.

Barrie, C.T. 1995. Zircon thermometry of high-temperature rhyolites near volcanic-associated massive sulfide deposits, Abitibi subprovince, Canada. Geology 23, 169-172.

Brown, S.J.A., Barley, M.E., Krapez, B. and Cas, R.A.F., 2002. The Late Archaean Melita Complex, Eastern Goldfields, Western Australia: Shallow submarine bimodal volcanism in a rifted arc environment. Journal of Volcanology and Geothermal Research, 115, 303-327.

Myers, J.A., 1990. Precambrian tectonic evolution of part of Gondwana, southwestern Australia. Geology, 18, 537-540.

Myers, J.S., 1997. Preface: Archaean of the Eastern Goldfields of Western Australia- regional overview. Precambrian Research, 83, 1-10.

Swager, C.P., 1997. Tectono-stratigraphy of late Archaean greenstone terranes in the Southern Eastern Goldfields, Western Australia. Precambrian Research, 83, 11-42.

Wyman, D.A., 1999. A 2.7 Ga depleted tholeiite suite: evidence of plume-arc interaction in the Abitibi greenstone belt, Canada. Precambrian Research, 97, 27-42.

Wyman, D.A., Kerrich, R. and Groves, D.I., 1999. Lode gold deposits and Archaean mantle plume-island arc interaction, Abitibi Subprovince, Canada. Journal of Geology, 107, 715-725.

Embedded insights into the Wallaby gold deposit, Western Australia

Susan Drieberg[1], John L. Walshe[2], Scott Halley[3], Greg Hall[3]

[1]*pmd*CRC, Centre for Global Metallogeny, School of Earth and Geographical Sciences, University of Western Australia, Crawley, WA 6009*

[2]*pmd*CRC, CSIRO Exploration and Mining, PO Box 1130, Bentley, WA 6102*
[3]*Placer Dome Asia Pacific*

Susan_Drieberg@placerdome.com

The embedded researcher concept has evolved through interactions between the minerals industry and academia that identified a need for direct, real-time transfer of research results into on-going exploration and mining activities. With this goal in mind, the embedded researcher interacts closely with mine site personnel delivering results as they are generated and also acts as the contact point for other researchers to obtain samples, gain site access, etc. An embedded researcher has been on site at the Wallaby gold mine since January 2004 focusing on two main unresolved issues: (1) the relative timing of magmatic intrusions and their relationship to gold mineralization, and (2) structural and chemical controls on gold grade distribution.

The Wallaby gold deposit is located 25km southwest of Laverton within the Eastern Goldfields Province of Western Australia. Gold mineralisation is hosted in a >1500m thick, polymict, matrix-supported conglomerate that has been intruded by a differentiated alkali syenite suite of dykes. The dykes occur as two main shoots plunging 50° to the south and extending to >1km in depth. The dykes range in composition from relatively early monzonite and carbonatite through younger syenite and porphyritic syenite. Both pre-ore and post-ore lamprophyre dykes are also present.

Alteration distal to the Wallaby deposit consists of a pre-ore regional chlorite-calcite-pyrite±pyrrhotite±chloritoid alteration formed under lower greenschist facies metamorphism (Wall and Mason, 2001). Proximal alteration is composed of actinolite-magnetite±epidote±pyrite that forms a pipe-like body mantling the syenite dyke suite (Wall and Mason, 2001). The actinolite-magnetite alteration event was accompanied by the formation of calc-silicate veins and abundant carbonate-rich veins with variable amounts of biotite, magnetite, and garnet, implying a relatively high temperature of formation. Early magmatic intrusions such as monzonite and carbonatite are overprinted by the actinolite-magnetite alteration while younger syenite and porphyritic syenite intrusions are not overprinted. Gold mineralisation is wholly contained within the actinolite-magnetite alteration pipe and occurs as a series of flat-lying ore lodes linked by small, steep, high-grade ore lenses. Gold-related alteration is composed of albite-ferroan dolomite-pyrite with abundant quartz-carbonate veins, and is hosted in structures that have previously undergone biotite-carbonate±pyrite alteration. The gold ore event crosscuts the conglomerate and the majority of magmatic intrusions, and overprints both actinolite-magnetite and biotite alteration.

While gold-related alteration post-dates the majority of intrusive activity and its associated actinolite-magnetite alteration, it is not known for certain whether the gold ore event and magmatism are directly related or whether there was a significant hiatus between these two events. Recent detailed mapping and reinvestigation of diamond drill core has identified a close spatial and paragenetic link between gold mineralisation and syenite magmatism. The

presence of pegmatite bodies, miarolitic cavities, and extensive magmatic-hydrothermal breccia pipes provide evidence that the syenite and porphyritic syenite dykes, the youngest intrusive phases, exsolved a CO_2-rich volatile phase. In addition, syenite dykes intrude along the same flat-lying structures that host gold mineralisation and rare post-ore syenite dykes have been documented. Geochronological studies currently in progress will help to constrain this close spatial and temporal link between gold mineralisation and syenite magmatism.

One problem encountered in the mining of the Wallaby gold deposit has been that the controls on gold grade distribution within the flat-lying ore lenses are not understood. To address this issue, an individual ore lens was modeled to investigate the relationships between geometry and gold grade. The modeling has revealed northwest and northeast trending high-grade zones within the ore lens. These high-grade zones occur at the inflection points between relatively flat-lying and steeply dipping segments of the ore lens. These features are interpreted as a ramp-flat style of structural control on gold grade distribution. Utilization of this knowledge better constrains open pit grade control data and provides confidence in the geological model used to plan the development of underground mining operations.

Reference

Wall, V. and Mason, D., 2001. Wallaby petrology: Geological review of the Wallaby lode-gold project, Laverton Region, Western Australia. Placer Dome Company Report, 44 pp.

Crustal fluids in tectonic evolution and mineral systems: evidence from the Yilgarn Craton

B.J. Drummond[1], B.E. Hobbs[2], R.W. Hobbs[3] and B.R. Goleby[1]

[1] *pmd*CRC, Geocsience Australia, GPO Box 378, Canberra ACT 2601*
[2] *pmd*CRC, CSIRO Exploration and Mining, PO Box 1130 Bentley, WA 6102*
[3] *Department of Earth Sciences*, *University of Durham, UK*
Barry.Drummond@ga.gov.au

Introduction

In seismic reflection sections, some crust-penetrating shear zones appear as bright reflections whereas others do not. Those that are reflective often have a close spatial relationship to areas of altered rock, and in some cases to mineral deposits. Examples in areas of interest to the pmd*CRC include the Adelheid Fault and Marimo Structure in the Western and Eastern Successions of the Mount Isa Inlier, respectively, the Bardoc and Boorara Shear Zones in the Eastern Goldfields Province of the Yilgarn Craton in WA; and a number of shear zones in the Broken Hill area. Furthermore, the Western Fold Belt Mt Isa and the Eastern Goldfields Province contain sub-horizontal detachments, or shear zones, in the (present-day) upper crust that are seismically reflective.

In a number of cases, the reflections must come from the intrinsic reflectivity of the shear zones, rather than contrasts between the rocks either side of the shear zones. The causes of intrinsic shear zone reflectivity have been the subject of debate within the literature. Physical models based on laboratory measurements of rock properties suggest two causes – seismic anisotropy caused by crystal alignment and chemical alteration within the fault and wall rocks of the shear zone. Both of these effects would indicate fluid movement within the shear zone, but the relative effects are unclear, and neither effect can easily explain the high amplitudes of the reflections that are often observed.

Modelling Shear Zone Reflectivity – The Yilgarn Craton Detachment

Synthetic seismogram modeling of shear zone reflectivity showed the effects that 3D morphology on the surfaces of shear zones has when the shear zones are imaged in 2D seismic sections. The synthetic seismogram studies used the detachment surface in the Eastern Goldfields Province as an example. The research indicated a number of empirical tests that can be used to distinguish between a fault (modelled as single thin layer within a rock of uniform physical properties) and a shear zone (multiple anastamosing layers of different thicknesses embedded within a uniform rock) (Drummond et al., 2004b) (Figure 1). The modelling also indicated that the amplitudes of the signals would be much higher because of the effects of tuning between layers, and because of seismic energy being reflected into the plane of the seismic section from structure outside the plane of the section[1]. The results of the modelling allow the sub-horizontal detachment imaged in the Eastern Goldfields Province to be characterised into regions of thick shear zones 10-20km across (in the plane of the seismic sections) consisting of multiple layers, linked by faults, also with an extent of 10-20km.

[1] Present research is being directed to develop methods for determining the minimum amount of alteration needed to explain the strength of the reflections, so this can be linked to other physical properties such as magnetic susceptibility and density to determine how much alteration is needed for faults and shear zones to be interpreted in regional potential field data.

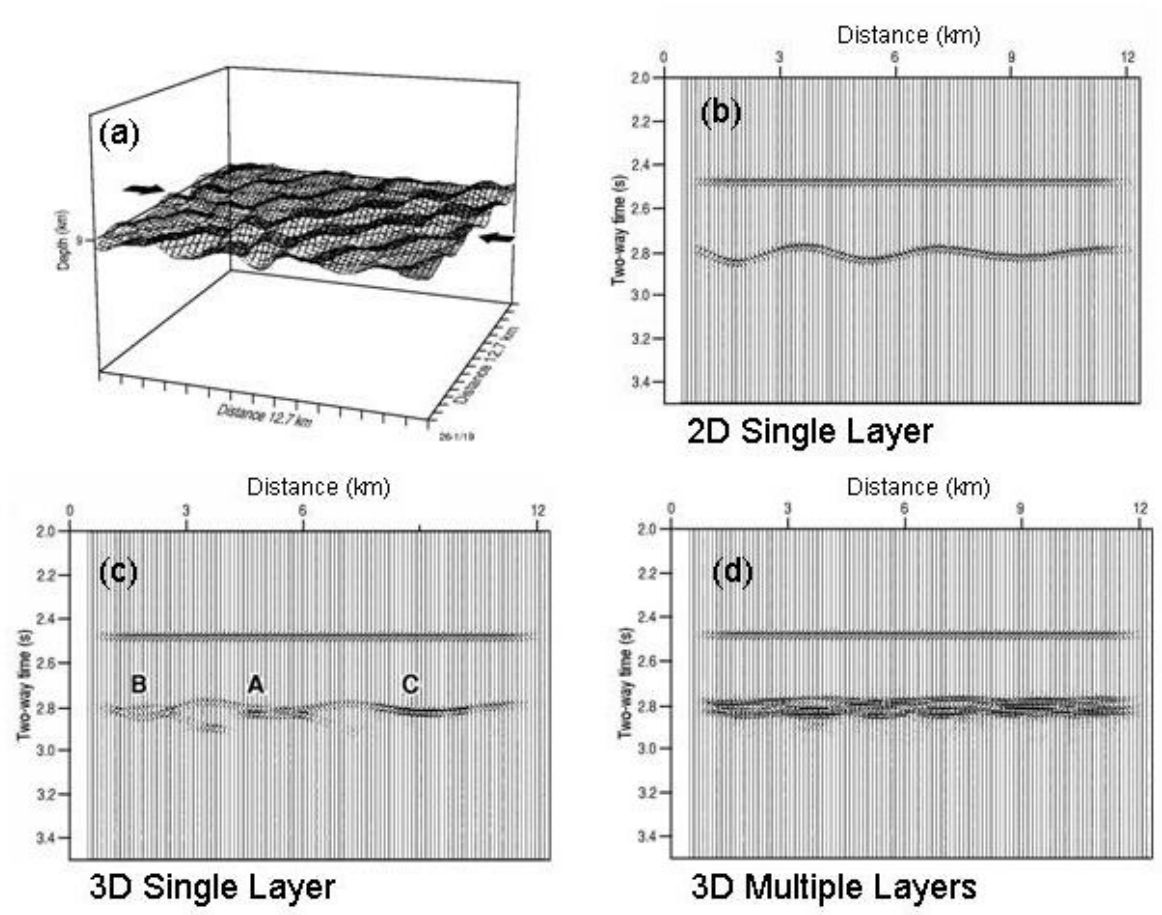

Figure 1: (a) 3D synthetic surface used to create synthetic seismograms. Note that the surface has a degree of roughness achieved by adding topography with a range of wavelengths that vary in relief and are randomly out of phase. The arrows mark the position of the line of 2D seismic section, which crosses the antiforms and synforms obliquely. (b) Migrated synthetic seismogram for a single 2D layer. The reflection just below 2.4s Two Way Time is a reference which, when displayed at the same amplitude scale in (b), (c) and (d) allows the amplitudes of the reflections from the deeper fault and shear zone near 2.8s to be compared directly. (c) Migrated synthetic seismogram for a single 3D layer (fault); the difference between (b) and (c) indicates the influence of out-of-plane reflector topography in a 2D seismic section. (d) Migrated synthetic seismogram for a band of reflectors (shear zone cf fault) created by using the layer in (a) eight times shifted in amplitude, thickness and phase so no two reflecting layers in the model are coherent. The difference in form between (c) and (d) indicates the effects of a thick zone of multiple reflectors compared to a single thin layer. (Modified from Drummond et al., 2004b)

The Detachment and Fluids

Drummond et al. (2000) drew parallels between the reflection character of the regional detachment and the bright reflectors imaged at 15-18km depth in Tibet. The Tibetan reflectors have been interpreted as fluids (brines or magmas). Drummond et al. (2004a) suggested that overpressured fluids focusing at that depth in an orogenic setting would provide weak zones which would be a locus for detachment formation. Zones of fluid focusing in the Archaean would be characterized today by shear zones in which rocks with altered anisotropic fabric wrap around lenses of protocrust. These zones would be linked laterally by faults characterized by single or only a few layers which broke through regions of little or no fluids.

In the seismic data available to date in the Kalgoorlie region of the Eastern Goldfields Province, former fluid rich zones are interpreted on the basis of detachment reflection character under the western sides of the Kalgoorlie (eg. Figure 2) and Mt Pleasant antiforms, and the eastern side of the Scotia-Kanowna antiform. Fluids in these zones would break into the brittle upper crust, presumably through deformation-induced permeability facilitated by high fluid pressures. In these three antiforms, concave-upwards reflectors link from the detachment upwards into the

core of the antiform. They can be interpreted as faults because of their reflection character, and would be excellent pathways for fluids from the detachment to migrate upwards into the antiforms. In the Kalgoorlie and Mt Pleasant antiforms, the direction of the faults is such as to have directed the fluids towards regions of known mineralization.

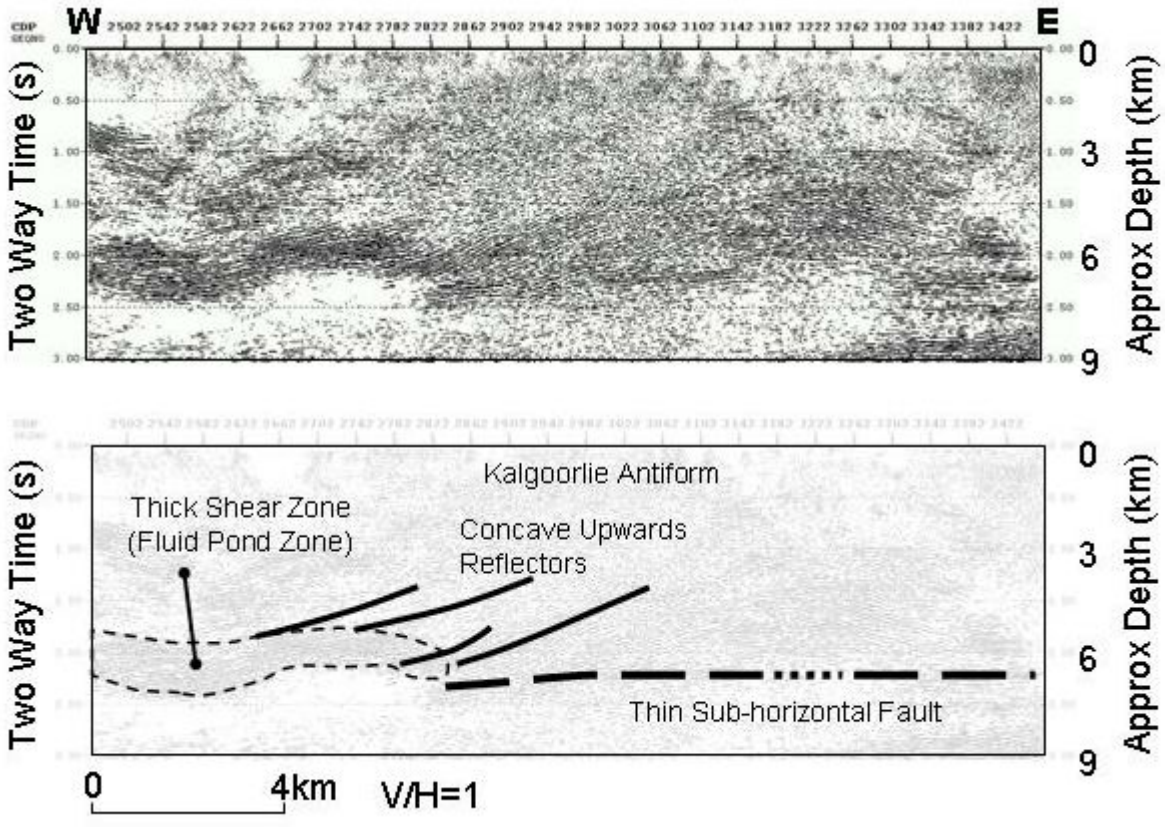

Figure 2: Top: EW seismic section from Line 99AGS-Y3 across the Kalgoorlie antiform. Bottom: Interpretation. The detachment in this region consists of a shear zone in the bottom left and a thin, sub-horizontal fault on the right. Concave upwards reflectors extend upwards from the shear zone into the Kalgoorlie antiform.

Deformation-driven induced permeability creation and destruction can lead to transitory fluid-rich zones at a range of depths in the crust (Cox, et al., 1990; Connolly & Podladchikov, 2004). In Tibet, the implied fluid-rich zones formed at a similar depth over distances of more than a hundred kilometres, and are reflective because the fluid-rich zones have a large seismic impedance contrast with the country rock. In the Kalgoorlie region, the detachment surface did not follow a compositional boundary everywhere. In some areas it is interpreted as the boundary between the greenstone succession and felsic basement, but in other areas it is through felsic basement below the greenstones. It is interpreted to be reflective in places because of chemical alteration and deformation induced anisotropy.

Detachment surfaces are not ubiquitous. However, other regions where detachment formation is not so pervasive have reflections that can be interpreted to result from alteration and anisotropy caused by fluid flux. For example, in the Laverton-Leonora region, sub-horizontal reflectors and linked concave upwards reflectors similar to those in the antiforms around Kalgoorlie are observed. In the seismic section in Figure 3, the reflections can be divided into two groups. In the top part of the diagram the regional geology is interpreted as a layered sequence in the upper left forming a roll over anticline on an amorphous piece of rock that may be granite. The form lines marking geological boundaries are dashed where there is uncertainty, but in most cases can be fairly confidently carried through other reflections that have a different orientation. Superimposed on the reflections that are interpreted as geological boundaries are a series of other reflections (bottom part of the figure) that sub-divide into sub-horizontal and feathering-

upward reflections. The sub-horizontal reflectors (H1, H2, and possibly a third, H3) can be interpreted as previous fluid rich zones that are now reflective because of alteration. Anisotropy due to deformation-induced fabric is not favoured as an explanation of these reflections because none of them offsets the reflectors attributed to the geological boundaries. Furthermore, the reflections are more like those of faults in the synthetic data than shear zones. Note that H1 lies in the core of an anticline and therefore was probably structurally related. In contrast, H2 cuts across stratigraphy, and would therefore have been controlled by fluid pressures. The feathering-upward reflectors would be breach faults driven by fluid pressures. They parallel but are separate from the boundary between the stratified rocks and the underlying inferred granite, and at depths close to H1 and H2 cross-cut the stratigraphy. The reflectivity of the breach faults would be due to alteration along the faults.

If this interpretation is correct, fluids would have moved systematically upwards and to the west through the crust in this region. We cannot tell from the available images whether the fluids were derived from the deep crust or from the stratified rocks to the east. The position of the fluid pathways regionally may have been controlled by the boundary between the stratified rocks and the ?granite, which can be followed in various forms down to the base of the crust where it offsets the Moho, but the actual pathways were not controlled locally by the stratigraphy or local structure.

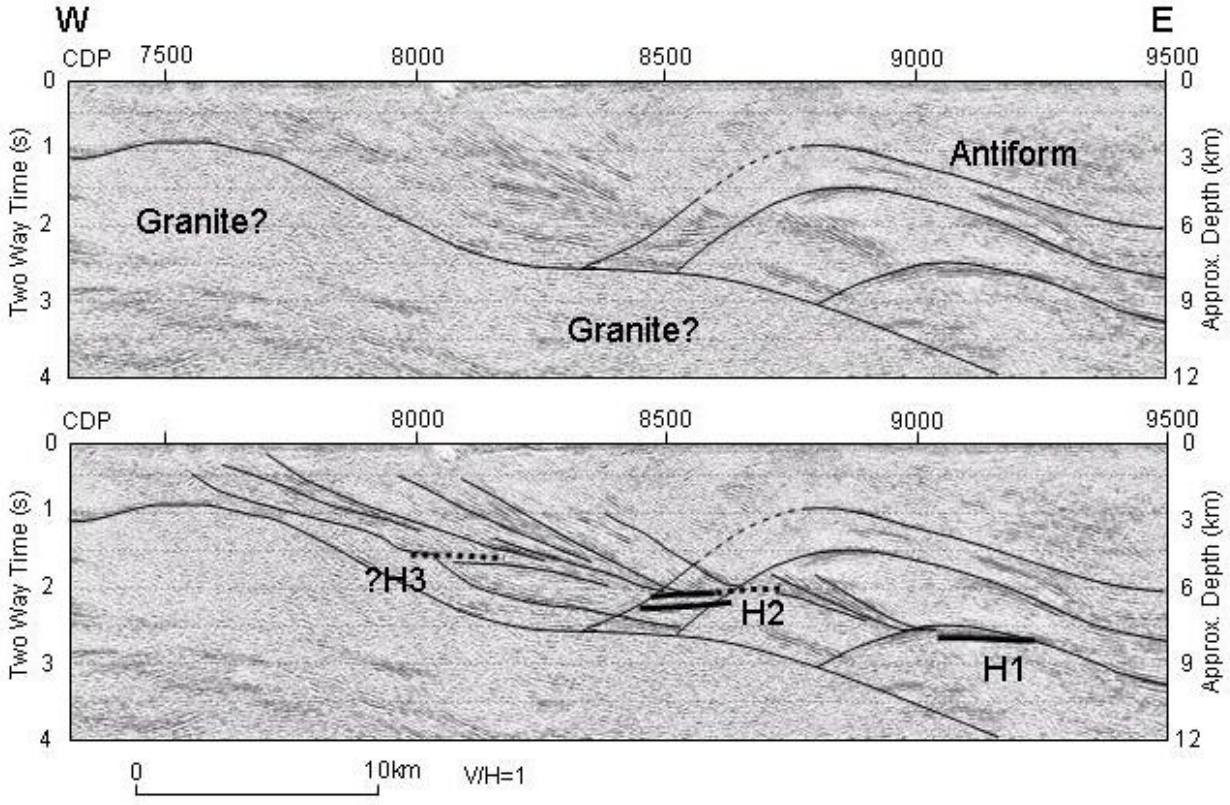

Figure 3: Top: Migrated seismic section from east of Laverton in Western Australia. Black lines show geometry of rock packages (dashed where uncertain) .Bottom: Sub-horizontal reflectors (H1, H2 and possibly H3) shown as thick lines link with concave upwards reflectors shown as thinner lines.

Acknowledgements

BJD & BRG publish with the permission of the CEO of Geoscience Australia. We thank the staff of ANSIR for acquiring and processing the seismic data.

References

Connolly, J.A.D. and Podladchikov, Yu.Yu, 2004. Fluid flow in compressive tectonic settings: implications for mid-crustal seismic reflectors and downward fluid migration. Journal of Geophysical Research, in press.

Cox, S.F, Etheridge, M.A. and Wall, V.J., 1990. Fluid pressure regimes and fluid dynamics during deformation of low-grade metamorphic terranes. Implications for the genesis of mesothermal gold deposits. In: Robert, F., Sheahan, P.A. and Green, S.B., eds., Greenstone Gold and Crustal Evolution. Nuna Conference Volume. Geological Association of Canada, 46-53.

Drummond, B.J., Cox, S.F. and Goleby, B.R., 2000. The role of fluids in the formation of regional-scale detachment surfaces. 9th International Symposium on Deep Seismic Profiling of the Continents and their Margins, Ulvik, Norway, 18-23 June, 2000, Abstracts, 51.

Drummond, B.J. and Goleby, B.R., 2004a. The role of crustal fluids in the tectonic evolution of the Eastern Goldfields Province of the Archaean Yilgarn Craton, Western Australia. Second International Symposium on Slip and Flow Processes in and below the Seismogenic Region, Tokyo, March 2004, (no pagination).

Drummond, B.J., Hobbs, R.W. and Goleby, B.R., 2004b. The effects of out-of-plane seismic energy on reflections in crustal-scale 2D seismic sections. Tectonophysics, submitted.

Adding value to exploration – Reducing time and cost to discovery in Western Victoria

L. Jonathon Dugdale

Exploration Manager, Eastern Australia, MPIMines

jdugdale@sgm.mpimines.com.au

Predictive mineral discovery in Western Victoria

The adage "Gold is where you find it" is effectively an indictment on the gold exploration industry. The industry has been driven by empirical exploration for 25 years and depended on luck to gain genuine success.

As a small-medium company MPIMines cannot afford to depend on being the "lucky company". Most small-medium sized companies go broke eventually. Exploration as a whole is a loss making business.

To quote our former Managing Director, the late Ken Fletcher, "Jon, we cannot afford to grid drill our prospects under cover – we'll go broke before we find the orebody". In other words, he was challenging us to deliver a step change reduction in our time and cost to discovery.

This is the reason MPI became involved with the predictive mineral discovery CRC. Our objectives as a company were aligned with the "mission statements" of the pmd*CRC. Our expectations of the pmd*CRC were not that we were buying into "silver bullet" exploration techniques, but rather, a commitment to the development of predictive models augmented by cutting edge techniques that could be melded into exploration programs in order to reduce the time and cost to discovery.

The case history presented below from the Stawell Corridor, in Western Victoria, illustrates how the location of concealed gold ore-bodies can be predicted both within active mining centres and under barren cover sequences. This is an active case history.

Gold Discovery at Stawell

The Stawell Gold Mine is located in Western Victoria, Australia (Figure 1). Stawell is an historic Goldfield having produced 2.7 Million ounces of gold between 1853 and 1926. No further mining took place until 1982 when Western Mining Corporation and Central Norseman Gold Mines in joint venture re-opened the mine commencing the Magdala Decline and Wonga Open Cut. WMC operated the mine until 1992 when the current owners Mining Project Investors Pty Ltd (MPI) in joint venture with Pittston Mineral ventures purchased the operation and one exploration tenement to the north. MPI, now MPI Mines Ltd., purchased Pittston's interest in the joint venture at the end of February 2004. Since MPI's involvement from 1992, the mine has produced over 1 million ounces of gold and discovered over 2.2 million ounces into resources. This brings the total hard rock endowment of the Stawell Goldfield to over 5 million ounces of gold.

The discovery of additional resources at Stawell, in particular the Golden Gift, has been in large part a predictive mineral discovery story. It was recognised that the steeply plunging Magdala orebodies systematically repeat down the western flank of the moderate northerly plunging Magdala basalt dome. This led to continued prediction and discovery of new ore-shoots down plunge. However, the available target area decreases down plunge above the South Fault. Exposure of the South Fault underground clearly indicated that the South Fault was post-ore

and that the remainder of the ore system should be present below the South Fault, somewhere. It was also recognised that the north plunging Magdala dome was the northern part of an offset doubly plunging basalt dome, the remaining south plunging end of which lay below the South Fault.

A long established research relationship with the University of Melbourne, through Professor Chris Wilson, was called upon to help solve the movement sense and extent of displacement on the South Fault and find the offset ore system. This initial work, by Dr John Miller, indicated that the South Fault offset had an early southwest component of movement followed by later west directed transport (Miller, et al 2001). This information was combined with results of Magnetic modelling by geophysicist Kim Francombe and a best case scenario for the southern end of the offset doubly plunging dome was presented. The first drillhole, MD 2064, intersected mineralised "volcanogenics" and basalt immediately below the South Fault at –910m RL, producing an intercept of 3.2m @ 4 g Au/t. A second hole, MD 2122, was drilled further east and intersected basalt below the South Fault until holes end at 1250m below surface. A third hole, MD 2167, drilled during October 1998 was angled between these holes and intersected three repeated zones of mineralised volcanogenics with visible gold, located below the South Fault on basalt contacts. Intersections of 16.2m @ 5.15g Au/t, 19.0m @ 7.21 g Au/t and 2.85m @ 7.12 g Au/t were produced. Follow up drilling on four approximately 300m spaced sections scoped a mineralised zone ~1200m long and 300m deep from -900m to -1200m below surface, representing approximately 1 million scoped ounces. Resource definition drilling has so far defined 650,000 ounces of indicated and inferred resources (Figure 2). Development of the Golden Gift has recently commenced.

Exploration and Discovery in the Stawell Corridor

Interpretation of aeromagnetic and gravity imagery indicates that the Stawell Corridor passes under cover north of Stawell and continues under cover of deepening Murray Basin sediments as far as 150km north of Stawell, west of Warracknabeal. This recognition by MPI was followed by the consolidation of contiguous exploration licences over a 140km strike length of the interpreted northern extension of the Stawell Corridor (Figure 1).

It was recognised that successful exploration within buried portions of the Stawell Corridor would require a well researched predictive model. Previous grid RAB drilling and some diamond drilling of regional structures had failed to enhance targets and although initial trialling of surface geochemical techniques appeared to produce encouraging results this was also abandoned in favour of a predictive model based on detailed characterisation of the Stawell ore-body and remote detection of key characteristics using geophysics.

The key predictive characteristic of the Stawell orebody is an association between the ore-system and a large tholeiitic basalt unit – the Magdala Basalt (Vandenberg et al., 2000). The northwest trending Magdala Basalt dome has a doubly plunging 1km wide unit of basalt in its core and is over 3km long. It is enveloped by a package of sulphidic, iron enriched, sedimentary rocks termed "volcanogenics" that host the majority of the ore-grade mineralization. Ore formation was associated with brittle re-activation and hydrothermal fluid flow along major reverse fault systems mostly localised on the western flank of the Magdala Dome (Miller et al., 2001), such as Central Lode. Fluid flow modelling within the predictive mineral discovery CRC program has demonstrated that the geometry and of the basalt dome and the contrasting rock properties between the basalt, "volcanogenics" and Mine Schist are the main controlling factors controlling the location of (D4) ore shoots at Stawell (Schaubs., et al 2004). Other factors such as chemical controls will be the subject of further work. However, this demonstrated association between the Magdala Dome and the ore bodies at Stawell is enough to present a powerful primary targeting tool.

The second stage in the development of the predictive model was the characterisation of the key geological elements of the Stawell ore system. It was known from previous WMC

petrophysics that Magdala basalt and "volcanogenics" were magnetic. "Dome shaped" magnetic anomalies within 5km west of interpreted extensions of the Coongee Break were selected as priority targets. The Wildwood dome, 2km northwest of Stawell, had been previously drilled by WMC and was known to be similar to the Magdala dome and also mineralised on the east flank (e.g., WLWD 113 : 15.1m @ 2.8 g Au/t). Other targets selected during this first phase included Caledonian, Wal Wal, Lubeck, Ashens, Jung, Byrneville, Kewell, Wallup and Cannum for a total of 10 conceptual domes. The Kewell target in particular was highlighted, pre drilling, in an internal memo on the 12th August 1998: "The similarity (to Stawell) is striking. The likelihood of mineralization being present in volcanogenic sediments on the western margin of the dome……. is considered to be high" (Dugdale, 1998).

Aircore drilling was selected as the principle tool for collecting bedrock samples for lithology and geochemistry. Initial testing was "highjacked" by the need to test empirical surface geochemical "anomalies" that turned out to be spurious. It was not until aircore hole MAC 42 that the centre of the Kewell magnetic target was tested. Basalt of the Magdala style was intersected and the contacts were subsequently tested with close spaced drilling in order to locate mineralised volcanogenics. On the 3 April 2000 MAC 057 intersected mineralised volcanogenics on the western flank, with a peak result of 6m @ 1.67 g Au/t from 121m including 1m @ 5.30 g Au/t.

Subsequent aircore drilling, on 400m spaced traverses, defined a 3km long, apparently doubly plunging, truncated basalt dome with mineralised volcanogenics on both flanks. An initial program of two diamond drillholes tested under the peak gold in aircore results producing a technically successful result confirming the presence of volcanogenics of the Magdala style in KD001 and a laminated quartz reef and volcanogenic hosted basalt contact mineralisation including 0.5m @ 1.6 g Au/t in KD002.

Despite the lack of an ore-grade intercept, these initial drill tests were considered technically successful, representing confirmation of the original geological concept. However, it was recognised that with a limited exploration budget the next round of diamond drill holes would need to produce an ore grade intercept for the prospect to survive. This would require additional research in order to develop sophisticated ranking criteria for selecting specific drilling targets in order to reduce the time and cost to genuine discovery. Two parallel approaches were taken; firstly, the initiation of an internal study to geochemically characterize the Stawell ore system and, secondly, MPI became an initial sponsor of the predictive mineral discovery CRC in order to gain access to cutting edge fluid-flow modelling technology.

Geochemical characterization of Stawell produced a series of mineralisation indices to be applied to regional aircore drilling, so that sparse sampling could be ranked using an ICP suite of correlating elements, which is using more than just gold.

Within the pmd*CRC, a specific research project, T1, was initiated, focusing on western Victoria. Additional geophysical data were collected over key prospects, including Kewell. In particular, detailed gravity data proved a very effective filter for basalt domes versus other magnetic features. Inversion modeling of gravity and magnetics assisted construction of 3-dimensional basalt dome models. Finite element meshes were then constructed for numerical simulation modeling of fluid flow and dilation at the time of mineralisation (Schaubs et al., 2004). Stress orientations and rock properties were as determined through previous Stawell ARC research. The combined results of ENE-WSW + E-W compression produced generally high fluid flow on the upper shoulders of the dome, particularly the shallow plunging WSW flank and steeply plunging ENE flank (Schaubs., et al 2004). Dilation was concentrated on the upper shoulders of the dome. The intersection of these areas of high fluid flow and dilation with the interface are a 1.6km long zone on the SW flank and a smaller zone on the northern nose (Figure 3). These zones are coincident with elevated aircore geochemistry.

The results of the geochemical characterization and fluid flow-dilation modeling were combined to produce specific diamond drilling targets. The first target selected for drilling was the

southern end of the dome on section 5967600mN. Drillhole KD003 intersected a brecciated quartz lode followed by a thick section of mineralised volcanogenics including a basalt bound "Waterloo" with visible gold, on a shallow west dipping basalt contact. Intersections included 4.2m @ 3.46 g Au/t from the hangingwall lode and 4.1m @ 12.6 g Au/t from the Waterloo (Figure 4).

Further drilling is in progress and time will tell whether Kewell is a significant discovery. However at this early stage it appears this may represent the first new goldfield discovery in Victoria for over 100 years and is an example of reducing time and cost through predictive mineral discovery. **It is estimated that in both the Golden Gift and Kewell examples the application of predictive mineral discovery techniques has at-least halved the number of critical early stage diamond drillholes required to make the discoveries**.

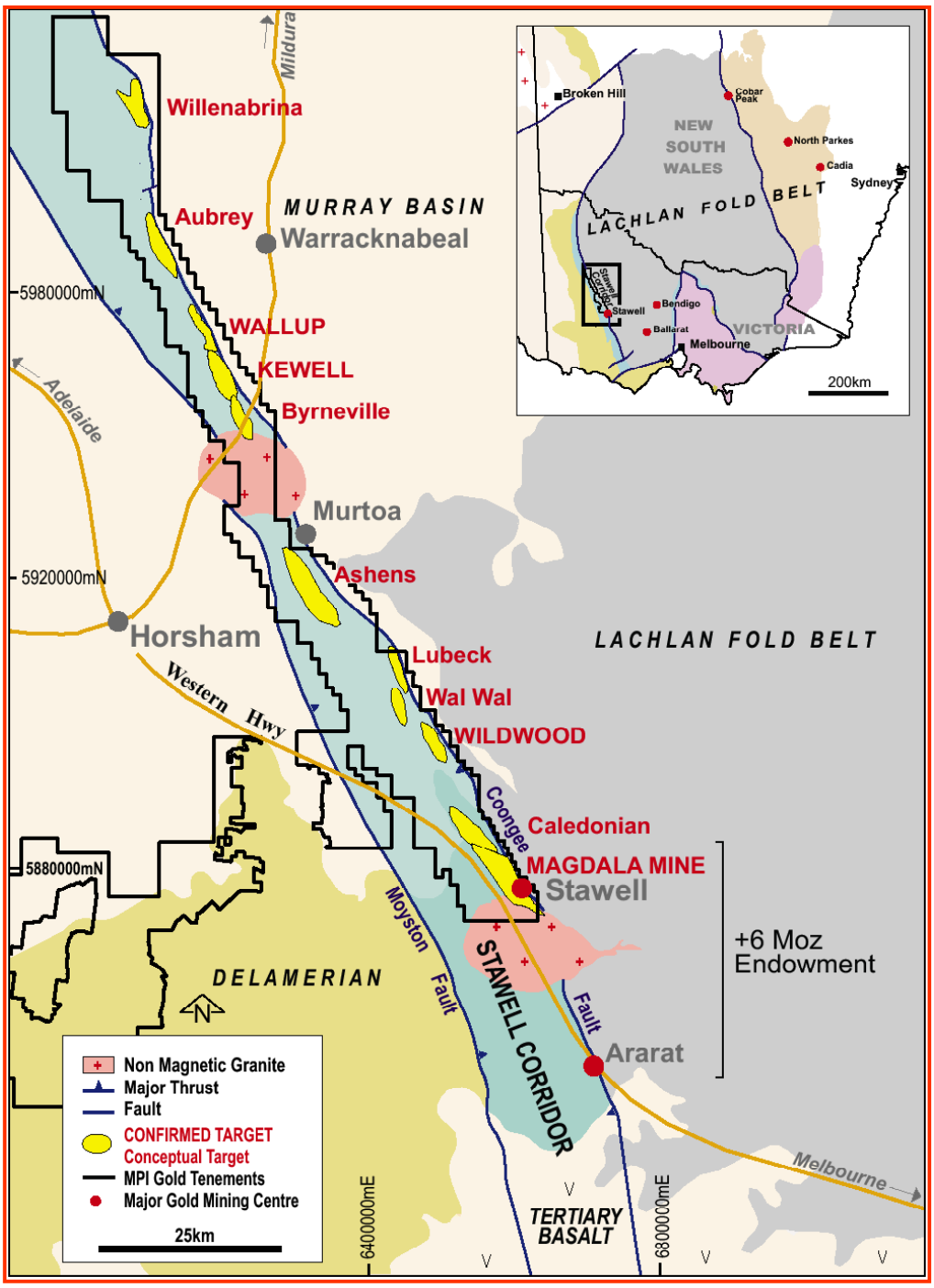

Figure 1. Stawell Corridor and targets, Western Victoria

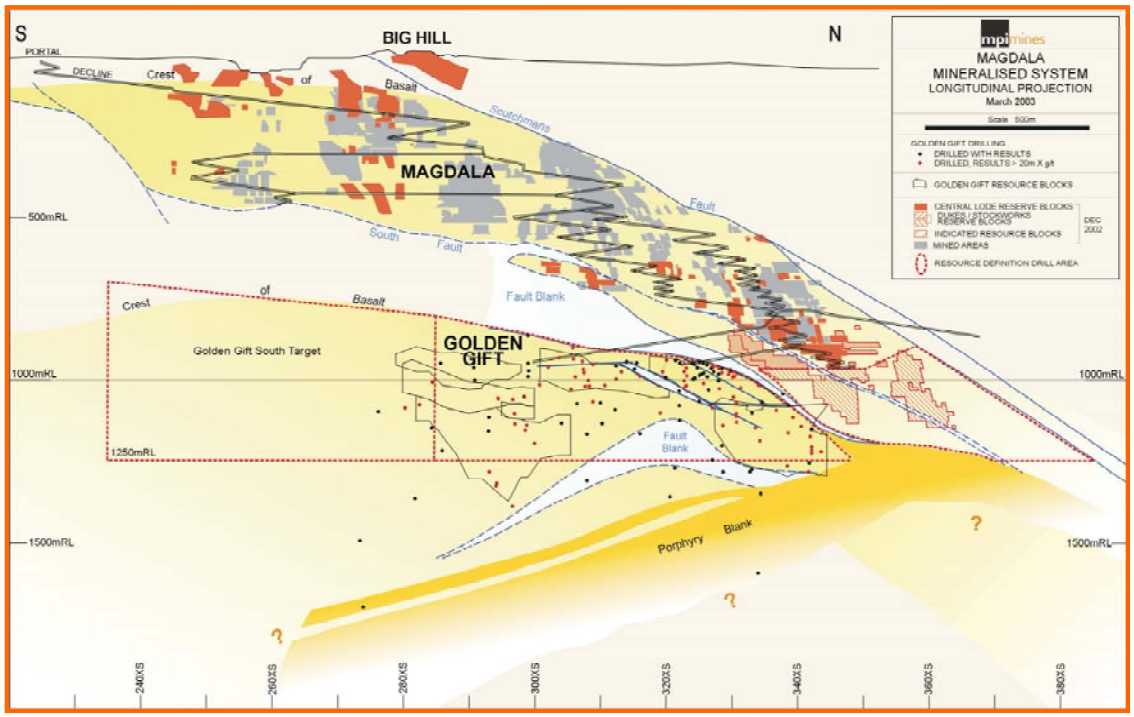

Figure 2. Stawell Mineralised System, Longitudinal Projection

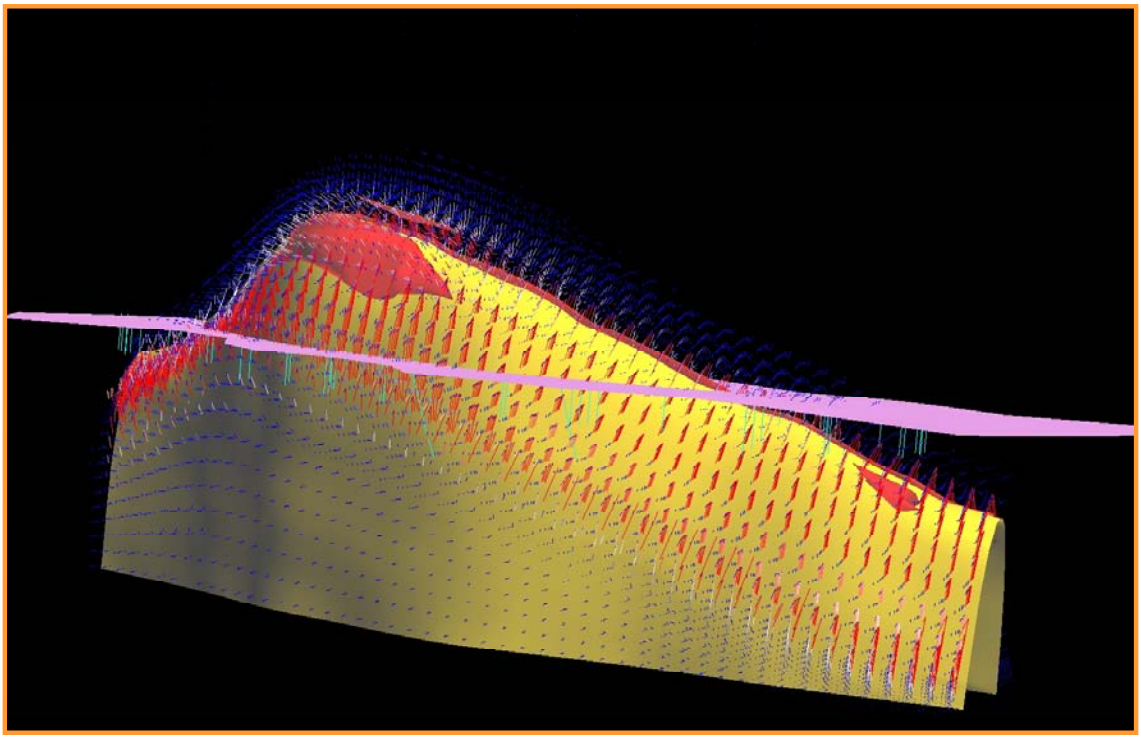

Figure 3. Kewell Dome Fluid Flow Model, looking north

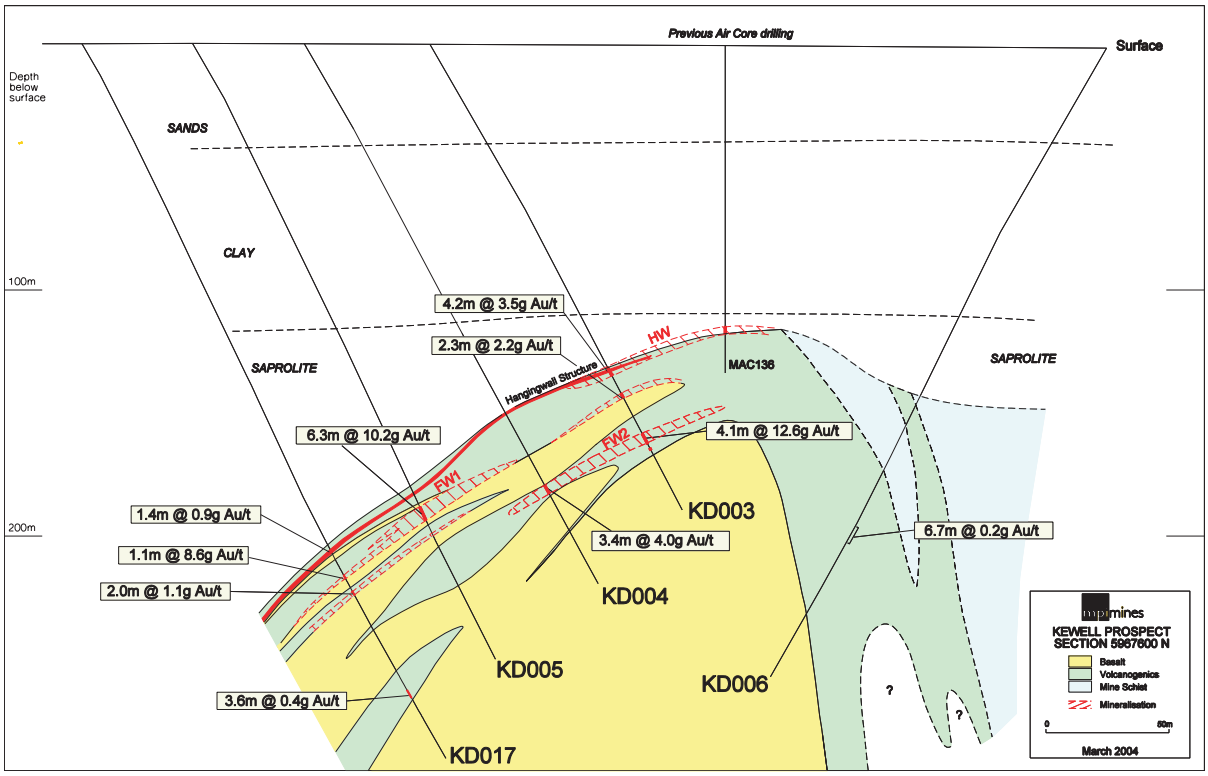

Figure 4. Kewell Dome Cross Section 5967600mN

Acknowledgements

Acknowledgements are made of the important contributions of MPI's Ken Fletcher, David Burt, Brian Phillips, John Rowe, Dean Fredericksen, Mike Gane, Shane Mele, Steve Vincent and Adam Elliston. Acknowledgement is made of the equally important contributions of researchers Prof. Chris Wilson, Dr John Miller, Dr Tim Rawlings, Dr Peter Schaubs and geophysicists Kim Francombe and Bob Smith.

References

Dugdale, L.J., 1998. Murtoa – Western Victoria, New Project Proposal. MPIMines internal memo, 1998.

Miller, J.McL., Dugdale, L.J. and Wilson, C.J.L., 2001. Variable hangingwall palaeotransport during Silurian and Devonian thrusting in the western Lachlan Fold Belt: missing gold lodes, synchronous Melbourne Trough sedimentation and Grampians Group fold interference. Australian Journal of Earth Sciences, 48, 901-909.

Schaubs, P., Rawling, T., Dugdale, J. and Wilson, C.J.L., 2004. Factors controlling the location of gold mineralisation around basalt domes, Stawell Zone, Central Victoria, Some insights from Deformation – Fluid Flow Models. Geological Society of Australia, Abstracts, 73, 118.

Vandenberg, A.H.M., Willman, C.E., Maher, S., Simons B.A., Cayley, R.A., Taylor, D.H. Morand, V.J., Moore, D.H. and Radojkovic, A., 2000. The Tasman Fold Belt System in Victoria. Geological Survey of Victoria Special Publication.

Geochronological constraints on tourmaline alteration at Mount Isa, NW Queensland

R.J. Duncan and A.R. Wilde

*pmd*CRC, School of Geosciences, Monash University, Melbourne, VIC 3800*

rduncan@mail.earth.monash.edu.au

Tourmaline alteration has been recognized as the result of sodic metasomatic events and in many instances is related to base and precious metal deposits in a variety of geologic environments (e.g. Frietsch et al., 1997; Lynch and Ortega, 1997; Slack et al., 1993; Robert and Brown, 1984). Tourmaline-rich rocks are exposed around the copper and lead-zinc orebodies at Mount Isa in the mid-Proterozoic Western Fold Belt. The most striking are quartz-tourmaline vein systems, and accompanying tourmalinization of sedimentary and volcanic wall rocks.

Mathias and Clark (1975) documented accessory tourmaline as part of the silica-dolomite alteration halo around the post-peak metamorphic copper orebodies. However, our field observations have found that tourmaline alteration is more pervasive than has been previously recorded. Based on structural relationships and internal characteristics it is reasonable to assume that several tourmaline vein generations exist. The majority of examples studied to date indicate the tourmaline is pre-peak metamorphism and pre-D_2 in timing. In most cases the tourmaline veins are deformed into meso-scale D_2 folds and are micro-fractured and overprinted by a quartz-biotite-chlorite metamorphic assemblage. Primary fluid inclusions within tourmaline are hypersaline and contain elevated base metal contents.

The absolute age of the tourmaline-bearing veins remains uncertain. Pb-Pb SHRIMP analyses of zircons from quartz-tourmaline-feldspar veins were interpreted to indicate formation at 1532±7 Ma, contemporaneous with regional metamorphism and D_2 (Connors and Page, 1995). Our observations of similar zircons reveal complex zoning and metamict core regions, leading us to question the validity of this age. Older ages of 1626±2 and 1653±3 Ma were obtained from xenocrystic zircons and are thought to be inherited from nearby batholiths (Connors and Page, 1995). We suggest these older dates are closer to the true vein age, with the younger ages representing extensive dynamic recrystallization during regional deformation.

These differing timing criteria support two theories, that tourmaline veins resulted from either (1) an older alteration event related to lead-zinc mineralization, or (2) a later stage of partial melting during metamorphism. The presence of primary sphalerite and pyrite inclusions in the tourmaline suggests the first scenario is most likely. If this is correct, tourmaline alteration is one of two distal metasomatic facies related to lead-zinc mineralization at Mount Isa. Pb-Pb step leaching of monomineralic tourmaline separates may provide a direct geochronological framework for this alteration type. Boron isotope analyses will be used to potentially determine the source of the fluids responsible for this alteration.

References

Connors, K. A. and Page, R. W., 1995. Relationships between magmatism, metamorphism and deformation in the western Mount Isa Inlier, Australia. Precambrian Research, 71, 131-153.

Frietsch, R., Tuisku, P., Martinsson, O. and Perdahl, J., 1997, Early Proterozoic Cu-(Au) and Fe ore deposits associated with regional Na-Cl metasomatism in northern Fennoscandia. Ore Geology Reviews, 12, 1-34.

Lynch, G. and Ortega, J., 1997. Hydrothermal alteration and tourmaline-albite equilibria at the Coxheath porphyry Cu-Mo-Au deposit, Nova Scotia. Canadian Mineralogist, 35, 79-94.

Mathias, B. V. and Clark, G. J., 1975. Mount Isa copper and silver-lead-zinc orebodies - Isa and Hilton mines. Economic Geology of Australia and Papua New Guinea: 1. Metals. Australasian Institute of Mining and Metallurgy, Monograph Series, 5, 351-371.

Slack, J. F., Palmer, M. R., Stevens, B. P. J. and Barnes, R. G., 1993, Origin and significance of tourmaline-rich rocks in the Broken Hill district, Australia. Economic Geology, 88, 505-541.

Robert, F. and Brown, A. C., 1984. Progressive alteration associated with gold-quartz-tourmaline veins at the Sigma mine, Abitibi greenstone belt, Quebec. Economic Geology, 79, 393-399.

New exploration techniques for Iron-oxide-Cu-Au deposits under cover in the Eastern Succession, Mt Isa Inlier

Mark Edmiston

*pmd*CRC, School of Earth Sciences, James Cook University, Townsville, QLD 4811*

mark.edmiston@jcu.edu.au

The Mt Isa Eastern Succession is a world class base metal and Iron-Oxide Copper Gold (IOCG) province. With much of the exposed bedrock already explored focus, must now turn to areas under different degrees of cover. Most of the recent discoveries (e.g. Ernest Henry, Osborne and Cannington) have been made using geophysical techniques to look beneath the cover. Extensive geophysical databases exist for the area, using which much can be done to further determine the geophysical expression of IOCG deposits.

IOCG deposits in the Eastern Succession can be classified into three (arguably four) distinct geological settings (Williams et al*.,* 2001). The physical properties of these types of deposits are not well understood. Their magnetic signature can be magnetite or hematite dominated while their gravity signature is highly dependant on the tectonic setting. Previously much geophysical interpretation has been mainly done qualitatively. Quantitative analysis has involved 3D inversion of potential field (magnetics and gravity) data, but this approach still requires a comprehensive geological understanding to account for the infinite number of source distributions that can produce a given data set. Multi-scale, wavelet based edge analysis or 'worming' is proving to be a fast and powerful way of extracting information from potential field data that has previously been hidden in traditional displays of geophysical data.

The worming technique has been successful in identifying Pb-Zn deposits in the Irish Base metal province. However, because the true 'meaning' of worms in an geological sense is not understood for the Eastern Succession, the full potential of the worms for the exploration of IOCG deposits in the Mt Isa Region has not so far been realized. Future IOCG deposits in the Mt Isa Eastern Succession are expected to be discovered under cover of varying unknown depth. This makes worms a very suitable exploration tool as they greatly improve inferences about the scale, shape and importantly the depth of source anomalies.

The aims of this project are to determine whether IOCG deposits in the Eastern Succession can be accurately classified in terms of their geophysical signature. This will involve the use of worms as discussed above as well as the use of comprehensive geophysical modeling to confirm results. This research will hopefully lead to new ways of classifying geophysical potential field data which can then be applied to finding new ore deposits quickly within vast geophysical data sets.

Acknowledgements

I thank Tom Blenkinsop, Barry Murphy and Fractal Geoscience for their notes on worms.

References

Williams, P.J. and Pollard, P.J., 2001. Australian Proterozoic Iron Oxide-Cu-Au Deposits: An Overview with New Metallogenic and Exploration Data from the Cloncurry District, Northwest Queensland. Exploration and Mining Geology, 10, 191-213.

Evidence of multi-stage ore genesis at the Century zinc deposit, Northwestern Queensland, Australia

Leonardo Feltrin and Nicholas H.S. Oliver

*pmd*CRC, Economic Geology Research Unit, School of Earth Sciences, James Cook University, Townsville, QLD 4811*

Leonardo.Feltrin@jcu.edu.au

The Northern Australian Zinc Belt represents one of the most important metallogenic provinces in the world, hosting several Pb-Zn deposits in Palaeoproterozoic to Mesoproterozoic rocks. The metamorphic grade of the host rocks is variable across the region, with the highest conditions reached in the southeastern part of the Mt. Isa Block in the Eastern Fold Belt, where Broken Hill type deposits (e.g. Cannington Ag-Pb-Zn) are hosted in siliciclastic rocks which are highly deformed and metasomatised. In contrast, in the northwestern part of the Mt Isa Block, for deposits like HYC and Century (respectively in the McArthur basin and central Lawn Hill Platform), metamorphic conditions are very low grade to unmetamorphosed. Deformation here produced relatively open, gentle folding suggesting a limited influence of the 1590 – 1500 Ma Isan Orogeny. This variation in metamorphic facies is reflected in a different degree of complexity of ore textures. If we accept the statistical argument proposed by Marshall et al. (2000), then indeed, this increasing complexity would be proportional to the amount of remobilisation affecting pretectonic mineralisation. In turn, mineral deposits such as Century should have a higher proportion of unmodified primary ore and may preserve evidence of syngenesis.

In this contribution, we use 3D evaluation of grade distribution data, petrographic and microchemical studies to interpret the genesis of the Century zinc deposit. A sequence of a minimum of two hydrothermal events on the Lawn Hill Platform is proposed. This may have involved at least deposit scale remobilisation of pre-existing ore and possible multi-stage ore genesis.

Deposit Scale Background

The Century zinc deposit is a shale hosted deposit occurring in siliciclastic rocks of the Wide supersequence (Krassay et al., 2000) which are part of the Upper Lawn Hill Formation (McNamara Group). Andrews (1998) has classified the deposit host rock as part of the Pmh4s member. This consists of up to 300 m of laminated to massive siltstone-shale in which the stratabound deposit is localised in high grade laminae (these can be interpreted either as products of exhalation or selective replacement), and also as more discordant mineralisation with similar mineralogy (sphalerite, galena, pyrite and siderite). Locally, along major fault contacts chalcopyrite is the only Cu bearing mineral identifiable. Two different ore genetic models have been proposed for Century: (1) syngenetic to early diagenetic model supported by textural evidence proposed by Waltho and Andrews (1993), and (2) a late-diagenetic to syn-tectonic model, reminiscent perhaps of Mississippi Valley Type deposits, as proposed by Broadbent et al. (1998). In the latter model, the discordant yet stratabound nature of the mineralisation is particularly emphasised and used as one of the arguments to support late diagenetic replacement as the primary ore forming process. The age of the deposit has been estimated by Carr et al. (1996) using lead isotope ratios of galena and is approximately 1570± 6 Ma. (Ord et al., 2002). This age differs from the host rock which is apparently slightly older than Century (1595+/- 6 Ma, Page et al., 2000).

The deposit is presently hosted in a D2 structure, the Page Creek Syncline, and is cross-cut by later syn- to post- D3, northeast to east-west striking structures hosting a regional distributed network of Pb-Zn lodes with traces of Cu. This later deformation event is of regional character and reflects the c. 1530 Ma reactivation of older basement normal faults developed during the (c. 1710 - 1670 Ma) Mount Isa Rift. Some of the major faults in the Northern Lawn Hill Platform (e.g. Termite Range Fault next to Century and the Elizabeth Creek Fault Zone) represent well constrained examples of synsedimentary faulting during deposition of the McNamara Group (Krassay et al., 2000; Scott et al., 1998; Southgate et al., 2000). However, the brittle transpressional strike-slip system developed on the eastern side of the Termite Range Fault is interpreted as the product of a later tectonic stage of the Isan Orogeny (O'Dea et al., 1997), indicating likely reactivation of this fault structure. The overall D3 geometries at the deposit scale resemble a negative flower structure surrounding the main orebody, and are consistent with sinistral strike-slip movement along the Termite Range Fault. The northeast and east-west oriented structures are thus most likely related to the strike-slip style deformation occurring during the later stage of the Isan Orogeny.

Discussion and Results

To compute copper, lead and zinc distributions we have applied a computer based technique using GoCad to evaluate the relationships between deposit scale faults and 3D grade distributions. The results obtained with this approach have been cross validated with a detailed petrographic study of selected drill holes, located in zones identified as anomalous in Cu content. Copper distribution appears to be localised along later D3 faults that clearly offset the ore body stratigraphy, suggesting a post-sedimentary origin, which also post-dated the main lead-zinc event. The 3D distribution of copper is distinctly different, being localised and spatially separated from the Zn and the Pb ones. Copper occurring in disseminated chalcopyrite and small veinlets is interpreted to be syn- to post- D3 faulting. Selected samples of drill cores, intersecting the highest Cu anomaly identified in the 3D model, display brecciation and pervasive sideritic alteration, plus massive sphalerite and minor galena, quartz, pyrite, chalcopyrite and chlorite. Siderite assemblages are syn to postectonic occurring in regional and deposit scale D3 faults. They also present characteristic oscillatory zoning, a feature already described by Broadbent et al. (1998) for an earlier generation of siderite localised in the ore zone. This earlier siderite is interpreted as syn- to early diagenetic and related to under-compacted sediments (siderite nodules are wrapped by inflected bedding and cut by compaction stylolites). A comparison of these two generations of iron-rich carbonates suggests that the first occurred in a compressional phase whether the second developed during early extension, sedimentation and consequent loading.

The availability of sulphur is one of the factors that control the fractionation of Zn between siderite and sphalerite and most likely caused the oscillatory zoning on siderite crystals. This suggests that when siderite was growing the precipitation of sulphide was controlling its composition. We propose that in both cases siderite was growing contemporaneously with the emplacement of Zn-Pb mineralisation.

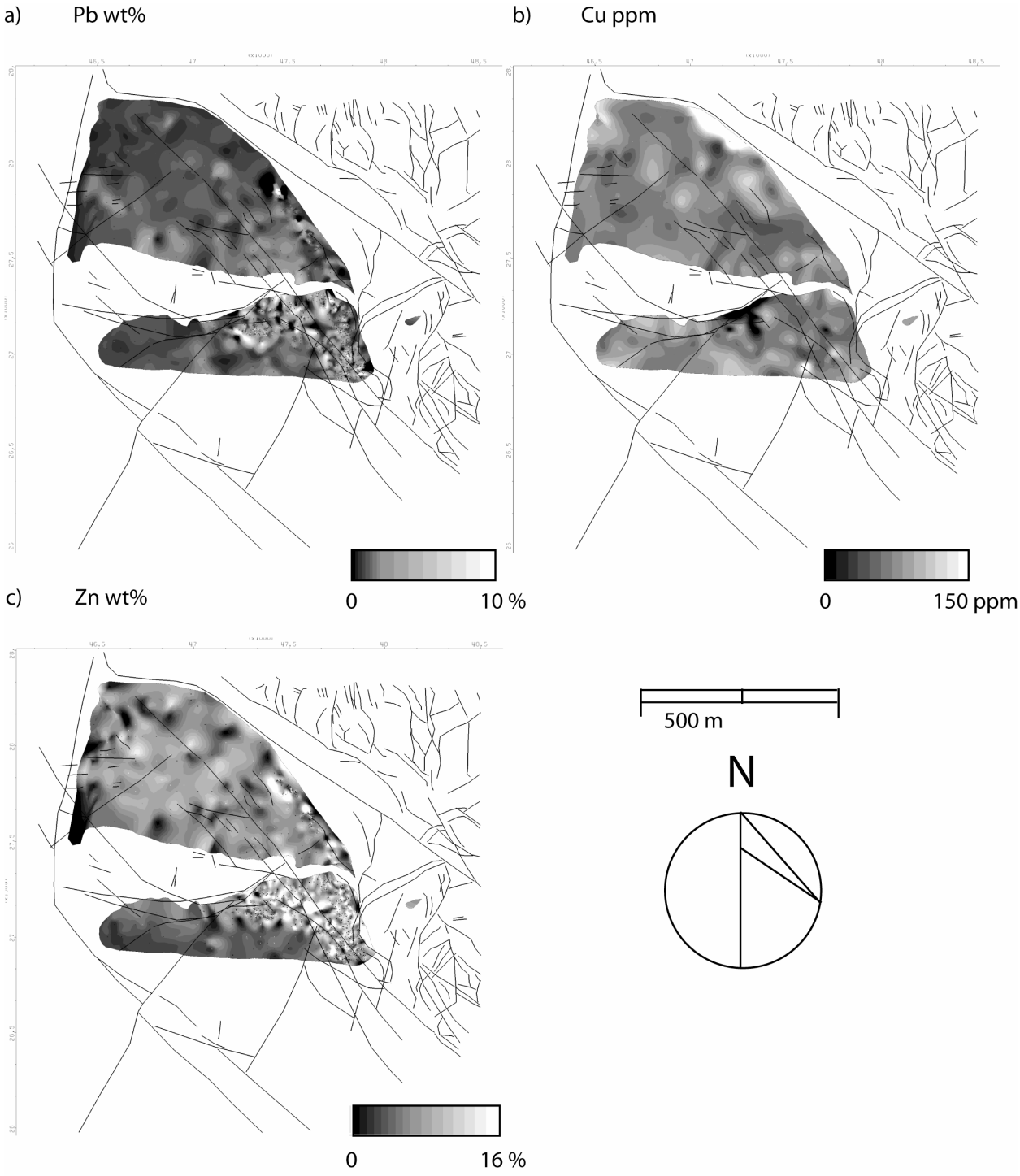

Fig. 1. GoCad vertical, inverse distance interpolation of lead, copper and zinc grades projected on top of a 3D polygonal surface representing an ore enriched horizon. The orebody is subdivided into three blocks that are intersected by secondary splays of major faults. (a) Pb distribution appears to reach highest values on the southeastern corner; separation of northern and southern block is interpreted to postdate Pb mineralisation. (b) Cu distribution averaged on surface 200 (mine stratigraphic code). Higher anomalies in Cu are localised preferentially along east-west and northwest striking faults. Bends and intersections favoured Cu deposition. (c) Zn grade resembles the Pb distribution on the southeastern corner, however the central part of the northern block is still Zn mineralised, where Pb is absent. Highest Cu values are positioned differently from highly Zn-Pb enriched domains. This evidence supports early emplacement of Zn-Pb mineralisation and post-D3 Copper deposition along strike-slip related faults.

Conclusions

The separation of a copper event from the main Zn-Pb event is commonly accepted in the Mt Isa inlier (Swager, 1985) and further supports our interpretation. This evidence coupled with different timing of zinc bearing siderites favours two possible models:

1. Two hydrothermal systems occurred, with a second event remobilising a pre-existing stratiform Pb-Zn-Cu mineralisation.

2. Two hydrothermal events occurred, in which the second event involved both remobilisation of early Zn-rich ore, and syntectonic emplacement of new Cu and possibly Zn-Pb ore.

Younger paragenetic timing for at least the copper-rich part of this system, plus two distinct lead isotope populations (Pb^{206}/Pb^{204} = 16.294-16.390; 16.436-16.503), (data from Richards, 1975; Bresser, 1992; and Broadbent et. al., 1998), might suggest that both syngenetic and diagenetic/tectonic processes were responsible for the mineralisation. However, although the Pb-Pb ages are apparently younger than the stratigraphy by 20 m.y, consistent ages of host-rock and mineralisation occur at both Mt Isa and HYC, with Mt Isa showing old (ca. 1650 Ma) ages for both Pb-Zn mineralization and sedimentation. At Century, different dating techniques were used to compare sedimentation and mineralization (U-Pb zircon for the sediments, Pb-Pb for mineralization). The strict geochronological interpretation of the dates is more rigid than the geological data suggests, and we interpret the difference in these ages to reflect either the introduction of at least some Pb into the system during the Isan Orogeny, or that the age differences are not meaningful. Remobilisation of at least some of the lead, new introduction of copper and possibly lead during the Isan Orogeny provide adequate alternatives to the earlier proposed models and the geochronological data. These considerations more likely suggest that a synsedimentary origin for the Century zinc deposit might have been the first stage of the metallogenic evolution of this system, as occurred elsewhere in the Mount Isa Inlier.

References

Andrews, S. J., 1998. Stratigraphy and depositional setting of the upper McNamara Group, Lawn Hills region, Northwest Queensland: Metallogeny of the McArthur River-Mount Isa-Cloncurry minerals province. Economic Geology, 93, 1132-1152.

Bresser, H. A., 1992. Origin of base metal vein mineralisation in the Lawn Hill mineral field, North-Western Queensland. James Cook University of North Queensland, Key Centre in Economic Geology, Unpublished Honours thesis,115 p.

Broadbent, G. C., Waltho, A. E., Berkman, D. A. and Mackenzie, D. H., 1998. Century zinc-lead-silver deposit. Australasian Institute of Mining and Metallurgy Monograph 22, 729-735.

Carr, G. R., Sun, S.-s., Page, R. W., Hinman, M., Baker, T., Rotherham, J. F., Richmond, J. M., Mark, G., and Williams, P. J., 1996. Recent developments in the use of lead isotope model ages in Proterozoic terrains. James Cook University of North Queensland, Geology Department, EGRU Contribution, 55, 33-35.

Krassay, A. A., Domagala, J., Bradshaw, B. E., and Southgate, P. N., 2000. Lowstand ramps, fans and deep-water Palaeoproterozoic and Mesoproterozoic facies of the Lawn Hill Platform; the Term, Lawn, Wide and Doom supersequences of the Isa Superbasin, northern Australia. Australian Journal of Earth Sciences, 47, 563-597.

Marshall, B., Spry, P. G. and Vokes, F. M., 2000. Discriminating between regional metamorphic remobilization and syntectonic emplacement in the genesis of massive sulfide ores. Reviews in Economic Geology, 11, 39-79.

O'Dea, M. G., Lister, G., MacCready, T., Betts, P. G., Oliver, N. H. S., Pound, K. S., Huang, W., Valenta, R. K., Burg, J.-P., and Ford, M., 1997. Geodynamic evolution of the Proterozoic Mount Isa terrain, Geological Society of London Special Publication, 121, 99-122.

Ord, A., Hobbs, B. E., Zhang, Y., Brown, M., Willetts, G., Sorjonen-Ward, P., Broadbent, G. C., Walshe, J. L. and Zhao, C., 2002. Geodynamic modelling of the Century deposit, Mt Isa Province, Queensland. Australian Journal of Earth Sciences, 49, 1011-1039.

Page, R. W., Jackson, M. J. and Krassay, A. A., 2000. Constraining sequence stratigraphy in North Australian basins; SHRIMP U-Pb zircon geochronology between Mt Isa and McArthur River. Australian Journal of Earth Sciences, 47, 431-459.

Richards, J. R., 1975. Lead isotope data on three North Australian galena localities. Mineralium Deposita, 10, 287-301.

Scott, D. L., Bradshaw, B. E. and Tarlowski, C. Z., 1998. The tectonostratigraphic history of the Proterozoic Northern Lawn Hill Platform, Australia: an integrated intracontinental basin analysis. Tectonophysics, 300, 329-358.

Southgate, P. N., Bradshaw, B. E., Domagala, J., Jackson, M. J., Idnurm, M., Krassay, A. A., Page, R. W., Sami, T. T., Scott, D. L., Lindsay, J. F., McConachie, B. A., and Tarlowski, C. Z., 2000. Chronostratigraphic basin framework for Palaeoproterozoic rocks (1730-1575 Ma) in northern Australia and implications for base-metal mineralization. Australian Journal of Earth Sciences, 47, 461-483.

Swager, C. P., 1985. Syndeformational carbonate-replacement model for the copper mineralization at Mount Isa, Northwest Queensland; a microstructural study: Economic Geology, 80, 107-125.

Waltho, A. E., and Andrews, S. J., 1993, The Century zinc-lead deposit, Northwest Queensland. In: Duncan, I. J., ed, The Australasian Institute of Mining and Metallurgy; centenary conference. Australasian Institute of Mining and Metallurgy, 41-61.

Models of the upper crust from wide-angle and reflection studies, Northeastern Yilgarn: Why we need both?

Tanya Fomin

*pmd*CRC and ANSIR, Geoscience Australia, GPO Box 38, Canberra ACT 2601*

Tanya.Fomin@ga.gov.au

Wide-angle seismic vibroseis data were collected during 2001 in the Northeastern Yilgarn Craton (Fig 1). This experiment focused on the Leonora-Laverton Tectonic Zone and was carried out coincident with the deep seismic reflection transect. The wide-angle survey supplements the reflection data by providing velocity information for the upper crust. This creates an opportunity to compare the velocity model derived from wide-angle data with a structural image obtained from the deep seismic reflection data.

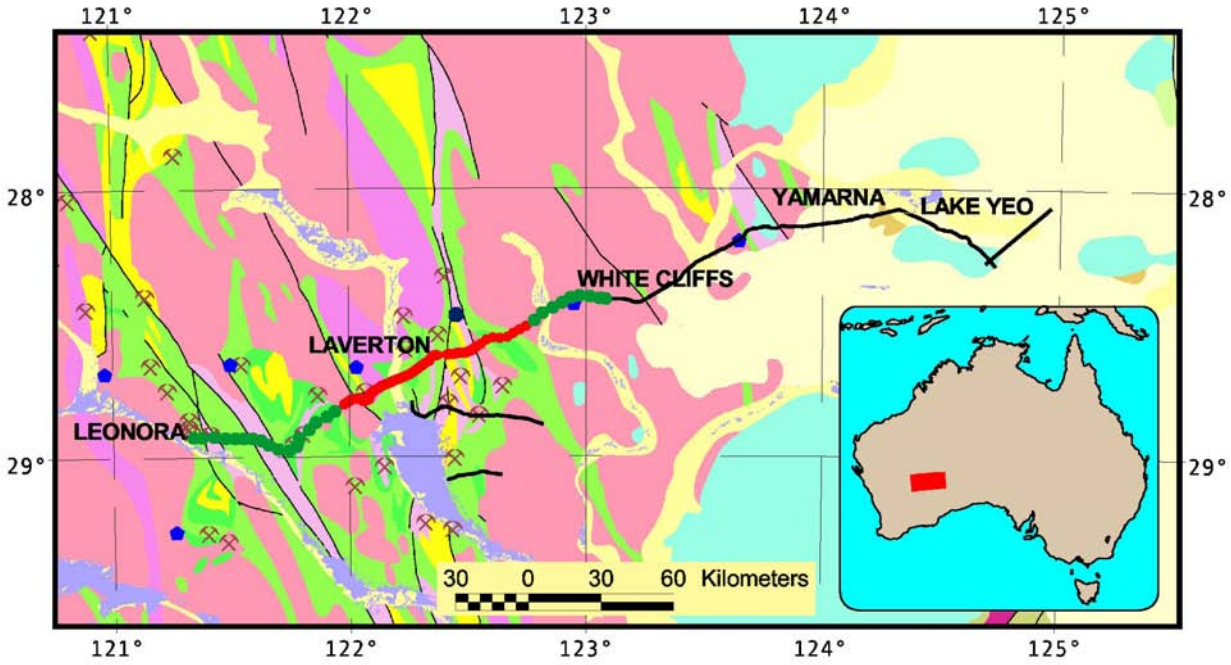

Figure 1. Location map of the 2001 Northeastern Yilgarn deep seismic survey. Wide-angle survey shown as a dots line coincident with a reflection regional transect.

A 2D velocity model produced with using forward modelling package based on the ray-tracing algorithm of Zelt and Smith (1992) shows a broad range of seismic velocity variation in the upper 16 km of the crust (Fig. 2). The highest velocities (6.5-6.7 km/s) are restricted to a ~ 2 km thick body in the western part of the line. The top of this body is modelled at 3-4 km depth. This body is interpreted to represent mafic facies within the Archaean Granite-Greenstone Belt. It is underlain by lower velocity rocks (6.0-6.1 km/s), most likely of granite-gneissic composition. It is important to note that the thickness of the low velocity layer increases from ~4 km to 8 km in the western part of the profile that is underneath the high-velocity body. It is concluded that some kind of balancing of high and low velocity material along the vertical profile through the crust can be observed, which is consistent with earlier observations by Goncharov et al. (1998).

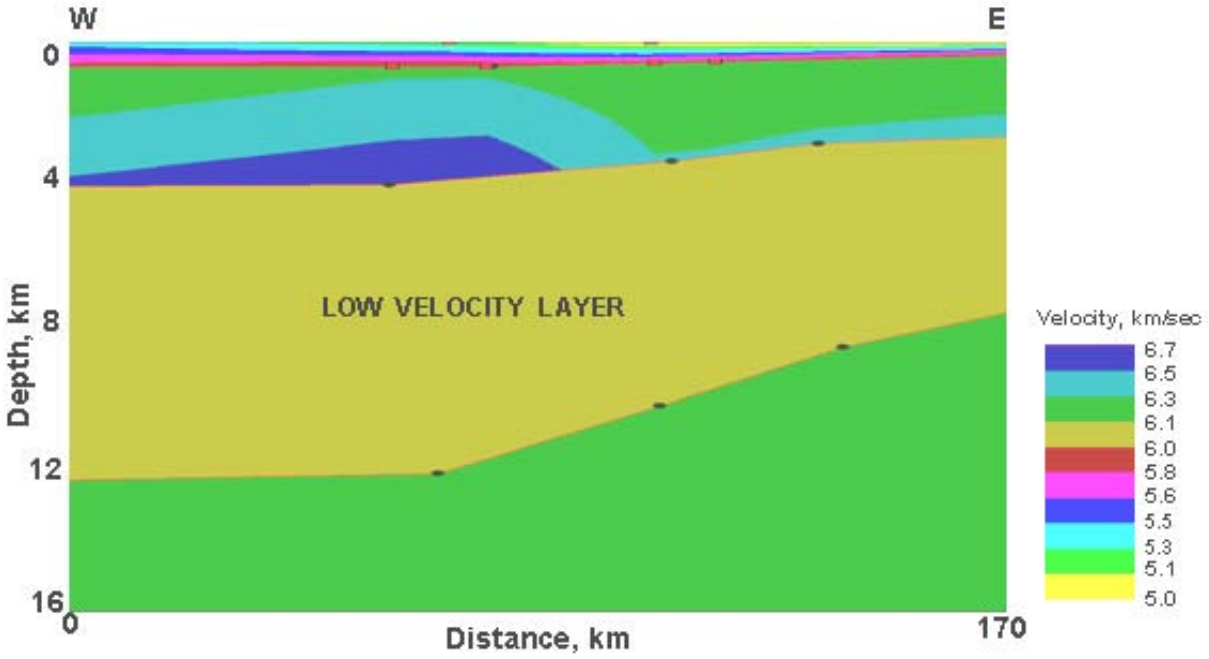

Figure 2D velocity model for upper crust, Leonora-Laverton Tectonic Zone, Western Australia.

The 2D velocity model (Fig. 2), originally developed in terms of depth , was converted to two-way time to allow easy comparison and interpretation with the seismic reflection data. The main conclusion is that reflection seismic technology which images structure within the upper crust quite well, fails to detect seismic velocity stratification. None of the interpreted seismic reflection horizons seem to correlate with velocity boundaries modelled from wide-angle data (Fig. 2). This apparent contradiction has a rather simple explanation.

The two major seismic technologies (reflection and wide-angle) measure different properties of the crust. Imaging crustal reflectivity is the major aim of conventional seismic reflection technology. Wide-angle reflection technology provides a more accurate estimation of the seismic velocity within the crust. Reflection horizons and changes in reflectivity patterns mapped by the reflection technique will not necessarily coincide with velocity boundaries imaged by refraction/wide-angle reflection technology.

The seismic velocity model derived from the wide-angle data was also used to depth-convert the seismic reflection. There is no substantial difference in the appearance of two-way time and depth scale images. This is because of very small velocity variations within the area of study. The average seismic velocity used for depth conversion, varies from 5.5 to 5.7 km/s for a constant depth level of 0.5 km. Similar velocity variations are estimated for deeper parts of the crust. For 4 km depth, the average velocity along the profile varies from 6.2 to 6.4 km/s.

A further interesting observation from the interpretation of reflection data and the velocity model is that the area where the high-velocity body was imaged appears to be relatively transparent in the reflection seismic image. There are far fewer reflective horizons interpreted in this area compared to the eastern and western flanks of the line. Such a correlation is suggestive of a relatively smooth (long wave length), probably metamorphism driven, influence on the velocity model of this area. Such metamorphism, likely to be associated with the formation of the greenstone belt, may have significantly overprinted the internal structure of this area, explaining why steeply dipping reflectors, well imaged to the east and west of the line, are not present here.

This comparison of wide-angle reflection and near-vertical reflection data recorded using a vibroseis source shows that a more accurate geological interpretation is possible using a

combination of these two techniques. However, a clear understanding of the advantages and limitations of both techniques is required when co-interpreting their results.

Acknowledgements

The author is grateful to Prof. Stewart Greenhalgh, Adelaide University, Prof. Brian Kennett, Australian National University and ANSIR for providing wide-angle recording equipment to collect the data and to the ANU staff for participation in the field work. I also thank the Yilgarn Y2 Project Team for providing the seismic interpretation of reflection data. Special thanks to Malcolm Nicoll for producing comparison images in GoCad software package.

References

Zelt, C.A. and Smith, R.B., 1992. Seismic travel time inversion for 2-D crustal velocity structure: Geophysical Journal International, 108, 16-34.

Goncharov, A.G., Lizinsky, M.D., Collins, C.D.N., Kalnin, K.A., Fomin, T.N., Drummond, B.J., Goleby, B.R.G., and Platonenkova, L.N., 1998. Intra-Crustal "Seismic Isostasy" in the Baltic Shield and Australian Precambrian Cratons from Deep Seismic Profiles and the Kola Superdeep Bore Hole Data. In: Braun J., Dooley J., Goleby B., Van der Hilst R. and Klootwijk, C., eds., Structure and Evolution of the Australian Continent. American Geophysical Union Geodynamics Series, 26, 119-138.

Significance of early high-temperature shear zones in the Broken Hill Block, NSW

Caroline J. Forbes, Peter G. Betts and Roberto Weinberg

*pmd*CRC, ACRC, School of Geosciences, Monash University, Clayton, VIC 3800*

caroline@earth.monash.edu.au

Introduction

High-temperature shear zones preserve crucial information regarding mid- to lower-crustal tectonic deformation and are critical structures controlling the evolution of extensional (rift and metamorphic core complex) environments, and within shortening (fold and thrust belt and nappe forming) settings. However, it is often difficult to recognise and interpret the tectonic context of high-temperature shear zones formed during the earliest phases of crustal deformation as they are often reactivated during later tectonism and (retrograde) metamorphism.

The Broken Hill Block, central western New South Wales (Fig. 1a, b) is representative of a mid-crustal terrane in which lithology parallel, high-temperature shear zones accommodated early deformation. However, recognition and interpretation of these structures is difficult due to intense poly-deformational and metamorphic overprinting during the Olarian (ca 1.6-1.58 Ga; Page et al., 2000) and Delamerian (ca 520-480 Ma; Harrison and McDougall, 1981) orogenies. This has resulted in controversies regarding the early history of the Block, which have been fuelled by the lack of definitive descriptions of the characteristics and local to regional structural settings of early high-temperature shear zones. Some workers suggest that the earliest episode of deformation involved nappe formation during the onset of the Olarian Orogeny (e.g. Hobbs et al., 1984), and others interpret an early ductile extensional event that occurred either during the deposition of the Willyama Supergroup (Gibson and Nutman, 2004) or immediately prior to orogenesis (Venn, 2001). This study aims to characterize an early high-temperature shear zone within the Broken Hill Block, and demonstrate the importance of a multi-disciplinary approach using detailed structural and metamorphic analysis of key structures preserving evidence of early deformation in drawing sound conclusions regarding the early tectonic regime active in complexly deformed and metamorphosed terranes.

The Round Hill Area

The Round Hill Area (Fig. 1b, c) has undergone multiple phases of deformation associated with amphibolite to granulite facies metamorphism, and preserves lithologies of the Broken Hill Main Lode within a well-exposed early high-temperature shear zone. The Round Hill Area has been subdivided here into the southern and northern areas (Fig. 1c), based on differences in strain, degree of partial melting and mineral assemblages within pelites, which possibly indicate variation in metamorphic grade.

Southern Round Hill Area

The Southern Round Hill Area (Fig. 1c) consists of partially melted metasediments with well defined leucosome and mesosome layers. Leucosomes are 8-10 cm width, commonly subparallel to layering and the earliest foliation (S1), consist of coarse grained quartz + feldspar and include large garnets. Mesosome layers comprise sillimanite-biotite-garnet gneiss and preserve a pervasive, well-developed high-grade fabric defined by fibrolitic sillimanite, biotite and aligned aggregates of feldspar and quartz. Feldspar grains are partially to totally retrogressed to sericite and fine-grained quartz. S1 wraps around garnet porphyroblasts which occasionally show dextral,

and commonly, sinistral asymmetry. S1 is sub-parallel to compositional layering and is not associated with any obvious folding in the Round Hill Area. A quartz, sillimanite and biotite mineral lineation is well developed on the S1 plane. The pervasive S1 fabric is overprinted by weakly to moderately developed biotite fabric (S2). S2 is ~1 mm spaced, and was not observed axial planar to any obvious folds. The third fabric (S3) is a well developed, ~2-5 mm spaced foliation defined by coarse grained sillimanite blades and biotite that overgrow and crenulate pre-existing fabrics, and cut through and overprint garnet porphyroblasts. S3 is often subparallel to, or at a low angle to, S1, but was observed axial planar to one isoclinal fold within the Southern Round Hill Area.

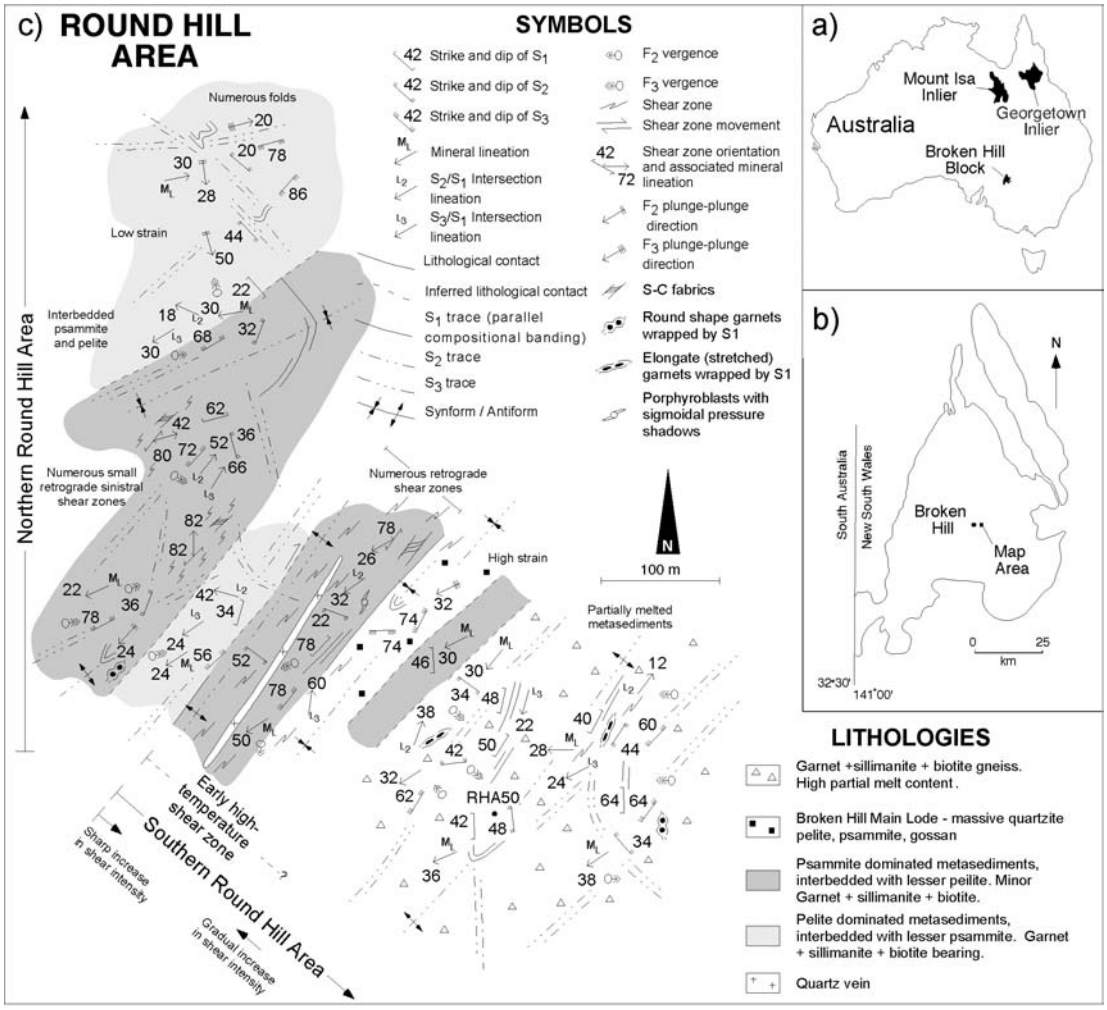

Figure 1. a) Location of selected Proterozoic terranes in eastern Australia; b) Location of the Round Hill Area in the Broken Hill Block; c) Geological map of the Round Hill Area.

Strain intensity gradually increases northwards towards a layering-parallel high-temperature shear zone (Fig. 1c), which separates the Northern Round Hill Area from the Southern Round Hill Area, and is reflected by the development of shear indicators and an increase in the length of sillimanite, biotite and quartz within the mineral lineation. Aspect ratios of garnet porphyroblasts increase from ~1:1 in the south to ~14:1 in the north of the area (Noble, 2000). The southern extension of the Broken Hill Main Lode is preserved within the high-temperature shear zone. Small, retrograde shear zones up to ~25 m wide anastamose through the northern extent of the area, and can be distinguished from the high-temperature shear zone as they are dominated by phyllitic, chlorite + sericite-rich metasediments that preserve a well-developed muscovite mineral lineation. The northern extent of the Southern Round Hill Area is defined by a sharp decrease in kinematic indicators.

Northern Round Hill Area

The lower strain Northern Round Hill Area (Fig. 1c) consists of interbedded psammite and pelite and shows no evidence of extensive partial melting. Psammitic layers preserve poorly to moderately developed foliations and consist of quartz, feldspar and minor biotite, sillimanite and garnet. Pelitic units are sillimanite and biotite rich and contain garnet porphyroblasts. Pelitic layers preserve multiple moderately to well developed foliations. The earliest foliation (S1) is sub-parallel to layering, defined by sillimanite, biotite and quartz and feldspar aggregates and wraps around garnet porphyroblasts. S1 was not recognized to be associated with folding. A variably developed mineral lineation defined by sillimanite, quartz and biotite occurs on the S1 plane. S1 is crenulated by a second foliation (S2), which is ~1mm spaced and defined by biotite. S2 is axial planar to inclined to recumbent, tight to open folds that are better developed in the north of the area. S3 crenulates the earlier foliations, and is defined by sillimanite and biotite. Towards the north of the area, S3 is also defined by stylolites and fractures. S3 is axial planar to subvertical, open, parallel folds that are better developed in the north.

Numerous retrograde shear zones occur sub-parallel to compositional layering and S1 throughout the Northern Round Hill Area. Pegmatites consisting of coarse grained quartz and feldspar and platy white mica are also preserved sub-parallel to compositional layering and S1. The pegmatites are up to 20m wide and are occasionally foliated by S3.

Metamorphic P-T paths

Analysis of the bulk rock chemistry has highlighted no major compositional variations within pelitic units. Pressure-Temperature (P-T) pseudosections using THERMOCALC were constructed for individual bulk rock compositions from selected samples, and used in conjunction with detailed petrography to investigate any major changes in P-T paths or peak P-T conditions across the high-temperature shear zone identified in the Southern Round Hill Area.

Preliminary petrography results show a pre-D1 metamorphic history in the Southern Round Hill Area, not identified in the field, involving multiple generations of garnet and sillimanite growth with biotite. These growth events may give clues to the setting of the Broken Hill Block prior to the development of the pervasive high-temperature S1 fabric preserved throughout the area. The extensive melting of metasediments in the Southern Round Hill Area that have similar bulk rock composition to metasediments in the Northern Round Hill Area, showing significantly less evidence of melting, implies a higher temperature P-T path in the south relative to the north. Evidence for a pre-S1 history has not been recognized in the Northern Round Hill Area, and it lacks multiple generations of garnet and sillimanite growth. However, this may be a function of minor differences in the bulk rock chemistry between samples, resulting in variations in the extent of the garnet field for pseudosections constructed across the Round Hill Area.

Discussion

Structural and metamorphic analysis of the Round Hill Area raises the question of the role of the layering-parallel high-temperature shear zone in the Southern Round Hill Area, which defines an area of intensive strain partitioning during early deformation in the Broken Hill Block. We are now working on identifying the P-T conditions of units above and below the high-temperature shear zone, particularly focusing on the prevailing conditions before and during D1 deformation and the development of the layer-parallel high-temperature shear zone and associated layer-parallel foliation defined by high-temperature minerals (S1 described in this study). Noble (2000) suggested an extensional origin for the early high-temperature shear zones based on their association with the pervasive layer-parallel fabric, coeval bi-modal volcanism, and juxtaposition of younger sediments over older, partially melted metasediments within the Round Hill and surrounding area, and our preliminary results so far support his assertion.

Resolution of an early extensional history for the Round Hill Area extends regionally to the Broken Hill Block, and it remains to be determined when the early shear zones were active and what influence their activity had on the regional thermal regime. Extensional activity during deposition of the Willyama Supergroup (Gibson and Nutman, 2004) at ~1.69-1.67 Ga implies a significant period of tectonic quiescence between early extension and orogenesis at ~1.6 Ga, during which time lithospheric reequilibration would have occurred, thus not accounting for the high-temperature/low-pressure metamorphism associated with the Olarian Orogeny. Extension just prior to orogenesis (Venn 2001) can explain regional high-temperature, low-pressure metamorphism during the Olarian Orogeny, although the mechanism for the fast switch between the extensional to shortening tectonic regimes is currently unclear. As the Broken Hill Main Lode is also hosted within the early high-temperature shear zone identified within the Round Hill Area, delineation of the active tectonic setting during times of mineralization will impact greatly on ore genesis models and perhaps exploration criteria.

Conclusion

Results of structural and metamorphic analysis of the Round Hill Area are helping define the early history of the Broken Hill Block prior to intensive shortening during the Olarian Orogeny. The Southern Round Hill Area is dominated by partially melted metasediments that preserve a well developed high-temperature mineral lineation. The Northern Round Hill Area appears to have undergone a lower-temperature metamorphic history and is dominated by interbedded psammite and pelite. A layering-parallel high-temperature D1 shear zone separates the Southern Round Hill Area from the Northern Round Hill Area, and separates units of potentially significantly differing metamorphic grade. An extensional origin for the layer-parallel high-temperature shear zone is being investigated using detailed structural and metamorphic analysis. Delineation of the early tectonic setting of the Broken Hill Block will have implications on the tectonic architecture of the Broken Hill Block prior to intense shortening and on the architecture of the area during ore genesis.

Acknowledgements

Dave Giles, Chris Doyle, Matt Noble and Bruce Schaefer are thanked for helpful discussion. John Clulow is thanked for assistance in the field.

References

Gibson, G. M. and Nutman, A. P., 2004. Detachment faulting and bimodal magmatism in the Palaeoproterozoic Willyama Supergroup, south-central Australia: keys to recognition of a multiply deformed Precambrian metamorphic core complex. Journal of the Geological Society of London, 161, 55-66.

Harrison, T. M. and McDougall, I., 1981. Excess ^{40}Ar in metamorphic rocks from Broken Hill, New South Wales: implications for $^{40}Ar/^{39}Ar$ age spectra and the thermal history of the region. Earth and Planetary Science Letters, 55, 123-149.

Hobbs, B. E., Archibald, N. J., Etheridge, M. A. and Wall, V. J., 1984. Tectonic history of the Broken Hill Block, Australia. In: Kroner, A. and Greiling, R., eds., Precambrian Tectonics Illustrated, E. Schweizerbart'sche: Nèagele u. Obermiller, Stuttgart, 353-368.

Noble, M., 2000. Geology of the Broken Hill Synform, N.S.W. Unpublished MSc. thesis, Monash University.

Page, R. W., Stevens, B. P. J., Gibson, G. M. Conor, C. H. H., 2000. Geochronology of Willyama Supergroup rocks between Olary and Broken Hill, and comparison to Northern Australia. Broken Hill Exploration Initiative: Abstracts of Papers presented at the May 2000 Conference in Broken Hill, Australian Geological Survey Organisation. 72-75.

Venn, C. J., 2001. The geodynamic evolution of the Mount Robe and Mount Franks region, Broken Hill Australia: Discovery of crustal-scale extensional shear zones and giant sheath folds. Unpublished. PhD thesis, Monash University.

The Fractal Distributions of base and precious metal systems, Mt Isa Inlier, Australia

Arianne Ford

*pmd*CRC, School of Earth Sciences, James Cook University, Townsville, QLD 4811*
Arianne.Ford@jcu.edu.au

Introduction

Mandelbrot (1983) suggested that mineral deposits in the earth's crust have a fractal distribution. Several studies of precious metal deposits have attempted to demonstrate that Mandelbrot's hypothesis is correct (eg. Carlson, 1991; Agterberg et. al, 1996; and Blenkinsop and Sanderson, 1999). A preliminary study has shown that base metal deposits may also exhibit a fractal distribution (Blenkinsop and Oliver, 2002).

The primary study area for this research, the Mt Isa Inlier, NW Queensland, Australia is a world famous Proterozoic base metal province which contains a variety of base and precious metal deposit types, including deposits of Cu, Pb-Zn-Ag, Iron oxide Cu-Au, Au, and U-REE. The inlier is therefore an ideal location to test whether the precious and base metals located within have fractal distributions. The aim of this study is to evaluate whether the five classes of deposit type (Cu, Cu-Au (including IOCG), Ag-Pb-Zn, Au and U-REE) have fractal distributions, and to compare any resulting fractal dimensions. The study is part of a larger project that will compare the fractal dimensions of different mineral deposit types in several areas (eg. Georgetown Province, Broken Hill) and to investigate the processes that lead to the fractal distributions.

Methods and Data Sources

Various methods are available for determining whether mineral deposits within a study area have a fractal distribution. Box-counting and radial-density approaches are commonly used (Carlson, 1991; Blenkinsop, 1994). This study uses a box counting algorithm to analyze the global spatial distribution of different deposit types. Further adjustments of this algorithm allow a regional analysis of the mineral deposit distributions to be performed by an incremental or shifting box-counting method.

The data used in the box-counting has been sourced from the Northwest Queensland Mineral Province Report (Queensland Department of Mines and Energy 2000). This study defines the largest box size used in the box-counting algorithm as the smallest box which covers all mineral deposit occurrences for a given deposit type within the study area. Regression of the linear part of the resultant log-log graph was performed and the resulting fractal dimension and related statistical data produced.

Results

While allowing a well-defined starting point, the fixed size for the largest box has proven to be problematic when analyzing the results of the box-counting method. When the results of the box-counting method are plotted on a log-log graph, the point for the largest box size inevitably has a box-count number of one. This value commonly falls below the line-of-best-fit for the linear part of each of the graphs, a problem that can be attributed to the fact that the largest box size is fixed by the geographical location of the mineral deposits within the study area. Analysis of log-log graphs has shown that regression of the line-of-best-fit for the linear part of these graphs gives excellent results when the point for the largest box size is ignored and the regression run over all box sizes greater than 10km.

Preliminary results show that each of the different mineral deposit types investigated for the Mount Isa Inlier has a different fractal dimension, indicating different degrees of clustering. For example, copper deposits are relatively dispersed, but gold deposits are highly clustered. This can be attributed to the fact that the different mineralizing systems have different geometries, and that the geological controls on each of these systems are different.

Deposit Type	No. of Deposits	Fractal Dimension	R	E
Cu	1869	1.426	0.988	0.032
Au	136	0.728	0.981	0.022
CuAu	416	1.402	0.980	0.063
IoCG	198	1.252	0.989	0.038
U-REE	144	0.902	0.993	0.016

Table 1: Fractal Dimensions for Global Mineral Deposit Distributions in the Mount Isa Inlier where R is the correlation coefficient and E is the standard error of regression

Current work on this project is focused on calculating the fractal dimensions of mineral deposits in other locations such as the Georgetown and Broken Hill provinces due to the similar geology that these regions share with the Mount Isa Inlier. Expansion of the box-counting method to review the regional variation in the fractal dimension is also being investigated. The incremental box-counting method coupled with a geometric progression (rather than an arithmetic progression) of box sizes will yield useful results for deposit types with a large enough number of deposits to be relevant.

Conclusions

The box-counting method used in this study shows that each of the different mineral deposit types investigated has a different fractal dimension. While an exact reason for these differences is unclear, indications are that the geological controls on the system are the main contributing factor.

References

Agterberg, F. P., Cheng, Q. and Wright, D. F., 1996. Fractal modelling of mineral deposits. In: Elbrond, J. and Tang, X., eds., Proceedings of the International Symposium on the Application of Computers and Operations Research in the Minerals Industries. Montreal, Canada, 43-53.

Blenkinsop, T.G., 1994. The fractal distribution of gold deposits. In: Kruhl, J.H., ed., Fractals and Dynamic systems in Geosciences. Springer, Berlin, 247-258.

Blenkinsop, T.G. and Sanderson, D.J., 1999. Are gold deposits in the crust fractals ? A study of gold mines in the Zimbabwe craton. Special Publication of the Geological Society of London, 155, 141-151.

Blenkinsop, T. G. and Oliver, N.H.S., 2003. Discrimination of precious/base metal mineral-izing systems by fractal analysis, Mt Isa, Australia. AGU/EUG 2003 Meeting, Nice France

Carlson, C. A., 1991. Spatial Distribution of Ore Deposits. Geology, 19, 111-114.

Mandelbrot, B. B., 1983. The fractal geometry of nature. New York, W.H. Freeman and Company, pp. 468.

Queensland Department of Mines and Energy, Taylor Wall & Associates, SRK Consulting Pty Ltd & ESRI Australia, 2000. North-west Queensland Mineral Province Report, Queensland Department of Mines and Energy, Brisbane.

Regional fluid compositions of the Mount Isa Eastern Succession, NW Queensland, Australia

B. Fu[1], T. Baker[1], N.H.S. Oliver[1], P.J. Williams[1], T. Ulrich[2], T.P. Mernagh[3], E. van Achterbergh[4], C.G. Ryan[4], L.J. Marshall[1], M.J. Rubenach[1], G. Mark[1 #] and B.W.D. Yardley[5]

*[1] pmd*CRC, EGRU, School of Earth Sciences, James Cook University, Townsville, QLD 4811*
[2] Department of Geology, Australian National University, Canberra, Australia
*[3] pmd*CRC, Geoscience Australia, GPO Box 378, Canberra, ACT 2601*
*[4] pmd*CRC, CSIRO Exploration and Mining, Sydney, Australia*
[5] Department of Earth Sciences, University of Leeds, Leeds, UK
[#] Present address: School of Geosciences, Monash University, Melbourne, Australia
bin.fu@jcu.edu.au

Introduction

The Mount Isa Eastern Succession in NW Queensland, Australia, is one of the economically most important iron oxide-copper-gold (IOCG) provinces in the world. The IOCG deposits or prospects in this district are commonly surrounded by sodic (-calcic) alteration, which typically formed prior to copper-gold mineralisation (e.g. Ernest Henry, Starra). There is, however, little known about the regional fluids (DeJong and Williams, 1995; Oliver, 1995). A detailed investigation of fluid inclusions in quartz veins from regional metamorphosed and hydrothermally altered rocks has been made for better understanding of the fluid geochemistry and processes using microthermometric methods and microanalytical techniques, including PIXE (proton-induced X-ray emission), Laser Raman and LA-ICP-MS (laser ablation inductively coupled plasma mass spectrometer).

Geological background

The Eastern Succession of the Mt Isa Block (including the Mary Kathleen Fold Belt and the Cloncurry district) consists of volcanic and sedimentary rocks that were deformed and metamorphosed under greenschist to amphibolite facies conditions during the Isan orogeny (1620-1580 Ma). Batholithic granite emplacement took place between 1540 and 1490 Ma, accompanied by retrograde metamorphism and late sodic (-calcic) alteration. Major Cu-Au deposits, such as Ernest Henry, Starra and Eloise, were formed in late breccias and brittle faults (e.g., Williams, 1998).

The regional sodic (-calcic) alteration occurs in three main settings: (1) regional fracture and breccia systems, some associated with fault zones, at variable distances from intrusions (e.g., Cloncurry Fault); (2) composite magmatic-hydrothermal vein and breccia systems adjacent or proximal to intrusions; and (3) intrusion-hosted magmatic-hydrothermal systems. In general, the path of fluid flow is channelized (structurally controlled) rather than pervasive. Multiple albitisation events are related to metamorphism, magmatism, hydrothermal alteration and brecciation. The sodic (-calcic) assemblages include albite, scapolite, clinopyroxene, actinolite, titanite and minor quartz.

Sample locations and analytical methods

Fluid inclusions in veins and host rocks related to albitisation have been investigated from Knobby, Tribulation, Lime Creek and Sunrise in the Mary Kathleen Fold Belt and from Mt Avarice, Roxmere-Marimo, Snake Creek and Gilded Rose in the Cloncurry district. All samples

were collected either from quartz-calcite-pyroxene±amphibole veins associated with albitisation in the metamorphosed calc-silicate and dolerite wall rocks or from breccias in the Mary Kathleen Group (Corella type) and Soldiers Cap Group (Gilded Rose type), which contain quartz clasts. Red hematite-K-feldspar alteration commonly occurs in the Gilded Rose breccias.

Microthermometric measurements of fluid inclusions were made on doubly polished, unmounted, approximately 300 μm thick sections using a Linkam MDS600 heating/freezing stage at James Cook University, coupled to a BX51 Olympus polarizing microscope, with liquid nitrogen as the cooling medium. The minimum temperature obtained was –195°C. The heating/freezing stage was calibrated with synthetic fluid inclusions (pure CO_2 in mixture of CO_2+H_2O, and pure H_2O). Reproducibility of the melting temperatures of both solid CO_2 and ice below 0°C was better than ± 0.1°C at heating rates of 0.5°C/minute. Laser Raman analyses were made with a multi-channel microspectrometer at Geoscience Australia, Canberra. PIXE analyses were conducted using a nuclear microprobe at CSIRO, North Ryde, Sydney. LA-ICP-MS analyses were performed at RSES, Australian National University, Canberra.

Fluid inclusions

Compositional fluid types

In the Mt Isa Eastern Succession, both aqueous and carbonic (CO_2-rich) inclusions are abundant in regional albitisation-related rocks or veins. Four main fluid compositional types have been identified as below. Monophase nitrogen and vapour, "empty" inclusions are much less abundant, and no CH_4-rich inclusions have been found in regional alteration.

Type I multisolid brine inclusions (L-V-nS, n ≥ 2). All multisolid inclusions contain a large halite cube together with one to five other solid phases such as sylvite, calcite, hematite and/or magnetite, and a vapour bubble (mostly 5 vol.%) at room temperature. Their size varies from ≤ 3 μm to ≥ 40 μm. No sulphides or sulphates have been identified by Laser Raman analysis. Only a few T_i (initial melting temperature of ice = eutectic temperature) and T_m data were obtained due to the absence of phase transitions on cooling. Most T_i values are below –50°C, indicative of the presence of Ca and/or other cations besides Na and K (Fig. 1a). The salinity is very high, as revealed by dissolution temperatures of halite and other salts such as sylvite up to 550°C. These inclusions are rare compared to their abundance in iron-oxide-copper-gold systems.

Type II halite-bearing brine inclusions (L-V+Halite). Type II liquid-rich aqueous inclusions contain only a halite cube and are the dominant type. They commonly occur along annealed microfractures. T_i values range from –70 to –50°C, showing a Ca-dominated fluid (Fig. 1b). The dissolution temperature of halite (T_{hs}: 170 to 330°C) is commonly 50 to >100°C higher than the homogenisation temperature of the vapour bubble (T_h, 105 to 190°C).

Type III biphase aqueous inclusions (L-V). Biphase aqueous inclusions commonly occur along annealed microfractures. T_i occurs at approximately –20.8°C, consistent with an NaCl-H_2O system. T_h ranges from 87 to 200°C.

Type IV CO_2-rich inclusions. CO_2-rich inclusions are abundant in some localities of regional albitisation. Most CO_2-rich inclusions are ≤ 15 μm in diameter. Most T_m (final melting temperature) values of CO_2-rich inclusions are very close to or equal to the triple point of pure CO_2 at –56.6°C, indicating only very small amounts of other gas species such as N_2 or CH_4 (≤ 3 mol.%). This has been confirmed by Laser Raman analyses. Most carbonic inclusions are pure CO_2. In some cases, N_2 content is up to 3 mol.%. The CO_2-rich inclusions have a wide range of T_h (homogenisation temperature) values, from –37.0 to +30.2°C, corresponding to variable density/molar volume. Some CO_2-rich inclusions without visible water phase contain one or two solid phases (calcite, nahcolite or unidentified solids).

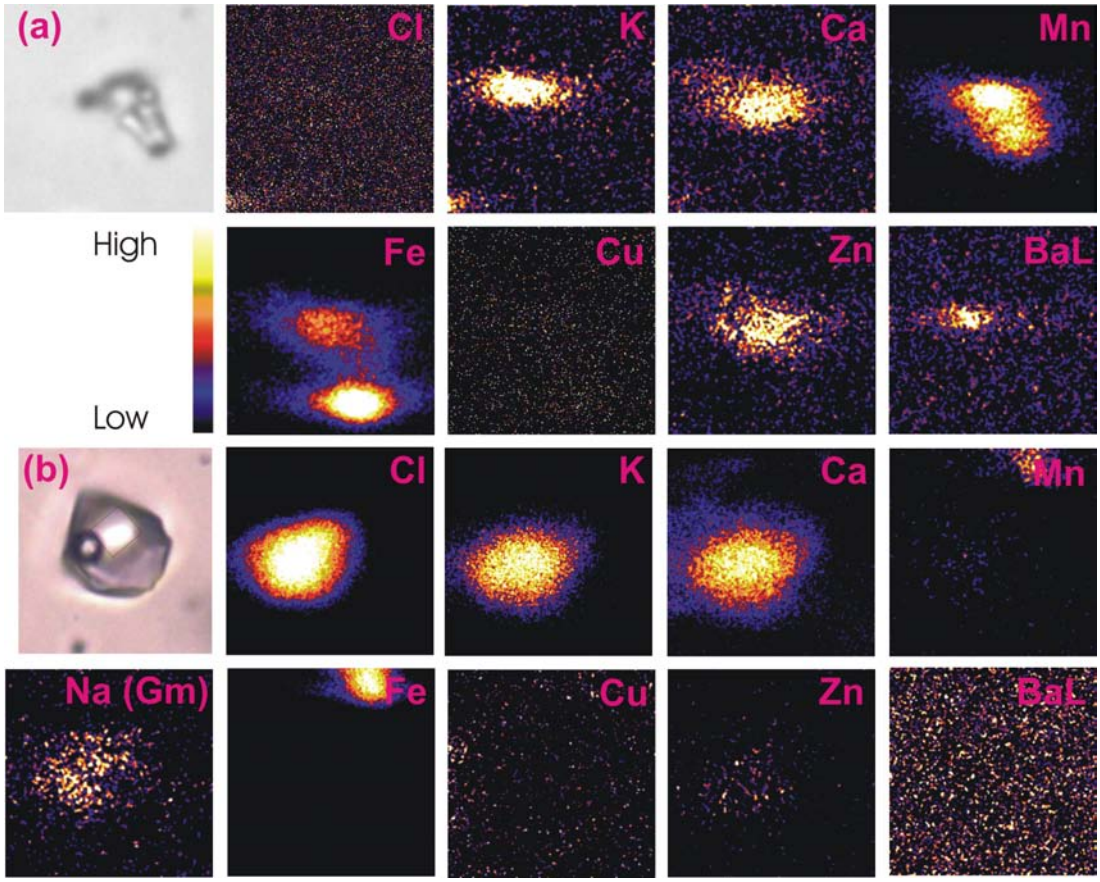

Figure 1. Comparison of type I (a) and type II (b) inclusions from Mary Kathleen. Gm – Gamma image. Inclusion size: (a) 10x6 μm, inclusion B1, Sample 02CC31-1, Knobby; (b) 9x8 μm, inclusion B8, Sample 02CC94B, Lime Creek. Type I inclusions in regional alteration are much less common than those in ore deposits and characterised by abundant Mn, Fe and Ba, distinctive from type II inclusions (halite).

Some Ca- and Na-rich inclusions (i.e., L+V+halite) are trail-bound and crosscut clusters of CO_2 ± N_2 inclusions producing calcite (see Figure 2 of Fu et al. 2003). This is a line of evidence for mixing of partly miscible fluids.

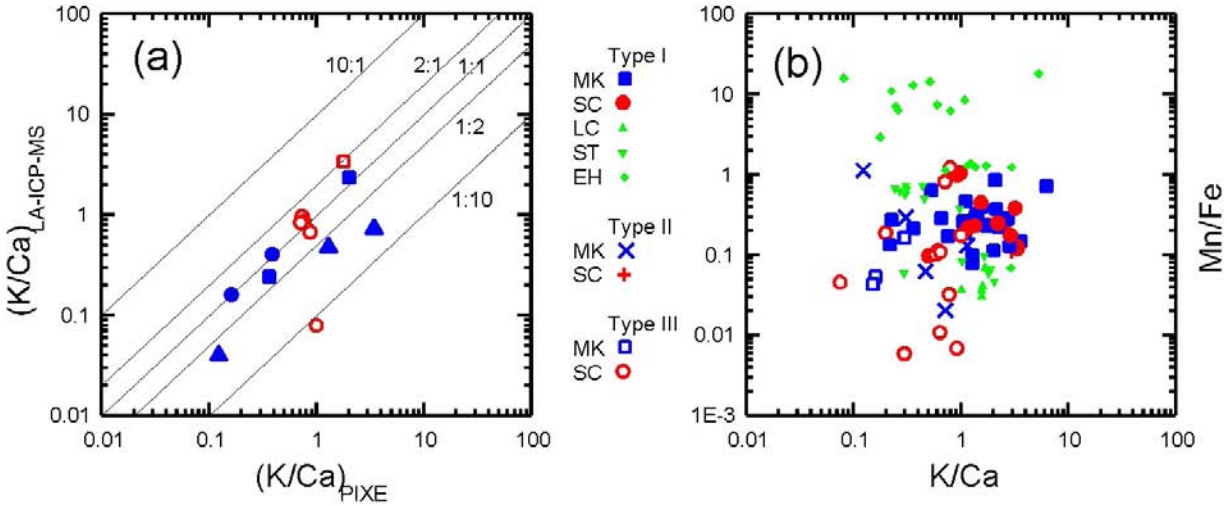

Figure 2. (a) Comparison of PIXE and LA-ICP-MS result: K/Ca ratio; and (b) plots of K/Ca versus Mn/Fe for all PIXE and LA-ICP-MS data from Mary Kathleen (MK) and Snake Creek (SC). There are only a few data from Mt Avarice and Gilded Rose and are not plotted here. Other PIXE Data sources: Lightning Creek (LC) prospect, Perring et al., 2000; Starra (ST) Cu-Au deposit, Williams et al., 2001; Ernest Henry (EH) Cu-Au deposit, Mark et al., 1999.

Microanalytical results

Both PIXE and LA-ICP-MS analyses indicate large amounts of Na, K, Ca, Fe and Mn in types I and II inclusions. Mo, Ag, Sn and Sb are below the limit of detection of PIXE. The Cu concentrations in all types of fluid inclusions are $\leq$ 550 ppm, the majority of which are below the limit of detection of both PIXE and LA-ICP-MS. Both microanalytical methods gave comparable results: K/Ca ratio for the same fluid inclusions analysed mostly lies within the area between lines of 2:1 and 1:2 (Fig. 2a).

K/Ca ratio for the respective fluid type from Snake Creek is somewhat higher than that from Mary Kathleen on average (Fig. 2b). There are no other significant differences in fluid composition between Mary Kathleen and Snake Creek. High-salinity brines (types I & II) are distinct from low-salinity fluids (type III) (Fig. 2b). For instance, K/Ca ratio in types I and II inclusions from Mary Kathleen and Snake Creek is much higher than type III inclusions.

Discussion and conclusions

The slight difference in major fluid components between Mary Kathleen and Snake Creek is probably controlled by the fluid-rock interaction (calc-silicate v. siliciclastic rocks). In other words, fluid is somewhat rock-buffered. It is noteworthy that some type I inclusions from Ernest Henry have higher Mn/Fe ratios, up to 18 (Mark et al., 1999), and that some from Lightning Creek prospect have much higher Cu/Zn ratios, up to 27 (Perring et al., 2000), than all others from regional alteration and ore deposits. Furthermore, type I inclusions are much less common in regional alteration than ore deposits.

In conclusion, late Ca-rich, halite-bearing brine inclusions are much more abundant than early K/Fe-rich, multisolid brine inclusions in regional alteration. This is distinctive from ore deposits. The copper concentration in regional fluids associated with albitisation is lower than that in some deposits or prospects (Lightning Creek: Perring et al., 2000; Starra: Williams et al., 2001).

References

DeJong, G. and Williams, P.J., 1995. Giant metasomatic system formed during exhumation of mid-crustal Proterozoic rocks in the vicinity of the Cloncurry Fault, northwest Queensland. Austalian Journal of Earth Sciences 42, 281-290.

Fu, B., Williams, P.J. Oliver, N.H.S., Dong, G., Pollard, P.J. and Mark, G.M., 2003. Fluid mixing versus unmixing as an ore-forming process in the Cloncurry Fe-oxide-Cu-Au District, NW Queensland, Australia: evidence from fluid inclusions. Journal of Geochemical Exploration, 78-79, 617-622.

Mark, G., Williams, P., Oliver, N.H.S., Crookes, R.A., Valenta, R.K.and Gow, P.A., 1999. Characteristics and Origin of the Ernst Henry Iron Oxide-Copper-Gold Hydrothermal System. Results of the 1999 Collaborative SPIRT Research Project (Unpublished). James Cook University, Townsville.

Oliver, N.H.S., 1995. Hydrothermal history of the Mary Kathleen Fold Belt, Mt Isa Block, Queensland. Australian Journal of Earth Sciences, 42, 267-279.

Perring, C.S., Pollard, P.J., Dong, G., Nunn, A.J. and Blake, K.L., 2000. The Lightning Creek Sill Complex, Cloncurry District, Northwest Queensland: a source of fluids for Fe oxide Cu-Au mineralization and sodic-calcic alteration. Economic Geology, 95, 1067-1089.

Williams, P.J., 1998. Metalliferous economic geology of the Mt Isa Eastern Succession, Queensland. Australian Journal of Earth Sciences, 45, 329-341.

Williams, P.J., Dong, G., Ryan, C.G., Pollard, P.J., Rotherham, J.F., Mernagh, T.P. and Chapman, L.H., 2001. Geochemistry of hypersaline fluid inclusions from the Starra (Fe oxide)-Au-Cu deposit, Cloncurry District, Queensland. Economic Geology, 96, 875-883.

Geochemical characterisation of the Golden Mile stratigraphy and implications for the structural architecture

Louis Gauthier[1], Steffen Hagemann[1] and Francois Robert[2]

*[1]pmd*CRC, Centre for Global Metallogeny, School of Earth and Geographical Sciences, University of Western Australia, Crawley, WA 6009*
[2]Barrick Gold Corporation

gauth101@segs.uwa.edu.au

A synthesis of an extensive major and trace element geochemical database allows a better understanding of the internal stratigraphy of the Paringa Basalt and Golden Mile Dolerite, which host the Golden Mile deposit. A better comprehension of the host stratigraphy is a critical element to define the structural architecture of the Golden Mile Deposit. Major and trace element geochemistry of the Paringa Basalt and Golden Mile Dolerite are used in three different ways to define the structural Architecture: (1) Consistent geochemical fractionation trends within the Paringa Basalt and individual units of the layered Golden Mile Dolerite are used as younging indicators, (2) Major faults are documented by offsets in the fractionation trend of the Paringa Basalt, and (3) Early syn-volcanic faults are interpreted by abrupt changes in thickness and composition of the Paringa Basalt and Golden Mile Dolerite.

The Paringa Basalt sequence consists of a 400 to 700m thick accumulation of basaltic flows grading from a high magnesium basalt (>10wt% MgO, anhydrous basis) with ubiquitous variolitic and local spinifex textures at the base, to a gradually more fractionated tholeiitic basalt (3 to 10 wt% MgO). The upper portion of the Paringa Basalt is characterised by pillow and flow breccia textures with a general increase of interflow sedimentary rocks. The Paringa Basalt displays a gradual fractionation trend with increasingly more evolved compositions towards the stratigraphic top, characterised by increasing Zr, TiO_2, Al_2O_3, V, Fe_2O_3 and decreasing MgO, Ni, Cr. The top 50 to 100m section of the Paringa Basalt sequence consists of a high iron tholeiite in sharp contact with the underlying Tholeiitic Basalt. It is characterised by a high content of TiO_2 (1.6 to 1.8 wt%), Fe_2O_3 (14 to 16 wt%), Zr (100 to 130 ppm), P_2O_5 (0.2 wt%) and low MgO (4 to 5 wt%). The High Iron Tholeiite also displays a normal fractionation trend.

The Golden Mile Dolerite (GMD) is a differentiated layered gabbroic sill of approximately 700m in thickness. The intrusion has been subdivided in 10 units based on petrographic and geochemical characteristics. Unit 1 and 10 form the basal and upper chilled margins, respectively. Unit 2 and 3, the basal cumulate units, display very high Cr, Ni, MgO with a decreasing trend upward into the intrusion. Unit 4 and 5 consist of medium grained sub-ophitic textured gabbro with a generally flat geochemical pattern. Units 6, 7 and 8 are the magnetite-rich units (10-15 wt% magnetite). Unit 6 displays very strong enrichment in elements with strong partition coefficient into magnetite, such as V, Cr, Ni and Cu. These elements are in turn strongly depleted in units 7 and 8. Units 6 and 7 display gradual enrichment trends in Zr, TiO_2 and Fe_2O_3 towards Unit 8. Unit 8 the granophyric unit, is characterised by high SiO_2, Zr, TiO_2, P_2O_5 and Fe_2O_3. Unit 9 displays a gradual fractionation trend characterised by higher Zr, V, TiO_2 and lower Cr, Ni, MgO towards the contact with Unit 8.

The GMD displays important lateral variations in terms of thickness, internal magmatic layering and geochemistry. The GMD in the east-dipping limb of the upright NW trending Kalgoorlie

Anticline is significantly thinner (200m) than the west-dipping limb (700m) and displays a gradual fractionation trend without the formation of magmatic layering. The fractionation trend indicates that the dolerite is eastward younging, which is consistent with the interpretation of this thinner dolerite being on the east-dipping limb of the Kalgoorlie Anticline. South of the Eastern Lode System, the GMD is slightly thinner (500m) and displays less well developed internal magmatic layering with significantly less abundant magnetite in Units 6, 7 and 8. This transition is gradual and not associated with the Adelaide Fault.

PIXE analysis of hydrothermal fluids in the Wernecke Mountains, Canada

David Gillen[1], Tim Baker[1], Julie Hunt[1,2], Chris Ryan[3] and Tin Tin Win[3]

*[1]pmd*CRC, School of Earth Sciences, James Cook University, Townsville, QLD 4811*
[2]Yukon Geology Program, Yukon Territory, Canada
[3]CSIRO Exploration and Mining, North Ryde, NSW

david.gillen@jcu.edu.au

Introduction

The main theories on the sources of fluids in Fe-oxide Cu-Au deposits centre on either a magmatic (Hitzman et al., 1992) or evaporitic origin (Barton and Johnson, 1996). The magmatic theory suggests that hot, saline ore-forming fluids are evolved from a crystallising magma. In the evaporitic source model, saline fluids are generated when circulating fluids interact with evaporites. Fluid mixing models are also suggested, where cooler, less saline fluids interact with, or postdate, hot highly saline fluids to create conditions suitable for precipitation of ore minerals (Oreskes and Einaudi, 1992).

Fe-oxide Cu-Au deposits in the Wernecke Mountains, Canada, and the Cloncurry District, Australia, allow the study of fluids from deposits which are similar in character, but which also display some key differences. The deposits from the two regions are similar in that they were formed by large hydrothermal systems, exhibit significant hydrothermal brecciation, and have similar ages. The Wernecke breccia has been dated at 1595 Ma, whereas dates obtained for the Cloncurry deposits lie in the range 1500 to 1540 and 1595 Ma. The main contrast between the two areas is the conspicuous absence of syn-mineralisation granitic intrusions in the Wernecke region. Studies in the Cloncurry district suggest a significant magmatic component to the fluids, in part consistent with the spatial and temporal association of economic deposits with the abundant intrusions in the region. Economic deposits are yet to be identified in the Wernecke region, and the absence of syn-mineralisation intrusions leaves a question mark over the source of the fluids that formed the extensive Fe-oxide Cu-Au breccias. The study of these two areas therefore provides an ideal opportunity to compare fluids of potentially quite different origins and thus improve our understanding of the types of fluids that can form Fe-oxide Cu-Au deposits and help in identifying the critical ingredients in ore deposit formation.

Geological Setting

The dominant rocks in the Wernecke Mountains belong to the Proterozoic Wernecke Supergroup (1840-1725 Ma). The sequence is divided into three main components, the basal unit being the Fairchild Lake Group, which consists of mainly siltstone. Layers of scapolite within a zone of sodic alteration (albite) are observed in the upper Fairchild Lake Group (Hunt et al., 2002) and may be an indication of pre-existing evaporite beds. Overlying this is the Quartet Group, made up of black carbonaceous shale, with minor siltstone and fine-grained sandstone, while uppermost is the Gillespie Lake Group dominated by dolostone. Minor intrusions are observed (dykes with ages of 1720 and 1270 Ma), and rare volcanic rocks (Thorkelson, 2000). Numerous breccia zones are present throughout the region and are associated with hydrothermal Fe-oxide-Cu-Au mineralisation. The brecciation in the region postdates the volumetrically minor Bonnet Plume River intrusions and has been dated at 1595 Ma (Thorkelson, 2000). Figure 1 represents the stratigraphy of the Wernecke Supergroup and illustrates the relative positions of each of the prospects sampled for this study.

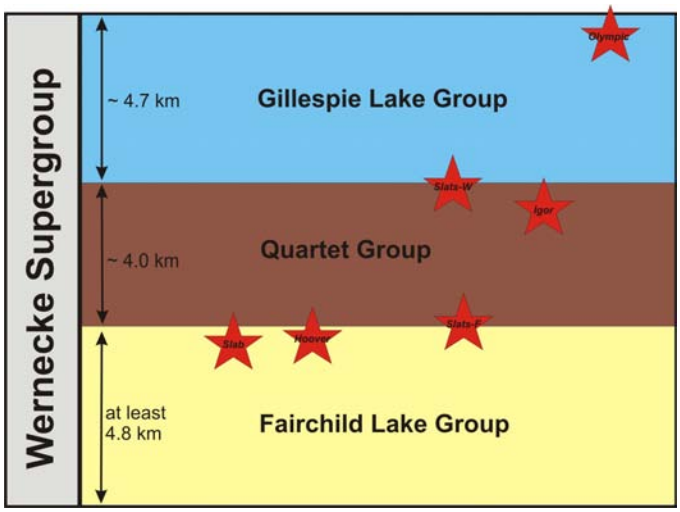

Figure 1 (left): Stratigraphy of the Wernecke Supergroup, and the relative locations of prospects.

Fluid Inclusion Microthermometry

Preliminary microthermometry has been performed on fluid inclusions in selected quartz samples from the Igor, Slab, Hoover and Olympic prospects, Wernecke Mountains. These samples were collected from quartz veins within and adjacent to breccia zones. The veins consist of quartz-carbonate (calcite, ankerite) with variable chalcopyrite ±pyrite ±magnetite ±hematite ±barite. The quartz contains both primary and secondary inclusions. The observed fluid inclusions are thought to represent syn to post brecciation fluids. Table 1 illustrates the fluid inclusion types observed at each of the deposits, along with a summary of the microthermometry results obtained from each location, and the proposed timing of the fluids measured, with respect to the breccia.

Prospect	Type	Tfm (°C)	Major fluid components	Salinity (wt% NaCl equiv)	Th vap (°C)	Th hal (°C)	Th (°C)	Timing[2]
Slab	L+V+S	-61 to -54	H_2O NaCl, Ca, K, Mn	~40*	167-230	202-261	202-261	Syn
Hoover	L+V+S	-55 to -49	H_2O, NaCl, Ca, K	?*	152-200	?	>200	Syn
Igor	L+V L+V+S	-56 to -38 - -32 to -21	H_2O, NaCl, Ca, K . H_2O, NaCl, Ca, K	30* 3-23	150-174 70-138	175-184 -	175-184 70-138	Syn-post
Olympic[1]	L+V L+V+S		H_2O, NaCl, K, Ca	~30?	~200	-	~200	Post

*Table 1: Thermometry data for fluid inclusions in quartz from four Fe-oxide Cu-Au prospects in the Wernecke region. Tfm= first melting temperature (eutectic) of a frozen inclusion upon heating. Th vap= temperature of vapour disappearance upon heating. Th hal= temperature of halite dissolution (where present). Th= final homogenisation temperature. Major fluid compositions inferred by microthermometry and confirmed and complemented by PIXE analyses. Salinities estimated by thermometry experiments, *(Nacl + $CaCl_2$). [1]Further data required at Olympic. [2]Timing is relative to the breccia.*

The main inclusion types are liquid rich (with 5 to 25% vapour) aqueous inclusions (L+V), and halite-bearing inclusions (L+V+S). Eutectic (first) melting temperatures indicate the fluids are NaCl dominated, with the majority of samples containing a significant calcium chloride content ($CaCl_2$). Salinities calculated from ice melting and halite dissolution temperatures range between 3 and 40 wt % NaCl and homogenisation temperatures range from 70 to 261 °C.

Proton Induced X-ray Emission (PIXE)

PIXE analyses have been carried out on individual fluid inclusions contained in the same quartz samples used for microthermometry experiments (and often the same inclusions). These analyses were undertaken with the aim of determining fluid compositions, by obtaining concentrations of a range of elements. It is hoped that such detailed compositional data will help in elucidating the character and source of fluids responsible for the brecciation and mineralisation in the Wernecke region.

Uncertainties in the current PIXE data are introduced by errors in the difficult task of estimating fluid inclusion depth and thickness. This has caused large variations in calculated chlorine concentrations; hence the preliminary data is currently being scrutinised to ensure the validity of the data for other elements. Methods being attempted to correct such errors, include fixing chlorine values to those inferred from salinities, which were calculated from microthermometry experiments. At present, elemental ratios are being used to highlight relative elemental abundances, minimising the effect of systematic errors in absolute concentrations.

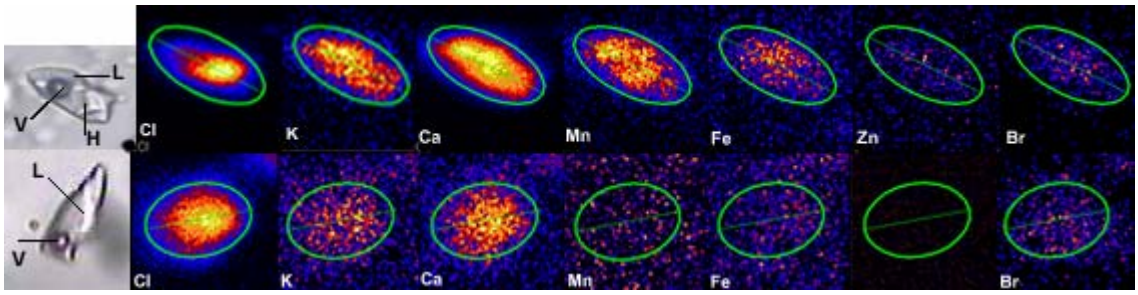

Figure 2: A fluid inclusion from the Slab prospect (2a)(top) and Igor (2b), shown with PIXE images displaying the abundances of Cl, K, Ca, Mn, Fe, Zn, and Br within the fluid. The inclusion in Figure 2a is approx 20µm long, and Figure 2b is approx 10µm. The location and intensity of the light coloured zones represent relative abundances of each element.

Preliminary PIXE data have identified some distinct differences in the fluid compositions from the four different prospects in the Wernecke region. The overall salinity of each of the fluids differs, although the majority are saline fluids, so of greater interest is the variation of certain elemental ratios when comparing each of the prospects. The Slab prospect contains the most saline fluids; they are rich in calcium, and have the highest Ca/K ratios of all the deposits. A photo of a halite-bearing (L+V+S) fluid inclusion from Slab is shown in Figure 2a, along with PIXE images of this inclusion. The images show the strong calcic nature of the fluids, and illustrates that significant components of Cl, Na, K, Mn and Fe are also present in the fluid. Figure 2b shows an inclusion from the Igor deposit, and its PIXE images. The difference between these two fluids is immediately apparent, with the Igor fluid showing less intense signals for Cl, K and Ca and lacking signals from the other elements.

Figure 3 below presents PIXE data from the four Wernecke prospects and illustrates the variation in fluids between each prospect. The plot also compares them with fluids from the Starra deposit of the Cloncurry region. Each of the prospects lies in a different area of the plot. The Igor fluids show the highest Ba/Fe ratios of all the prospects, which seems consistent with the presence of significant barite veining at this particular deposit. Interestingly Slab has attracted the most exploration interest of the prospects, possibly showing the greatest promise of the group in terms of economic potential, and the highly saline Slab fluids appear on this plot to be the most consistent with mineralising fluids from Starra. The ironstone-forming fluids from Starra are thought to be largely magmatic in character (Williams et al. 2001), and are seen to plot in their own area in Figure 3.

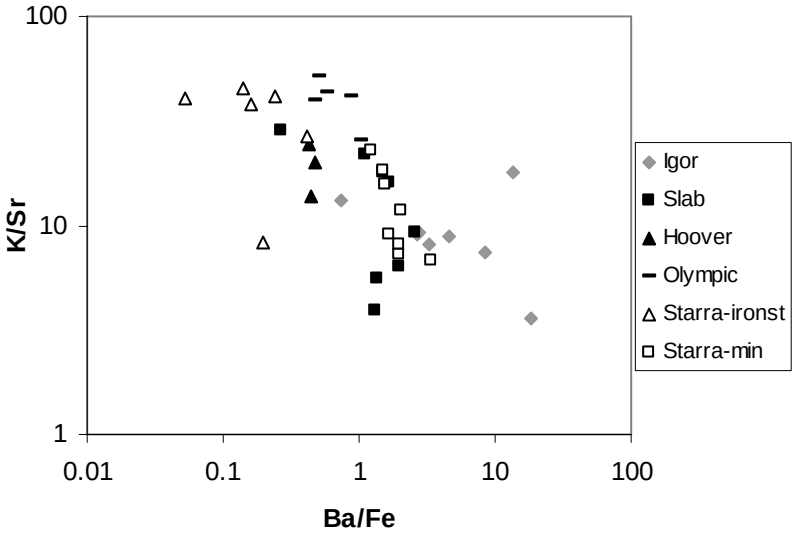

Figure 3 (above): K/Sr v Ba/Fe ratios for data obtained from PIXE analyses at four Wernecke prospects. Included are data from Williams et al. (2001) for inclusions at the Starra deposit, representing an ironstone-forming fluid and another fluid associated with the mineralisation.

Interpretation and discussion of fluid inclusion data

The study of fluid inclusions has revealed a distinct variation in fluids between the different prospects in the Wernecke Mountains. There are several factors that may have influenced each of the fluids and a combination of these may help to explain these variations in fluid character. The stratigraphic context of the respective prospects is the most obvious difference between them (Figure 1). This could affect fluid character in terms of temperature and pressure, variations in fluid-wall rock interaction due to change in host-rock, and proximity to features such as evaporites which can exert a significant influence on the character of circulating fluids. The influence of such factors seems to be evident in the presented data, with high Ba/Fe fluids at Igor closely linked with substantial barite found at the deposit. The high salinity of fluids at the Slab prospect may be related to its close proximity to evaporite beds, thought to have existed in the upper Fairchild Lake Group. The character of any upwelling hydrothermal fluid may have been influenced by interaction with such evaporites, for example by dissolution of halite horizons. In addition, it is perhaps no coincidence that the two most distinctly different fluids in the region are found at the deposits furthest apart in the stratigraphy (Slab and Olympic). Further scrutiny of the timing of fluid inclusions at Olympic is required and may help to explain this fluid contrast.

In considering fluid source, the apparent low homogenisation temperatures observed during microthermometry are not consistent with magmatic-derived fluids and are well below those commonly observed in the Cloncurry district (>300 °C). The more magmatic, ironstone-forming fluid from Starra also seems distinct from the Wernecke fluids. These observations seem consistent with the distinct lack of syn-mineralisation intrusions in the area and are more likely representative of some variety of basinal fluids. It is hoped that further analysis of the inclusions for halogens will provide further clues to the fluid's origin.

Acknowledgements

Funding for this project is provided by the Yukon Geological Survey, an APRS scholarship and the pmd*CRC.

References

Barton, M. D. and Johnson, D. A., 1996. Evaporitic-source model for igneous-related Fe-oxide-(REE-Cu-Au-U) mineralisation. Geology, 24, 259-262.

Hitzman, M. W., Oreskes, N. and Einaudi, M. T., 1992, Geological characteristics and tectonic setting of Proterozoic iron oxide (Cu-U-Au-REE) deposits. Precambrian Research, 58, 241-287.

Hunt, J.A., Laughton, J.R., Brideau, M-A., Thorkelson, D.J., Brookes, M.L. and Baker, T., 2002. New mapping around the Slab iron oxide-copper-gold occurrence, Wernecke Mountains (parts of NTS 106C/13, 106D/16, 106E/1 and 106F/4), Yukon. In: Emond, D.S., Weston L.H., and Lewis L.L., eds., Yukon Exploration and Geology 2001. Exploration and Geological Services Division, Yukon Region, Indian and Northern Affairs Canada, 125-138.

Oreskes, N. and Einaudi, M. T., 1992. Origin of hydrothermal fluids at Olympic Dam: Preliminary results from fluid inclusions and stable isotopes. Economic Geology, 87, 64-90.

Thorkelson, D. J., 2000. Geology and mineral occurrences of the Slats Creek, Fairchild Lake and "Dolores Creek" areas, Wernecke Mountains (106D/16, 106C/13, 106C/14), Yukon Territory. Exploration and Geological Services Division, Yukon, Indian and Northern Affairs Canada, Bulletin 10, 73 p.

Williams, P.J., Dong, G., Ryan, C.G., Pollard, P.J., Rotherham, J.G., Mernagh, T. and Chapman, L.H., 2001. Geochemistry of hypersaline fluid inclusions from the STarra (Fe oxide)-Au-Cu deposit, Cloncurry district, Queensland. Economic Geology, 96, 875-883.

A tomographic view of the Eastern Goldfields Province, Yilgarn Craton

B.R. Goleby[1,3], B.L.N. Kennett[2,3], T. Fomin[1,3], A.M. Reading[2], R. Blewett[1] and M. Nicoll[1]

*[1] pmd*CRC, Geoscience Australia GPO Box 378, Canberra ACT 2601*
[2] Research School of Earth Science, ANU, Canberra, ACT, 0200
[3] Australian National Seismic Imaging Resource (ANSIR)

Bruce.Goleby@ga.gov.au

Seismic Experiments

Our knowledge of the crustal architecture of the Yilgarn Craton has increased greatly over the last few years with the collection of a wide range of seismic data. This range in seismic data varies from lithospheric-scale studies using distant earthquakes as sources to obtain information on the craton scale and down to depths in excess of 350 km, through regional scale studies providing information at the province scale and down to depths of 30-40km to mine camp scale studies providing information on the local scale and down to the top few kilometres of the crust. The location of these different seismic surveys is shown in Figure 1.

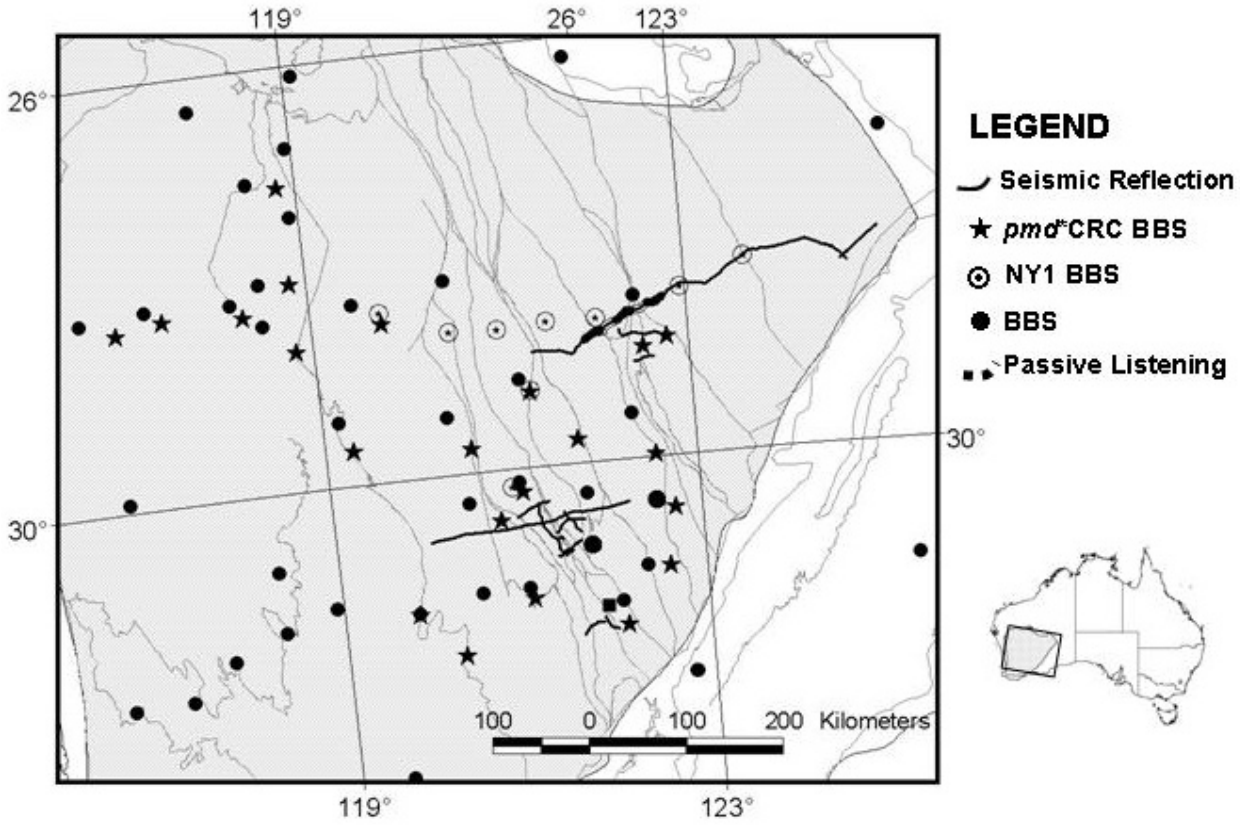

Figure 1. Map of the Yilgarn Craton showing location of the different seismic experiments undertaken during the last few years. BBS refers to Broadband Site. Dots are earlier BBS sites recorded by RSES, ANU. Seismic reflection traverses include the earlier Geoscience Australia and AGCRC traverses as well as the recent seismic work at regional and mine scale.

Lithospheric Scale Studies

At the craton scale, the Y2 project has undertaken a number of broadband instrument deployments to record P-wave, S-wave and surface wave variations across the Yilgarn Craton. The Research School of Earth Sciences, ANU, in conjunction with Y2 is developing P-wave, S-wave and surface wave velocity maps of the craton (VRML on pmd*CRC web site). A 350km deep, east-west S-wave seismic tomography cross section of the Yilgarn Craton is shown in Figure 2. The cross section shown is sub parallel to the deep seismic reflection traverse 01AGSNY1. An interesting observation is the presence of a body with a high S-wave velocity (> 4.8 km/sec) within the upper mantle. This body dips to the east, and has a series of step-wise 'normal' offsets coinciding approximately with the principal terrane boundaries as defined at the surface. The receiver function results are showing a significant variation in crustal and upper mantle velocities across the craton, with the Moho increasing in depth eastward across the craton.

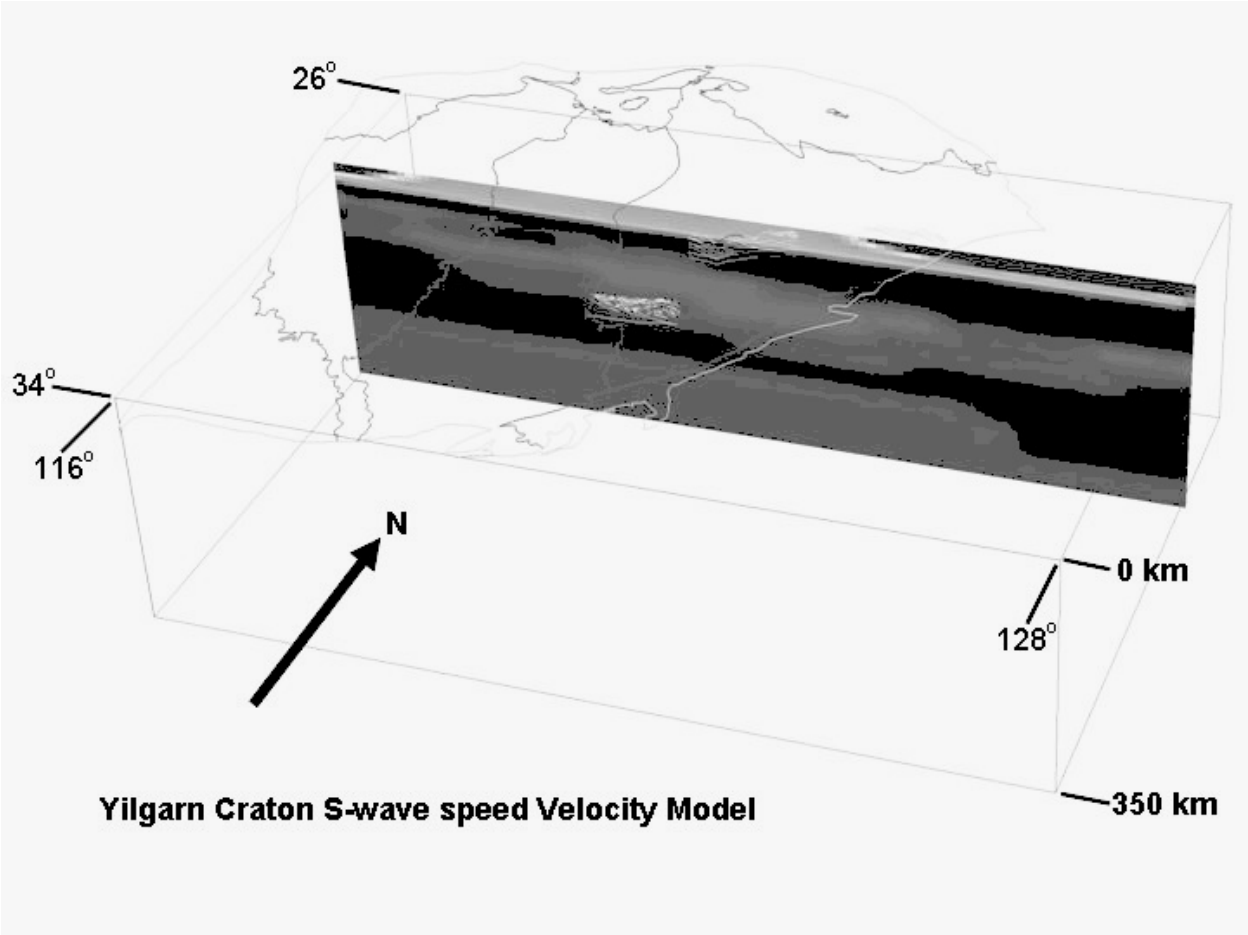

Figure 2. An east-west orientated S-wave tomographic cross section of the Yilgarn Craton. Lighter colours in cross section are areas where S-wave velocity is faster than the world average. Darker colours are areas where S-wave velocity is slower than the world average.

Regional Scale Studies

At the regional scale, deep crustal seismic reflection studies have provided excellent 2D crustal architecture information in the eastern part of the craton, which in turn, have provided information on the region's mineral systems (Goleby et al., 2003). These seismic data have imaged the numerous shear zones within the crust as well as details within the greenstone succession and indicate that the regions major orogenic gold deposits are spatially associated

with these major shear zones (Cassidy et al., 2003). The data from the broadband instrument deployments are also being used to compute receiver function estimates of the crustal velocity of the Yilgarn Craton. Receiver function results for the NY1 BBS sites (locations on Figure 1; data on Figure 3 as WV sites) show higher velocity material within the footwall of the Ida Fault, the western boundary to the Eastern Goldfields. This observation is consistent with observations made further south (Reading et al., 2003, data shown as WT sites on Figure 3). The results from the pmd*CRC BBS sites (Figure 1) are currently being processed. The results will provide information on the velocity structure of the Yilgarn Craton, in particular on the potential velocity differences between the mineralized Eastern Goldfields Province and the less mineralized Southern Cross and Murchison Provinces. Through the collection of seismic tomography data, the project will be able to link the velocity structure of the region to the 3D geological models being constructed of the Eastern Goldfields.

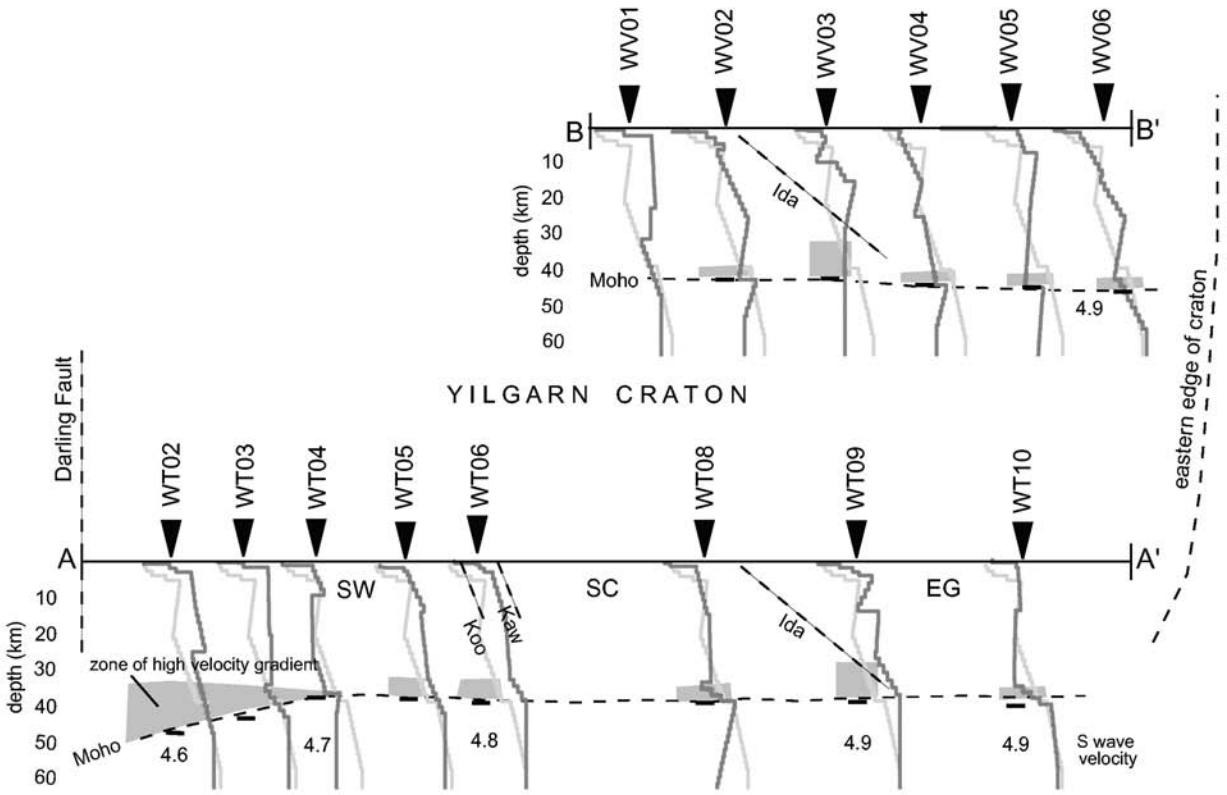

Figure 3. Crustal receiver function results for WT and WV lines, WA (WV line is shown on Figure 1 as NY1 BBS sites). Figure from Reading et al., 2003.

At a more detailed scale, a passive recording experiment was undertaken to record wide-angle data within the Leonora to Laverton area (Figure 1) to supplement the deep seismic reflection (01AGSNY1) data to obtain additional velocity information within the granite-greenstone succession that will be used to develop detailed velocity-lithological distributions in the top 7 km (Fomin et al., 2003; Fomin, this volume). These data show a region of higher velocity to the west of Laverton and a large mass of slow velocity lithosphere beneath Laverton region.

Mine Camp Studies

During the acquisition of the regional seismic reflection traverse, two mine camp-scale seismic traverses were recorded as part of a MERIWA project involving two of the regions' main gold exploring companies, AngloGold and Placer Granny Smith. These mine camp seismic traverses were recorded within the highly prospective Laverton Tectonic Zone and shear zones designed to target the upper 5-10 km of the granite-greenstone succession to obtain three-dimensional details within this mineralized zone. The resultant seismic reflection data, together with detailed

geological mapping of the area were integrated, so that the near surface information obtained by mapping, drilling and mining were linked to the deeper information obtained by the seismic reflection method.

Tomographic View

The integration of the results from these different scaled seismic data sets show a more variable velocity distribution and hence complex crustal architecture than initially inferred. The combined velocity, structural and geological data sets provide an image of the granite-greenstone succession and its underlying relatively low-density and low-velocity middle crust. The crustal architecture is indicative of a crustal scale (thin and thick-skinned fold –thrust belt), with regional folding and thrusting occurring during the main contractional episodes. These compressive episodes were separated by equally important extension episodes, with the seismic reflection data suggesting that extensional movement on shear zones was more common that previously thought. The major domain-bounding shear zones are also best interpreted as having late extension that followed an episode of earlier west-directed thrusting.

Acknowledgements

This paper is published with the permission of the Chief Executive Officer, Geoscience Australia, the Director of ANSIR and the Chief Executive Officer of the Predictive Mineral Discovery Cooperative Research Centre.

References

Cassidy, K.F., Blewett, R.S., Champion, D.C. and Goleby, B.R., 2003. Northeastern Yilgarn seismic reflection survey: Implications for orogenic Au systems. In: Goleby B.R., Blewett R.S., Groenewald P.B., Cassidy K.F., Champion D.C., Jones L.E.A., Korsch R.J., Shevchenko S. and Apak S.N., eds., The 2001 Northeastern Yilgarn Deep Seismic Reflection Survey. Geoscience Australia Record, 2003/28, 127-143.

Fomin, T., Crawford, A. and Johnstone, D., 2003. A wide-angle reflection experiment with Vibroseis sources as part of a multidisciplinary seismic study of the Leonora-Laverton Tectonic Zone, Northeastern Yilgarn Craton. Exploration Geophysics, 34, 147-150.

Fomin, T., 2004. Models of the upper crust from wide-angle and reflection studies, Northeastern Yilgarn: Why we need both? This volume.

Goleby, B.R., Blewett, R.S., Groenewald, P.B., Cassidy, K.F., Champion, D.C., Korsch, R.J., Whitaker, A., Jones, L.E.A., Bell, B., and Carlson, G., 2003. Seismic interpretation of the northeastern Yilgarn Craton seismic data. In: B.R. Goleby, R.S. Blewett, P.B. Groenewald, K.F. Cassidy, D.C. Champion, L.E.A. Jones, R.J. Korsch, S. Shevchenko and S.N. Apak., eds., The 2001 Northeastern Yilgarn Deep Seismic Reflection Survey. Geoscience Australia, Record, 2003/28, 85-112.

Reading, A.M., Kennett, B.L.N. and Dentith, M.C., 2003. Seismic structure of the Yilgarn Craton, Western Australia. Australian Journal of Earth Sciences, 50, 427-438.

Preliminary Re-Os dating of the Mount Isa copper ores, Northwest Queensland

M.J. Gregory, A.R. Wilde, R.R. Keays and B.F. Schaefer

*pmd*CRC, School of Geosciences, Monash University, Melbourne, VIC 3800*

melissa.gregory@mail.earth.monash.edu.au

The absolute timing of sulphide deposition in the Mount Isa copper orebodies remains controversial and poorly constrained. Previous studies have not directly dated the ore phases and have focused on alteration assemblages, which are interpreted to have the same timing as the ore sulphides.

Preliminary Re-Os isotopic analyses have been obtained from six samples (including whole rock and sulphide separates) from the Mount Isa copper and lead-zinc orebodies. They generate a Re-Os isochron age of 1370 $\pm$ 80 Ma, and an initial $^{187}Os/^{188}Os$ ratio of 0.20 $\pm$ 0.25 (MSWD = 49). Two samples of the host sediment (Urquhart Shale), were also dated using the K-Ar system, giving ages of 1356 $\pm$ 27 Ma and 1134 $\pm$ 22 Ma, partly consistent with the Re-Os results. Overall, these ages are considerably younger than the age of 1523-1505 Ma inferred for copper mineralisation at Mount Isa, using $^{40}Ar/^{39}Ar$ dating of hydrothermal biotite (Perkins et al., 1999).

Well over 100 samples from within a twenty kilometre radius of the Mount Isa base-metal deposits have been dated in the past using a variety of techniques. A substantial subset of these data has been ignored due to the fact they have yielded dates that are considered too young to be of significance to mineralisation. For example, the combined Rb-Sr dataset from Farquharson and Richards (1975) and Page (1978) generates an isochron age of 1323 $\pm$ 12 Ma using 152 analyses of tuff samples from the Urquhart Shale. The initial $^{87}Sr/^{86}Sr$ of 0.7418 $\pm$ 0.0061 is very radiogenic and is indicative of a resetting event at this time. The Re-Os data imply the resetting of the Rb-Sr system within the sediments may be related to copper mineralisation.

$^{40}Ar/^{39}Ar$ data from Spikings et al. (2002) and Perkins et al. (1999) show a group of unexplained dates which are consistent with our Re-Os results. They dated sericites and hornblendes from fault zones within the mine and from the Mount Isa Fault Zone, with a range in results from 1440 Ma to 1325 Ma. These dates have been interpreted as either a fluid flow event along the Mount Isa Fault (Perkins et al., 1999), or as a time of cooling and uplift (Spikings et al., 2002). This data in combination with new Re-Os dates, suggests these events were in some way associated with copper mineralisation at Mount Isa.

An extensive Re-Os sampling and analytical program, along with detailed paragenetic studies, will be undertaken in the near future to determine the importance of these preliminary results. This aims to significantly reduce the error and uncertainty on the data and the outcomes will have important implications in the understanding of the genesis of the Mount Isa copper system.

References

Farquharson, R. B. and Richards, J. R., 1975. Isotopic remobilization in the Mount Isa tuff beds. Chemical Geology, 16, 73-88.

Page, R. W., 1978. Response of U/Pb zircon and Rb/Sr total-rock and mineral systems to low-grade regional metamorphism in Proterozoic igneous rocks, Mount Isa, Australia. Journal of the Geological Society of Australia, 25, 141-163.

Perkins, C., Heinrich, C. A. and Wyborn, L. A. I., 1999. $^{40}Ar/^{39}Ar$ geochronology of copper mineralization and regional alteration, Mount Isa, Australia. Economic Geology, 94, 23-36.

Spikings, R. A., Foster, D. A., Kohn, B. P. and Lister, G. S., 2002. Post-orogenic (<1500 Ma) thermal history of the Proterozoic Eastern fold belt, Mount Isa Inlier, Australia. Precambrian Research, 109, 103-144.

Y3 project: Camp- to deposit-scale multiple alteration footprints

Steffen G. Hagemann [1], Peter Neumayr [1], John L. Walshe [2]
*[1]pmd*CRC, Centre for Global Metallogeny, School of Earth and Geographical Sciences, University of Western Australia, Crawley, WA 6009*
*[2] pmd*CRC, Exploration and Mining Division, CSIRO, PO Box 1130, Bentley, WA 6102*
shageman@segs.uwa.edu.au

Vision

The projects' vision is to predict the alteration and geochemical signature of the "gold-related" hydrothermal event(s) within complex, overprinted gold mineral systems, and to predict fertile areas within hydrothermal alteration systems, by developing mineralogical and geochemical criteria.

Aims

The Y3 projects aims are to:

- Develop a generic model to predict the alteration and geochemical signatures of the hydrothermal alteration events, including the gold event(s),
- Develop geochemical criteria to characterize and predict Au-transporting and barren hydrothermal systems,
- Decipher the early history of major fault zones, associated structural domes and anticlines through tectonic, stratigraphic, metamorphic and alteration studies of spatially associated mafic-ultramafic horizons and related ore deposits,
- Model Au (metal) transport and deposition to distinguish and predict barren and mineralized hydrothermal fluid systems.

Innovation

In order to achieve this ambitious vision, research is carried out at a range of scales from camp to deposit and even to ore-shoot scale. Detailed textural and microanalytical studies are also conducted at a microscale. Spatial data on a camp- to deposit-scale are possibly the most useful for direct application in exploration. However, observations at all other scales are critical to test working models. Observed patterns are expected to be repetitive at most if not all scales. The project applies a range of methods to develop petrographical data, whole-rock geochemical analyses, stable isotope data, fluid inclusion analyses as well as innovative spectral logging data (e.g., PIMA, ASD).
All data sets are integrated into 2D and 3D models. These models will be constructed in time slices, that is hydrothermal alteration is depicted in 4D. Detailed, high-tech analytical techniques are applied to determine whole-rock geochemical and stable isotope signals of alteration as well as the geochemical composition of end-member hydrothermal fluids. These serve as critical input parameters into geochemical models to test different metal transport and deposition mechanisms.

Achieve the step change

The Y3 project aims to achieve a step change by:

- Construction of 4D hydrothermal alteration/fluid models,

- Using low-detection, modern analytical techniques,
- Developing new geochemical models for hydrothermal fluid tracing and gold mineralization, and by
- Translating geochemical tracers and 4D hydrothermal models into vectors to ore.

A dynamic view of orogenesis and the development of the Eastern Yilgarn Craton

P. A. Henson[1], R.S. Blewett[1], D.C. Champion[1], B.R. Goleby[1] and K.F. Cassidy[2]

*[1] pmd*CRC, Geoscience Australia, GPO box 378, Canberra ACT 2601*
*[2] pmd*CRC, Geoscience Australia, c/-GSWA, 100 Plain St, East Perth, WA 6004*

Paul.Henson@ga.gov.au

Outline

The widely accepted tectonic history of the Eastern Yilgarn Craton, WA involves D_1 (N-S) thrusting and recumbent folding, D_{2e} (E-W extension), D_2 upright folding, and later D_3-D_4 strike-slip faulting (Swager, 1997) (Table 1). Recent findings indicate that the broadly E-W contractional event (D_2) is more complex and significant to mineralisation than previously interpreted. Evidence for this is integrally linked to the formation of siliciclastic basin sequences including: the Kurrawang, Merougil, Penny Dam, Pig Well-Yilgangi, which are commonly referred to as 'late basins'. The Kurrawang Syncline has been described as an extensional basin, developed during D_{2e} (Swager, 1997). Map patterns question this hypothesis due to the syncline overprinting D_2 folds which, in turn, are folded by a coaxial contractional event (Blewett et al., 2004a). This temporal link implies that it developed as a single part of the D_2 event and not during D_{2e} (extension prior to D_2 contraction). We propose that D_2 was not a single event, instead it developed during a complex episodic process involving switching of contraction and coaxial extension between ~2665 and ~2655 Ma ('D_2' = **D_{2a}, D_{2E}, D_{2b}**) (Blewett et al., 2004a). In addition, a subsequent orthogonal deformation (N-S contraction, **D_3**) has been identified as producing doming and localized thrusting.

Swager, 1997		**This study**	
DE	N-S? extension	**D_E**	N-S extension
D_1	N-S contraction	**D_1**	N-S? contraction
		D_{2a}	E-W contraction
D_{2e}	E-W extension	**D_{2E}**	E-W extension ('late basins')
D_2	E-W contraction	**D_{2b}**	E-W contraction
		D_3	~N-S contraction
D_3	E(NE)-W(SW) contraction	**D_4**	E(NE)-W(SW) contraction
D_4	E-W regional contraction	**D_5**	E-W regional contraction

Table 1: A comparison of the Swager (1997) deformation nomenclature with the current understanding of deformation events in the Eastern Yilgarn Craton

Orogenic surge

Several processes could explain the occurrence of extension events operating in a broadly contractional setting including: (1) slab roll back; (2) vertical block 'escape' or channel flow; (3)

post orogenic collapse; (4) underplating and wedge extension; and (5) slab detachment/break off, although the process of orogenic surge best explains the observed deformation within the upper and middle crust. Orogenic surge develops at the frontal region (toe) of a foreland fold and thrust belt (Lister et al., 2001). It requires topographic relief to develop until the critical taper in the frontal wedge becomes unstable driving the frontal thrust to extrude westwards over the foreland above a gently dipping basal detachment/thrust. The effect is that the region is thrown into extension during a broadly contractional stress field. This is thought to be facilitated by crustal thickening and subsequent uplift of the thrust belt until gravitational instability causes σ1 to switch from a horizontal stress field to a vertical one (Figure 1). Contemporaneous localized extension results in the formation of 'late basins' (fining-up sequences), which develop in localized extensional regimes during the tectonic switching event.

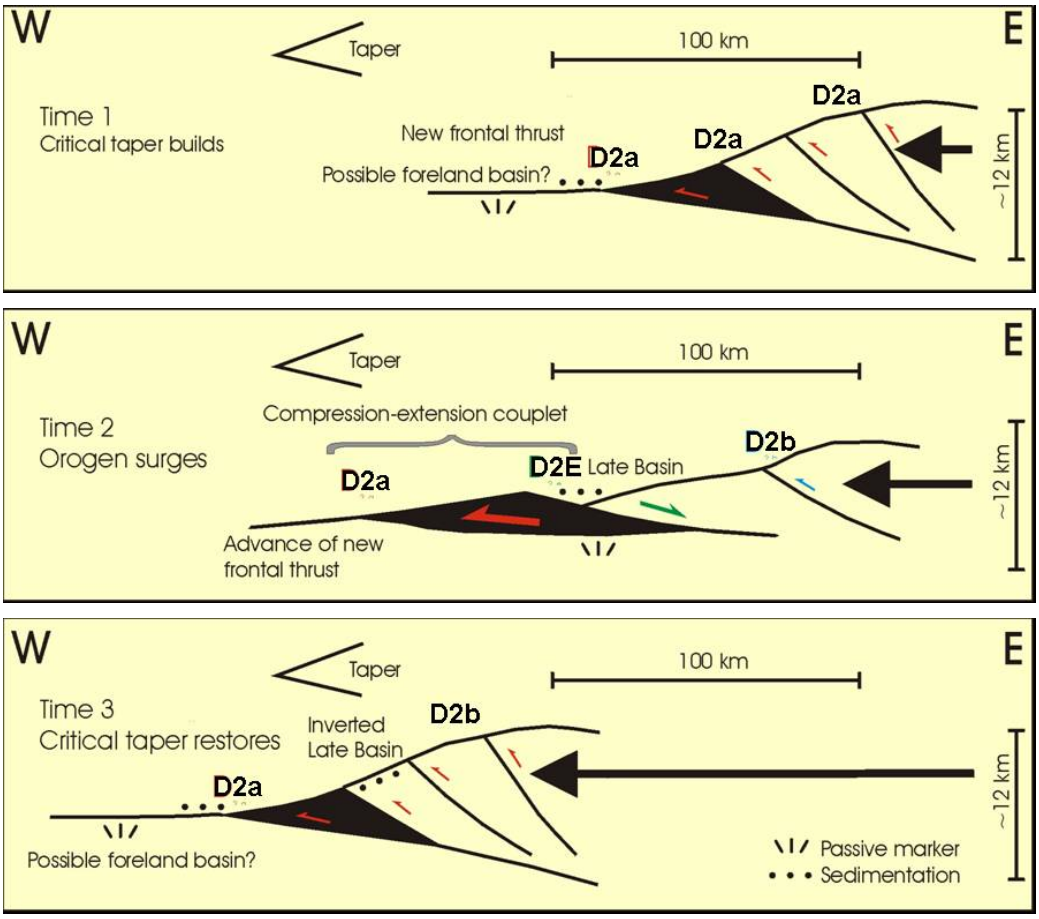

Figure 1: Three schematic drawings (Time1; Time 2; Time 3) depicting the ***D_{2a}, D_{2E}, D_{2b}*** *process through time within the upper crust*

Geochronological evidence within the 'late basins' indicate that individual basins across the Yilgarn Craton young to the west, implying that the process of tectonic switching occurred several times, and is in fact diachronous across the region (Blewett et al., 2004b). This process requires significant interaction between the middle and upper crust during broadly west-directed thrusting. Extensive shortening (>30%) of the middle-crust is represented in the deep seismic line (Figure 2) as a series of large imbricate thrust wedges, working semi-autonomously from the lower and upper crust and separated by what could be broadly referred to as roof and floor thrusts.

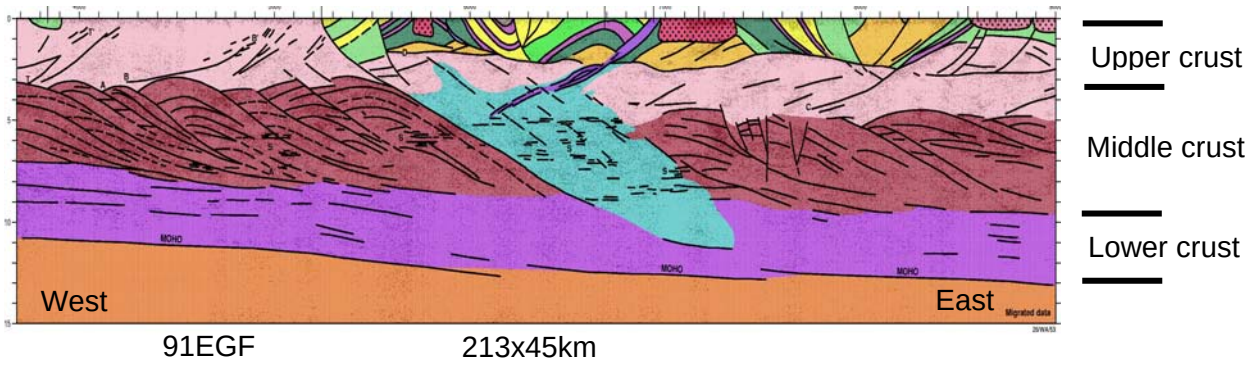

Figure 2: Image of the 91EGF seismic line through the Eastern Goldfields Province displaying variable deformation character at three different levels in the crust.

Roof and floor thrusts (low angle shear zones – LASH's) first identified by Goleby et al. (2002) between the middle crustal imbricates and the lower and upper crust, facilitate the variable vertical character of observed deformation through the whole crust. They allow individual components (upper-middle-lower) of the crust to operate semi-autonomously. Shortening within the middle crust had significant effects on the deformation experienced within the upper crust, creating subsequent uplift that propagated westward across the craton.

Explanation of the process

It is relatively simple to envisage the tectonic surge process happening once in isolation, although it is not the case in the Yilgarn, with the tectonic switching process (contraction and extension) occurring several times. We invoke the idea that the middle-crust thickens beneath the upper-crust and, hence, develops a topographic front (topographic high) whereby σ1 can switch to sub-vertical at a critical stage of crustal uplift. As the thrust front within the middle crust propagates westward, it piggybacks (elevates and compresses, '$\mathbf{D_{2b}}$') the newly formed 'late basins', while continuing to construct a new frontal wedge within the upper crust that will subsequently be thrown into extension via the surge process again (switching the σ1 stress field from sub-horizontal to sub-vertical). Propagation via this process from east to west explains the diachronous ages observed in the 'late basins' and possibly associated granites, syenites and lamprophyre sequences, and produces a way of explaining the tectonic process in 4D.

Fluid focusing

Pre-existing structural weaknesses in the upper crust would play a part in both fluid flow and the orientation of reactivated structures. Therefore understanding the nature of these structures prior to the deformation of D_2 is important. Unfortunately little is known about the orientation and location of extensional structures due to extensive tectonic overprinting and the lack of detailed regional sedimentological and metamorphic studies. Pre-D_2 structural weaknesses and their propensity to be reactivated may provide fluid pathways that could be utilized during subsequent deformations.

Interpretations of seismic reflection data within the Kalgoorlie-Ora Banda and Leonora-Laverton regions have identified low-angle domical shears (LASH's – roof thrust of the middle-crust) within the gneissic basement, interpreted as D_1? or D_2 thrust surfaces. Along east-west oriented seismic lines, these LASH's are clearly folded into broad antiforms and locally disrupted (interpreted to reflect continued D_2 contraction - $\mathbf{D_{2a}}$, $\mathbf{D_{2b}}$). Detailed 3D modelling of both east-west and north-south seismic lines in the Kalgoorlie-Ora Banda region shows that these LASH's are also folded in a north-south direction ($\mathbf{D_3}$), producing a pronounced dome and basin interference pattern or topography. A number of important deposits (e.g., Kanowna Belle, Golden Mile) are located in the region above these domes, suggesting a relationship between domes and gold mineralization. Late structural breaches ($\mathbf{D_4}$-$\mathbf{D_5}$) of the domes associated with deformation may allow focussing of gold rich fluids within the domical structures to migrate into zones of mineralization, via a similar mechanism to oil migration. The seismic reflections

associated with these domes clearly indicate they are located within the gneissic basement and not associated with the base of greenstone, posing questions as to why there is a significant velocity contrast within coherent gneiss. One hypothesis is that their initial formation was due to shearing along the brittle-ductile transition zone (zone between upper-crust and mid-crust) and possibly facilitated by focussed fluids.

The LASH's display a complex structural history and are now clearly at a much higher crustal level due to erosion following several orthogonal deformations. One example is the domical shear beneath Kanowna Belle. It is a dome approximately 30km across with depths ranging from 4km in the centre to 9km at its margin. Although varied, metamorphic grade indicates that 5-8km of material has been eroded, placing the LASH's close to the brittle ductile transition during their formation. The presence of vertically stacked LASH's, if produced at the brittle-ductile transition as suggested, can be then used to provide relative histories of uplift and burial for the region. Seismic reflection data were critical in identifying these features and, while the solid geology does not clearly represent these features, there are broadly identifiable long-wavelength east-west trending regional folds (**D_3**).

Predictions

There is debate about whether gold is early or late, or both (*cf.* Bateman et al., 2001; Groves et al., 2000). We predict that gold is 'early' and related to mode switching and integrally related to the late basins and intrusive events (e.g. Fimiston lodes). Gold is also 'late' and is associated with the development of a domical fluid-metal system, through several superimposed orthogonal events (e.g. Mt Charlotte, Kanowna Belle). On breaching by late-stage faults, a highly focussed fluid/metal is effectively transferred to a trap (=deposit).

References

Bateman, R.J., Hagemann, S.G., McCuaig, C., T.C. and Swager, C.P., 2001. Protracted gold mineralization throughout orogenesis in the Kalgoorlie camp, Yilgarn Craton, Western Australia: Structural, mineralogical, and geochemical evolution. Geological Survey of Western Australia Record 2001/17, 63-95.

Blewett, R.S., Cassidy, K.F., Champion, D.C., Henson, P.A. and Goleby, B.R., 2004a. Episodicity of Archaean Tectonics: An Orogenic Surge Model for the Eastern Yilgarn Craton. In: McPhie, J. and McGoldrick, P. (eds), Dynamic Earth: Past, Present and Future. Geological Society of Australia, Abstracts, 73, 146.

Blewett, R.S., Cassidy, K.F., Champion, D.C., Henson, P.A., Goleby, B.S., Jones, L. and Groenewald, P.B., 2004b. The Wangkathaa Orogeny: an example of episodic regional 'D_2' in the late Archaean Eastern Goldfields Province, Western Australia. Precambrian Research, 130, 139-159.

Goleby, B., Blewett, R.S., Champion, D.C., Korsch, R.J., Bell, B., Groenewald, P.B., Jones, L.E.A., Whitaker, A.J., Cassidy, K.F. and Carlsen, G.M., 2002. Deep seismic profiling in the NE Yilgarn: insights into its crustal architecture. Australian Institute of Geoscientists Bulletin, 36, 63-66.

Groves, D.I., Goldfarb, R.J., Knox-Robinson, C.M., Ojala, J., Gardoll, S., Yun, G.Y. and Holyland, P., 2000. Late kinematic timing of orogenic gold deposits and the significance for computer-based exploration techniques with emphasis on the Yilgarn Block, Western Australia. Ore Geology. Reviews, 17, 1-38.

Lister, G.S., Forster, M.A. and Rawling, T.J., 2001. Episodicity during orogenesis. In: J.A. Miller, R.E. Holdsworth, I.S. Buick, and M. Hand (eds.), Continental reactivation and reworking Geological Society of London Special Publications, 184, 89-113.

Swager, C.P., 1997. Tectono-stratigraphy of late Archaean greenstone terranes in the southern Eastern Goldfields, Western Australia. Precambrian Research, 83, 11-42.

Using 3D 'map patterns' to elucidate the tectonic history of the Eastern Yilgarn

P. A. Henson[1], R.S. Blewett[1], D.C. Champion[1], B.R. Goleby[1] and K.F. Cassidy[2]

*[1] pmd*CRC, Geoscience Australia, GPO box 378, Canberra ACT 2601*
*[2] pmd*CRC, Geoscience Australia, c/-GSWA, 100 Plain St, East Perth, WA 6004*

Paul.Henson@ga.gov.au

The widely accepted tectonic history of the Eastern Yilgarn Craton, WA involves D_e extension, D_1 (N-S) thrusting and recumbent folding, D_{2E} (E-W extension), D_2 upright folding, and later D_3-D_4 strike-slip faulting (Swager, 1997 and references therein). Careful examination of 2D map patterns shows that this paradigm has a number of inconsistencies (Blewett et al., 2004a, 2004b). The process of building a 3D map of the Kalgoorlie-Kambalda region has meant that these inconsistencies must be accounted for if we are to understand the processes that led to the formation of the architecture (fluid flow pathways), and the drivers of fluids flow.

The process of building a 3D map has a degree of rigour far beyond that of a 2D map. In the past, geologists 'hid' problems under the "yellow bits" of a map (Qa). The advent of routine potential field geophysics meant that the cover was 'stripped' and a new quantum of relationships and understanding was revealed by the process of interpreting a solid geology map of the area. A similar quantum of advance of understanding occurs during the act of taking a 2D solid geology map and building a 3D map from it. One can no longer 'hide' one's problems at depth, because every map feature has a clear relationship in time and space with adjacent features. Unlike a 2D solid geology map, in a 3D map a linear fault becomes a plane that intersects other planes, and a map unit polygon becomes a rock volume.

In the Eastern Yilgarn, we have merged our own, published and industry solid geology maps into a seamless coverage and using the extensive seismic reflection data, magnetic and gravity data (and their derivatives such as worms), and drawn a series of regional geological cross sections (tested by potential-field models) to build a new model. The process has posed many questions and provided some answers regarding the deformation event history as it was understood (paradigm). This contribution outlines some of the more important questions and answers that have been unearthed. It also poses some hypotheses and appropriate tests for unanswered questions.

De and initiation of the Kalgoorlie-Kambalda dome?

In building the 3D map, it is apparent that there are significant changes in stratigraphy, especially the so-called **upper** basalt. These units were described by Swager and Griffin (1990), and were used partly to subdivide the Kalgoorlie region into a number of terranes or domains. Conners et al. (2002) suggested that the stratigraphic variations in the thickness of the **lower** basalt were north to south in the Kambalda area, and possibly controlled by N-S extension (D_e?). To the north in the Leonora and Laverton region, Williams (1993) and

Hammond and Nesbit (1992, 1993) suggested that extension was ~N-S and associated with the exhumation of the granite domes as well as deposition of the greenstones themselves.

Hammond and Nesbit (1993) posed three important and related questions regarding the early extensional events:

1.Was there a single regional detachment that has been now segmented;

2.Are there a series of separate extensional or basin-forming events, and;

3.Did extension occur during a single brief episode, or was it diachronous over a considerable period of time?

We can add the following questions to Hammond and Nesbit's list:

1.Can the inferred N-S extension explain the east to west changes in basalt stratigraphy; or does it relate to an E.W. external event and;
2.Have these early shear zones 'set' the tectonic grain for all subsequent events, especially the main 'D_2' event?
3.Are the D_1 structures in fact D_e ones?

Do we have any answers to these fundamental questions?

Map patterns around the Scotia-Kanowna dome show that the boral units of the Black Flag Group down cuts the entire upper basalt to the komatiite stratigraphic level. This 'unconformity' (as it is shown) is not accounted for by the paradigm. Could this be an example of extensional excision of the upper basalt, with large-scale extension occurring within what is traditionally lumped as the Black Flag Group (Spargoville Formation of Krapež et al., 2000). This observation does not tell us much about the extension direction, but it does provide timing information. It suggests that extension at ~2675 Ma may have occurred in the Kalgoorlie region, as reflected by the major unconformity at the top of the Spargoville Formation (Krapež et al., 2000). In support of a significant extensional event at around 2675 Ma, high-grade gneisses and their associated fabrics were exhumed rapidly, because relatively undeformed or unmetamorphosed granites cross cut the gneissic fabrics and their ages, although younger, are within error. (Champion, unpublished GA data).

The implications of this are that at least part of the excision is structural and later than the deposition of the lower parts of the Kambalda Group stratigraphy, and therefore stratigraphic thickness changes may not be solely a function of growth fault development.

Where and what is D1?

Why is it important to find D_1? Firstly, because a number of important deposits (e.g., Kanowna Belle, Golden Mile) are located within domal structures in the host greenstones, and above domal shear zones sited in the underlying gneissic crust (Henson et al., 2004). Such a geometrical coincidence may imply a genetic relationship between greenstone and 'basement' domes and gold mineralisation. Secondly, in order to restore the greenstone sequences to their depositional positions we need to ascertain whether D_1 was a N-S contractional and not an extensional (part of D_e) event.

The development of the domes was the product of the positive interference of N-S trending folds with E-W trending folds (Type I interference or dome-and-basin map patterns). If domes and gold are related, then both the relative and absolute timing of the interfering fold events is critical to understanding the mineral system. Typically, the N-S folding is envisaged to be a D_2 event, so the question is: do these F_2 folds overprint E-W folds (F_1), or

are they overprinted by E-W folds (D_3)? Either way, the pattern is the same, but the timing is quite different.

As discussed above, the N-S antiformal structure of the Kalgoorlie to Kambalda corridor could have been initiated during D_e extension, and further tightened during D_2 inversion of this geometry. This aspect of the timing does not change the basic geometry, although its recognition may be important if can be shown that there was a syn-extensional gold event (e.g., Williams et al., 1989).

What is the evidence for ~N-S contraction? Based on examining the 3D map patterns, the following observations can be made:

1.The N-S seismic reflection lines show marked long-wavelength undulations of the detachment. This suggests that the detachment is broadly folded about ~E-W axes.
2. Similarly, there are long-wavelength periclinal plunges to most of the F_2 folds in the Kalgoorlie region, reflecting an open folding about ~E-W axes. These folds overprint all of the greenstone stratigraphy and granite domes, illustrating that at least one N-S shortening event was late, that is post late-basins.
3. The 'classic' D_1 thrusts which repeat stratigraphy at Kanowna-Belle (Fitzroy thrust) and also at Kambalda (Tramways and Republican thrusts) all cut F_2 regional folds and or overprint the main S_2 foliation.

Based on observations in the Kalgoorlie region at least, the evidence for significant D_1 thrust duplication of stratigraphy is weak. Furthermore, the use of komatiites as a regional marker is questionable, especially if they can be shown to be intrusive as well extrusive. Many of the F_{2a} folds deform earlier structural elements, but can these folds and fabrics be unequivocally demonstrated to be a function of D_1 compression or are they a result of D_e extension?

We describe this post-D_2 deformation event of ~N-S (NW-SE) compression as D_3 (Henson et al., 2004), which is interpreted to be the same event that controls mineralisation at Kambalda (e.g., Gressier & Kolkert, 2002). This suggests that if a domal structural control was important for gold mineralisation, then this mineralisation event was late.

Are the late basins pre-D2 strike-slip basins, or syn- D2 inverted thrust basins?

Until recently, there were two published views regarding the formation of the late basins, which include the Kurrawang, Merougil, Penny Dam, and Pig Well-Yilgangi basins. Swager (1997) suggested that they were associated with a post D_1 and a pre D_2 extensional event before the major D2 thrusting and folding event. Krapež et al. (2000) suggested that they also occupied the time between D1 and D2, but were the result of an unnamed (unassigned) strike-slip event.

In contrast, Blewett et al. (2004a) suggested that the broadly E-W compressional event (D_2) was more complex and significant to mineralisation than previously interpreted (Henson et al., 2004). Primary evidence for rejecting the previous two hypotheses is apparent in the 2D map patterns as well as the seismic reflection data (not available to the previous workers at their time of writing). The late basins are herein considered to have developed during a complex episodic process involving switching of compression and coaxial extension between ~2665 and ~2655 Ma ('D_2' = **D_{2a}, D_{2E}, D_{2b}**) (Blewett et al., 2004a; Henson et al., 2004). The association of these basins with extensional magmatic rocks (e.g., porphyries, syenites, lamprophyres, and mafic granites), and their combined relationship with an 'early'

gold event (eg. Granny Smith), suggests that tectonic mode switching (see Henson et al.,2004) was an important process in mineralisation.

Seismic reflection profiles that intersect the Kurrawang and Pig Well-Yilgangi basins also show that the late basins have a complex relationship to 'D_2' structures. These profiles, combined with map patterns, show that the late basins do not have geometries consistent with strike-slip basins. For example, the Pig Well-Yilgangi basin is folded into a broad syncline (D_{2b}), but it overlies a pre-folded (D_{2a}) sequence in its basement. The Kurrawang basin has a central fault that is a splay from the west-dipping Zuleika fault near the basin's western margin. This fault has a thrust geometry (west over east) and it appears to have exposed a narrow window of Black Flag Group basement in the centre of the Kurrawang basin. The Kurrawang basin appears to consist of two synclines with a central faulted anticline (D_{2b}). These observations are key information needed to restore the late basins to a pre-folded (D_{2b}) position in order to understand the role that basinal fluids may have had on the 'early' gold event.

References

Blewett, R.S., Cassidy, K.F., Champion, D.C., Henson, P.A. and Goleby, B.R., 2004a. Episodicity of Archaean Tectonics: An Orogenic Surge Model for the Eastern Yilgarn Craton. In: McPhie, J. and McGoldrick, P., eds., Dynamic Earth: Past, Present and Future. Geological Society of Australia, Abstracts, 73, 146.

Blewett, R.S., Cassidy, K.F., Champion, D.C., Henson, P.A., Goleby, B.S., Jones, L. and Groenewald, P.B., 2004b. The Wangkathaa Orogeny: an example of episodic regional 'D_2' in the late Archaean Eastern Goldfields Province, Western Australia. Precambrian Research, 130, 139-159.

Gressier, J.M., and Kolkert, R., 2002. Structural controls on gold mineralisation of the Argo Deposit, Western Australia. Australian Institute of Geoscientists, Bulletin, 36, 72-74.

Hammond, R.L. and Nisbet, B.W., 1992. Towards a structural and tectonic framework for the Norseman-Wiluna Greenstone Belt, Western Australia. In: J.E. Glover and Ho S.E., eds., The Archaean–Terrains, processes and metallogeny. University of Western Australia, Geology Department and University Extension, Publication, 22, 39-50.

Hammond, R.L. and Nisbet, B.W., 1993. Archaean crustal processes as indicated by the structural geology, Eastern Goldfields Province of Western Australia. In: Williams P.R. and Haldane J. A., (eds.), Kalgoorlie 93–an international conference on crustal evolution, metallogeny, and exploration of the Eastern Goldfields. Australian Geological Survey Organisation Record 1993/54, 105–114.

Henson, P. A., Blewett, R.S., Champion, D.C., Goleby, B.R. and Cassidy, K.F., 2004. A Dynamic view of orogenesis and the development of the Eastern Yilgarn. this volume

Krapež, B., Brown, S.J.A., Hand, J., Barley, M.E. and Cas, R.A.F., 2000. Age constraints on recycled crustal and supracrustal sources of Archaean metasedimentary sequences, Eastern Goldfields Province, Western Australia. Evidence from SHRIMP zircon dating. Tectonophysics, 322, 89-133.

Swager, C.P., 1997. Tectono-stratigraphy of late Archaean greenstone terranes in the southern Eastern Goldfields, Western Australia. Precambrian Research, 83, 11-42.

Swager, C.P. and Griffin, T.J., 1990. An early thrust duplex in the Kalgoorlie-Kambalda greenstone belt, Eastern Goldfields Province, Western Australia. Precambrian Research, 48, 63-73.

Williams, P.R., 1993. A new hypothesis for the evolution of the Eastern Goldfields Province. In: Williams, P.R. and Haldane, J.A., eds., Kalgoorlie 93–an international conference on crustal evolution, metallogeny, and exploration of the Eastern Goldfields. Australian Geological Survey Organisation Record, 1993/54, 73-83.

Williams, P.R., Etheridge, M.A., Witt, W. and Swager, C.P., 1989. Gold potential of early shear zones near Leonora, WA. Bureau of Mineral Resources Research Newsletter, 10, 6-7.

3D structural model for northern Leichhardt River Fault Trough and adjacent Lawn Hill Platform, Mt Isa

P. A. Henson[1], George Gibson[1], Simon Debenham[1], Aleks Kalinowski[1], Mike Barlow[1], Avon McIntyre[1] & Laurie Hutton[2]

*[1]pmd*CRC, Geoscience Australia, GPO Box 378 Canberra ACT 2601*
[2]Queensland Department of Natural Resources and Mines, Block A, 80 Meiers Road Indooroopilly QLD 4068

Paul.Henson@ga.gov.au

Outline

A 3D map constrained from multidisciplinary datasets has been constructed for the Mt Isa, Western Succession, greatly improving our understanding of the tectonostratighaphic framework and mineral systems. 3D map input has come from three semi-autonomous work modules producing complementary data that can be viewed and analysed within the same georeferenced framework: (1) sedimentary basin analysis and sequence stratigraphy; (2) structural analysis allied with potential field modelling; and (3) PIMA-calibrated and ground-truthed remotely sensed imagery. Marrying these techniques within a single project has provided a powerful tool for geological interpretations, which have historically been conducted in isolation. This approach requires all interpretations to be geologically feasible, testable and internally consistent. The ultimate aim is an assessment of basin architecture and fault geometries and how these may have served to focus fluid flow at the time of regional alteration and mineralization. Initial emphasis has been on the Leichhardt Superbasin rather than the younger Calvert and Mt Isa Superbasins where NABRE conducted much of its research effort.

Depth constraints using potential field data

Potential field validation of serial structural cross-sections combined with structural readings and solid geology have been used to constrain depth and relative thickness of stratigraphic units. The 3D may also incorporates geological interpretations of steep gradients observed within the gravity field data. These gradients are believed to reflect major structures and/or faults that controlled the early basin architecture and sedimentation patterns. Early basin architecture (e.g. Myally Subgroup) and fault geometries have often been overprinted by younger structures, unconformably overlain by younger basinal sequences, and generally preserve little of the early rift geometry and basin architecture. Identification of the early structures and basin architecture is critical as without an understanding of the original basin template, it is difficult to comprehend let alone predict which structures and fluid pathways are likely to have been active during subsequent deformations. Inversion modelling of the aeromagnetic data has provided a constraint on depth to magnetic basement, highlighting a distinct division between the Mt Isa Western Succession and its eastern counterpart.

As part of the construction and understanding of basin architecture, magnetic and gravity data have been used to provide constraints beyond surface profiles. Typically perturbations on the gravity and magnetic fields are sourced from just a

couple of contrasting rock types, in this case Proterozoic volcanic units and granitic intrusions of various ages within the Leichhardt-Kalkadoon basement.

Up to now, potential field modelling has been undertaken on a 2-2.5 dimensional basis. These basin 'slices' are constructed from surface mapping and conceptual ideas of fault planes, sedimentary thicknesses and deformation regimes (Figure 1).

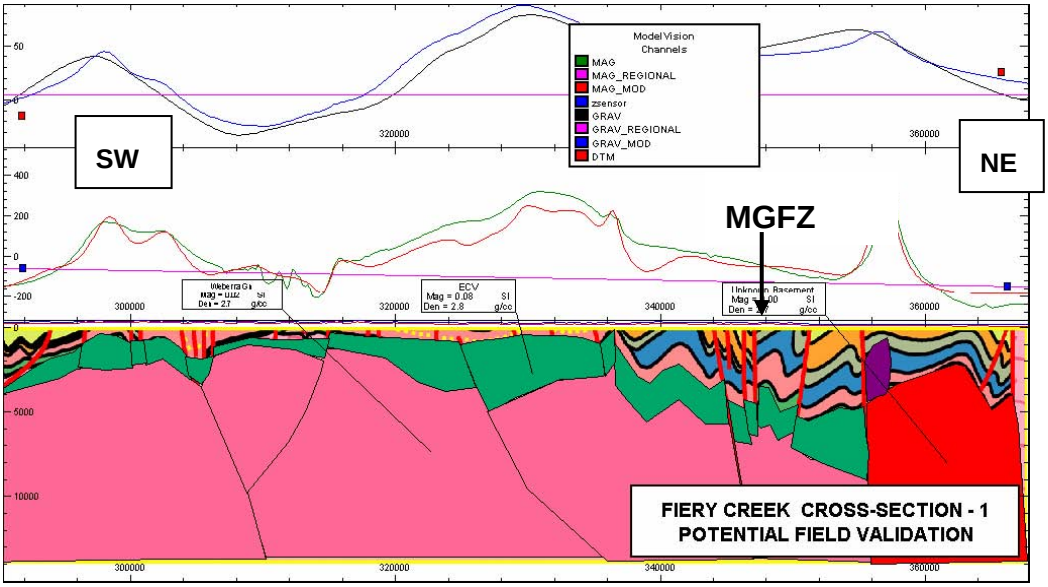

Figure1: Potential field validation of a serial cross-section using ModelVision

More recently the validation process has been extended to three dimensions through UBC's smooth model inversion, where the fit with the smoothest boundary conditions represents the optimal (or 'unique') solution (Figure 2).

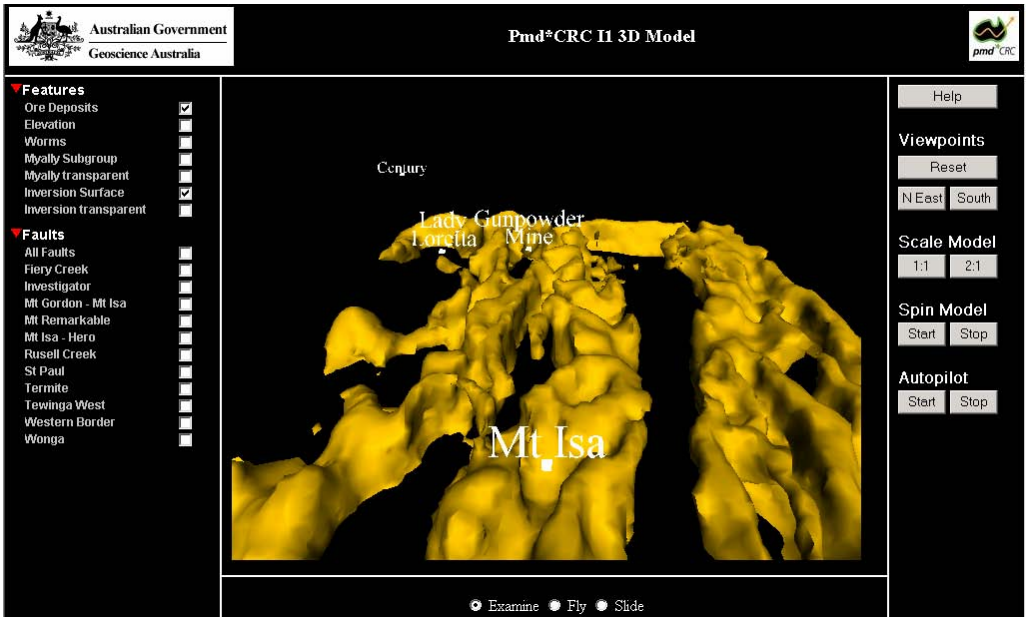

Figure 2: Image of the 3D inversion surface, derived from aeromagnetic data

Future work will incorporate boundary information and knowledge of fault planes to tightly constrain the inversion, with the final objective of independently testing our model construct for the Mt Isa Basin.

The combination of these techniques has highlighted relatively thin Eastern Creek Volcanics (ECV) beneath the sedimentary sequences in the Leichhardt River Fault Trough (cf. earlier suggestions). A corollary of this statement is that the Leichhardt-

Kalkadoon basement always lies at comparatively shallow depths beneath Mt Guide Quartzite and Eastern Creek Volcanics. These factors allow improved constraints on depth to basement to be built into the 3D map.

Re-orientation during D_2- D_3

The Leichhardt River Fault Trough (Western Succession) is dominated by a pronounced north-south oriented structural grain of late D_2-D_3 age, incorporating discrete high-strain zones (HSZ) separated by ~35km. These high strain corridors include the Mt Gordon Fault Zone (MGFZ), and serve as hosts to several major deposits (Mt Isa, George Fisher, Hilton and Gunpowder mines). Orthogonal east-west trending faults (i.e. Investigator Fault) exist between these HSZ's and locally preserve younger stratigraphic units of the Mt Isa Group (Bull Creek Syncline, Crystal Creek). In the Fiery Creek Dome region, the MGFZ delineates a major change in orientation of structural grain. Major faults north of the dome are mutually orthogonal, trending NW-SE (Termite Range Fault, which is thought to be genetically linked to the Century Mine) or NE-SW (e.g. Fiery Creek Fault). Additional evidence for reorientation can be drawn from vector analysis of the aeromagnetic 'worms'. They change orientation SE of the MGFZ and display a distinct flattening profile relative to those NW of the MGFZ.

One possible explanation of this change in structural trend is that the area SE of the MGFZ has, in fact, been rotated in a clockwise sense with respect to the area NW of the fault during a phase of dextral strike-slip, giving rise to a mega-kink. Removing this reorientation and restoring basin architecture to its original configuration at the time of Myally Subgroup deposition implies northwest trending growth faults were dominant and regional extension was broadly NE–SW (Figure 3).

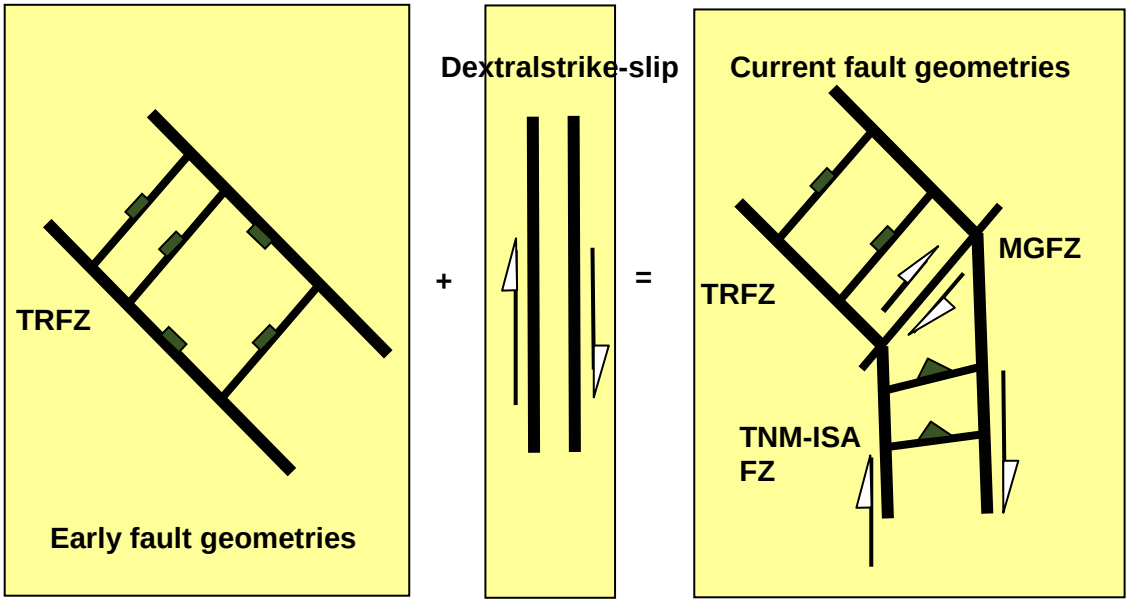

Figure 3: Schematic illustration displaying early fault geometries and the effects of imposing a late dextral strike-slip system to it: Termite Range fault zone (TRFZ), Mount Gordon Fault Zone (MGFZ), Twenty-nine mile and Mt Isa Fault Zone (TNM-ISAFZ)

Field relationships indicate that the MGFZ contains both strike-slip and thrust geometries facilitated by dextral strike-slip faulting. Rotation and associated accommodation problems would therefore produce significant dilation and fracture induced porosity regionally during this event.

Initial basin forming growth faults: their implications for fluid flow and mineralisation

Sequence stratigraphy and the construction of regional 3D stratigraphic thicknesses for the Western Succession have confirmed and highlighted the location of early growth faults. Early extension (during Myally Group deposition) was NE-SW prior to the process of dextral rotation. Growth faults with NE-SW and NW-SE orientations were contemporaneous. Subsequent deformation reactivated these structures during the Isan Orogeny (D_1, D_2, and D_3) and, therefore, the location of early growth faults is aided by the identification of stratigraphic thickening and systematic facies variations towards structures. Structures may have been extensively re-orientated and folded, and in some cases obscured by younger overlying (cover) units that do not record the geometries of the underlying fault (blind faults). Early faults associated with basin formation display prolonged histories of reactivation and provide suitable pathways for the propagation of mineralised fluids during subsequent deformations. One example is the Paroo Fault, which is a folded, gently dipping structure that currently displaces the ECV's in a normal sense (Betts and Lister, 2002) and bears resemblance to an early growth fault that has been subject to subsequent deformation. In its hangingwall is the Mt Isa Pb-Zn-Cu system that has undergone two major episodes of mineralisation associated with hydrothermal fluids.

b_0 and illite crystallinity (IC) to determine the depth of burial and temperature

Metamorphic studies of the Western Succession are limited by the relatively low metamorphic grade and comparatively indifferent mineralogical response to changing metamorphic conditions. Changes in pressure-temperature conditions are nevertheless a critical aspect in understanding the structural evolution of the Leichhardt River Fault Trough through time. To address this issue and establish approximate thermal gradients for the basin during different deformational events both Illite crystallinity and white mica b_0 cell dimensions were measured for widely separated geographical localities. Illite crystallinity provides a crude temperature measure whereas b_0 provides an estimate of the peak pressure conditions (Sassi and Scolari, 1974). Both methods combine to produce pressure-temperature estimates for very low metamorphic grade rocks. b_0 and IC analyses have been obtained from both S_1 and S_2 fabrics. Further sample collection will be directed towards increasing sample density in regions where anomalous metamorphic variations have been identified.

Conclusions

Identification of early basin forming faults has provided additional understanding of the original basin architecture and associated fluid corridors. Geophysical interpretations gained from 'worm' interpretation, potential field modelling and inversion modelling have highlighted the distribution and geometry of units at depth. In addition, metamorphic studies are providing relative depths of burial through time which is helping to define the tectonic history of the region.

References

Sassi, F., Scolari, A., 1974. The b_0 value of the potassium white micas as a barometric indicator in low grade metamorphism of pelitic schists. Contributions to Mineralogy and Petrology, 45, 143-152.

Betts, P.G. & Lister, G.S., 2002. Geodynamically indicated targeting strategy for Shale-hosted massive sulfide Pb-Zn-Ag mineralization in the Western Fold Belt, Mt Isa terrane. Australian Journal of Earth Sciences, 49, 985-1010.

Komatiite alteration assemblages in the Kambalda Domain, Western Australia

M. Heydari, S. Hagemann and P. Neumayr
*pmd*CRC, Centre for Global Metallogeny, School of Earth of Geographical Sciences, University of Western Australia, Crawley, WA 6009*
mheydari@segs.uwa.edu.au

Introduction

The main objective of this PhD project is to investigate whether komatiite units were fluid and metal reservoirs for gold hydrothermal systems, through field, geochemical and isotopic studies of alteration mineral assemblages in key gold mineralised and unmineralised geologic settings of the Kalgoorlie-Kambalda domain. The working areas include Hannan Lake area south of the Golden Mile gold deposit, New Celebration gold deposits and Otter-Juan and Long-Victor nickel mine complexes in the Kambalda dome. The project aims to document various ultramafic alteration assemblages with respect to the mineralisation and structural elements in microscopic, macroscopic and domain scale.

Alteration assemblages

In the Kalgoorlie-Kambalda corridor, metamorphic and hydrothermal alteration events have produced a range of mineral assemblages in ultramafic rocks. Optical microscopy, quantitative X-ray analysis and carbonate staining methods were utilized to characterise the alteration phases. Chlorite, antigorite, chrysotile, magnesite, dolomite and plagioclase set in a granular to porphyroblastic texture are the most common alteration phases in the study areas. Serpentinisation is the earliest phase of alteration in the area. During this event nearly all of the primary olivine minerals have been replaced with antigorite or chrysotile. In the Hannan Lake area, the talc-dolomite assemblage has partly replaced clinochrysotile. Both field and microscopic timing relationships demonstrate the ingress of CO_2 fluids into an early chrysotile altered rock that has led to the formation of porphyroblasts and veins of magnesite and dolomite. The overall restriction of talc-carbonated komatiite occurrence to the vicinity of the major fault in the area suggests a structural control on carbonate alteration. In the Kambalda dome, despite the nearly complete carbonation of the western flank, remnants of incompletely carbonated komatiite are still preserved in the eastern flank (e.g. brecciation of early serpentinised komatiite due to influx of CO_2 rich fluids).

Stable isotope systematic of the carbonates in komatiite

A total number of 15 carbonate minerals in komatiite samples from the Otter-Juan nickel mine were analysed to demonstrate the carbon and oxygen isotope characteristics of alteration fluids (Figure 1). Ferroan calcite and dolomite were the main carbonate phases. The results show a relatively narrow $\delta^{13}C$ (PDB) range of carbonates in komatiites (-4 to –6‰). Although carbon isotope composition of metamorphic fluids can represent a wide variation depending on the redox conditions during their precipitation (Schandl and Naldrett, 1992; McCuaig and Kerrich, 1998), the results suggest similarity with the already recognized mantle-driven and structurally controlled carbonation (Groves et al., 1988).

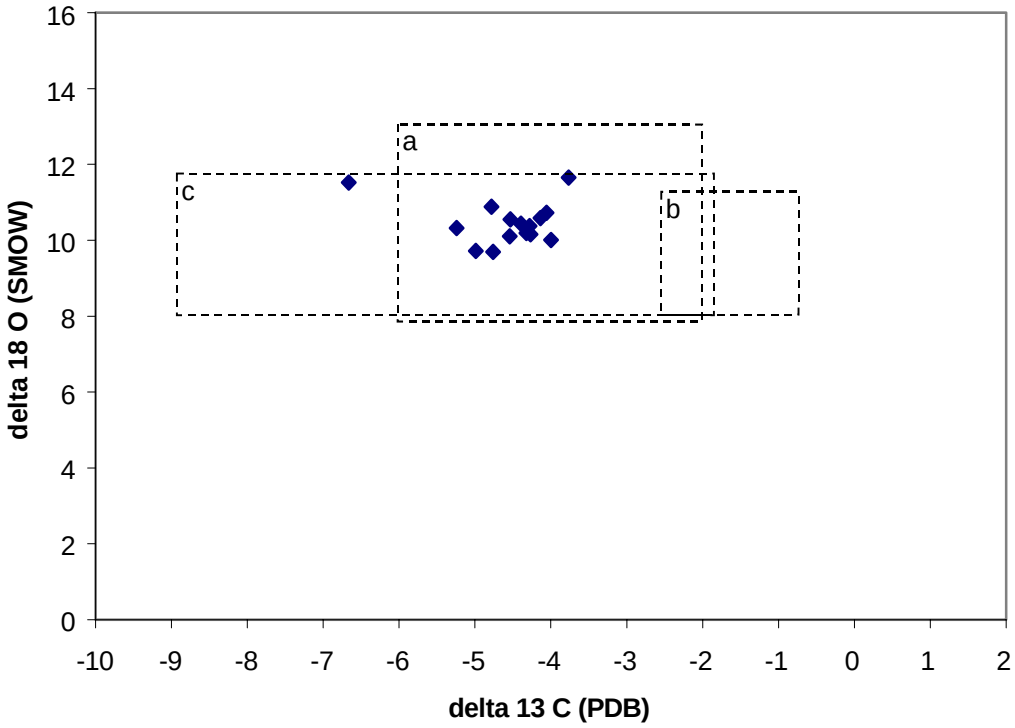

Figure 1. Oxygen and carbon isotope composition of carbonate minerals in komatiites from Otter-Juan mine, Kambalda with respect to

a: regional structurally controlled carbonation (Groves et al., 1988),

b: sea-floor alteration (Groves et al., 1988) and c: gold related alteration in St Ives gold camp (Y3 project results).

Preliminary results

Preliminary results of this study indicate that:

1. Based on the field and microscopic evidence, at least one phase of carbonation postdated the serpentinisation of komatiites.
2. The carbon isotope signature of carbonate minerals in the Kambalda samples is different when compared to those of sea floor alteration and suggests rather a mantle driven or magmatic source for the fluids.
3. There is a similarity in the carbon isotope composition of carbonates in the komatiites of this study with those in the St Ives lode gold deposits (Y3 project results).

References

Groves, D.I., Golding, Z.D., Rock, N.M.S., Barley, M.E., and McNaughton, N.J., 1988. Archaean carbon reservoirs and their relevance to the fluid source for gold deposits. Nature, 331, 254-257.

McCuaig, T.C. and Kerrich, R., 1998. P-T-t-deformation-fluid characteristics of lode gold deposits: Evidence from alteration systematics. Ore Geology Reviews, 12, 381-453.

Schandl, E.S. and Naldrett, A.J., 1992. CO_2 metasomatism of serpentinites, south of Timmins, Ontario. Canadian Mineralogist, 30, 93-108.

The structural, hydrothermal alteration and fluid evolution of the New Celebration lode-gold deposits: multiple deformation events and two stages of gold mineralization

Joanna Hodge[1], Sian Nichols[2], Steffen Hagemann[1] and Peter Neumayr[1]

*[1]pmd*CRC, Centre for Global Metallogeny, University of Western Australia, 35 Stirling Highway, Crawley, WA 6009*
[2]Harmony Gold Mining Co. Ltd., PO Box 2125, Boulder, WA 6432

hodgej02@segs.uwa.edu.au

Introduction

The Boulder segment of the Boulder-Lefroy fault zone, a first-order, trans-crustal fault system (Swager, 1989), hosts the Archean New Celebration lode gold deposits. Although first-order fault systems do host gold mineralization (e.g. Kerr Addison gold deposits in the Cadillac Tectonic Zone in Abitibi; Poulsen et al., 2000), second- and third-order fault systems are more typical hosts (e.g. Eisenlohr et al., 1989).

This study aims to: 1) quantify the P-T-X-fO_2-t conditions of fluids associated with different mineralizing events, and 2) constrain the fluids within deposit- and regional-scale tectonostratigraphic frameworks. New Celebration is a key location to evaluate fluid pathways and evolution, and provides valuable insights into the role regional scale structures play in focusing both mineralizing and non-mineralizing fluids.

Regional Geology

The New Celebration deposits are located approximately 35km southeast of Kalgoorlie in the Kambalda domain of the Kalgoorlie terrane of the Eastern Goldfields Province of Western Australia. The deposits are hosted within the Boulder segment of the Boulder-Lefroy Fault Zone, a trans-crustal fault system that forms part of the eastern boundary of the Kambalda domain. The Kambalda domain consists of a 6-9 km thick, elongate volcano-sedimentary sequence, which is metamorphosed to upper greenschist-lower amphibolite facies and bounded to the east and west by wide (up to 1km), NNW-trending anastamosing shear zones (Swager and Griffin (1990).

Lithostratigraphy of the New Celebration deposits

The stratigraphic sequence at New Celebration consists of a basal komatiite overlain by a strongly differentiated mafic unit, intruded by a number of plagioclase and quartz-feldspar porphyries and minor lamprophyres. Apart from the felsic intrusions, all rocks seen at New Celebration are metamorphosed to upper greenschist facies.

Structural and magmatic evolution

Nichols (2003) identified three main deformation events at New Celebration, which are tentatively correlated with regional deformation events. The earliest deformation event ($D2_{NC}$) recognized at New Celebration is defined by vertically dipping conformable stratigraphic contacts such as those between the sub-units of differentiated dolerites and represents regional D2, NNW-striking upright folds of Swager (1989) and Swager and Griffin (1990). Penetrative NNW-trending shear foliation in mafic and ultramafic rocks, well-developed S-C fabric in mafic rocks and plagioclase-rich porphyry dykes, and mineral elongations, S-C intersection lineations and slickenline lineations observed in the open pit define $D3_{NC}$. The S3 foliation has an average orientation of 82° towards 260°

and 87° towards 29°, which represent S- and C-foliation planes, respectively. The $D3_{NC}$ tentatively correlates with regional ENE-WSW shortening, and sinistral strike- and dip-slip faulting of Swager (1989) and Swager and Griffin (1990). Penetrative S- (81° towards 312°) and C- (58° towards 292°) foliation observed in the ultramafic footwall and the mafic hanging wall and NNW dipping structures that crosscut $S3_{NC}$ shear foliation in the pit represent $D4_{NC}$. Late curviplanar faults that crosscut all other structures are assigned to D_{4+nNC}

Nichols (2003) distinguished two magmatic events at New Celebration, based on mineralogy, deformation style and crosscutting relationships. Early, intensely altered, plagioclase-rich M_1 porphyries have a penetrative $S3_{NC}$ foliation and later, weakly hydrothermally altered, M_2 quartz-feldspar porphyries are unfoliated and preserve primary igneous textures. The north-northwest trending $S3_{NC}$ foliation observed in the surrounding mafic and ultramafic rocks wraps around the late porphyries. The development of $S3_{NC}$ deformation fabrics in M_1 porphyries, their lack in M_2 porphyries and the presence of brittle fracture networks on the M_2 porphyry margins suggest that emplacement of both intrusion types occurred during $D3_{NC}$, but at different times within the same deformation event and under changing tectonic conditions.

Gold mineralization and hydrothermal alteration

Evidence from open pit mapping, diamond core logging, detailed geochemistry, and petrography indicates that komatiite, differentiated, metamorphosed dolerite and porphyry dykes host gold mineralization at New Celebration. Nichols (2003) identified two gold mineralizing events and four mineralization styles at New Celebration. The early gold event consists of Mylonite- and Porphyry-style mineralisation and late gold consists of Contact- and Fracture-style mineralization.

Early gold mineralization

Quartz-ankerite-biotite-sericite mylonite hosts Mylonite-style mineralization. Gold either occurs as round inclusions in euhedral, zoned, “dirty” pyrite, also containing other sulfides (galena) and tellurides (calaverite, petzite), or as fine-grained anhedral disseminated grains within silicate. Distal alteration consists of bio-ser-ank-±py±mt whereas proximal alteration comprises ank-bio-py±ser (Nichols, 2003).

Plagioclase-rich porphyry dykes (M_1) host Porphyry-style mineralization. All M_1 dykes are pervasively alb-bio-py-ank±ser altered. Accessory sulfides (chalcopyrite, galena), oxides (hematite, magnetite), phosphates (monazite) and tellurides (hessite, altaite, melonite and tetradymite) also occur (Nichols, 2003). Pyrite hosts gold as rounded inclusions or along grain fractures. Disseminated gold also occurs along albite grain boundaries adjacent to pyrite.

In both early mineralization styles, pyrite predominantly hosts gold. Pyrite is aligned parallel to $S3_{NC}$ foliation planes. Ankerite and hydrothermal quartz pressure shadows are developed at pyrite grain margins, which indicates pyrite and gold were deposited prior to, or contemporaneous with, $D3_{NC}$ deformation (Nichols, 2003).

Late gold mineralization

The high-Mg basalt-M_2 porphyry contacts host Contact-style gold mineralization. Contact-style mineralization has a well-developed alteration halo, which consists of a distal ank-bio-chl zone with accessory mt, an outer proximal ank-bio-ser zone and an inner proximal ank-ser zone. Abundant coarse-grained pyrite immediately adjacent to the contact is characteristic. Gold forms inclusions in pyrite or along pyrite grain boundaries, and within disseminated pyrite along foliation planes in the high-Mg basalt (Nichols, 2003).

Thin (1-2mm wide) fractures filled with hydrothermal alteration minerals are developed at the margins of M_2 quartz-feldspar porphyries and host Fracture-style mineralization.

Distal alteration consists of widespread (>20m) pervasive ank-ser alteration whereas proximal alteration consists of py-ser-ank restricted to the fracture fill. Pyrite hosts gold as inclusions or along grain boundaries (Nichols, 2003).

Vein Paragenesis

Preliminary investigations indicate that the New Celebration vein system consists of (Table 1): (1) syn-$D2_{NC}$ veins that developed prior to the early gold event; (2) $D3_{NC}$ veins which predate early gold mineralization; (3) $D3_{NC}$ syn-early gold veins; (4) $D4_{NC}$ veins which predate late-stage gold mineralization; and (5) $D4_{NC}$ veins synchronous with late-stage gold mineralization.

$D2_{NC}$ Veins

Type 1 $D2_{NC}$ veins consists of foliation-parallel quartz-calcite "boudins" which are only observed in mylonites and strongly foliated M_1 feldspar porphyries. Quartz and calcite grains within pre-$D3_{NC}$ veins show dynamic recrystallization by grain boundary migration (Passchier and Trouw, 1996). Grain boundaries are commonly highly irregular and bulge into adjacent grains. Calcite twins typically terminate before grain boundaries. Undulose extinction and lattice-preferred orientation in quartz grains suggest recrystallization by sub-grain rotation (Passchier and Trouw, 1996).

Table 1: Summary of the geological characteristics of the New Celebration vein system

Deformation Event	Vein Generation	Host Rock	Vein Type	Mineralogy	Width	Structure	Alteration Halo
$D2_{NC}$	Pre-gold veins -Early gold event	Bio-ank mylonites, M1 plg porphyries	1	qtz, cb	200-1200µ	Foliation parallel deformed quartz boudins	Ankerite?
$D3_{NC}$		Bio-cb mylonites, chl schists	2	qtz, cb	400-2000µ	Zoned veins, cross-cut by foliation	Ankerite
$D3_{NC}$		Mafic, ultramafic chl-cb schists	3	cc	400µ	Thin veins, cross-cut By foliation	None
$D3_{NC}$	Syn-gold veins -early gold event	M1 plg porphyry	4	qtz, cc, py,	600-2400µ	Foliation sub-parallel. Biotite edges veins	Ankerite
$D4_{NC}$	Pre-gold veins -Late gold event	M2 fsp-qtz porphyry	5	qtz, (cb, ser)	400-4000µ	Buck quartz, forms vein breccia arrays	None
$D4_{NC}$	Syn-gold veins -late gold event	M2 fsp-qtz porphyry	6	ser, chl, py	20-200 µ	Thin fracture veinlets	None

Abbreviations: ank – ankerite; bio – biotite; cb – carbonate; cc – calcite; chl – chlorite; plg – plagioclase; py – pyrite; qtz - quartz

$D3_{NC}$ Veins

Types 2 and 3 veins consist of quartz-calcite and calcite-only veins, and have developed oblique to foliation. The veins and the foliation exhibit mutually crosscutting relationships. These veins predominantly occur within mylonites, and mafic and ultramafic schists. Partial recrystallization of quartz has occurred where foliation planes crosscut the veins. In these areas, quartz grains have irregular grain boundaries, show sub-grain development and exhibit undulose extinction, indicating they have undergone dynamic recrystallization. The M_1 feldspar porphyries host type 4 veins, which are predominantly composed of quartz and calcite with accessory pyrite and are surrounded by a wide ankerite alteration zone. Zoned, inclusion-rich pyrite often clusters along vein selvedges. Grains typically exhibit a "dirty", inclusion-rich core surrounded by a "clean", inclusion free rim. Inclusions typically comprise abundant silicates, minor sulfides (galena, sphalerite) and rare gold. Quartz grains within the veins have undergone partial dynamic recrystallization by grain boundary migration and sub-grain rotation. Sub-grain development is minor, and predominantly concentrated along the vein edge. Relict grains exhibit undulose extinction and lattice-preferred orientation.

$D4_{NC}$ veins

Type 4 veins consist of quartz, calcite and sericite. The veins are composed almost entirely of coarse-grained clear quartz overprinted by accessory calcite and rare sericite. The veins locally form breccias within M_2 quartz-feldspar porphyries. Quartz within type

4 veins show evidence of dynamic recrystallization by grain boundary migration. Evidence for this includes diffuse and highly irregular grain boundaries.

Type 5 late gold event-related veins are composed of sericite, chlorite and pyrite and form thin stringer veins. These veins only occur in M_2 quartz-feldspar porphyries. Where the $D4_{NC}$ veins crosscut the earlier quartz breccia, they have generally developed along the quartz grain boundaries. Pyrite occurs as large subhedral to euhedral grains or as aggregates of fine subhedral to euhedral crystals, and commonly contains abundant silicate and sulfide inclusions. Pyrite hosts gold as rounded inclusions and localized gold occurs along pyrite grain boundaries.

Preliminary Fluid Inclusion Data

Detailed fluid inclusion petrography on primary, pseudosecondary and secondary fluid inclusions trapped in type 2 qtz-cb veins in Mylonite-style and type 5 qtz veins in Fracture-style samples revealed five inclusion types: (1) dark, irregularly shaped single-phase inclusions, possibly CH_4; (2) two-phase, clear, ovoid liquid-rich inclusions; (3) clear, rounded vapour-rich two-phase inclusions; (4) darkish, irregularly shaped, three-phase H_2O-CO_2 inclusions; and (5) clear, irregularly shaped, three-phase liquid-vapour-solid inclusions. A fluid inclusion assemblage consisting of types 1 and 2 occur in clusters of primary inclusions in quartz grains within $D2_{NC}$ quartz boudins. Quartz within the boudins has likely been recrystallized, based on petrographic evidence, therefore, the fluid inclusion assemblages may represent $D3_{NC}$ fluids and not the original $D2_{NC}$ vein-forming fluids. Types 1, 2, 3 and 4 form a fluid inclusion assemblage that occurs in primary clusters and pseudosecondary trails in $D3_{NC}$ qtz-cb veins. Primary inclusion clusters occur in quartz grains immediately adjacent to gold-hosting pyrite crystals, whereas pseudosecondary inclusion trails occupy fractures that parallel foliation planes, which crosscut Type 2 qtz-cb veins. Inclusion types 1 through 5 consist of a fluid inclusion assemblage that occurs as primary clusters in $D4_{NC}$ gold-hosting quartz veins.

Preliminary Sulfur Isotope Results

Bulk sulfur isotope analysis of pyrite from 10 representative samples from the four mineralization styles reveals distinctly different $\delta^{34}S$ wrt CDT signatures that do not overlap significantly. The values range from -7.12‰ $\delta^{34}S$ wrt CDT from Fracture-style mineralization, to +2.03‰ $\delta^{34}S$ wrt CDT from Mylonite-style mineralization.

Further Work

Planned work includes further detailed fluid inclusion petrography, microthermometry, Laser Raman analysis and LA-ICP-MS analysis to constrain the P-T-X-fO_2-t conditions of the hydrothermal fluids associated with the evolution of the New Celebration gold deposits. Further work also includes dating of hydrothermal monazite, $^{40}Ar/^{39}Ar$ dating of pyrite and Pb-Pb step leaching of sulfides and oxides to establish the timing of different mineralizing events, and further detailed in situ sulfur isotope analysis to constrain redox conditions and fluid sources.

References

Eisenlohr, B.N., Groves, D.I. and Partington, G.A., 1989. Crustal scale shear zones and their significance to Archaean gold mineralization in Western Australia. Mineralium Deposita, 24, 1-8.

Nichols, S., 2003. Structural Control, Hydrothermal Alteration and Relative Timing of Gold Mineralization at the New Celebration Gold Deposits, Kalgoorlie, Western Australia. BSc (Hons) thesis, University of Western Australia, Crawley, WA.

Passchier, C. W. and Trouw, R. A. J., 1998. Microtectonics. Springer, Berlin, 289 p.

Poulsen, K.H., Robert, R. and Dube, B., 2000. Geologic classification of Canadian gold deposits. Geological Survey of Canada, Bulletin 540, 106p.

Swager, C.P., 1989. Structure of Kalgoorlie greenstones-regional deformation history and implications for structural setting of the Golden Mile deposits. Geological Survey of Western Australia Report 25, 59-84.

Swager, C. P. and Griffin, T. J., 1990. Geology of the Archaean Kalgoorlie Terrane, (northern and southern sheets): Western Australia Geological Survey, 1:250,000 Geological Map.

4D visualisation: bringing animation to geoscience

A.A. Kalinowski[1], P.A. Henson[1], R.S. Blewett[1], D.C. Champion[1], B.R. Goleby[1] and K.F. Cassidy [2]

*[1] pmd*CRC, Geoscience Australia, GPO box 378, Canberra ACT 2601*
*[2] pmd*CRC, Geoscience Australia, c/- GSWA, 100 Plain St, East Perth, WA 6004*
Aleks.Kalinowski@ga.gov.au

Animation in geology

Using a three dimensional animation package more commonly applied to the games and entertainment industry, we have created a four dimensional movie (3D plus time) demonstrating new concepts related to the tectonic evolution of the Eastern Goldfields. In particular, we targeted two critical facets of the tectonic processes responsible for the development of the gold mineral system(s). Firstly, we visualise the switching of tectonic regimes from compression to extension (orogenic surge and 'early' mineralisation); and secondly the formation and breaching of a domical detachment resulting in localisation of fluid flow and 'late' mineralisation. We aim to describe the process and benefits of working in four dimensions (3D animation). The science behind the animations is more fully explained in Henson *et al.* (2004), although, the concepts are briefly described here for completeness.

The science behind the movie

Orogenic Surge

This is a concept adapted from Lister et al. (2001) (Fig. 1) that explains the switching of tectonic modes from compression to extension during the E-W directed 'D2' shortening event in the Eastern Goldfields. The modified process both allows for multiple episodes of extension during a dominantly compressive regime and best fits the timing and features, specifically the late basins and associated granitoid, syenite, and lamprophyric intrusions observed in the Eastern Goldfields (Blewett et al., 2004a, b). The first movie is centred on demonstrating exactly how the surge process works to produce two compressive phases - D_{2A} and D_{2B} - separated by a phase of extension, D_{2E}. Essentially an unstable thrust wedge builds due to thrust stacking in the middle crust, at the thrust front on the overriding plate during collision (D_{2A}). At some point (D_{2E}) this wedge collapses over the foreland to produce long, N-S trending basins adjacent to inverted D_{2A} thrusts. The basins are then deformed and uplifted (inverted) as D_{2B} progresses through the same area and reactivates the extensional faults as thrusts. The modified process is illustrated in the storyboard that we developed for the animation (Fig. 2). The surge is important because it explains the relationship between 'early' gold, late basins, and deep-sourced magmas.

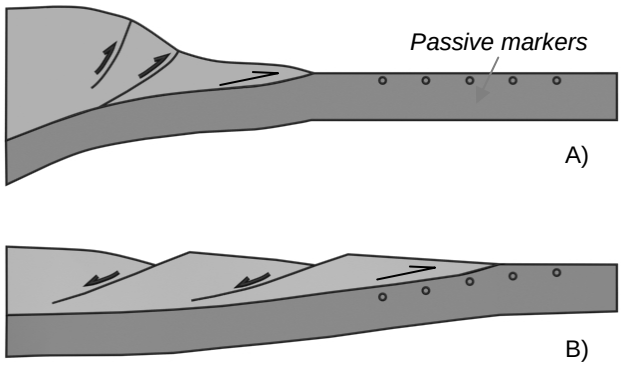

Figure 1. Initial concept of the geometry of orogenic surge (after Lister et al, 2001). A) Over-thickening of the orogenic wedge with a new frontal thrust. B) The orogen has collapsed over the foreland.

Domical Detachment

Doming of the mid-crustal detachment is a consequence of initial E-W shortening (D_3) followed by N-S shortening (D_3). Folding of the detachment causes fluids to build up beneath the domes. Eventually the domes are breached due to continuing shortening and the collected fluids are then free to travel through the new conduits into the middle and upper crust. Areas of breaching of the detachment hence localise mineralisation.

Animating geological processes

While 3D maps represent the present state of a study area, 3D animation is a tool that shifts the focus to the geological processes that formed the existing geology by adding the time component (motion).

Although animations look complicated, creating them is actually rather easy using a simple procedure (Fig. 3). There are three principal stages: an initial concept or problem (Fig. 1); a detailed storyboard illustrating the geological process under investigation (Fig. 2); and the final 3D movie (Fig. 4 and 5).

To make the movie we used the Discreet™ 3D animation package 3ds max®, a product commonly used for animations and special effects in cinema, television and the games industry. The program gives the user full control and no constraints. However, it is possible to create constraints, such as scale, timing, and referencing of objects relative to a specified location. The primary function of animations, however, is to convey ideas and concepts to an audience, making the cartoon-like feel of the final product immaterial. It is an excellent educational and presentation tool, and also potentially an effective means of putting forward geological concepts for numerical modelling.

The storyboard is the essential ingredient to making the movie (Fig. 2). It serves both as the focus for the science and as the basis of the animation. Storyboarding promotes and focuses group discussion and decision-making regarding the problem at hand. The geological process in question must be transparent and able to undergo close scrutiny not only in three dimensions but also in time, and flaws in the science are quickly exposed under thorough group review. It is not easy to create a seamless geological process from several known static states, and this method can facilitate the process. In some ways storyboarding is midway between a thought experiment and a laboratory experiment.

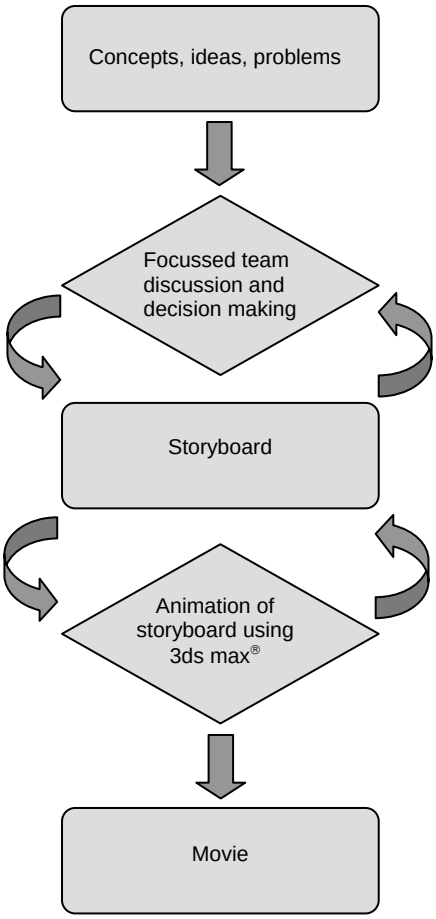

Figure 3. Flowchart describing the suggested animation process. The storyboard is the key element.

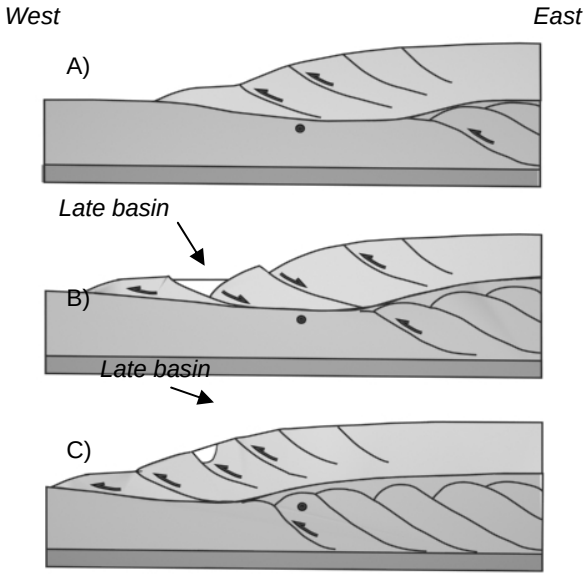

Figure 2. Excerpts from storyboard used to produce the animation showing key elements of the surge process. "Mid-crustal shortening drives D_2 in the upper crust".

A) SSW-directed D_{2A} causes diachronous reactivation of pre-existing N-S trending faults to build up an unstable wedge. B) The wedge collapses to form a N-S trending 'late basin' in D_{2E}. C)The basin formed at B is deformed and uplifted as a result of D_{2B}, as D_2 progresses from east to west.

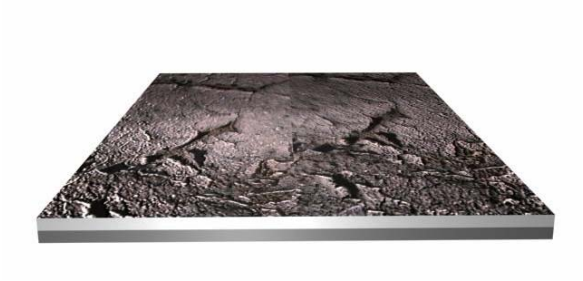

A) *looking towards north*

B) *looking towards north*

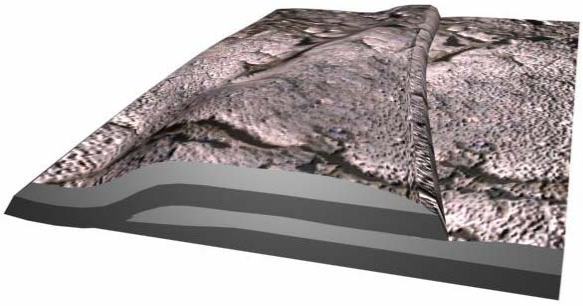

D) *looking towards south*

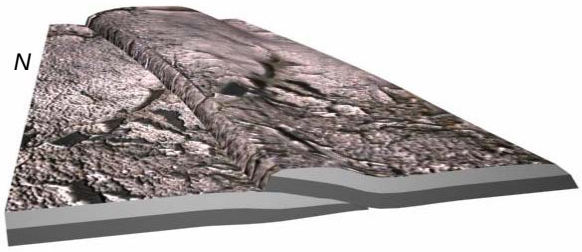

C) *looking towards north*

Figure 4 (above). 3D images from early orogenic surge animation. A) Undeformed upper crust with simple stratigraphy with view to the north. B) E-over-W thrusting begins in the northern part of the area due to SSW-directed D_{2A}. C) E-over-W thrusting continues along the length of the fault as D_2 progresses westwards. D) Same as C but with view to the south.

A)

Figure 5 (below and left). 3D images from simple animation demonstrating doming of the mid-crustal detachment. A) Undeformed detachment. B) Detachment after E-W compression (D_2). C) Domical detachment forms after N-S compression (D_3). Arrows indicate north.

B)

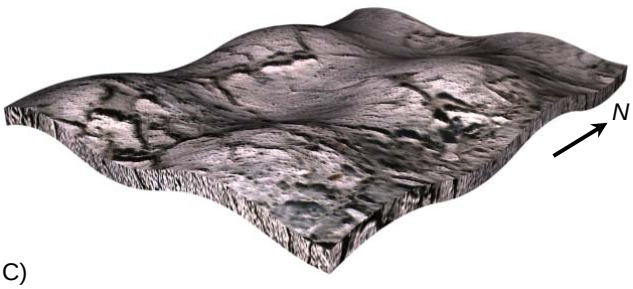

C)

So why animate?

Animation is the logical next step to working in three dimensions. One of the significant advantages to animation is the ability to present concepts clearly, visually, and in a condensed form. When considering a mineral system, we attempt to understand geological processes such as geodynamics and architecture, basin formation and magmatism, fluid flow and chemical reactions, and metamorphism. Animation provides a focus for the team and allows us to take a multidisciplinary approach to developing and testing our ideas

References

Blewett, R.S., Cassidy, K.F., Champion, D.C., Henson, P.A. and Goleby, B.R. 2004a. Episodicity of Archaean Tectonics: An Orogenic Surge Model for the Eastern Yilgarn Craton. In: McPhie, J. and McGoldrick, P., eds., Dynamic Earth: Past, Present and Future. Geological Society of Australia, Abstracts, 73, 146.

Blewett, R.S., Cassidy, K.F., Champion, D.C., Henson, P.A., Goleby, B.R., Jones, L. and Groenewald, P.B., 2004b. The Wangkathaa Orogeny: An Example of Episodic Regional 'D_2' in the Late Archaean Eastern Goldfields Province, Western Australia. Precambrian Research, 130, 139-159

Henson, P.A., Blewett, R.S., Champion, D.C., Goleby, B.R. and Cassidy, K.F., 2004. A Dynamic View of orogenesis and the development of the Eastern Yilgarn Craton. This volume.

Lister, G. S., Forster, M. A., and Rawling, T. J., 2001. Episodicity During Orogenesis. In: Miller, J. A., Holdsworth, R. E., Buick, I. S. and Hand, M., eds., Continental Reactivation and Reworking. Geological Society of London, Special Publication, 184, 89-113.

Insights into the Age and Genesis of Mt Isa Cu-Pb-Zn sulfide ores from Re-Os Isotopes

Reid Keays[1], Melissa Gregory[3], Travis Murphy[2] , Andy Wilde[3] and Bruce Schaefer[1]

*[1] pmd*CRC, VIEPS, School of Geosciences, Monash University, VIC 3800*
[2]Department of Geology, James Cook University, 411 QLD, Townsville, Australia
*[3] pmd*CRC, MORE, School of Geosciences, Monash University, VIC 3800*
rkeays@mail.earth.monash.edu.au

The genetic relationship between the Cu and Pb-Zn ore bodies at Mt Isa has long been subject to debate, with most recent studies arguing in favour of genetic models which have these world class ore bodies forming at different times from different ore-forming fluids. Most studies have concluded that the Cu ores formed during or after D_2 deformation, although the absolute age of this deformation remains poorly constrained. The relative age of the Pb-Zn orebodies is less clear-cut. Many early studies have proposed formation at the same time as or shortly after deposition of their host-rocks, the Urquhart Shale, for which the best available estimate of depositional age is ~1655 Ma. Recent studies of the distribution of high grade ore at George Fisher, however, clearly demonstrate the influence of later deformation events (Murphy, in prep.). Resolution of the debate has been hampered by the inability to establish the absolute age of either the Cu or Pb-Zn ores and indeed of the D_2 deformation.

The Re-Os isotope system is unique amongst geochronological systems in having the ability to directly date ore minerals. In addition, it can provide valuable information on the source of the Os in the ores. If the Mt Isa Cu and Pb-Zn ores formed at different times and from different ore fluids, then it is probable that these ores would have different initial Os isotope ($Os_{(i)}$) ratios (i.e., the composition of Os in the ore-forming fluids at the time of ore formation).

A preliminary Re-Os isotope investigation of samples from both the Mt Isa Cu and the Pb-Zn ores (see also Gregory et al. this volume) as well as samples from the George Fisher Pb-Zn mine indicates that ages of the Cu ores are within analytical error of the ages for the Pb-Zn ores and that all the ores have the same $Os_{(i)}$. Pooling all of the data together produces a 12 point isochron which yields an age of 1380 $\pm$ 47 Ma (MSWD146) with an $Os_{(i)}$ = 0.13 $\pm$ 0.096, a value that is almost identical to that of the mantle. The Cu ores contain up to 0.4 ppb Os, a factor of 50 times the Os content of barren Urquhart Shale and significantly higher than most crustal rocks. In addition, whereas the $Os_{(i)}$ of the ores is mantle-like and non-radiogenic, that of the Urquhart Shale is crustal in character and strongly radiogenic. Hence, both the Re-Os isotope signature of the ores and their high Os contents suggest that the Os in the ores was derived from a mantle source.

These preliminary Re-Os isotope results suggest that the Mt Isa and George Fisher Cu and Pb-Zn ores were formed at the same time as part of a giant mineralizing system that involved the mantle or mantle-derived rocks or magmas of the same age as the ores. It is unlikely that the Re-Os isotope signatures are the product of either thermal or metasomatic overprinting of pre-existing mineralization. However, these preliminary conclusions are based on an isochron with a relatively high MSWD and the pooling of paragenetically disparate samples may not be appropriate. Additional sampling and analysis will attempt to resolve this uncertainty.

Application of reactive transport modelling to the Mount Isa Copper mineralised system

Michael Kühn[1], Peter Alt-Epping[1], Klaus Gessner[1] and Andy Wilde[2]

*[1]pmd*CRC, CSIRO Exploration and Mining, 26 Dick Perry Avenue, Kensington, WA 6102*
*[2]pmd*CRC, School of Geosciences, Monash University, Clayton, VIC 3800*

michael.kuehn@csiro.au

Introduction

One distinct feature of the Mount Isa Fe-sulphide copper mineralising system is a massive silica body in the Urquhart Shale, which predates the copper deposit. Quartz occurs mainly as an infill in veins and breccias, suggesting high fracture permeability at the time of quartz formation. The combination of locally high fracture permeability and an inferred high geotherm may be sufficient for hydrothermal convection to occur on the scale of the mineralised system. The focus of this paper is to investigate if 3D free convection in faults and fractured rock units is a possible process responsible for driving fluid flow and depositing quartz on the scale of the Mount Isa Copper system. Reactive transport simulation of the quartz rock alteration patterns has been used to test whether the convection scenario can reproduce the silicification observed in the field. Based on the observed flow fields, 1D models with complex chemistry have been used to investigate scenarios of copper deposition and associated alteration reactions in the Urquhart Shale.

Significance of free convection in the Mount Isa fracture system

Fluid convection in faults is increasingly recognised as an important mechanism for fluid flow and mass transport in hydrothermal systems (Zhao et al., 2003; Alt-Epping et al. 2004). It is influenced not only by heat transport processes within the fault but also by lateral heat transfer to and from the surrounding rock mass. This has been shown theoretically by Zhao et al. (2003) and Murphy (1979). Bächler et al. (2003) showed that numerical simulation of free convection on Rhine Graben faults reproduces the measured thermal pattern of geothermal anomalies. The aim of this first part of the study was to investigate under which circumstances free convection within the Paroo and Mount Isa faults and fractured rock mass occurs, and what the resulting silica body looks like.

The **S**imulator for **HE**at and **MA**ss **T**ransport (SHEMAT, Clauser, 2003) has been applied to a 3D model of the Mount Isa system to investigate onset and development of free convection as a function of the permeability of major geologic units, salinity of the inherent formation water, and the applied system boundaries. The 3D architecture used in the modelling is shown in Figure 1. The numerical simulations focus on how the permeabilities of the different geological units, especially the Urquhart Shale, impact on the flow field, temperature distribution and, ultimately, the dissolution and precipitation of quartz. The thermal boundaries are fixed to a temperature of 179°C at the top and 300°C at the bottom with a geothermal gradient of approximately 40°C km^{-1}. The 3D chemical simulations are run for a uniform initial distribution of quartz throughout the model domain and are used to identify areas of quartz precipitation and dissolution.

The Rayleigh number (Ra) indicates the tendency towards free convection, that is, flow driven purely by density differences. Ra is based on the ratio of buoyant forces, which drive

convective fluid flow, to the viscous forces inhibiting fluid movement. The theoretical value or critical Ra, at which a system starts to convect is $4 \cdot \pi^2$ ($\approx$39.48). The difficulty with the theoretical Ra is the fact that it is based on homogeneous systems with averaged fluid and rock properties. It is impossible to determine Ra for a heterogeneous model as shown in Figure 1. However, under the assumption that both faults are vertical and homogeneous, the Mount Isa Fault would have a Ra number of 53 (system height $\approx$3000 m) and the Paroo Fault one of 35 (system height $\approx$2000m). The fact that one value is above and one below the critical Ra underlines that numerical simulation of the hydraulic conditions in the Mount Isa system is essential.

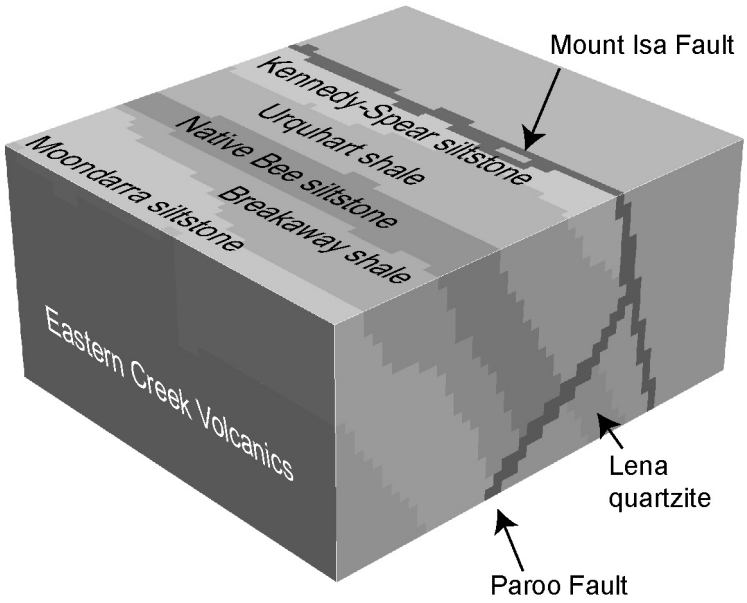

Figure 1. Mount Isa three dimensional architecture in SHEMAT. The model domain is 6098 m N-S, 5429 m E-W, and 2974 m high and is subdivided in eight different units.

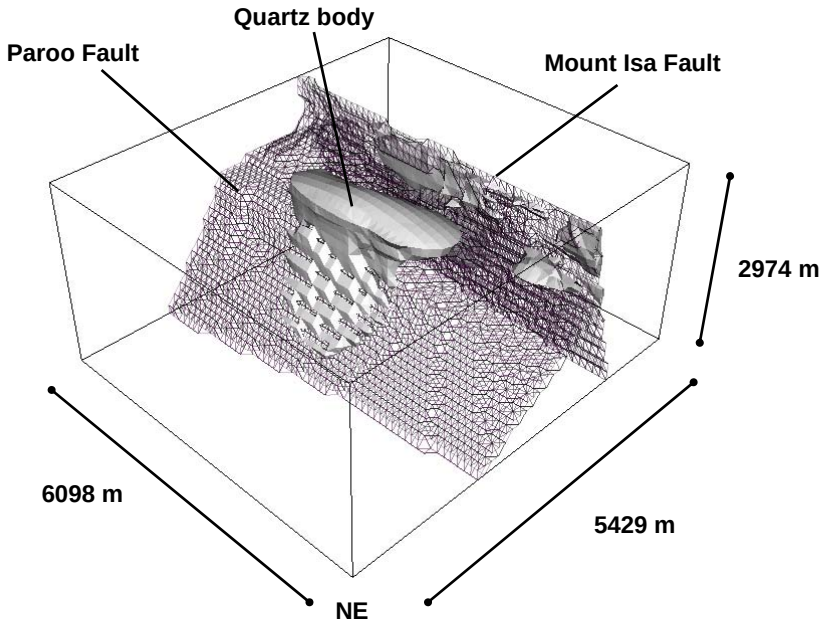

Figure 2. Rock alteration index of quartz displayed as isosurface of 25 % increase indicating areas of potential quartz precipitation. The wire frame represents the Mount Isa and Paroo faults. Silicification occurs within faults and mainly within the Urquhart Shale.

The results of the reactive transport simulations show that the permeability distribution is the controlling factor for the convection and mineral alteration patterns. In Mount Isa, a massive silica body occurs immediately above the Paroo Fault, near the centre of the modelled architecture. A model with a low permeable Urquhart Shale shows free convection in both faults, but with downward flow in the centre of the model and upward flow near the northern and southern margins of the domain. The patterns of dissolution and precipitation are produced by fluid movement across thermal gradients: silicification occurs within the up flow zones and dissolution within the down flow zones. No quartz precipitates within the Urquhart Shale with assigned low permeability. When the permeability of the Urquhart Shale is increased to that of the faults, convection patterns exhibit upward flow in the centre. Although silicification is now located in the centre of the model, it is too far detached from the Paroo Fault. With decreasing permeability of the Urquhart Shale, the centre of quartz precipitation moves closer to the Paroo fault. The best result, as shown in Figure 2, is obtained with a heterogeneous permeability distribution within the Urquhart Shale that decreases linearly from fault values down to country rock values. Shape and location of quartz precipitation in this case are very similar to field observations.

Looking at chemical processes in detail – The Urquhart Shale

The three-dimensional fluid flow modelling with SHEMAT has helped constrain flow patterns within the Mount Isa mineralised system for simulation with the code OS3D (Steefel and Yabusaki 1996). One fluid flow scenario which is consistent for a range of boundary conditions and permeability distributions is the upward flow from the Paroo Fault into the stratified Urquhart Shale. If one assumes that fluids moving along the Paroo Fault are metal-bearing, it is crucial to understand what the chemical implications are when such fluids move into and along the units of the Urquhart Shale. This scenario has been investigated in detail by down-scaling the 3D regional-scale model to a 1D vertical flowpath model in which the processes are tracked in the fluid and the rock as the fluid moves along the compositionally different units in the Urquhart Shale. The purpose of this study is to examine which of the units in the Urquhart Shale is the most effective for the deposition of copper, and why. Furthermore, the spatial associations of the Cu deposit is computed, including alteration minerals and other ore-bearing minerals such as sphalerite or galena. Unravelling the spatial associations of ore and alteration minerals is not only an essential tool for the understanding of the Mount Isa system but it is also invaluable information for targeting new ore deposits.

Preliminary results from 1D reactive transport simulations in the Urquhart Shale indicate that the efficiency of Cu deposition is strongly controlled by the amounts of primary sulphides (e.g. pyrite) in the rock. The grade of the deposit and the spatial distribution of deposit formation and alteration processes are controlled by the primary mineralogy and the porosity and permeability of the rock (Figure 3). The porosity not only represents the space available for ore deposition but also controls the flow velocity and volumetric fluxes of metal-bearing fluid through the rock. Porosity changes are a function of rock deformation and mineral precipitation/dissolution reactions.

Conclusions

Reactive transport modelling is essential for predicting the flow geometry and mineral alteration patterns of a highly complex thermally driven 3D system like Mount Isa. It has been shown that free convection in faults and fractured rock masses is likely to dominate the hydraulic system at Mount Isa. The silicification patterns generated with reactive transport simulations successfully reproduce the location, size and shape of the silica alteration observed at Mount Isa.

1D reactive transport simulations demonstrate that the simple process of through-flow of a metal-bearing fluid can create pore-space through the dissolution of primary minerals. This

leads to an increase of space available for ore-deposition and to an increase of fluid residence times. Both effects significantly enhance the efficiency of ore deposition.

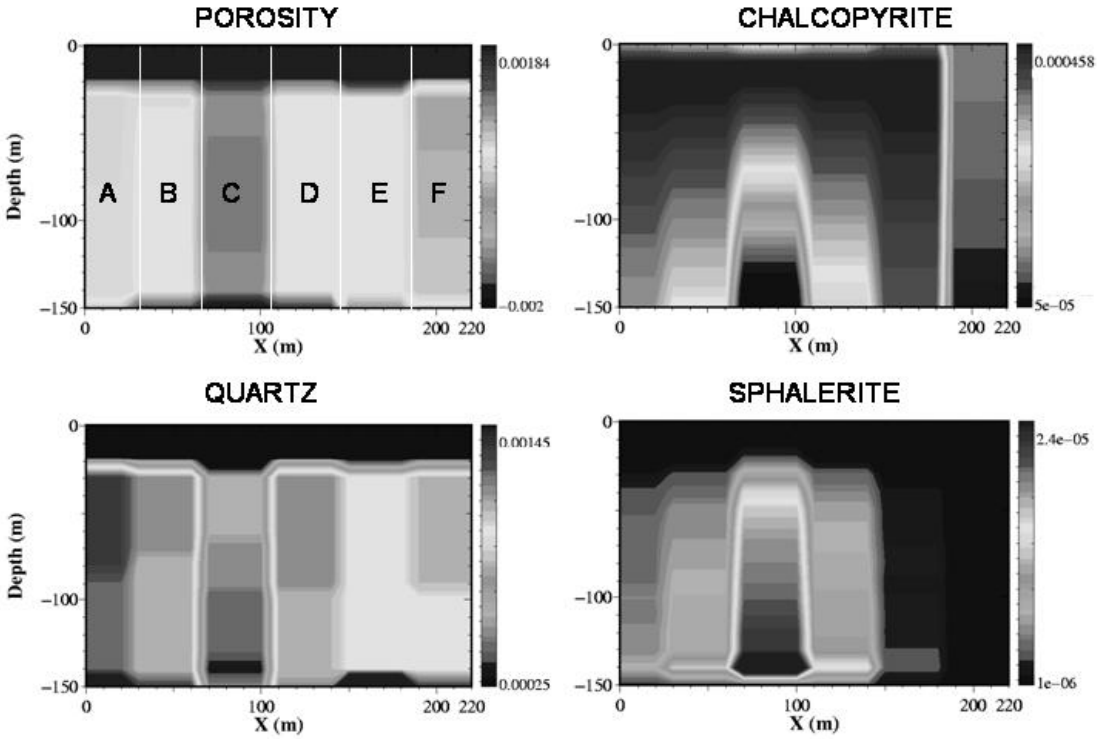

Figure 3. Examples of mineralogical profiles along fluid pathways through the Urquhart shale. The distributions of ore and alteration minerals, shown as volume percentage changes, are linked to the porosity/permeability distribution in the rock.

Acknowledgements

The authors would like to thank the Mount Isa Exploration Office of Xstrata Copper Australia Pty. Ltd. for financial support and the contribution of valuable field data.

References

Alt-Epping, P., Zhao, C., Hobbs, B.E., Ord, A. and Hornby, P., 2004. Reactive transport modelling in a three-dimensional fault zone with finger-like convective flow regime. Geofluids (submitted).

Bächler, D., Kohl ,T. and Rybach, L., 2003. Impact of graben-parallel faults on hydrothermal convection – Rhine Graben case study. Physics and Chemistry of the Earth, 28, 431-441.

Clauser, C., 2003. Numerical simulation of reactive flow in hot aquifers - SHEMAT and Processing SHEMAT. Springer Verlag, Heidelberg, 332p.

Murphy, H.D., 1979. Convective instabilities in vertical fractures and faults. Journal of Geophysical Research, 84(B11), 6121- 6130.

Steefel, C.I. and Yabusaki, S.B., 1996. OS3D/GIMRT – Software for Modeling Multicomponent-Multidimensional Reactive Transport. User Manual & Programmer's Guide. Pacific Northwest National Laboratory, Richland, Washington. Report PNL-11166, 55p.

Zhao, C., Hobbs, B.E., Mühlhaus, H.B., Ord, A. and Lin, G., 2003. Convective instability of 3-D fluid saturated geological fault zones heated from below. Geophysics Journal International, 155, 213-220.

Systematic analysis of Archaean gold deposits in a global context

Terry Lees
*pmd*CRC, School of Geosciences, Monash University, Clayton VIC 3800*
terry.lees@sci.monash.edu.au

Introduction

The paper describes the application of systematic taxonomy to hydrothermal mineral deposits. The approach has been taken from biology, with the aim of looking at similarities and relationships between various mineral deposits and groups, and deriving key characters of these groups.

A major part of the analysis has been the development of a mineral deposit database containing characters derived from the literature and mine visits. Presently there are 455 disparate, global, hydrothermal mineral deposits, selected on the basis of containing comprehensive (at least reliable) data available in the literature (typically at least two references); that they encompass a broad range of conventional classes ("VHMS", "MVT", "porphyry Cu" etc.).

A list of characters was developed to describe observable features of the deposits in terms of fluid inclusion data, ore deposit texture and geometry, reaction processes, host rock, ore mineralogy and chemistry and alteration mineralogy and chemistry. Criteria for the characters include generally available in the literature, that they describe key features of various deposits and deposit classes and they are observable features ("facts") that are not, as far as possible, interpretations. Most of the 150 characters were scored on the basis of 0=absent, 1=minor component or by-product, 2=major or abundant. Absolute values (eg. ore grades) were not considered appropriate because of poorer data availability and lack of standard reporting; however, some data related to fluid inclusions and ages are in absolute terms. In deposits not comprehensively described, lack of a character is taken to mean "unknown" and scored as "9999".

Data were run through several biological programs developed for phenetic (similarity) and phylogenetic (cladistic) analysis to assess relationships. Although several types of software have been used in prior tests, here we are concerned with PATN (Belbin, 1995), a largely phenetic software. PATN determine different levels of division (How many groups?) and lists and characters for those groups.

The mineral deposit database and analysis of it represent a new tool for the minerals industry, to define groups of deposits based on their characteristics, in turn enabling better genetic and exploration models. The tool has application to project generation in poorly known terranes (What deposit types occur here and what are they like?) and in well-known terranes (What are the natural groups and controlling factors?). In light of these results, exploration models may need to be reviewed. An example is in the Archaean gold deposits, where most deposits fit the traditional "shear-zone hosted" or "orogenic" model but some deposits and groups appear different.

Systematic Analysis of Global Mineral Deposit data

Analysis of the global data set produced a dendrogram which was simplified and (with interpretation) condensed into various groups; often the classic deposit styles (Table 1), with the main group characters. 21 deposit groups appear to reflect natural mineral deposit classes. Fewer groups appear not to encompass the full range of natural deposit styles, while more groups just subdivide the earlier ones.

Table 1. 21 groups with geological description and selected group characters (those with highest percentage scores in characterisation)

Group	Geological description	Group Characters (from the A1 mineral deposi database)
1/21	Sediment-hosted dissem Cu/Au/U	parallel S0, quartz
2/21	Carbonate-hosted Pb-Zn	Dolomite, galena, sphalerite, Pb, Zn
3/21	High-T carbonate replacement	Rock reaction, pyrite, quartz
4/21	Skarn Pb Zn Cu Au W	Rock reaction, limestone, replacement, garnet
5/21	Sed-hosted massive sulphide Pb-Zn	shale-siltstone, massive sulphide, pyrite, sphalerite Zn
6/21	VHMS	Volcano-sediment, massive sulphide, Layered parallel S0, sphalerite, Cu, Zn, chlorite, quartz sericite/musc
7/21	Metamorphic-hosted massive sulphide	massive sulphide, quartz, sphalerite, Zn
8/21	Epithermal Au plus others	Vein, quartz, Au
9/21	Vein, porphyry, replacement Sn W	Fluid pH<7, porphyry, quartz
10/21	Breccia-hosted Au-U-Cu	Unmixing, Foverpressure, Breccia, bx-irregular chlorite
11/21	Vein/replacement polymetallic	Cooling, Ft/bx, fault/SZ, quartz
12/21	Porphyry Cu-Au	Porphyry, Cu, K feldspar
13/21	High mm grade Au-other	Rock reaction, quartz, Au
14/21	Au (possibly Granite-related?)	Volcanic mafic, quartz, Au, quartz, sericite/musc silicate other
15/21	Fe rich (oxide/sulphide)	MM host, Replacement, Recrystallised, quartz, Au biotite
16/21 *	ElSoldado (group of 1)	fluid pH<7, Vfels, Vint, pipe, multiple lens, Manto bornite, calcite, Au, quartz, sericite/musc, silicate other
17/21	Unusual Fe	Salinity, CO_2, MM host, folded, amphibole
18/21	Skarn-like Fe Cu U	CO_2, MM host, replacement
19/21	Ironstone-hosted Au	Rock reaction, replacement, quartz, Au, Fe, U
20/21	Archaean Orogenic Au	Salinity, Ft/bx, Vein, quartz, Au
21/21	Archaean, Proterozoic Orogenic and Palaeozoic (slate-belt) Au	Vein, quartz, Au

Although all characters contribute to division, characteristics of a particular group are not necessarily those that distinguish groups. An example is that ‘massive sulphide’ and ‘sphalerite’ are characteristic of both SHMS and VHMS deposits but the main distinguishing characters might be ‘FW stringer zone’ and ‘arsenic’. Group characters are those which describe attributes of the group - those which score highly whether or not they separate this from their groups. Distinguishing characters are those that, either by presence or absence, separate one group from others.

Major groups include most classical styles (eg. VHMS, epithermal Au-Ag, porphyry Cu-Au) with reasonable divisions and sub-groups, eg. Carbonate-hosted deposits are split between high-T replacement deposits and another group with “Irish” and “MVT”. There are also many differences; IOCG is not a simple coherent group but several Fe-rich groups; skarns separated into Pb-Zn-Ag-W and Fe-Cu-Au.

Metamorphic grade is an important criteria as it is reflected in many characters (mineralogy). Metamorphic hosted Pb-Zn (group 7) have subgroups of probable VHMS affinity and BHT; metamorphic Cu-Fe-Au deposits form a separate group (13).

Archaean gold deposits are considered in more detail as an example of systematic analysis.

Archaean Gold Deposits in a Global Context

In a global context, there is considerable variation within Archaean Au deposits. In the global analysis, there are three large groups dominated by Archaean Au deposits;

- mainly Archaean Au deposits in ironstone hosts is a mixture of Archaean and Proterozoic hosts with iron from various pre-ore sources;
- archetypal "Archaean orogenic Au" in greenstone belts;
- mix of Archaean, Proterozoic and Palaeozoic orogenic Au mainly in sediments.

The differences are complex and not just in host rock, metamorphic grade (with associated mineralogy) or commodity.

Archaean gold deposits also occur within three other groups:

- Siscoe C and Centurion Binduli sit comfortably among a group of epithermal to mesothermal gold deposits of the Pacific rim (group 8)
- Group 13 consists of Au deposits in very high metamorphic grade rocks (Big Bell, Challenger) along with deposits described as metamorphosed VHMS (Aitik, Mt Gibson, Werner Lake).
- Group 14 consists of Boddington, Boliden, Bousquet and Campbell, show possible granitic affinities with common characters of tourmaline and at least partly hosted by granite/porphyry, pipe-like, amphibole, biotite, tourmaline, Bi, Sb, Te.

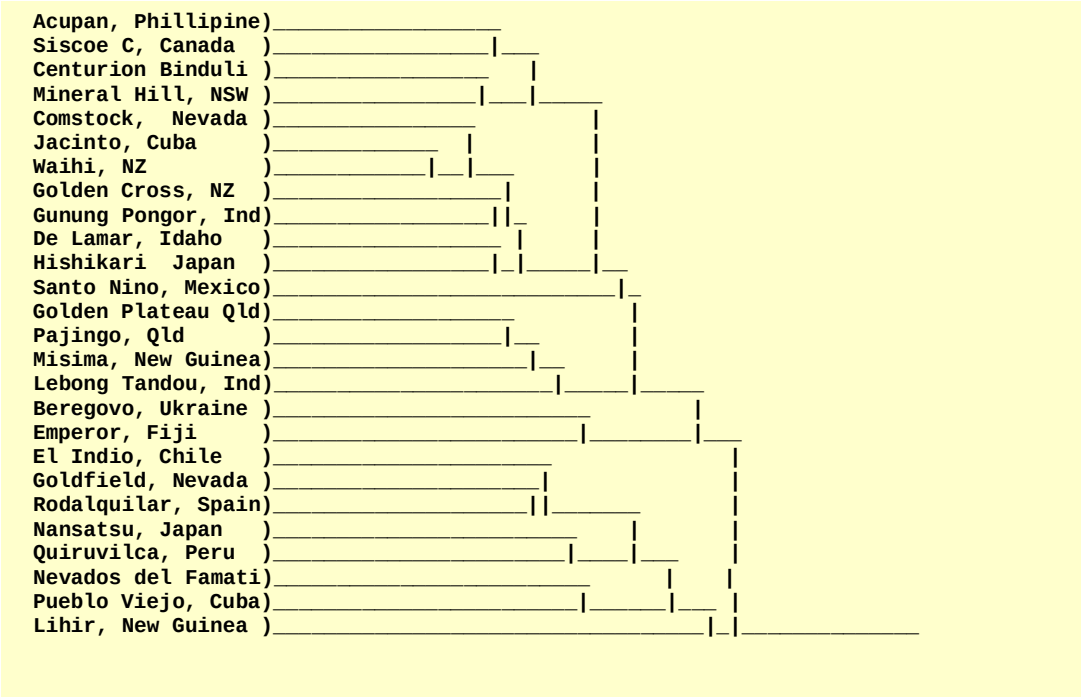

Fig. 1. Part of the global dendrogram showing epithermal to mesothermal gold deposits (group 8). Archaean deposits Siscoe C and Centurion Binduli (WA) occur in this group. The horizontal axis represents similarity of characters, increasing to the left.

Considering the Archaean deposits in this phenetic analysis and global context, the variation amongst these deposits and interspersal within other coherent groups implies a wide variation in deposit style. Examples of epithermal, volcanic-associated and intrusive-associated styles are

present as well as typical "orogenic Au" with possible variations such as ironstone-hosted and sediment-hosted types. The strong similarities of particular deposits with epithermal and VHMS groups imply different processes (genetics) had influence. Archaean Au deposits appear to be complex and exploration models should reflect the complexity and variation.

Reference

Belbin, L., 1995. PATN Technical Reference. CSIRO (unpublished).

Systematic analysis of the A1 faults database

Terry Lees[1] and Steve Fraser[2]
*[1]pmd*CRC, School of Geosciences,Monash University, Clayton, VIC 3800*
[2]CSIRO Exploration and Mining, Pullenvale, Brisbane
terry.lees@sci.monash.edu.au

Introduction

The A1 Faults Database consists of some 200 characters with a mixture of data types (ordinal; eg. ages; nominal, e.g. fault kinematics and tectonic settings; and binary i.e.yes/no). Invariant (i.e. only one class represented - unknown not used) were removed. Earlier analyses had indicated strong bias into age-related groups. As many characters in the database include age data (e.g. age of fault, age of intrusion) these ages were removed from the subsequent analysis (presented here) except for one very broad and nominal age character. The data analysed consisted of 118 faults (including a blank) with 80 characters, although some characters are poorly populated.

For the analysis, data were treated as follows:

- Ordinal data were left as is (except age data which were removed for other reasons; see below);
- Nominal classes were coded (this is fine for the dendrogram but presents a problem for definition of group characters);
- Orientation data were coded into groups (eg. 0-15° = 1)
- Binary data coded as No=0, Yes=1.

Because of the diverse types of data and their treatment, group and distinguishing characters derived from the analysis are not exhaustive and other factors may be relevant.

Data were run through a program developed for phenetic (similarity) analysis in biology, PATN (Belbin, 1995). PATN determines different levels of division (How many groups?) and lists and characters for those groups.

CSIRO Exploration & Mining have developed a version of Kohonen's (1982, 2000) Self-Organizing Map (SOM) technique aimed specifically at geological and exploration problems. SOM is a powerful tool for the objective analysis of multiple and complex data sets and it has been widely used for data analysis in the fields of finance, industrial control and speech analysis. The Self Organizing Map procedure is essentially an unsupervised "data-mining" or "clustering" tool for complex data sets.

The SOM method takes a set of multi-dimensional data and reduces it to a 2-dimensional map that essentially retaining the topology of the input data points. (That is, data points that are close to one-another in Euclidean N-D space will be close to each other in the 2-D feature space.) For each sample in the data set, the best fitting location (code-vector) in the feature-space map is found, and the closeness of fit to this location determined. These code vectors are then mapped onto the 2-D node map by a non-parametric regression. The SOM output is typically viewed via a "unified distance matrix" (*U-matrix*) that allows a user to graphically visualize the structure of the SOM output as a pseudo three-dimensional "landscape". It is standard to use a "temperature" colour-scale so that adjacent nodes that are close together in Euclidean space are shown in blue(s), whereby adjacent nodes that have big separations in Euclidean space are coloured in oranges and red. This representation gives rise to a topographic analogy in that there are plains of (blue) nodes that are similar, separated by walls of brighter coloured nodes that represent class-boundaries or samples belonging to different clusters.

The SOM procedure has the advantage over traditional “multivariate” methods, in that it can handle both linear and non-linear relationships between data inputs. It also can be applied to both continuous (e.g. geochemical assay values) and categorical (assigned or named) variables, making it ideal for the analysis of disparate data sets. Furthermore, no prior knowledge is required as to the nature, or number, of "groupings" within the data set. These features are why the SOM technique is preferred over other more ‘conventional’ analysis methods such as traditional clustering (both hard and fuzzy), factor analysis and principal components.

PATN Analysis of the A1 Fault Database

Two analyses were performed; the first analysis divided faults into 6 groups, as shown in Figure 1 and Table 1. These groups appear to correspond to broad ages (eras) of the faults; however, as virtually all age data were removed, these actually represent differences in fault morphology. This is further exemplified when group 4 (Precambrian) is clearly subdivided into Archaean and Proterozoic faults.

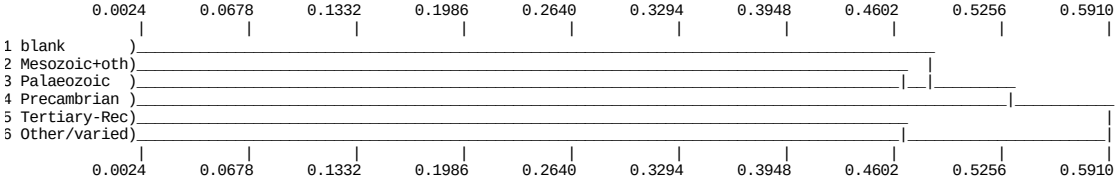

Fig. 1. Summary of Fault Groups. Largely into broad ages despite only 1 of 80 characters containing any age data, thus the division represents differences in fault morphology. Note the degree of similarity (increasing to the left) for these fault groups is poor.

The division is largely on the basis of broad characteristics:

- Fault geometry (length, width, depth)
- Mineralisation factors (endowment, proximity of deposits to fault, fluid chemistry)
- Metamorphism factors (retrograde, grade present, change in grade across fault)
- Presence of basement and ophiolites.

The second analysis into 11 groups separates the Archaean and Proterozoic faults. At this level, the Gowk Fault in Iran is very different from the others due to the lack of metamorphism but also has little other data for comparison. Some otherwise seemingly coherent groups are split. If there are too many groups in such a small and poorly populated dataset, this would be expected to happen. The main characters causing split into groups (both 6 group and 11 group) are: Mineralised, dip geometry, depth extent, width, active, ophiolites, inversion, retrograde metamorphism, MIME (Is the mineralisation on the fault related to the regionally Most Important Mineralising Event?) and endowment of mineral resources.

SOM Analysis

Analysis of an older, smaller version of the database by SOM is shown in Figure 2. Age data and invariant characters were not included in the analysis. Clusters of deposits (Figs 2, 3) appear to be at least partly based on broad ages. Although “maps” individual characters are derived, it is not possible to derive relative contributions of each character to the overall product.

Discussion

Both PATN and SOM analyses of the A1 Faults database show a similar and intriguing picture. Although minimal age data are included in the analyses, faults are sorted into groups approximating general ages. Characters apart from age, such as metamorphic grade, presence of basement, and fault geometry determine these broad groups.

These first analyses of the A1 database show some interesting results; however main constraints are not enough faults (from experience of the deposits database need >> 200), lack of data in many fields and that much of the data is nominal.

These first attempts at analyzing the A1 Faults Database show groupings and patterns that are potentially meaningful and further investigation is warranted. However, limitations in the database, such as the need for more samples, and the apparent sparsity of data in some fields could be limiting factors.

Table 1. Group membership of PATN analysis of 118 faults, 6 groups (fault names from A1 Fault database).

Group, Name, number	**Membership**
1 Outgroup	blank
2 Mesozoic / other faults (16)	Karatau Fault, Talas Ferghana Fault, Battle Mountain-Eureka Trend, Getchell Fault Zone, Jerritt Canyon Trend, Kiewa Kancoona Fault Zone, Gilmore Fault Zone, Indi Fault Zone, Errabiddy Shear Zone, Halls Reward, Atacama Fault Zone, Sumatra Fault, Juneau Gold Belt, Sangruntau-Tamdytau, Muruntau-Daugyztau, Gowk Fault.
3 Palaeozoic Faults (9)	Moyston Fault, Stawell Ararat Fault Zone, Heathcote Fault, Governor Fault Zone, Mount Wellington Fault Zone, Avoca Fault, Lake George – Copperhania Fault, Peel Manning Fault System, Yarrol Fault.
4 Archaean and Proterozoic Faults (73)	Post Fault System, Sons of Gwalia Shear Zone, Pleasant Grove-Huntingdon Valley Shear Zone, Tyennan Fault, Larder Cadillac, Modoc Fault Zone, Duketon Fault, Claypan Fault, Ida Fault, Bardoc Boorara Shear, Boulder Lefroy Fault, Kieth Kilkenny, Menzies Shear Zone, Zuleika Shear Zone, Mt McClure Fault, Ockerburry Shear Zone, Perserverence Fault, Mt George Shear Zone, Ninnis Fault, Hogans Paris Shear Zone, Moongarnoo Shear Zone, Moilers Shear Zone, Celia Shear Zone, Koolyanobbing Shear Zone, Murchison Fault, Goodin Fault, Jenkin Fault, Moriarty Shear Zone, Abattoir Shear Zone, Mount Hunt Fault, Bullabulling Shear Zone, Mt Monger Fault, Kanowna Shear Zone, Mulgarrie Fault, Melita Fault, Murrin Fault, Laverton Shear Zone, Henty Fault, Termite Range Fault, Oyarbide Fault, Great Lyell Fault, Rosebery Fault, Pine Mountain Thrust, Retina Fault, Hurricane Fault, Kingsborough FaultFault, Kondaparinga Fault, Arthur Lineament, Mt Rose Bee Fault, Corridor, Rufus Fault Zone, Gorge Creek Fault, Mt Annable Fault, May Downs Fault, Mount Gordon Fault Zone, Mount Isa Fault, Mount Remarkable Fault System, Ballara Corella River Fault, Overhang Shear, Pilgrim Fault, Quilalar Fault Zone, Selwyn Shear, Cloncurry Overthrust, Levuka Trend, Fountain Range Fault, Wonomo Fault, Globe Vauxhall Shear Zone, Cloncurry Fault, Redbank Fault, Woodroffe Thrust, Mann Thrust, Clarendon , Brevard Fault, Burdekin River Fault.
5 Tertiary to Recent Faults (9)	Turkestan Suture, New Guinea Suture, Alpine Ft, TanchengI, Tancheng II, TanchengIII, TanchengIV, Ailao Shan – Red River Shear Zone, Baikal Rift System.
6 Various/other Faults (10)	South Armorican Shear Zone, Cundeelee Fault, Heywood Fault, Coramup Fault, Errabiddy Fault, Teddy Mount Fault, Clarke River Mylonite Zone, Clarke River Fault, Gray Creek Fault Zone, Palmerville Fault.

References

Belbin, L., 1995. PATN Technical Reference. CSIRO (unpublished).

Kohonen, T., 1982. Self Organized Formation of Topological Correct Feature Maps. Biolofical Cyberbetics, 43, 59-96.

Kohonen, T., 2000. Self-Organizing Maps. Third Extended Edition, Springer Series in Information Sciences, Vol. 30, Springer, Berlin, Heidelberg, New York.

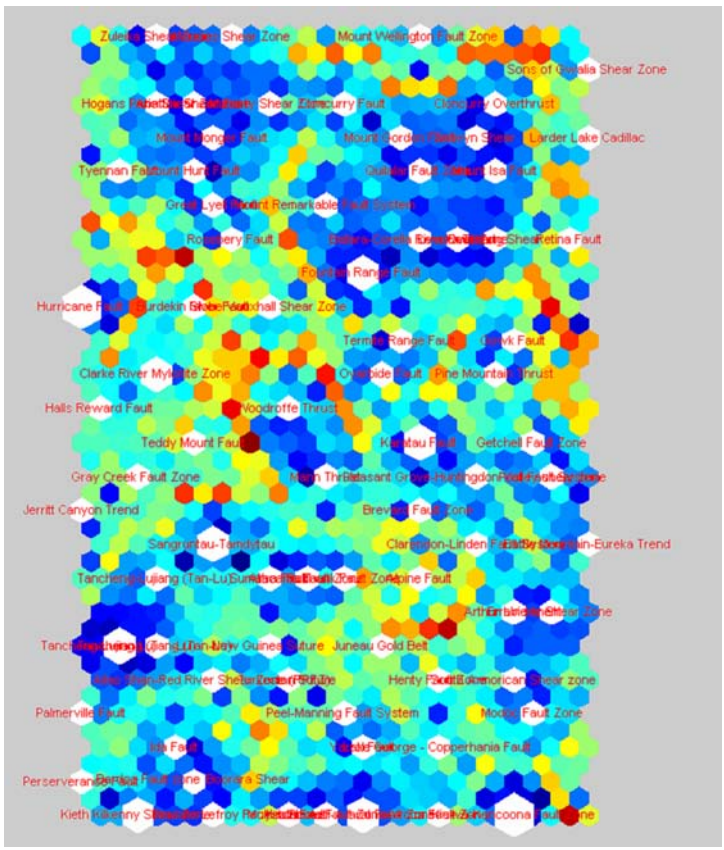

Fig. 2. SOM groups of 88 faults. Note clear separation into clusters within blue areas.

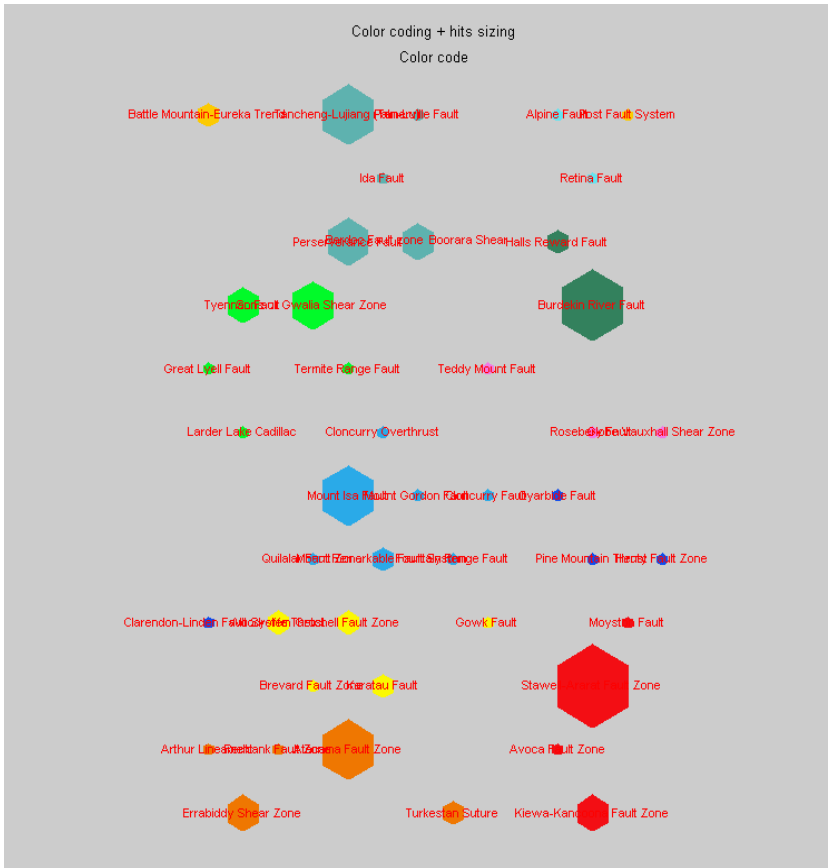

Fig. 3. Membership for 10 SOM groups (colour coded). Note clear separation into clusters with similar age.

Crustal architecture from geophysics: Reprocessing the Mt Isa Seismic Transect

Piter Lepong[1], Bruce Goleby[2] and Tom Blenkinsop[1]

*[1]pmd*CRC, School of Earth Sciences, James Cook University, Townsville, QLD 4811*
*[2]pmd*CRC, Geoscience Australia, GPO BOX 378, Canberra, ACT 2601*
Piter.Lepong@jcu.edu.au

Introduction

The Mt Isa deep seismic section was acquired and processed in about 10 years ago. Interpretation of the deep seismic transect indicates that the Eastern Fold Belt is dominated by large-scale horizontal offsets of supracrustal rocks that were decoupled from the basement along a subhorizontal detachment that spawned numerous east-dipping thrust faults (MacCready et al., 1998). This west-directed fold and thrust system was then broadly warped and dissected by a number of reverse and strike-slip faults that involve the basement and may link to a major mid-crustal structure (inferred from alignment of high-velocity rocks interpreted from seismic refraction).

On the other hand, surface geology and potential field data (i.e. gravity and aeromagnetic data) indicate that the major structure of the Mt Isa Eastern Succession is generally steeply dipping and extends down to the middle of the crust in contrast to the shallowly dipping seismic interpretation. The resolution of this paradox is a vital for understanding the formation of mineral deposits and depends essentially on understanding the deep structure of the crust.

Seismic sections can not directly image structures with steep to vertical dips. Any interpretation of the crustal structure from seismic sections alone may therefore be biased towards shallow-dipping structures. The Mt Isa area offers an opportunity to evaluate crustal structure in three dimensions by combining interpretation of seismic sections with potential field data and advanced geological knowledge. This article presents reprocessing of the seismic section to investigate if it is possible to increase temporal and spatial seismic resolution and facilitate more accurate interpretation of the data.

Reprocessing of Deep Seismic Transect

The Mt Isa deep seismic transect were reprocessed using the Disco/Focus seismic data processing system using updated techniques and algorithm processing methods. Processing sequences and parameters used by Goleby et al. (1996) provided a useful starting point for designing the processing sequence for this data set. The data were reprocessed through a basic sequence of noise attenuation, spiking deconvolution, dip moveout and scaling prior to stack. The post-stack data were subsequently migrated using the Kirchhoff algorithm. Further filtering was applied post-migration. Preprocessing included demultiplex, editing, gain recovery, field geometry and field statics mostly adopted from previous processing. This reprocessing focused on increasing the signal to noise ratio within the seismic records and improving continuity of the reflection events. The following is a summary of the updated techniques and parameters used in this current reprocessing sequence.

Deconvolution (Pre-Stack)

To increase temporal resolution and sometimes, to remove the effects of multiples, deconvolution is applied before stack. The Wiener-Levinson algorithm was used to sharpen

seismic events and extend the frequency bandwidth. Spiking deconvolution used 160-millisecond operator length and 0.1% pre-whitening parameters applied to all traces in two gates window, near and far offset.

Spectrum Balancing

Spectrum Balancing is particularly useful for balancing the spectrum of the data contaminated by source generated noise. The input is prestack data, sampled at 4 milliseconds. Spectral whitening is achieved using four frequency bands. The AGC length is set to 500 milliseconds. The frequency and amplitude parameters supplied to control output trace.

Bandpass Filter

Filtering for temporal frequency (in time) and also for spatial frequency (in wavenumber) is applied in this processing. A band pass filters with slopes in decibels per octave is applied to traces in all shots. A four time gate is designated for filtering with a 160 millisecond length. Lower frequencies are attenuated at 18 decibels per octave and higher frequencies are attenuated at different ranges of decibels per octave.

Dip Moveout

The Dip Moveout (DMO) correction applied before stack used the F-K DMO algorithm as described by Cabera and Levy (1989). The input to this DMO routine are Normal Moveout (NMO) corrected shot records. The group interval for this data is 20 m. The maximum frequency of the data is approximately 75 Hz. The minimum time start of DMO operation is 150 milliseconds.

Kirchhoff Migration

The objective of migration is to move (migrate) data from an observed point of reference to the point of actual origin. Implemented ideally, this procedure essentially collapses diffractions to a single point, and spatially orients dipping events to their correct position. A poststack data set is migrated for all traces using time space Kirchhoff migration. The imaging operation is based on an algorithm derived from the description of Kirchhoff migration in Stolt and Benson (1986). The CDP trace spacing is 20 m and the dip limit is 70º with an interpolation filter. The velocity model used for the migration has previously been stored in the database.

Summary and Conclusion

The reprocessing methodology described here resulted in seismic profiles with increased temporal and spatial resolution, which should facilitate more accurate interpretation of the data. The major difference in the sections between the original processing and current processing is attributed to the application of spiking deconvolution, dip moveout and Kirchhoff migration. The application of DMO eliminated the dip dependency of the NMO velocity field and removed the midpoint noise on dipping events. The DMO technique appeared to be very efficient in areas of the Mt Isa Inlier where structure is associated with steeply dipping features. The overall quality of the reprocessed data shows better noise suppression and increase of continuity reflection events, especially after DMO and post-stack Kirchhoff migration section (Figure 2) compare to original processing after Finite Difference migration (Figure 1).

Figure-1. After Finite Difference Migration

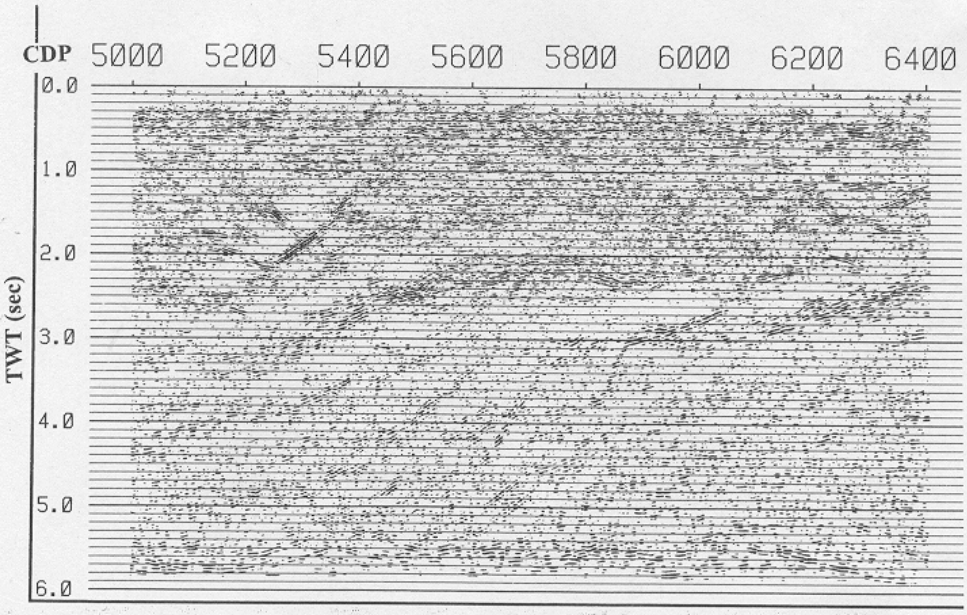

Figure-2. Applied DMO and Post-Stack Kirchhoff Migration

Clearly visible improvements in the new profiles are:

1) Much better signal to noise ratio

2) Greater length and continuity of reflections in some areas

3) More reflections visible in the interval from 4 to 10 s two way travel time, which is characterized on both the former and newly processed sections by homogeneity.

4) Apparent reflections on the previous sections are not visible on the newly processed sections because they may be diffractions removed by the new migration technique.

The new profile casts doubt on the evidence for a moderate easterly dip for the Cloncurry fault. Reflectors previously considered to be continuous with the surface trace of the Cloncurry fault may be due to the inverted fold limb of the Snake Creek anticline. Under the Duck Creek anticline, west-dipping reflectors that were previously interpreted as part of a gently dipping folded decollement are not apparent in the newly processed section. These two examples illustrate that the model of west vergent thin-skinned thrust tectonics that was a consequence of the previous seismic section needs to be questioned.

Acknowledgements

I would like to thank to ***pmd****CRC* and to staff of Geoscience Australia, particularly Leonie Jones, for their help and cooperation during the reprocessing of the seismic data.

References

Cabera, J. and Levy, S., 1989. Shot Dip Moveout with Logarithmic Transform. Geophysics, 54, 1038-1041.

Goleby, B.R., Drummond, B.J. and MacCready, T., 1996. The Mount Isa Deep Seismic Transect. Australian Geological Survey Organization, Research Newsletter, 24, 6-8.

MacCready, T., Goleby, B.R., Goncharov, A., Drummond, B.J. and Lister,G.S., 1998. A Framework of Overprinting Orogens Based on Interpretation of the Mount Isa Deep Seismic Transect. Economic Geology, 93, 1422-1434.

Stolt, R.H. and Benson, K.H., 1986. Seismic Migration. London , Geophysical Press Ltd, 382 pp.

The geochemistry of magmatic fluids, Cloncurry district, Australia: relations to IOCG systems

G. Mark[1,2], T. Baker[2], P. Williams[2], R. Mustard[2], C. Ryan[3] and T. Mernagh[4]
*[1]pmd*CRC, School of Geosciences, Monash University, Clayton, VIC 3168*
*[2]pmd*CRC, School of Earth Sciences, James Cook University, Townsville, QLD 4811*
*[3]pmd*CRC, Division of Mining and Exploration, CSIRO, Clayton, VIC 3168*
*[4]pmd*CRC, Geoscience Australia, Symonston, ACT 2609*
Geordie@mail.earth.monash.edu.au

Introduction

The origin of the fluids associated with Fe oxide-Cu-Au mineralisation is controversial, and hydrothermal models invoked for the derivation of the ligands and metals include both magmatic and non-magmatic variants (Hitzman et al. 1992; Barton and Johnson, 2000; Pollard, 2000). This controversy is due in part to the close temporal and, less commonly observed, spatial association between intrusive activity and fluids that formed the regional hydrothermal systems, and those that produced Cu-Au mineralisation. One of the main points of contention revolves around the role and significance of coeval intrusions and their contribution of metals (Fe, Cu and Au) and sulphur to ore-forming processes. Consequently, resolving the relative significance of various fluid sources in hydrothermal systems is of fundamental importance to understanding how these systems were generated.

The Cloncurry district, Mount Isa Inlier is probably the most well documented Fe oxide-Cu-Au terrane (Hitzman, 2000), and is the best-suited to resolve the role and significance of fluids from different parentages in ore formation. This study has chosen an initial focus on characterizing the geochemistry of saline brines exsolved from magmatic intrusions emplaced synchronously with Cu-Au mineralization for two main reasons: 1. A magmatic contribution is invoked to play a role in the formation of all Fe oxide-Cu-Au deposits in the district (*cf.* Williams and Pollard, 2003, and references therein); and 2. The few published compositional data on magmatic brines from the Lightning Creek prospect reveal high concentrations of Fe and Cu.

The results presented here are from samples selected from intrusive phases emplaced immediately prior to and during the formation of a km-scale magmatic-hydrothermal breccia system within the Mount Angelay igneous complex (MAIC) (cf. Mark et al., 1999). The main objectives of this paper are to present new data on the geochemistry of the magmatic brines, and discuss their relations to brines from Fe oxide-Cu-Au deposits and similar magmatic-hydrothermal systems within the Squirrel Hills Granite.

Cloncurry District

The Paleoproterozoic cover sequence rocks (1.78-1.61 Ga) in the district were intruded by a series of syn- to post-peak metamorphic intrusions that form the Williams and Naraku Batholiths, which were predominantly emplaced between 1.55-1.50 Ga. Intrusions of this age have an outcrop exposure >1500 km^2, and are predominantly potassic, although rare sodic intrusions of similar age do occur. The main K-rich phases of the batholiths were emplaced in an intracratonic environment, and have a pre-, syn- and post-D_3 timing. These intrusions are largely composed of metaluminous, alkaline to subalkaline, magnetite-bearing granitoids and typically plot as 'A-type' on geochemical discrimination diagrams. The age of Cu-Au mineralisation in the Cloncurry district has been controversial, and its relationship to the regional magmatic and hydrothermal system was until recently largely speculative, although new Ar-Ar plateau ages, $Re\text{-}Os_{Molybdenite\ ages}$ and $U\text{-}Pb_{\ rutile\ and\ titanite}$ (ca. 1.59-1.50 Ga) from mineralisation-related hydrothermal minerals support a broadly coeval association between magmatism and

epigenetic Cu-Au mineralization. However, despite this temporal association, close spatial relations between intrusions and Cu-Au deposits are rarely observed.

Geology of the Mount Angelay Igneous Complex

The MAIC (ca 1525 Ma) is largely composed of K-rich, magnetite-bearing intrusive rocks that range in composition from quartz monzodiorite to biotite syenogranite and are cut by late, petrogenetically-related, alkali pegmatites and Na-rich balloon-textured albitites. This suite of intrusive rocks exhibit 'A-type' geochemical characteristics, and possess Y-undeleted, Sr-depleted compositions that implicate a derivation from partial melting of the mid-crust (<1.0-0.8 GPa; >850^{o}C). Mantle derived dioritic intrusions were emplaced during the earliest phases of the complex's evolution, and are spatially associated with the localized occurrence of rocks of mingled and mixed derivation. A large, km-scale magmatic-hydrothermal breccia-vein system is hosted within the main phase of the MAIC, where the system grades from composite breccias filled with synchronously formed magmatic intrusions (e.g. pegmatites and albitites) and hydrothermal mineral precipitates in the topographic lows, to fracture-related hydrothermal vein systems in the topographic highs. Estimated temperatures from stable isotope mineral pair equilibrium (albite and quartz) for the evolved magmatic phases and hydrothermal precipitates indicate formation temperatures *ca.* 550 ^{o}C, which are consistent with temperature constraints from similar rocks elsewhere (cf. Mark and Foster, 2000; Perring et al., 2000; Mark et al., 2004). This system exhibits many geochemical and mineralogical similarities to the magmatic-hydrothermal system associated with the formation of the Lightning Creek Fe oxide-(Cu-Au) prospect in the Squirrel Hills Granite (cf. Perring et al., 2000; Pollard, 2001).

Characteristics of magmatic fluids

We present here data from primary$^{\#}$ fluid inclusions trapped in quartz within biotite syenogranite and alkali pegmatite that respectively were emplaced immediately prior to, and during the formation of a kilometre-scale magmatic hydrothermal breccia-vein system in the MAIC (cf. Mark et al., 1999). Magmatic quartz contains populations of hypersaline, multi-solid brine inclusions together with two-phase aqueous brine inclusions. These trapped brines are arranged throughout quartz as individual or clustered populations of inclusions, or occur along fracture-controlled linear arrays. CO_2-rich inclusions containing rare narcolite daughter minerals are present within quartz in syenogranite, but are apparently absent in alkali pegmatite. The multi-solid, hypersaline brines in both intrusions commonly contain between two and six daughter minerals, which include combinations of halite, ferropyrosmalite and magnetite, and more rarely sylvite, kutnahorite (Mn carbonate), hematite, andradite, diopside and calcite. The results of laser Raman spectrographic analysis of the liquid and gaseous phases show that they are primarily composed of H_2O with no detectable CO_2 or nitrogen (for all measured brine inclusions).

Preliminary microthermometric analysis of the brine inclusions reveals that homogenization temperatures range from 313^{o}C to > 517^{o}C, where most heating experiments show that fluid inclusions remain incompletely homogenized at temperatures exceeding 500^{o}C (although a population of inclusions homogenize between 313^{o}C and 440^{o}C). The temperature range exhibited by these inclusions is consistent with the fluid's probable magmatic derivation, and is consistent with other geothermometric constraints.

Proton Induced X-ray Emission (PIXE) analysis was carried out on fluid inclusion populations from the biotite syenogranite and alkali pegmatite. Sample preparation, analysis and data reduction were undertaken in accordance with the methods described by Ryan (1999) and Williams et al. (2001). In this study, shallow (<30 μm) primary brine inclusions trapped in euhedral-subhedral quartz were analysed to determine the concentration of Cl, K, Ca, Mn, Fe, Cu, An, As, Br, Rb, Sr, Ba and Pb.

In total, data for 33 PIXE brine analyses are presented here, and are compared to data from brines from intrusive phases of the Squirrel Hills Granite and the Starra Au-Cu hydrothermal system. Of the 33 analyses, 16 are of brines from the biotite syenogranite and the remaining are from alkali pegmatite. PIXE analyses show that all brines have a Br:Cl ratio < 0.005 (Fig. 1), with all but four having <0.002. These ratios overlap with, or are lower than values typically ascribed for magmatic brines and are much lower than those associated with sedimentary-hosted Cu sulphide mineralization at Mount Isa (Williams et al., 2001). Fluid inclusions from both intrusion types mainly contain percent-level concentrations of Ca (~0.8-5.1 wt %) and K (~0.4-3.6 wt %) with generally lower concentrations of Fe (0.2-4.2 wt %) and Mn (0.2-1.2 wt %). Ba typically occurs at concentrations on the order of 1000's ppm (0.1-0.8 wt %), whereas Rb resides at these concentrations within multi-solid brine inclusions within pegmatite but elsewhere occurs at levels below detection (<200-600 ppm). Sr, as opposed to Rb, exhibits

ranges in concentration from 350 to 780 ppm in multi-solid brine inclusions from the biotite syenogranite, whereas outside this population Sr occurs at concentrations below the level of detection (<1000-300 ppm). Cu, Zn, As and Pb concentrations are low, generally < 400 ppm, although a few inclusions contain > 1000 ppm of one or more of the metals.

Comparisons of the geochemistry of fluid inclusion populations show that there is a systematic change in the concentration of elements with magma evolution, where the younger rocks contain fluids that tend to have lower Sr, Ba, Ca and Ba/Fe, and higher K, Rb, Pb, Fe, Mn, Zn and As than magmatic fluids hosted in older biotite syenogranite (Fig. 2). For the most part these trends parallel geochemical changes arising from fractional crystallization during magma evolution, and as such fluid composition apparently largely correlates to bulk melt composition. However, data for Fe, Mn, Cu, Zn and As, appear to be at odds with trends in wholerock geochemistry and are higher in fluids derived from more highly evolved intrusions with lower Fe, Mn, Cu, Zn and As. This antithetic relationship can be used to suggest that the geological mechanisms involved in the metal enrichment processes shown here act independently to those governing fluid-melt partitioning for the alkali and alkaline earth elements.

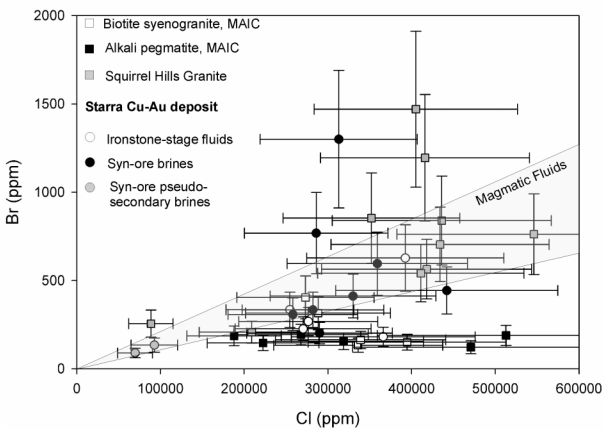

Figure 1 (left). Cl v Br composition of selected magmatic and ore-forming brines, Cloncurry district. Error bars shown are 30 % of the coordinate value. Additional data from brines from the Squirrel Hills Granite (Williams, unpublished and Starra Au-Cu deposit (Williams et al., 2001). The field for magmatic fluid are taken from data for volcanic fumaroles in Bohlke and Irwin (1992).

Figure 2 (below). Geochemistry of brines from selected intrusions and ore deposits. Symbols as in Fig. 1.

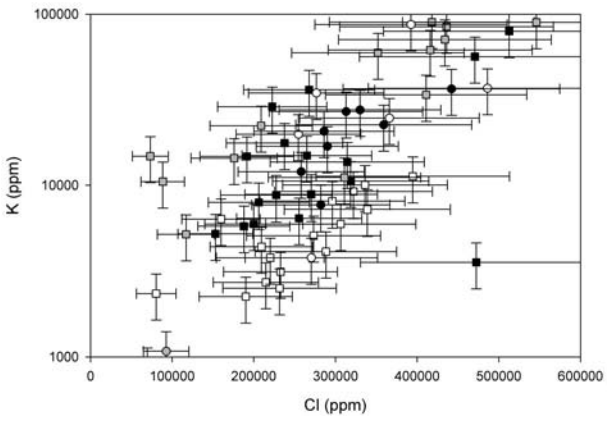

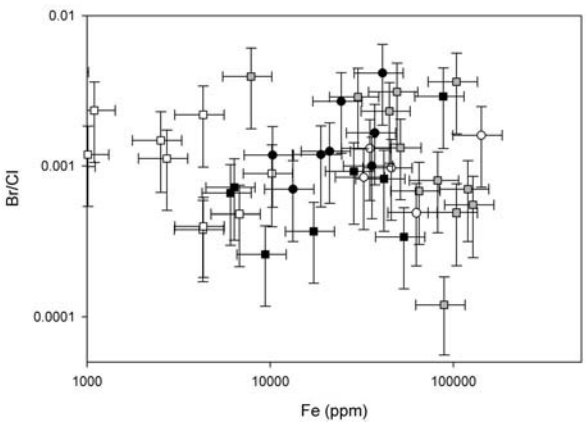

PIXE data (including data from Perring et al., 2000; Williams, unpublished) of magmatic brines from the MAIC and the Squirrel Hills Granite two intrusive masses that share similarities in their intrusive age (1.53-1.51 Ga) and petrogenesis exhibit substantial overlaps in their bulk geochemistry (Fig 2). One major, and potentially economically significant exception is a subset of brine inclusions from the Squirrel Hills Granite, first presented by Perring et al. (2000), which contain high Fe (9-13 wt %), Cu (1-2 wt %) and Ba (0.5-1.0 wt %) and exhibit demonstrable genetic associations with Fe oxide mineralization at the Lightning Creek prospect. As indicated in the data from the MAIC, the distribution of alkali and alkaline earth elements within magmatic brines appears to bear a direct correlation with the composition of the melt. Hence the similarity in the concentration of these elements within brines derived from the Squirrel Hills Granite and MAIC is consistent with the source intrusions having near identical petrogenetic histories and wholerock compositions.

Magmatic fluids, hydrothermal alteration and Fe oxide-Cu-Au mineralization

Primary CO_2–rich fluid inclusions have been identified in both of the igneous systems discussed above, where the timing of CO_2 exsolution appears to correlate to magmatic-hydrothermal brecciation (e.g. MAIC), fluid exsolution and high temperature albitization (cf. Perring et al.,

2000; Pollard, 2001). Similar fluid inclusions appear to be associated with ore-stage mineralization in all significant Fe oxide-(Cu-Au) deposits in the Cloncurry district (cf. Williams and Pollard, 2003, and references therein). More recent results show an intimate role between the timing of CO_2-brine unmixing and magnetite-copper mineralization (Mustard et al., 2004). Comparison of the geochemistry of brines from the MAIC to those from the Starra Au-Cu deposit (Williams et al., 2001) shows that the magmatic brines are dissimilar to all three types of fluids involved in mineralization at the deposit. This relation also holds for most of the brines from the Squirrel Hills Granite, which like those from the MAIC contain low Fe and Cu (cf. Figs 1 and 2). However, the occurrence of a small population of brine inclusions in the Squirrel Hills Granite (Perring et al., 2000), highlights the potential significance of magmatic fluids to ore genesis, but further work is required to unravel the relations between magma composition and petrogenesis, and the nature and evolution of their exsolved fluids. The existence of a small group of inclusions with radically different, but internally consistent compositions in the Squirrel Hills Granite indicates that their geochemistry was probably generated by mechanisms other than those controlling the distribution of alkali and alkaline earth elements. These processes could have influenced the geochemistry of these brines chemistry either at the point of brine exsolution (via fluid unmixing) or early in the genesis of hydrothermal evolution.

Acknowledgements

This work was funded by the pmd*CRC, and a JCU small grant managed by PJW. GM is a Logan Fellow funded by Monash University. The authors would like to thank Damien Foster and Justin Tolman for their assistance and advice.

References

Barton, M.D. and Johnson, D.A., 2000. Alternative brine sources for Fe oxide (-Cu-Au) systems: Implication for hydrothermal alteration and metals. In: Porter, T.M., ed, Hydrothermal Iron Oxide Copper-Gold and Related Deposits: A Global Perspective. Australian Mineral Foundation, 27-42.

Bohlke, J.K. and Irwin, J.J., 1992. Laser microprobe analyses of Cl, Br, I and K in fluid inclusions: Implications for sources of salinity in some ancient hydrothermal fluids: Geochimica et Cosmochimica Acta, 56, 203-225.

Hitzman M.W., Oreskes N. and Einaudi M.T., 1992. Geological characteristics and tectonic setting of Proterozoic iron oxide (Cu-U-Au-REE) deposits. Precambrian Research 58, 241-287.

Mark, G., Darval, M., Tolman, J., Foster, D.R.W., Williams, P.J. and Pollard, P.J., 1999. Magmas and regional alteration, Cloncurry district, NW Queensland, Australia. In: Stanley, C.J. et al., eds., Mineral Deposits: Processes to Processing. Balkema, Rotterdam, 385-388.

Mark, G. and Foster, D.R.W., 2000. Magmatic albite-actinolite-apatite-rich rocks from the Cloncurry district, Northwest Queensland, Australia. Lithos, 51, 223-245.

Mark, G., Foster, D.R.W., Pollard, P.J., Williams, P.J., Tolman, J. and Darvall, M., 2004. Magmatic fluid input during large-scale Na-Ca alteration in the Cloncurry district, NW Queensland, Australia. Terra Nova, 16, 54-61.

Mustard, R., Baker, T., Williams, P.J., Mernagh, T, Ryan, C., van Achterbergh, E. and Adshead, D. 2004. The role of unmixing in magnetite - copper deposition in the Fe oxide-Cu-Au systems. This volume.

Perring C.S. Pollard P.J., Dong G., Nunn A.J. and Blake K.L., 2000. The Lightning creek sill complex, Cloncurry district, northwest Queensland: A source of fluids for Fe oxide Cu-Au mineralisation and sodic-calcic alteration. Economic Geology, 95, 1067-1089.

Pollard, P.J., Mark, G. and Mitchell, L. C., 1998. Geochemistry of post-1540 Ma granites in the Cloncurry district, northwest Queensland: relationships to regional sodic-alteration and Cu-Au-Co mineralisation. Economic Geology, 93, 1330-1344.

Pollard P.J., 2001. Sodic(-calcic) alteration associated with Fe-oxide-Cu-Au deposits: an origin via unmixing of magmatic-derived H_2O-CO_2-salt fluids. Mineralium Deposita, 36, 93-100.

Ryan, C.G., 1999. Advances in fluid inclusion analysis using the nuclear microprobe. Nuclear Instruments and Methods in Physics Research, B54, 523-532.

Williams, P.J. and Pollard, P.J., 2003. Australian Proterozoic iron oxide-Cu-Au deposits: an overview with new metallogenic and exploration data from the Cloncurry district, northwest Queensland. Exploration and Mining Geology, 10, 191-213.

Williams P.J., Dong Guoyi, Ryan C.G., Pollard P.J., Rotherham J., Mernagh T.P. and Chapman L.H., 2001. Geochemistry of hypersaline fluid inclusions from the Starra (Fe oxide)-Cu-Au deposit, Cloncurry district, Queensland. Economic Geology, 96, 875-884.

Sr-Nd isotopic insights into the evolution of the Cloncurry district, Mount Isa Inlier

G. Mark[1], R. Mustard[2], D.R.W. Foster[2] and P.J. Pollard[2]

*[1] pmd*CRC, School of Geosciences, Monash University, Clayton, VIC 3168*
*[2] pmd*CRC, School of Earth Sciences, James Cook University, Townsville, QLD 4811*
Geordie@mail.earth.monash.edu.au

Introduction

Fe oxide-(Cu-Au) deposits are increasingly recognized as an economically valuable type of hydrothermal deposit due to their large size (100's->1000's Mt), and their endowment with a diverse range of metals (e.g. Cu, Fe, Au, Ag). This family of deposits encompasses a group of occurrences that were predominantly formed during Precambrian times (e.g. Olympic Dam deposit, Australia; Aitik deposit, Sweden; Sue Dianne deposit, Canada), but which exhibit considerable diversity in mineralogy, geochemistry and metal endowment. The nature and origin of Fe oxide Cu-Au deposits is highly controversial, particularly their relationships to magmatism and regional hydrothermal alteration. The main points of contention include: 1. The role of coeval intrusions as a source of heat and or fluids + metals; 2. The role of evaporite-rich country rocks (or their metamorphic equivalents) in providing fluids and ligands; 3. The degree of basinal/meteoric fluid infiltration; and 4. The capacity of regional fluids to move and transport metals from country rocks into the zones of Cu-Au mineralization (Williams and Pollard, 2001; Oliver et al., in press). However, little work has addressed how the nature, timing and distribution of Fe oxide-(Cu-Au) mineralization correlates with intrusive rock composition, and how intrusive compositions link with the tectono-thermal evolution of an orogenic belt. Addressing this important question will help to resolve the geodynamic setting of IOCG systems, and provide a framework for assessing the relative importance of the contentious issues above. The main difficulty in satisfactorily understanding these relations in most IOCG terranes is a lack of high-resolution age constraints for the timing of thermal peaks, magmatism and hydrothermal mineralization. However, the Mount Isa Inlier, and in particular the Cloncurry district represents one of the few exceptions, and thus is an ideal terrane to access these relations.

We present here Sr and Nd isotopic data figures 1 and 2 on the composition of magmatic intrusions emplaced after the thermal peak of the Isan Orogeny (ca.1600-1500 Ma). These data, combined with whole rock geochemistry and geochronological data, provide insights into the nature and composition of the crust; the role of the mantle in crustal evolution, orogenesis and magmatism; and constrain aspects of the crust's thermal character. The isotopic dataset also provides a baseline to more easily assess the contribution of different intrusions to the mineralized hydrothermal systems formed at various times during the orogeny. Consequently, the aims of this paper are to: 1. Determine the nature, composition and thermal character of the crust beneath the Cloncurry district during the Isan orogeny; and 2. To discuss the potential of radiogenic isotopes for fingerprinting magmatic fluid contributions to ore-forming systems.

Cloncurry District

The Cloncurry district forms the eastern exposed margin of the Mount Isa Inlier, and is endowed with numerous epigenetic Cu-Au deposits hosted within Paleoproterozoic carbonate-evaporite and siliciclastic metasedimentary rock sequences and metavolcanic rocks that were deposited during periods of intracrustal rifting (ca. 1.78-1.72 Ga and 1.67-1.65 Ga). In the west these sequences overlie older granite and felsic volcanic rocks dating to the Barramundi Orogeny. The cover sequences underwent a protracted period of deformation and metamorphism during the Isan Orogeny (ca. 1.60-1.50 Ga; O'Dea et al., 1997; Page and Sun, 1998) within which, three main fabrics are typically identified, although more complicated tectonothermal histories have been recorded in the vicinity of hydrothermal ore deposits and Isan-age igneous intrusive rocks. Regional metamorphism ranges in grade from greenschist to upper amphibolite facies; however the timing of this remains poorly constrained and is complicated by evidence for multiple thermal episodes

(Rubenach and Lewthwaite, 2002). Nevertheless, published age constraints indicate that the metamorphic peak occurred ca. 1.60-1.58 Ga across much of the district (Page and Sun, 1998; Hand and Rubatto, 2000; Giles and Nutman, 2002).

The Paleoproterozoic cover sequence rocks are intruded by a series of syn- to post-peak metamorphic intrusions that predominantly consist of four chemically distinctive suites of igneous rocks: 1. Abyssal pegmatites (ca. 1590 Ma); 2. Y-depleted, Sr-undepleted (TTG series) intrusions (ca. 1550 Ma); 3. Sodic, Y-undepleted, alkaline intrusions (ca 1540-1500 Ma); and, 4. K-rich, Y-undepleted intrusive complexes (ca 1540-1500 Ma). The abyssal pegmatites are the products of partial melting during metamorphism (Mark et al., 1998) while the remaining three suites form part of the Williams and Naraku Batholiths. These batholithic intrusions have an outcrop exposure >1500 km^2, and are predominantly potassic, although rare sodic intrusions of comparable age are also present. The potassic phases of the batholiths are largely composed of metaluminous, alkaline to subalkaline, magnetite-bearing granitoids that largely plot within 'A-type' fields on geochemical discrimination diagrams, although field relationships suggest a syn- to post-tectonic timing for the majority of the intrusions (Pollard et al., 1998). Potassic intrusions range from diorite to syenogranite to pegmatite, and are typically more oxidized than older counterparts in the western half of the Mount Isa Inlier (cf. Wyborn, 1998).

These intrusions exhibit a temporal, and less commonly observed spatial relation to regionally extensive hydrothermal alteration and Cu-Au mineralization. The close relations between magmatism, regional alteration and mineralisation (1590-1500 Ma) has engendered a range of highly contentious arguments over the degree to which intrusions played a passive (e.g. source of thermal input to drive fluid convection) or active (e.g. direct input of saline fluids, metals or sulphur) role in the generation of the hydrothermal systems, and the formation of localized base metal mineralization (Williams and Pollard 2001, and references therein). Stable isotope, fluid inclusion and geochemical data from a range of deposits and regional hydrothermal systems provide evidence for a substantial role for magmatic fluids in the formation of these systems (Williams and Pollard, 2001, and references therein; Oliver et al., in press).

Results

Abyssal pegmatites and host metasedimentary rocks

The ca. 1590 Ma pegmatites and psammitic metasedimentary host rocks of the Soldiers Cap Group (ca. 1670 Ma) collected from around the Cannington Ag-Pb-Zn and Osborne Cu-Au mines exhibit similar Sr and Nd isotopic compositions, and contain highly radiogenic initial $^{87}Sr/^{86}Sr$ of 0.710896-0.718505 and 0.705919-0.716103 respectively, and yield depleted mantle model ages (T_{DM}) of 2447-2508 Ma and 2520-2565 Ma respectively. The similarity in the isotopic composition of the rock types is consistent with the pegmatites having formed by partial melting of the host sedimentary package during upper amphibolite facies metamorphism (>670^oC; 300-500 MPa) at 1600-1580 Ma (cf. Mark et al., 1998; Giles and Nutman, 2002). The late Archaean to early Proterozoic T_{DM} are much older than that of the intrusions of the Williams and Naraku Batholiths, although they overlap with some similarly aged units of the Mount Norna Quartzite (T_{DM} 2131-2510 Ma*). For the most part, however, the samples studied here most closely resemble the felsic basement rocks (e.g. Leichhardt Volcanics, T_{DM} 2506 Ma; Yaringa Metamorphics, T_{DM} 2489 Ma*), as well as some of the older cover sequence 2 packages rich in calc-silicate rocks (T_{DM}: 2314-2730 Ma*) and coeval felsic intrusions (e.g. Levian Granite, 1746 ± 8 Ma; T_{DM} 2442 Ma*). Given these considerations the results most likely show that these Soldiers Cap Group metasedimentary rocks that host the Osborne and Cannington deposits are largely sourced from basement material which most likely formed a topographic high ca. 1670 Ma (cf. O'Dea et al., 1997).

Williams and Naraku Batholiths

Representative samples of Y-depleted, Sr-undepleted trondhjemite (ca. 1550 Ma) and Y-undepleted sodic and K-rich intrusions (1540-1500 Ma) have mixed crust-mantle initial $^{87}Sr/^{86}Sr$ (0.696800-711170) and εNd (-1.0 to –3.4), and exhibit a range in T_{DM} between 2081 and 2301 Ma. In detail, trondhjemite has higher initial $^{87}Sr/^{86}Sr$ (0.711170) than both the Y-undepleted sodic and K-rich intrusions that predominantly range from 0.706726 to 0.708487, and 0.696800 to 0.706476 respectively, although one two-mica granite (Wallaby Granite) contains highly radiogenic initial

$^{87}Sr/^{86}Sr$ (0.806158) with a T_{DM} of 2246 Ma. Compared to the supracrustal rocks, and most of the older igneous rocks, these intrusive rocks contain an average REE component that was removed at a much later time (ca. 2200 Ma), and apart from minor inclusion of xenocrystic zircons show very little evidence for significant interaction with materials removed from the depleted mantle at earlier times. This conclusion is best demonstrated in the data from the suite of potassic intrusions that show systematic, and asymptotic mixing relationships between wholerock T_{DM} and SiO_2. This relationship shows that the felsic, crustally-derived intrusions (>65 wt% SiO_2) were derived from crustal material separated from the depleted mantle ca. 2200-2250 Ma, and that these intrusions locally mingled and mixed with coeval mantle-derived mafic intrusions which preserve a systematic increase in T_{DM} with the progressive incorporation of more felsic melt (c.f. Figure 3).

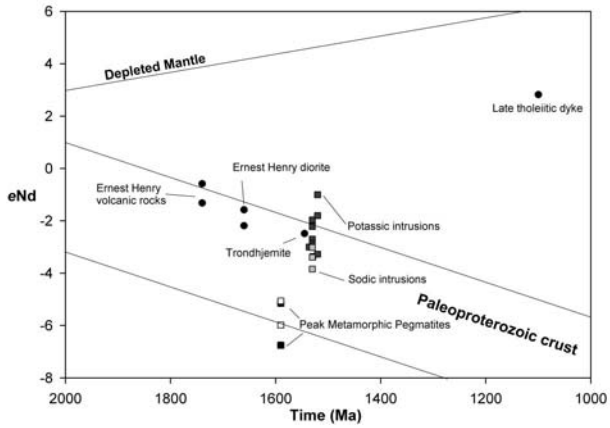

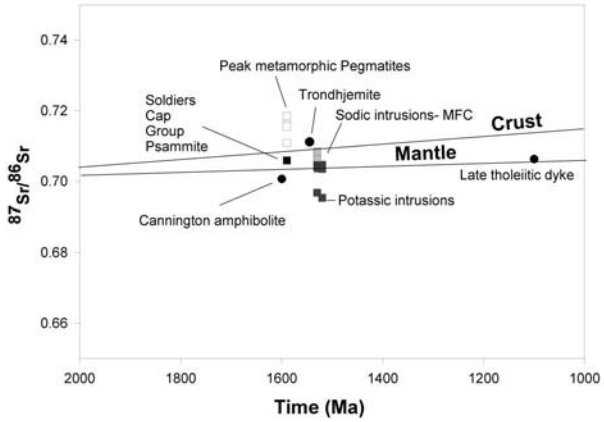

Figure 1 (top right. Initial $^{87}Sr/^{86}Sr$ at the time of the emplacement of the magmatic rocks, or at the thermal metamorphic peak ca. 1590 Ma.

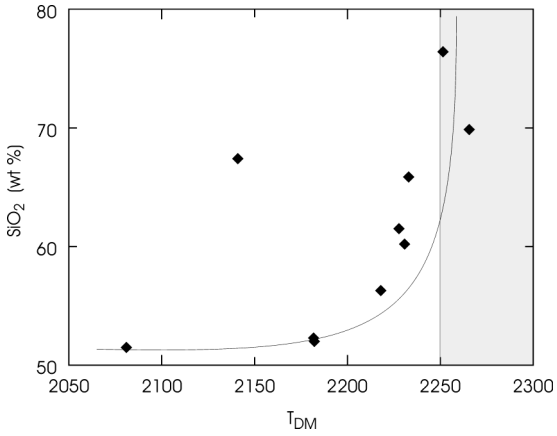

Figure 2 (top left). Initial $^{144}Nd/^{143}Nd$ (as εNd) at the time of the emplacement of the magmatic rocks, or at the thermal metamorphic peak ca. 1590 Ma.

Figure 3 (left). Calculated two-stage depleted mantle-model age against wholerock SiO_2 for selected potassic intrusions of the Williams and Naraku Batholiths. Note the asymptotic character of the line-of-best-fit that appears to show that the REE reservoir for the felsic intrusive rocks was probably removed from the mantle prior to 2220-2250 Ma, whereas the mafic rocks exhibit incorporation of juvenile mantle.

The close correlation in the T_{DM} and initial $^{87}Sr/^{86}Sr$ of the sodic and K-rich intrusions shows that they were formed from material of broadly similar isotopic character and, combined with their near identical REE patterns and Y-undepleted geochemistry, indicates derivation from contemporaneous melting reactions (<1.0-0.8 GPa; >850^{o}C) in the same regions of the crust. Similarity in the isotopic composition of these intrusions with the trondhjemitic intrusions (*ca.* 1550 Ma) suggest that the source regions for both periods of melting was crustal material removed from the depleted mantle during the early Proterozoic, and that the Y-depleted character of the older melts is due to melting reactions at deeper crustal levels (Pollard et al., 1998; Wyborn, 1998).

The results of this isotope study shows that the crust is composed of two main REE reservoirs which, when taken as a bulk composition, indicate removal from the depleted mantle at ca. 2400-2600 Ma and ca. 2200 Ma (cf. McCulloch, 1987). These reservoirs were most likely continually diluted by the episodic emplacement of mantle derived magmas during the main periods of orogenesis from the Barramundi through to the Isan Orogeny (cf. Page and Sun, 1998). In the Cloncurry district the younger intrusions of the Williams and Naraku Batholiths are predominantly derived from melting the 2200 Ma reservoir with minor interaction with mantle-derived mafic melt, whereas the abyssal pegmatites that formed in the early stages of the Isan Orogeny (1590 Ma) as well as the older supracrustal rocks and felsic intrusions interacted to a much higher degree with the 2400-2600 Ma crustal reservoir.

Implications for unravelling the genesis of ore systems and regional alteration

The protracted period over which hydrothermal alteration and mineralization occurred in the Cloncurry district (1590-1500 Ma) means that intrusions from different intrusive suites contributed to the hydrothermal systems at different times over the entire duration of the district's metallogenic history. The input of fluids by compositionally distinct magmas into the regional hydrothermal systems, and locally the ore-forming systems, significantly downplays the potential role of intrusions of specific composition in the genesis of Fe oxide-(Cu-Au) mineralization. This apparent diversity in intrusive rock composition over time may also play some part in the diversity in the composition and nature of mineralized ore systems in the district.

As an example, from published ages and field relationships, our present understanding of the Osborne Cu-Au deposit indicates that it was produced much earlier (1590 Ma) than the other Cu-Au systems in the district, and formed in close association with abyssal pegmatites, whereas the other deposits formed synchronously with the emplacement of the Williams and Naraku Batholiths. Therefore, if this interpretation is correct, and considering the isotopic results shown above, it is clear that fluids exsolved from the abyssal pegmatites should exhibit radically different isotopic compositions (reflecting that of the parent melt) than the later intrusions. As such, the deposits formed in association with the introduction of magmatic fluids at different stages of the Isan Orogeny should exhibit differences in their isotopic composition, e.g. we here anticipate that the isotopic composition of the Osborne deposit will be radically different to the younger examples. Isotopic (crustal scale) 'stratigraphy' provides a powerful tool that can be applied to problems such as reconstructing crustal history, the role and significance of magmatic fluids and the interplays of fluid-rock interaction in the genesis of Fe oxide-(Cu-Au) deposits in the Cloncurry district, and also to deconstructing the hydrodynamic mechanisms for how regionally extensive hydrothermal systems were formed and evolved.

Acknowledgements

GM is a Logan Fellow funded by Monash University. The authors would like to thank Mike Rubenach, Tom Blenkinsop and Nick Oliver for their assistance and advice.

References

Giles, D. and Nutman, A.P., 2002. SHRIMP U-Pb monazite dating of 1600-1580 Ma amphibolite facies metamorphism in the southeastern Mt Isa Block, Australia. Australian Journal of Earth Sciences, 49, 455-465.

Hand, M. and Rubatto, D., 2002. The scale of the thermal problem in the Mount Isa Inlier. In: Preiss, V.P., ed., Geoscience 2000: expanding horizons: Geological Society of Australia, Abstracts, 67, 475.

Mark, G., Phillips, G.N. and Pollard, P.J., 1998. Highly selective partial melting of pelitic gneiss at Cannington, Cloncurry district, Queensland. Australian Journal of Earth Sciences, 45, 169-176.

McCulloch, M.T., 1987. Sm-Nd isotopic constraints on the evolution of Precambrian crust in the Australian continent. In: A. Kroner, ed, Proterozoic Lithospheric Evolution. American Geophysical Union, Washington, 115-130.

O'Dea, M. G., Lister, G.S., MacCready, T., Betts, P.G., Oliver, N.H.S., Pound, K.S., Huang, W. and Valenta, R.K., 1997. Geodynamic evolution of the Proterozoic Mount Isa terrain. In: Burg, J.P. and Ford, M., eds., Orogeny through time. Geological Society of London, Special Publication, 121, 99-122.

Oliver, N.H.S., Mark, G., Cleverley, J.S., Pollard, P.J., Fu, B., Marshall, L.J., Rubenach, M.J., Williams, P.J. and Baker, T., The role of sodic alteration in the genesis of iron oxide-copper-gold deposits, eastern Mt Isa Block, Australia. Economic Geology (in press).

Page, R.W. and Sun, S-S. 1998. Aspects of geochronology and crustal evolution in the Eastern Fold Belt, Mount Isa Inlier. Australian Journal of Earth Sciences, 45, 343-362.

Pollard, P.J., Mark, G. and Mitchell, L.C., 1998, Geochemistry of post-1540 granites spatially associated within regional sodic-calcic alteration and Cu-Au-Co mineralisation, Cloncurry district, northwest Queensland. Economic Geology, 93, 1330-1344.

Rubenach, M.J. and Lewthwaite, K.A. 2002. Metasomatic albitites and related biotite-rich schists from a low-pressure polymetamorphic terrane, Snake Creek Anticline, Mount Isa Inlier, north-eastern Australia. Microstructures and P-T-d paths. Journal of Metamorphic Geology, 20, 191-202.

Williams, P.J. and Pollard, P.J., 2001. Australian Proterozoic iron oxide-Cu-Au deposits: an overview with new metallogenic and exploration data from the cloncurry district, northwest Queensland. Exploration and Mining Geology, 10,191-213.

Wyborn, L.A.I., 1998. The younger ~1500 Ma granites of the Williams and Naraku Batholiths, Cloncurry district, eastern Mount Isa Inlier: geochemistry, origin, metallogenic significance and exploration indicators. Australian Journal of Earth Sciences, 45, 397-412.

[*]Data from the Mount Isa Inlier geochronolgy database on the GA website: www.ga.gov.au.

Testing the 'Fool's Clock' and tales from fluid inclusions

J.McL Miller, M. Kendrick and D. Phillips

*pmd*CRC, School of Earth Sciences, University of Melbourne, VIC 3010*

jmm@unimelb.edu.au

Testing the 'Fool's Clock'

Introduction

The possibility of dating 'pyrite' using the $^{40}Ar/^{39}Ar$ technique was first investigated by York et al. (1982), who obtained a reasonable, although imprecise, age for pyrite grains from an Archaean ore deposit. More recently, Smith et al. (2001) used a $^{40}Ar/^{39}Ar$ laser probe to analyse single pyrite grains (0.1 – 0.3 mm) from two igneous rocks and obtained apparently reliable and precise ages. Smith et al. (2001) further suggested that pyrite grains will be retentive of argon and less susceptible to problems associated with argon loss and ^{39}Ar recoil.

One of the goals of the current H4 project is to evaluate the potential for dating mineralization events via $^{40}Ar/^{39}Ar$ analyses of pyrite grains containing inclusions of white mica. Initial studies on pyrite from the Stawell gold mine in Western Victoria revealed sufficient potassium in <0.5 mm grains for single grain $^{40}Ar/^{39}Ar$ laser probe analyses and confirmed the retentivity of argon in the pyrite structure. This paper presents additional results for pyrite samples from the Mt Charlotte and Kanowna-Belle gold deposits in the Yilgarn Craton.

Sample and Analytical Procedures

Ore-stage pyrite grains (0.2 – 0.5 mm), containing white mica inclusions, were separated from Mt Charlotte (MC263-1) and Kanowna-Belle (GDD438) samples. In addition, a matrix sericite separate was prepared from sample GDD438. $^{40}Ar/^{39}Ar$ analyses were carried out using a Nd-YAG laser and a MM5400 mass spectrometer. Reported ages have been corrected for system blanks, mass discrimination, reactor interferences, fluence gradients and atmospheric contamination. Errors on ages are 1σ and include uncertainties in the J-value (±0.35%).

Analytical Results

$^{40}Ar/^{39}Ar$ laser step-heating analyses were carried out on a number of single pyrite grains from the Mt Charlotte and Kanowna Belle samples. The Mt Charlotte pyrite grains yielded very reproducible results, with some grains producing flat age spectra. Other grains exhibited younger ages from the lowest temperature step, suggestive of minor argon loss. When plotted on an inverse isochron diagram, the high temperature analyses give an age of 2596 ± 9 Ma (1σ) and a $^{40}Ar/^{36}Ar$ intercept value of 293 ± 3 (Fig. 1).

In contrast to the Mt Charlotte sample, pyrite grains from Kanowna-Belle yielded more discordant results, with the lowest temperature steps characterized by anomalously old apparent ages (up to 3.3 Ga), and the highest temperature steps giving the youngest ages (to 1.9 Ga). Importantly, most total-gas ages are in the range 2570 – 2660 Ma, which are significantly older than maximum ages obtained from a matrix sericite sample (2500 Ma) from the same sample (Figure 1). The matrix sample produced a staircase-shaped age spectrum, indicating significant partial argon loss at some time in the Proterozoic.

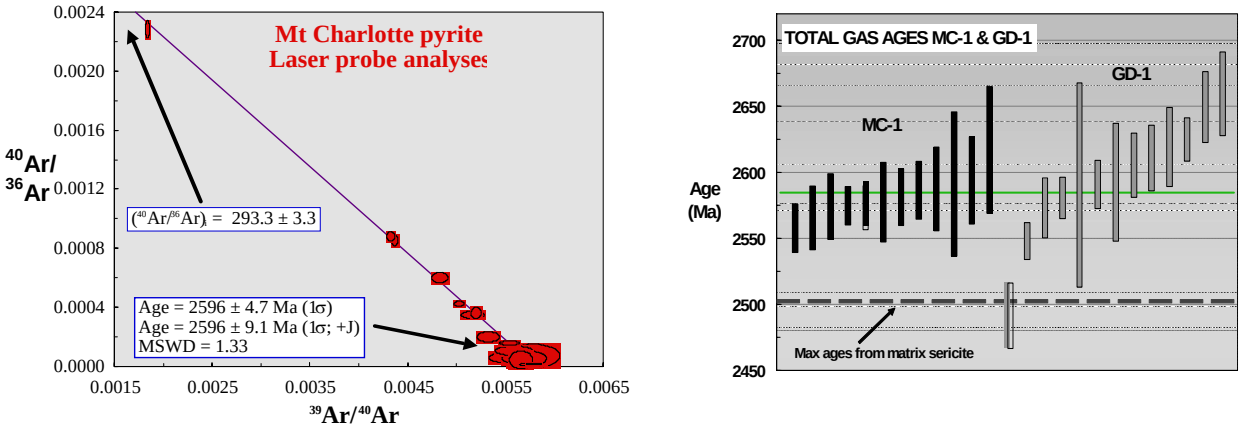

Fig. 1. Inverse isochron diagram showing high temperature $^{40}Ar/^{39}Ar$ laser probe analyses for single pyrite grains from Mt Charlotte sample MC-1 (left) and diagram of total gas ages from Mount Charlotte and Kanowna-Belle pyrites (right).

Discussion

The isochron age of 2596 ± 9 Ma obtained from the Mt Charlotte pyrite grains is within error of $^{40}Ar/^{39}Ar$ ages (mean age = 2602 ± 8 Ma) obtained by Kent and McDougall (1995). Our results confirm that individual pyrite grains (<0.5 mm) contain sufficient white mica for $^{40}Ar/^{39}Ar$ step-heating analyses and can provide precise and reliable age information. These results also demonstrate the advantage of undertaking step-heating analyses to investigate argon loss effects, presumably related to white mica grains connected to grain surfaces by fractures.

The argon loss profile associated with the Kanowna-Belle matrix sericite likely relates to partial overprinting by Proterozoic dykes and faults. A possible explanation for the Kanowna-Belle pyrite results is that this overprint event caused partial loss of argon from white mica inclusions to the mica-pyrite interface region within the pyrite grains. This weakly-held argon was then released during the initial heating steps, yielding old apparent ages. If correct, then the total-gas ages should provide the best estimate of the time of white mica entrapment within the pyrite. However, as it is not possible to determine argon loss effects from total-gas ages, all ages are strictly minimum estimates for the time of pyrite formation. In this case, the oldest apparent ages may provide the best estimate for initial pyrite formation and hence gold mineralization (~2655-2665 Ma), although multiple stages of pyrite growth and excess ^{40}Ar must be considered.

Noble gases and Halogens in fluid inclusions

Introduction

The isotopic noble gas (^{40}Ar, ^{36}Ar, ^{84}Kr and ^{129}Xe) and halogen (Cl, Br and I) composition of fluid inclusions can be determined simultaneously by noble gas mass spectrometry of irradiated samples (extended ^{40}Ar-^{39}Ar methodology). The technique is a powerful tool for studying hydrothermal ore deposit, and examples are given for two contrasting fluid systems: (1) High T, high salinity, Porphyry Copper Deposits (PCD), where the technique enables: quantitative determination of mantle (magmatic), crustal and surface derived fluid components; identification of devolatalisation processes, and age constraints of hydrothermal quartz veins (Kendrick et al., 2001a, 2001b). (2) Low T, Pb-Zn-rich, crustal fluids involved in sediment-hosted, Mississippi Valley-Type (MVT) deposits where, in addition to evidence on fluid origin, the technique enables; delineation of brine provinces (10-100's of km) (Kendrick et al., 2002a); identification of specific fluid-rock interactions (Kendrick et al., 2002b), and/or the involvement of basement lithologies; inferences on timing and; construction of deposit models (Kendrick et al., 2004).

Methodology and samples

Neutron irradiation of the halogens (Cl, Br, I) and various cations found in mineralizing fluids (Ca, K, Ba) produce isotopes of Ar, Kr or Xe. It is therefore possible to measure simultaneously noble gas isotopes, halogens and selected cations via noble gas mass spectrometry of irradiated samples. This technique is

several orders of magnitude more sensitive than conventional techniques for the detection of halogens and makes analysis of fluid inclusion wafers possible.

Quartz vein PCD samples were selected from the inner Potassic and outer Propylitic zones of Bingham Canyon, Silverbell, Pinto Valley, Mission, Ray and Globe-Miami, USA. Complimentary He isotope analyses were obtained from non-irradiated coexisting sulphide phases. Fluorite, barite, sphalerite and calcite samples where selected from MVT districts in the UK (S. Pennine), USA (Tri-State, Viburnum Trend, Illinois-Kentucky) and Scandinavian sandstone-hosted Pb-Zn (Laisvall, Vassbo, Osen). He isotope analyses were obtained from fluorite and sulphide phases.

Halogens

The Br/Cl and I/Cl values of PCD fluids overlap those of mantle diamond (Johnson et al., 2000) suggesting a mantle/magmatic source for salinity. Crustal fluids involved in MVT mineralization consist of predominantly evaporated seawater, but halite dissolution waters are important at Hansonburg, USA (Bohlke and Irwin, 1992) and mixed brines are significant in the South Pennine Orefield, UK (Kendrick et al., 2002a). I/Cl ratios are ubiquitously above what can be accounted for by evaporation of seawater alone, and indicate fluid interaction with I-rich organic sediments. Evolution of fluids to higher I/Cl values in the outer zone of Silverbell PCD, provide evidence for a formation water involvement in PCD mineralization (Kendrick et al., 2001b).

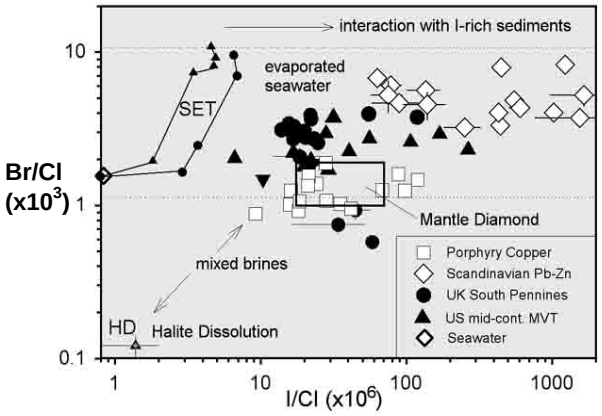

Fig 2. Halogen data for PCD and MVT deposits. The South Pennine orefield and US MVT are distinguished from Scandinavian Pb-Zn. The Seawater Evaporation Trajectory, mantle diamond field and the Hansonburg MVT representative of Halite dissolution water are shown for reference (Zherebstova and Volkova, 1966; 1966; Bohlke and Irwin, 1992; Johnson et al., 2000).

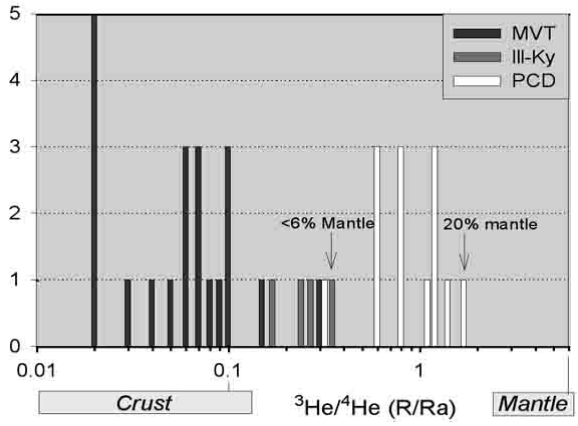

Fig 3. Helium data for PCD and MVT deposits. 'MVT' comprises the South Pennine Orefield and Scandinavian Pb-Zn deposits. This time the Illinois-Kentucky district is distinguished.

Helium

The helium $^{3}He/^{4}He$ ratio is expressed as an R/Ra value (atmospheric R/Ra = 1). However, due to the low atmospheric abundance of helium, the $^{3}He/^{4}He$ composition of crustal fluids results from mixing between crustal (R/Ra <0.1) and mantle (R/Ra >8) end-members only. The data indicate both the inner Potassic and the outer Propylitic zone in each of the PCD studied comprise mixed mantle and a sub-equal to dominant crustal component. The majority of 'MVT' deposits have low crustal $^{3}He/^{4}He$ values typical for basinal brines. However a minor mantle component (<6%) is present in fluorite-rich mineralization of the Illinois-Kentucky district, which is spatially associated with an alkaline igneous complex.

Helium and Argon

The radiogenic production ratios of $^{40}Ar^{*}/^{4}He$ for crust (0.2) and mantle (0.5) are distinct and fluid values outside these ranges indicate fluid mixing or noble gas fractionation. Low T fluids (<250 °C) are enriched in He due to the preferential retention of Ar in many crustal minerals. High T, PCD fluids are a mixture of

crust and mantle components and have preferentially lost He during devolatilisation; the ^{36}Ar concentration is lower than air saturated water (ASW) and Ar, Kr and Xe also exhibit fractionation supporting this interpretation (Kendrick et al., 2001b).

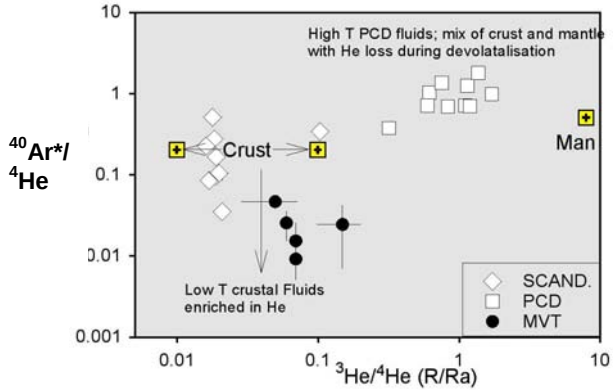

Fig 4. 40Ar/4He v. R/Ra for PCD, MVT and Scandinavian Pb-Zn. SCAND = Scandinavian Pb-Zn; sphalerite and fluorite. MVT = South Pennine Orefield, UK.*

Deposit	$^{40}Ar/^{36}Ar$	$^{3}He/^{4}He$ (R/Ra)	^{4}He and $^{40}Ar^*$ concentration
PCD	**300-3600**	**0.35-1.7**	**v. low**
MVT	**300-1500**	**0.05-0.1**	**high**
SCAND.	**300-16000**	**0.02**	**v.v. high**

Table 1: Typical values for 3 different styles of ore deposit

Helium, Argon and Krypton

The $^{40}Ar/^{36}Ar$ ratio provides information on mixing between an atmospheric (or surface derived meteoric/seawater) component (=295.5) and a radiogenic component that consists of mantle and/or crustal volatiles. The $^{84}Kr/^{36}Ar$ ratio is used to distinguish Atmospheric Ar introduced as air, meteoric water or seawater. Thus used in tandem, the $^{40}Ar/^{36}Ar$, $^{84}Kr/^{36}Ar$, $^{3}He/^{4}He$ and halogens provide information on: mantle, crustal, meteoric, seawater and air components.

Typical values of $^{40}Ar/^{36}Ar$, $^{3}He/^{4}He$ and the relative concentration of $^{40}Ar^*$ and ^{4}He are given in Table 1. In PCD systems the data suggests fluids in the Potassic and Propylitic zones are a mixture of magmatic, crustal formation water, and meteoric water. Formation water involvement at Silverbell is also suggested by I/Cl values that increase toward the outer propylitic zone. However, based on He data, the proportion of crust and mantle volatiles is similar in both the potassic and propylitic zones, approximately 1:(2-9) mantle:crust. In contrast, the involvement of meteoric water is just 10-40% in the inner pottasic zone but increases significantly in most of the outer propylitic zones, accounting for >90% of the fluid at Bingham Canyon. The low noble gas concentration provides evidence for devolatilisation during hydrothermal boiling.

Most sediment-hosted Pb-Zn deposits are formed by long-lived crustal brines with low R/Ra values. The high concentration of the crustally derived noble gases ($^{40}Ar^*$, ^{4}He) provides strong evidence of limited meteoric water involvement. ^{4}He contents were used in the South Pennine Orefield to infer a pre-mineralisation crustal residence time of ~50 Myr. The $^{40}Ar/^{36}Ar$ ratios and noble gas concentrations of Scandinavian sandstone-hosted Pb-Zn deposits are much greater than typical carbonate-hosted MVT districts. This suggests a longer pre-mineralisation crustal residence time of 100-200 Myr, compatible with a Caledonian (~425 Ma) mineralisation age and significant fluid-basement interaction. Critically, the difference in noble gas compositions between classic MVT and the Scandinavian Pb-Zn deposits can be related to the tectonic setting of Scandinavia. A fluid origin on the pre-collision continental margin is favoured, with migration driven by tectonic processes. Mineralisation does not appear to be related to gravity induced flow from a foreland basin, as is the case for most MVT deposits (see Kendrick et al., 2004).

Acknowledgements

Significant contributions to noble gas/halogen work on fluid inclusions have been made by R. Burgess, R. Pattrick and G. Turner (University of Manchester); A. Bjørlykke (Geological Survey of Norway and D. Leach (USGS).

References

Bohlke, J.K. and Irwin, J. J., 1992. Brine history indicated by argon, krypton, chlorine, bromine, and iodine analyses of fluid inclusions from the Mississippi valley type lead-fluorite-barite deposits at Hansonburg, New Mexico. Earth and Planetary Science Letters, 110, 51-55.

Johnson, L.H., Burgess, R., Turner, G., Milledge, H.J. and Harris, J. W., 2000. Noble gas and halogen geochemistry of mantle fluids; comparison of African and Canadian diamonds. Geochimica Cosmochimica Acta 64, 717-732.

Kendrick, M.A., Burgess, R., Pattrick, R.A.D., and Turner, G., 2001a. Halogen and Ar-Ar age determinations of inclusions within quartz veins from porphyry copper deposits using complementary noble gas extraction techniques. Chemical Geology, 177,351-370

Kendrick, M.A., Burgess, R., Pattrick, R.A.D., and Turner, G., 2001b. Fluid inclusion noble gas and halogen evidence on the origin of Cu-porphyry mineralising fluids. Geochimica Cosmochimica Acta 65, 2651-2668.

Kendrick, M.A., Burgess, R., Pattrick, R.A.D., and Turner, G., 2002a. Hydrothermal fluid origins in a fluorite-rich Mississippi valley-type district; combined noble gas (He, Ar, Kr) and halogen (Cl, Br, I) analysis of fluid inclusions from the South Pennine ore field, United Kingdom. Economic Geology 97, 435-451.

Kendrick, M.A., Burgess, R., Leach, D., and Pattrick, R.A.D., 2002b. Hydrothermal fluid origins in mississippi valley-type ore districts; combined noble gas (He, Ar, Kr) and halogen (Cl, Br, I) analysis of fluid inclusions from the Illinois-Kentucky fluorspar district, Viburnum Trend and Tri-State districts, Midcontinent United States. Economic Geology 97, 453-469;

Kendrick, M.A., Burgess, R., Harrison, D., and Bjørlykke, A., 2004. Noble gas and halogen evidence for the origin of Scandinavian sandstone-hosted Pb-Zn deposits, Geochimica Cosmochimica Acta, In Press.

Kent, A.J.R and McDougall, I.,1995. ^{40}Ar-^{39}Ar and U-Pb age constraints on the timing of gold mineralization in the Kalgoorlie gold field, Western Australia. Economic Geology, 90, 845-859.

Smith, P.E., Evensen, N.M., York, D., Szatmari, P., de Oliveira, D.C., 2001, Single-crystal ^{40}Ar-^{39}Ar dating: No fool's clock, Geology, 29, 403-406.

Zherebstova, L.K. and Volkova, N.N.1966. Experimental study of behaviour of trace elements in the process of natural solar evaporation of Black Sea water and Sasyk-Sivash brine. Geochemistry International., 3, p. 656-670.

York, D., Masliwec, A., Kuybida, P., Hanes, J.A., Hall, C.M., Kenyon, W.J., Spooner, E.T.C., Scott, S.D., 1982, ^{40}Ar-^{39}Ar dating of pyrite, Nature, 300, 52-53.

Pressure-temperature-time paths from P-T pseudosections and zoned garnets: implications for microstructural and metamorphic evolution of the Eastern Succession, Mt Isa Inlier

Mohammad Sayab and Michael Rubenach

*pmd*CRC, School of Earth Sciences, James Cook University, Townsville, QLD 4811*

Mohammad.Sayab@jcu.edu.au

Introduction

The Mt Isa Inlier of northwest Queensland contains multiply deformed and poly-metamorphosed middle Proterozoic meta-sedimentary rocks with extensive intrusive and extrusive complexes. A number of structurally-controlled Iron Oxide Copper Gold (IOCG) and Ag-Zn-Pb deposits are hosted within the inlier. It has been argued that the mineralization is controlled by discrete episodes of deformation and metamorphism (e.g., Adshead-Bell, 1998) ranging from ~1595Ma Osborne Cu-Au (Rebenach et al., 2001) to ~1505Ma Starra Au-Cu orebodies (Rotherham et al., 1998). Therefore, understanding tectonics and metamorphism is essential for prospectivety analysis and exploration for these deposits.

The Eastern Fold Belt of the Mt Isa Inlier hosts poly-metamorphic signatures of pro- and retrograde mineral assemblages. Examples of poly-metamorphic mineral assemblage include cordierite-staurolite-biotite-muscovite in the Snake Creek Anticline (Rubenach and Lewthwaite, 2002) and Rosebud Syncline of the Mary Kathleen Fold Belt (Reinhardt, 1992). The occurrence of such poly-metamorphic mineral assemblage implies that the Eastern Succession of the Mt Isa inlier has undergone discrete phases of metamorphism and associated deformation (e.g., Pattison et al., 1999).

This study seeks to understand the tectono-thermal evolution of the Eastern Succession of the Mt Isa Inlier. Detailed structural mapping and systematic sampling has been carried out in the key areas of the Eastern Succession to answer some of the fundamental and most critical questions, e.g., what is the link between the poly-metamorphic nature of the Eastern Succession with crustal-scale deformation episodes? We present our preliminary P-T results based on microstructural relationships and thermodynamic modeling from the Snake Creek Anticline, Tommy Creek Block and White Blow Formation of the Mary Kathleen Fold Belt (Fig. 1). Significantly, we have documented high-pressure estimates based on thermodynamic modeling of chemically zoned garnets, which are consistent with textural relationships and field observations, and have never been reported from any part of the Mt Isa Inlier.

P-T pseudosections and geo-theromobarometric constraints

P-T pseudosections, that is, maps of stable mineral assemblages in P-T-X space, have been prepared using XRF bulk rock major element chemistry, using the computer program THERMOCALC and an internally consistent thermodynamic database (Powell et al., 1998). This method can reliably model the P-T conditions of garnet core growth, based on the intersection of Fe, Mn and Ca compositional isopleths (Vance and Mahar, 1998). P-T pseudosections are able to explain the observed mineral assemblages, compositions, zonations and modes in the rocks with distinct bulk compositions with respect to a petrogenetic grid.

P-T paths for five samples were calculated in a 9-component model chemical system (MnCaNaKFMASH). Three samples came from Snake Creek anticline (SC122, SC189, SC192), one

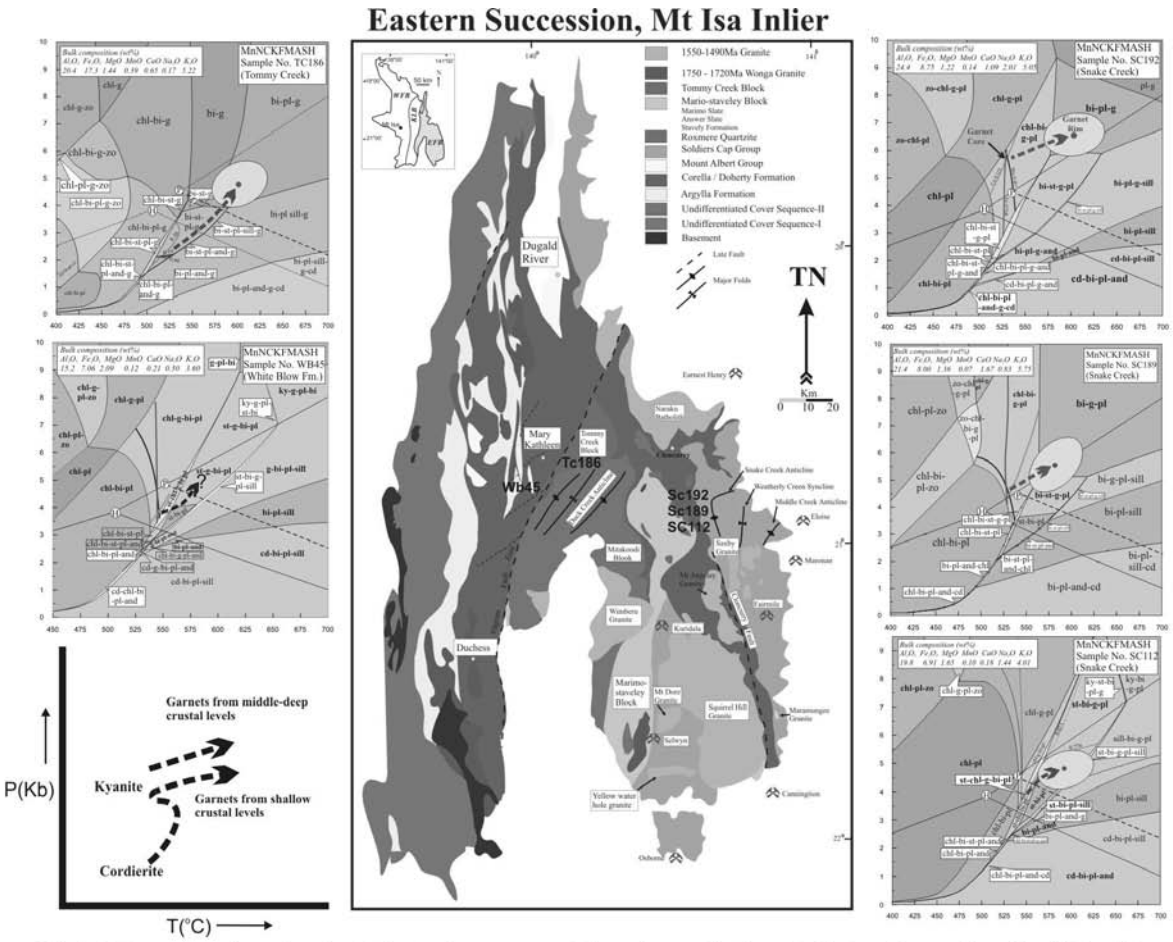

Fig.1. P-T pesudosections showing P-T paths from representative rock samples from the Eastern Succession of the Mt Isa Inlier. Sample number plus location is presented on the top right corner of the pseudosections, where XRF bulk rock composition (wt%) is on the top left.

from Tommy Creek Block (TC186) and one from White Blow Formation (WB45) (Fig. 1). To a first approximation, the pseudosections for sample SC192 and SC189 are consistent with the mineralogies of the rocks. For example, in sample SC192 chlorite and plagioclase inclusions occur in the core and median region of the garnets. No chlorite has been observed in the matrix. This textural relationship has successfully been modeled, where garnet core X_{Mn}, X_{Fe} and X_{Ca} compositional isopleths intersect uniquely in chl-bi-pl-grt stability field. Similarly, garnet rim, matrix plagioclase, biotite and muscovite geothermobarometric estimates by using the average P-T feature of THERMOCALC lies within the grt-pl-bi field, and is completely consistent with the pseudosection stability field. Texturally, the inclusion trails within the garnets are fine-grained as compared to the matrix minerals and are not continuous, i.e, the matrix foliation is strongly deflected around the porphyroblast. This suggests that the garnet growth occurred early in the deformation history (Passchier and Trouw, 1998). The core of the garnet growth occurred at 5.6-5.8kb/526^{o}C, whereas the garnet rim with matrix phases are found to be 6.5±1.1kb/602±27^{o}C. For sample SC189, garnet core growth occurred at 4.4-4.6kb/527-529^{o}C, whereas garnet rim has been modeled at 5.5±1.2kb/581±26^{o}C. These are the highest pressure estimates so far reported from any part of the Eastern Succession.

In samples SC122 and WB45, the garnet core compositional isopleths intersect at 3.7-3.9kb/548-550^{o}C and 3.7-4.5kb/544-547^{o}C, respectively. Garnets analyzed from these two samples were interpreted to be syntectonic, that is, inclusion trails are continuous with the matrix foliation. Both the rocks host more than 1cm size syntectonic staurolite, and it is clear from textural relationships that garnet grew first, as garnet is found inside the staurolite. For

sample SC122, garnet rim plus matrix mineral phases are modeled at 4.8±1.3kb/592±32^{o}C. No average P-T calculations have been made for sample WB45 as no plagioclase has been found in the matrix. However, as the pseudosection geometry and textures of WB45 are very similar to that of SC112, it is assumed that WB45 had similar paths to SC112. For sample TC189, garnet core formation is predicted to occur at 2.1-2.2kb/510-515^{o}C, whereas garnet rim plus matrix phases have been calculated at 4.8±1.1kb/600±29^{o}C (Fig. 1).

Tectonic implications

P-T paths from sample SC112, WB45 and TC186 appear to be the part of the classic anticlockwise P-T-t path proposed by Rubenach and Lewthwaite (2002). However, the P-T paths from samples SC192 and SC189 show near-isobaric heating at elevated pressure. Significantly, the garnets displaying elevated P-T growth conditions appear to be older based on textural evidence (i.e., truncated inclusion trails) than the relatively low-pressure samples (i.e., continuous inclusion trails). One of the possible interpretations is that as these two rock samples were collected near the vicinity of Cloncurry Fault, which is interpreted as thrust fault in a number of publications. It is suggested that the garnets from sample SC189 and SC192 began to grow at elevated P-T conditions at middle crustal levels, followed by rapid exhumation and cooling along the Cloncurry Fault.

Acknowledgements

MS is grateful to Tom Evans and Peter Welch for their help during the pseudosection calculations, and is also thankful to Damien Foster for discussion.

References:

Adshead-Bell, N. S., 1998. Evolution of the Starra and Selwyn High-Strain Zones, Eastern Fold Belt, Mount Isa Inlier: Implications for Au-Cu Mineralizations. Economic Geology, 93, 1450-1462.

Passchier, C. W. and Trouw, R. A. J., 1998. Microtectonics. Springer-Verlag, Berlin Heidelberg, 2nd corrected print, 1-283.

Pattison, D.R.M., Spear, F.S. and Cheney, J.T., 1999. Polymetamorphic origin of muscovite + cordierite + staurolite + biotite assemblages: implications for the metapelitic petrogenetic grid and for P-T paths. Journal of Metamorphic geology 17, 685-703.

Powell, R., Holland, T., and Worley, B., 1998. Calculating phase diagrams involving solid solutions via non-linear equations, with examples using THERMOCALC. Journal of Metamorphic Geology, 16, 577-588.

Reinhardt, J., 1992. Low-pressure, high-temperature metamorphism in a compressional tectonic setting: Mary Kathleen Fold Belt, northeastern Australia. Geological Magazine, 129, 41-57.

Rotherham, J. F., Blake, K. L., Cartwright, I. and Williams, P. J., 1998. Stable isotope evidence for the origin of the Mesoproterozoic Starra Au-Cu deposit, Cloncurry District, northwest Queensland. Economic Geology, 93, 1435-1449.

Rubenach, M. J. and Lewthwaite, K. A., 2002. Metasomatic albitites and related biotite-rich schists from a low-pressure polymetamorphic terrane, Snake Creek Anticline, Mount Isa Inlier, north-eastern Australia: microstructures and P-T-d paths. Journal of Metamorphic Geology, 20, 191-202.

Rubenach M. J., Adshead, N., Oliver, N. H. S., Tullemans, F., Esser, D. and Stein, H., 2001. The Osborne Cu-Au deposit: Geochronology, and genesis of mineralization in relation to host albitites and ironstones. In: Williams, P.J., ed, 2001: A hydrothermal odyssey. Economic Geology Research Unit, James Cook University, Contribution, 59, 172-173.

Vance, D. and Mahar, E., 1998. Pressure-temperature paths from P-T pseudosections and zoned garnets: potential, limitations and examples from the Zanskar Himalayas, NW India. Contributions to Mineralogy and Petrology, 132, 225-245.

Structural and mineralogical characteristics of the Menzies-Boorara Shear Zone, Yilgarn Craton – implications for variations in the gold potential of a major fault system

Anthony Morey, Frank Bierlein and Roberto Weinberg
*pmd*CRC, School of Geosciences, Monash University, Melbourne, VIC 3800*
Anthony.Morey@sci.monash.edu.au

Abstract

Gold mineralisation from five deposits within the Menzies-Boorara Shear Zone (MBSZ), Eastern Goldfields Province, Western Australia, is characterised by several similar features. These features have been used to constrain the regional Au mineralisation processes.

The MBSZ is a wide zone of intense shearing constrained to a narrow NNW-trending corridor bounded by granitic batholiths (Figure 1). Gold deposits within the MBSZ are geologically similar to the world-class gold deposits associated with the Boulder-Lefroy Shear Zone (BLSZ), however, significant variations also occur. These variations include: (i) the relative thickness of the greenstone package; (ii) the presence of nearby granites; (iii) a potentially different shear zone evolution; (iv) gold mineralisation being relatively late and (v) an apparent lack of Te-bearing minerals within the mineralised assemblages analysed from the MBSZ. These defferences may be used to help understand why the MBSZ is not as well endowed as the BLSZ. This paper presents preliminary results from field- and laboratory-based studies and provides some regional implications for variations in the gold endowment within the Eastern Goldfields Province of the Yilgarn Craton.

Introduction

To date, the MBSZ zone has yielded <100 t of gold, whereas the nearby Boulder-Lefroy Shear Zone (BLSZ) hosts the giant Golden Mile (>2500t), and two other world-class (>100 t) Au deposits (Hagemann and Cassidy, 2001). By assessing the structural relationships, petrogenesis and alteration characteristics of key gold deposits within the MBSZ, this project aims to understand the nature of gold mineralisation within the MBSZ and to then discuss genetic links between these and the more heavily endowed deposits associated with the BLSZ. This will potentially help define target areas for further exploration within the MBSZ, and elsewhere within the Eastern Goldfields Province.

It has been established that major lode-gold mineralisation within the Eastern Goldfield Province, is associated with second- to third-order faults, which splay off more regional, and lesser mineralised first-order faults and shear zones (e.g. Groves and Phillips, 1987; Eisenlohr et al., 1989). As a >100 km-long, major crustal discontinuity, the MBSZ is a primary shear zone, and its connecting, more-mineralised splay fault is the BLSZ. By studying the nature of gold mineralisation from the MBSZ, it is also possible to more quantitatively understand why there is such variation in gold endowment between primary and their higher-order connecting faults.

To characterise mineralisation within the MBSZ, five representative deposits – selected along its entire extent – have been chosen. From north to south, these deposits are; Yunndaga, New Boddington, Broad Arrow, Paddington and Golden Ridge (Figure 1).

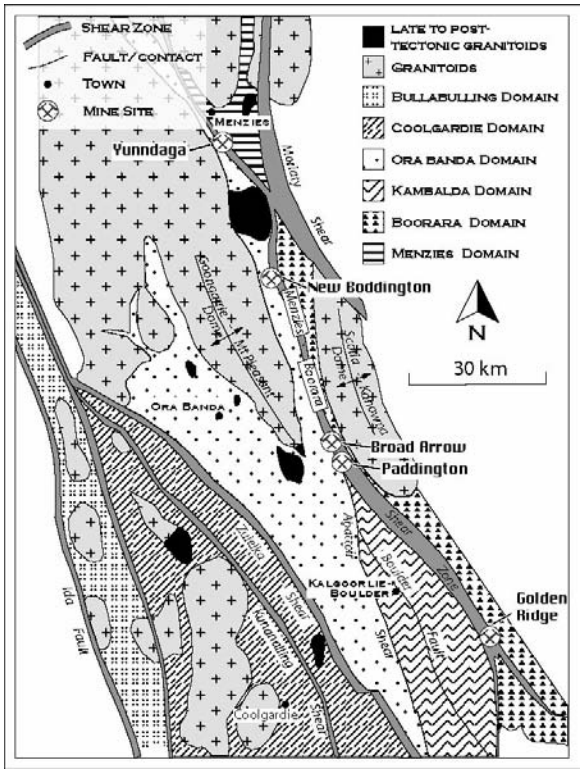

Figure 1: Geological map of the southern section of the Eastern Goldfields Province, showing the major shear zones and rock units. Modified after Witt (1993).

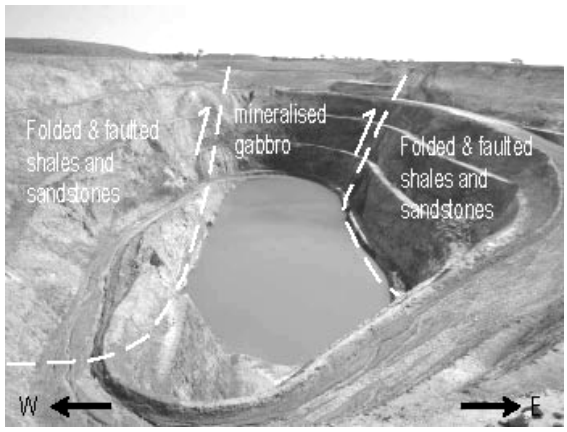

Figure 2: Photograph of Broad Arrow; a mineralised gabbro is bounded by less competent sedimentary rocks

Gold deposits of the Menzies-Boorara Shear Zone – defining characteristics

Field and structural relationships

All of the deposits investigated are situated within the NNW-trending shear zone (Figure 1). This is reflected at the mine scale as the geometry of all the major rock units dip steeply to the west and rock contacts are controlled by NNW-trending reverse faults and associated folds and foliations (Figures 2 and 3). Gold mineralisation is always hosted within a relatively competent, lesser-strained rock unit - except New Boddington, where deformation has developed more uniformly throughout all of the host rock sequences. In accordance with Witt (1993), the relatively more competent and more mineralised units vary in rock type from: mafic basalts, dolerites and gabbros (Yunndaga, New Boddington, Paddington and Broad Arrow), through to a felsic porphyry intrusive/dyke at Golden Ridge. All of these mineralised units are <100m thick. Within the bounding sedimentary rock sequences, deformation has been accommodated through dip-slip and strike-slip faults, shears, and folded structures. A representative pit photograph is shown in Figure 2. North to NW-trending (Yunndaga, Broad Arrow) and oblique (New Boddington, Paddington) strike-slip faults occur, however, reverse faulting and folding with associated dip-slip lineations dominate the structure of the highly strained bounding sedimentary units (Figure 3). This suggests that the evolution of the MBSZ was dominated by *reverse faulting and folding* (D_2 of Swager, 1997) and *strike-slip* (D_3) deformation did not significantly occur within this shear zone.

Nature of gold mineralisation

Gold within the MBSZ is predominantly associated with structurally-controlled lodes. There are numerous unmineralised veins at each locality but only the major Au-bearing structures are discussed below.

Veins bearing sulphides and gold are commonly planar and post-date the major NNW-trending shear foliation, as they cross-cut, and are not sheared by this foliation. At all localities, lode structures are observed as repetitive vein arrays that are 10's of metres in length. At Paddington and Golden Ridge, steeply-dipping continuous lodes also exist, at Paddington over 1 km in

length. At New Boddington, Paddington and Golden Ridge the repetitive lode structures dip shallowly to moderately, whereas at Yunndaga and Broad Arrow similar structures have moderate to steep dips.

The sulphide and gold assemblage occurs within the wall rock directly at, or proximal to the lode - wall rock interface. The lode mineralogy consists of quartz or quartz-carbonate composite veins. Centimetre-scale alteration haloes are also identified, and are characterised by carbonate – chlorite – silica ± sericite ± epidote hydrothermal alteration assemblages.

Fluid infiltration related to sulphide and gold deposition is complex and evidence exists for both singular and multiple events. Arsenopyrite precipitated relatively earlier, and was then overprinted by gold (Figure 4). It is as yet unconfirmed if these deposition events are genetically related, or if they represent independent influxes of hydrothermal fluids.

Figure 3: Upright, NNW-trending fold from Yunndaga

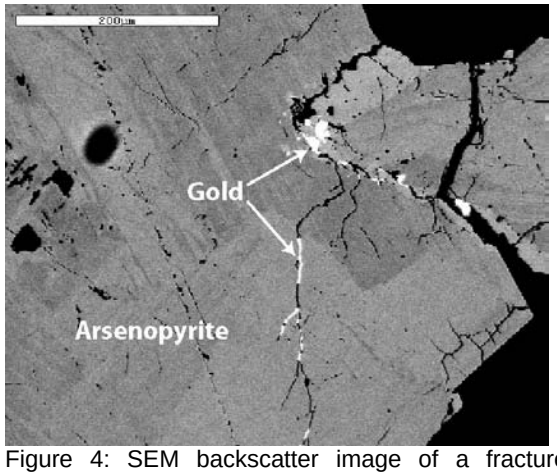

Figure 4: SEM backscatter image of a fractured arsenopyrite grain, with gold infilling these fractures

Comparisons with the Boulder-Lefroy Shear Zone

From field- and preliminary laboratory-based studies, gold mineralisation within the MBSZ is predominantly lode-related, and for efficient gold ore formation, Au-bearing fluids must be localized within a relatively competent rock unit. This allows for brittle-style fracturing, dilation, fluid focusing and Au mineralization (Weinberg et al., in press). This competent unit does not have to be a particular rock type, as mafic to felsic igneous rocks are all potential hosts to Au mineralisation. The importance of rheological contrasts is best exemplified by New Boddington, where the lack of a significant contrast explains its low gold endowment (0.4 t Au; Witt, 1993). Mineralised competent units within the MBSZ are also significantly narrower than similar mineralised rocks associated with the BLSZ, and this could further explain the lower endowment of the MBSZ. The need for a competency contrast, and limited width competent units within the MBSZ, could possibly account for its variable Au endowment.

The major structures from the five gold deposits investigated imply that D_2-style deformation was the dominant regional event, and that D_3 sinistral strike-slip faults were not significant within the MBSZ. D_3 deformation structures have been recognised from the BLSZ, and this implies that both shear zones have had a different tectonic evolution.

Our investigations show that Au endowment within the MBSZ is always late in relation to regional shear zone development, whereas the mineralisation events associated with the BLSZ are both early (i.e. Fimiston lodes) as well as late (i.e. Mt. Charlotte-type; Bateman et al., 2001). Moreover, Au-bearing telluride minerals are an important mineralogical association within the Boulder-Lefroy Shear Zone (Witt, 1993), however, telluride-bearing minerals are yet to be observed within Au deposits from the MBSZ. These results suggest differences in Au-bearing

fluid compositions, sources and timing relationships may have affected the gold endowment of the two shear zones.

Acknowledgements

The continuing support and input from Placer Dome, WMC, AngloGold and Harmony personnel has been greatly appreciated. Robert Douglass and Rachelle Pierson are also thanked for thin section and rock sample preparation.

References

Bateman, R.J., Hagemann, S.G., McCuaig, T.C. and Swager, C.P., 2001. Protracted gold mineralisation throughout Archaean orogeneses in the Kalgoorlie camp, Yilgarn Craton, Western Australia: structural, mineralogical, and geochemical evolution. In: Hagemann S.G., Neumayr P. and Witt W.K. eds., World-class gold camps and deposits in the eastern Yilgarn Craton, Western Australia, with special emphasis on the Eastern Goldfields Province., Western Australia Geological Survey, Record 2001/17, 63-89.

Eisenlohr, B.N., Groves, D.I. and Partington, G.A., 1989. Crustal-scale shear zones and their significance to Archaean gold mineralisation in Western Australia. Mineralium Deposita, 24, 1-8.

Groves, D.I. and Phillips, G.N., 1987, The genesis and tectonic controls on Archaean Gold deposits of the Western Australian Shield: a metamorphic-replacement model. Ore Geology Reviews, 2, p. 287-322.

Hagemann, S.G. and Cassidy, K.F., 2001. World-class gold camps and deposits in the Eastern Goldfields Province, Yilgarn Craton: diversity in host rocks, structural controls, and mineralisation styles. In Hagemann, S.G., Neumayr, P. and Witt, W.K., eds., World-class gold camps and deposits in the eastern Yilgarn Craton, Western Australia, with special emphasis on the Eastern Goldfields Province. Western Australia Geological Survey, Record 2001/17, 7-44.

Swager, C.P., 1997, Tectono-stratigraphy of late Archaean greenstone terranes in the southern Eastern Goldfields, Western Australia: Precambrian Research, v. 83, p. 11-42.

Swager, C.P., Griffin, T.J., Witt, W.K., Wyche, S., Ahmat, A.L., Hunter, W.M. and McGoldrick, P.J., 1995. Geology of the Archaean Kalgoorlie Terrane – an explanatory note (reprint of Record 1990/12): Geological Survey of Western Australia Report 48.

Weinberg, R.F., Hodkiewicz, P.F. and Groves, D.I., in press. What controls gold distribution in Archean terranes? Geology.

Witt, W.K., 1993. Gold mineralisation of the Menzies-Kambalda Region, Eastern Goldfields, Western Australia. Geological Survey of Western Australia Report 39.

Habitat of Yilgarn gold - from fault and worm analysis

Barry Murphy[1] and Terry Lees[2]

*[1]pmd*CRC, School of Earth Sciences, University of Melbourne, VIC 3010*
*[2]pmd*CRC, School of Geosciences, Monash University, Melbourne VIC 3800*

bmurphy@unimelb.edu.au

Rationale

The A1 project seeks to characterise and discriminate between penetrative faults that are permissive to mineralisation from those that appear not so prospective. Such faults populate the Tectonic Targets database, where a lower limit of 100km strike length is imposed on the input data. Although restrictive, this makes for easier management of a global database. However, in nature, populations of faults occur over a range of scales and, in this regard, the Yilgarn fault population is being assessed.

In the Yilgarn terrane, faults provide just one piece of the puzzle in unraveling gold genesis and deposition. Factors that are well known in the exploration context include: proximity to crustal-scale faults, anticlinal hinge zones, dilational jogs, strike changes, strong rheological contrasts and metamorphic grade. These have already been deployed for prospectivity analysis outcomes (Knox-Robinson, 2000; Gardoll et al., 2000).

Our research has been examining the magnitude of faults and potential field gradients and evaluating their impact on the distribution of gold deposits, ranked according to size. Intuitively, long strike-length faults are more penetrative than short strike-length faults. They offer more potential for tapping ore-bearing fluids and provide more permeable pathways for focusing such fluids. Of particular interest here are edge length and height persistence (a proxy for depth).

Methodology

Gold deposit data were derived from MINLOC (through the Geological Survey of Western Australia) and Ozmin (through Geoscience Australia). These were filtered to remove duplicates and non-gold occurrences, and the remaining 9,905 deposits were ranked according to size: 1 (occurrence or < 10 kg Au); 2 (10-100 kg Au); 3 (100-1000 kg Au), 4 (1000-10000 kg Au) and 5 (>10000 kg Au). Separate analysis of a global database (Lees, this volume) shows at least 5 categories of Archaean gold deposit. However, the sample number of such categories within the Yilgarn is small, so that we treat the deposits as a single group here.

Digital faults (Fig. 1) were extracted from the GSWA coverage, cleaned of duplicates and concatenated (i.e., joined contiguous lines). Fault lengths were computed and imaged.

The gravity data were wormed (FracWormer^{TM}) through a process of upward continuation to 60 km. The resultant data (Fig. 2) were interpreted in relation to the maximum upward continued height and the strike length of worm edges. In addition, linear vacancies (i.e. edges with no distinct density contrast that truncate a series of worms) were interpolated. The near-surface worms are weighted by the height of upward continuation (using Geoscope software) and nearest-neighbour analysis of the point data is performed to generate vector lines. The lines are concatenated and attributed with length and height persistence values, thereby providing a structural framework.

The aeromagnetic worm data has not, as yet, been incorporated in the analysis.

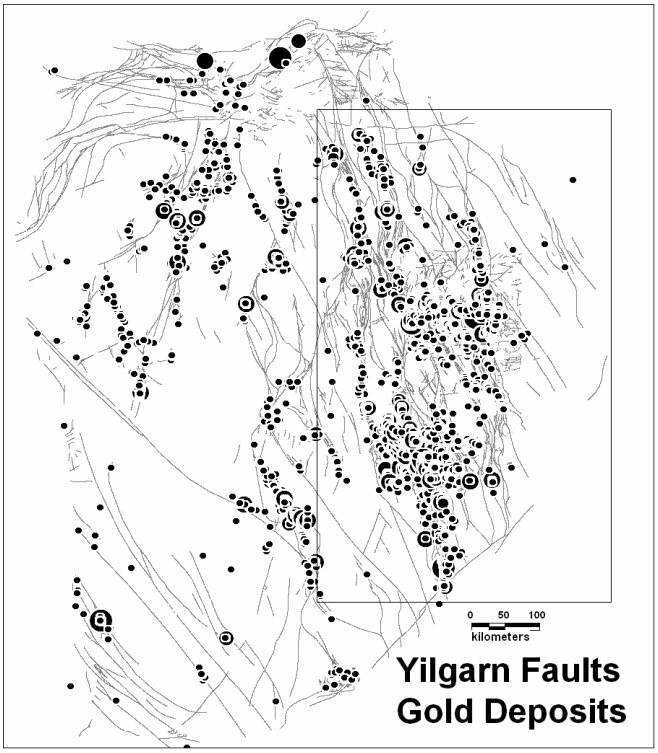

Figure 1: Yilgarn Faults and gold deposits (box shows area of gravity worm data)

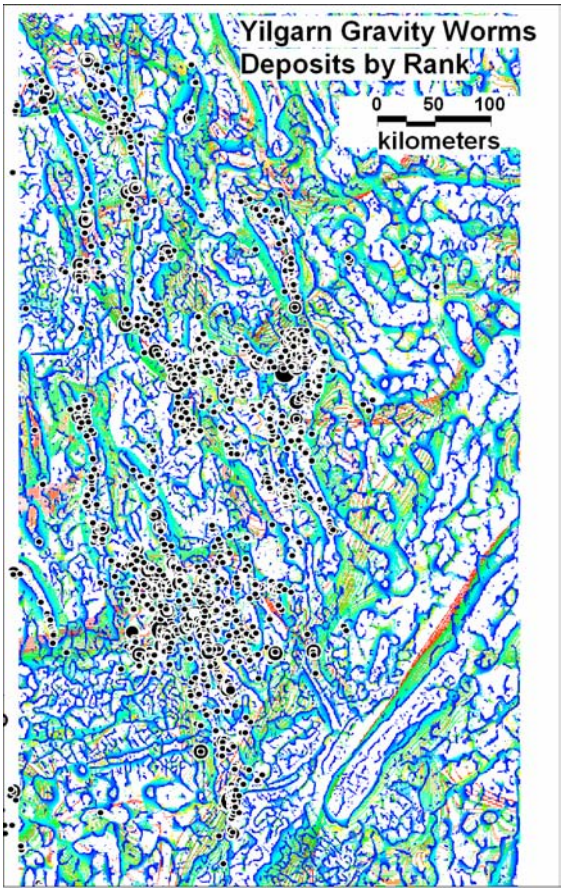

Figure 2: Gravity Worms (coloured by height) and gold deposits

Results

There is evidently more gold in proximity to faults (Fig. 1), echoing an exploration axiom in the Yilgarn – "the closer the fault, the larger the deposit". The partitioning of Au within 1km and 2km buffers (Fig. 3a) for faults of specified length windows shows an increase in the contained Au with proximity to small faults (Fig. 3b). This suggests that small faults localise the gold and/or that more small faults are mapped in the vicinity of gold deposits.

a) 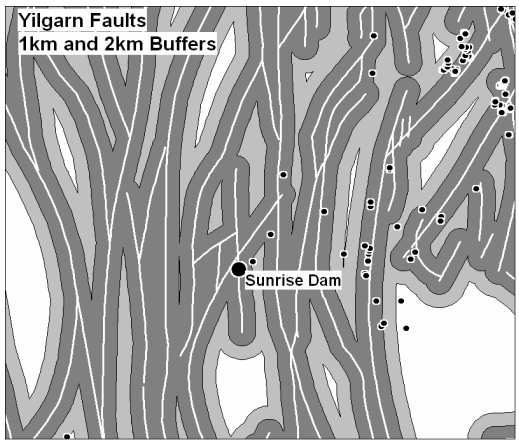

b) 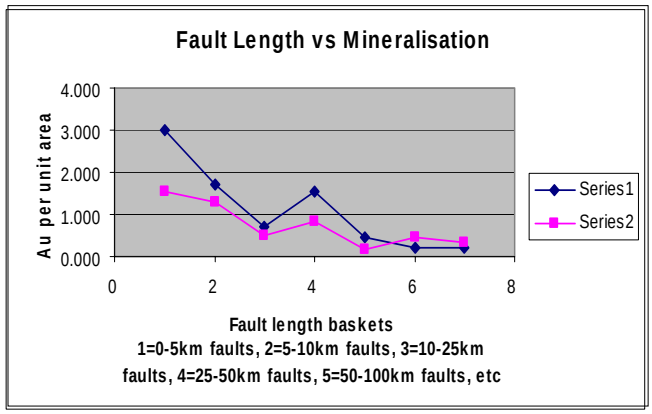

Figure 3: Fault buffers a) example map of 1km (dark grey) and 2km (light grey) buffers, b) plot of Au content per unit area (y axis) against fault length baskets (2km = series 1, 1 km = series 2)

The influence of fault length is examined in a windowed buffer analysis, with buffer size increasing according to fault length (Fig. 4a), and metal content measured within each buffer window. There is a positive correlation with proximity to long faults (Fig. 4b). An important aspect of this is that there is more gold within smaller buffer areas with increasing proximity to long faults.

a) 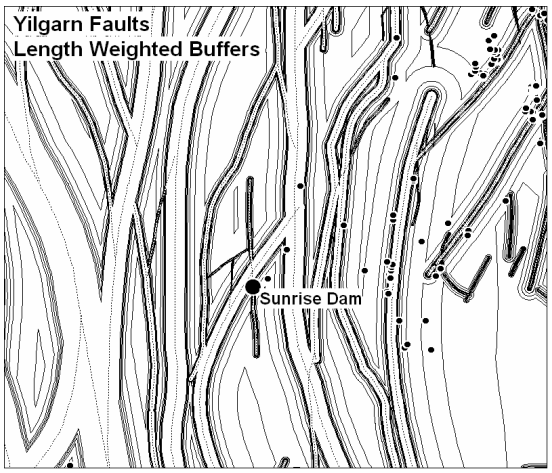

b) 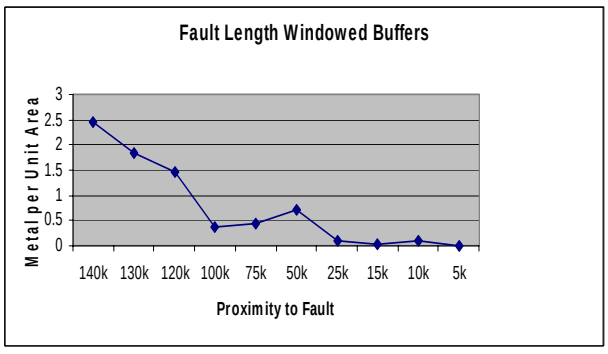

c)

Figure 4: Fault length, windowed buffers. a) example of buffer distributions, b) graph of buffer size (x axis) against metal content per unit area.

The gravity worm data is being evaluated in a similar fashion, using length and upward continued height ("persistence"). The interpreted framework of the gravity worms is displayed in relation to edge length and height persistence images (e.g. Fig 5). A number of geostatistical routines can be applied to the data. The widowed buffer analysis approach based on edge length functions (Fig. 6a) shows a strong increase in metal content per unit area with proximity to long strike length gravity worms, commensurate with decreasing buffer areas (Fig. 6b). Other

aspects of note are the association with penetrative edges (Fig. 5) and an association of deposits with edges that have a high density contrast (i.e." warm worms").

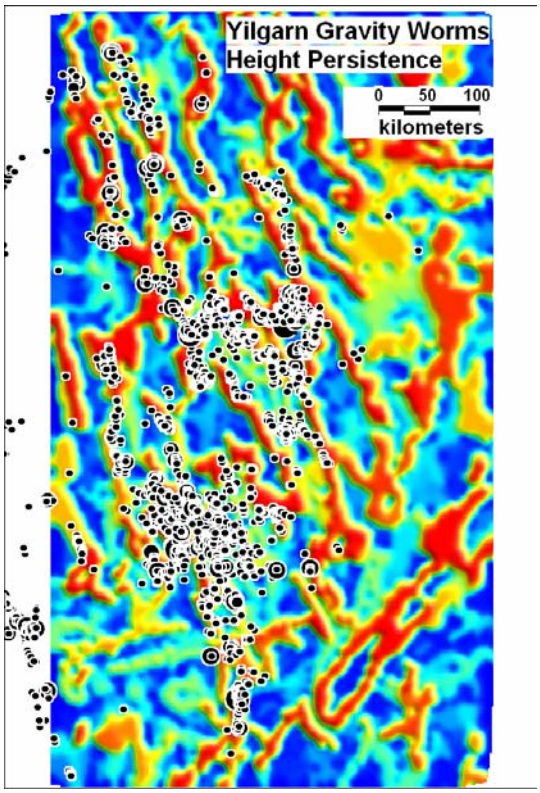

Figure 5: Yilgarn Gravity worm interpretation, upward continued height image and gold deposits

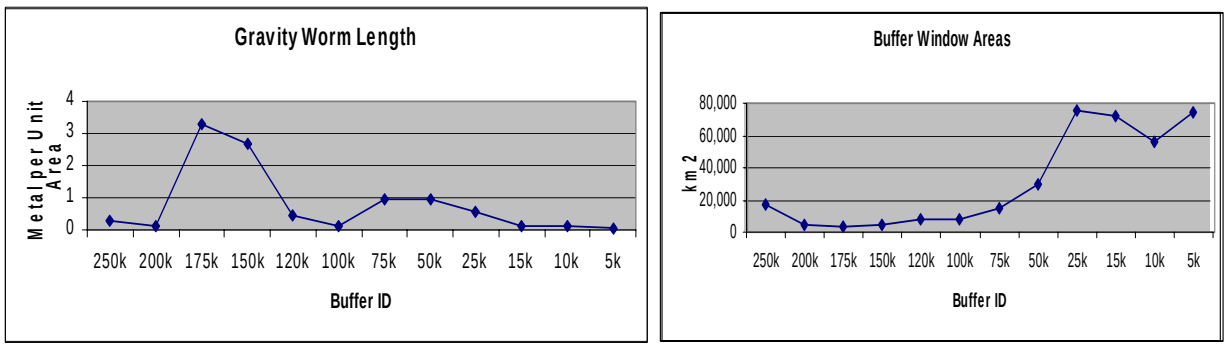

Figure 6: Yilgarn gravity worms, a) edge length buffers and metal content, b) buffer areas (km^2)

Overall, the approach is yielding results that may be of empirical value in application to predictive mineral discovery.

References

Knox-Robinson, C. M., 2000. Vectorial fuzzy logic: a novel technique for enhanced mineral prospectivity mapping, with reference to the orogenic gold mineralisation potential of the Kalgoorlie Terrane. Australian Journal of Earth Sciences, 47, 929-942.

Gardoll, S. J., Groves, D. I., Knox-Robinson, C. M., Yun, G. Y. and Elliott, N., 2000. Developing the tools for geological shape analysis, with regional- to local-scale examples from the Kalgoorlie Terrane. Australian Journal of Earth Sciences, 47, 943-953.

Crustal scale modelling of western Victoria

Barry Murphy[1], Tim Rawling[1], Chris Wilson[1] and Jon Dugdale[2]

[1] *pmd*CRC, School of Earth Sciences, University of Melbourne, VIC 3010*
[2]MPI Mines Ltd, Stawell, VIC

bmurphy@unimelb.edu.au

Rationale

This paper describes the visualisation of the structural framework of western Victoria via a 3D geological model (Fig. 1). Embedded within this are existing gold deposits, prospects and targets. Through a combination of geophysical forward modelling, numerical simulation and geospatial data inquiry, the 3D model will be used to inform the explorationist on prioritising resource opportunities in the region. The crustal scale of the model attempts to capture the "total mineral system" that generated the gold. The geodynamic setting places this region in a collision zone at the western edge of the Lachlan Fold Belt, and at the exposed eastern margin of the earlier Delamerian orogen (Miller et al., submitted).

Methodology

The model has been constructed through integrated analysis of a range of digital data sets, with a limited amount of field checking being undertaken. The 3D model is centred on the Stawell corridor and is based on 15 E-W oriented serial cross sections, spaced 5km apart, approximately 100km long and 20km deep (Fig. 1). The 1:100000 scale geological mapping provides a robust template for the model in the southern parts of the corridor, while much of the remaining area to the north is under Murray Basin cover. We utilise the regional aeromagnetics and gravity as a primary constraint in determining the crustal geometry, with the existing GA seismic profiles as a starting line for determining the shapes of major fault structures in the subsurface.

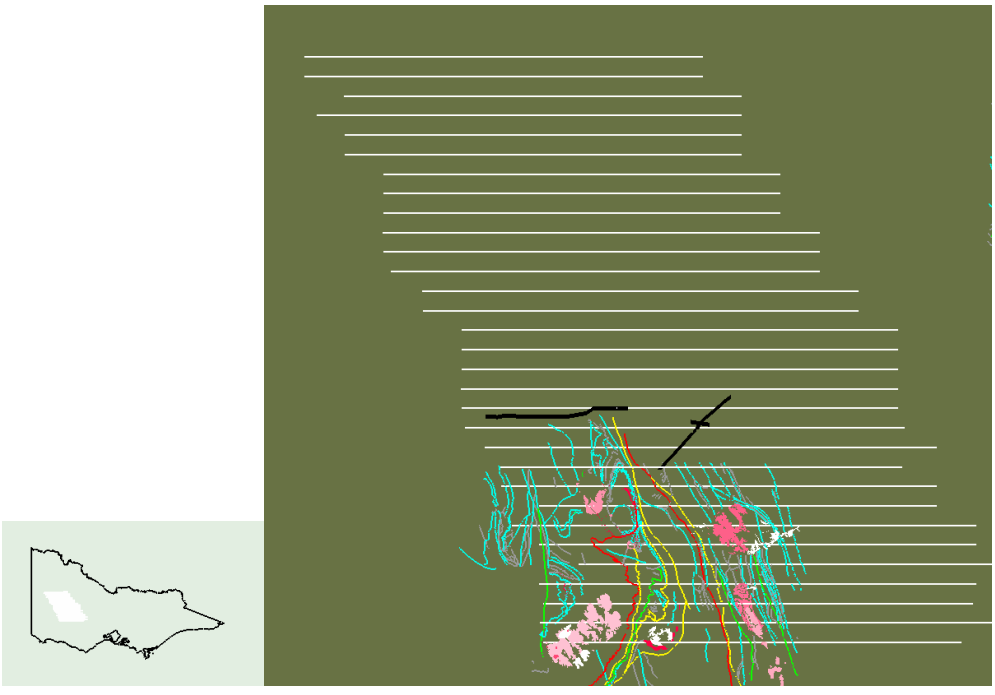

Figure 1. Location of modelled area (inset), positions of serial lines of section (white), seismic lines (black), 1:100k faults (coloured by strike length, and Devonian granites (reds). Cross section lines ca. 100km long.

The component lithostratigraphic packages being modelled include:

- Proterozoic basement (inferred from potential field data and geological relationships)
- Early Cambrian mafic to ultramafic oceanic suite and related sediments (host to Stawell deposit)
- Late Cambrian sediments and volcanics (e.g. Mt. Stavely Group, St Arnaud Beds)
- Silurian-Devonian sediments (e.g..Grampians Group)
- Intrusives (e.g. Devonian granitoids)

Edge detecting worms are used to reduce the ambiguity in delineating the positions and magnitudes of gradients in the potential field. This yields critical information on the location, dip, dip direction and extent of edges across which density contrasts are detected, e.g. faults and intrusive contacts. Naturally, contacts with no detectable density contrast are blind, but can be inferred through truncations and offsets in detected worms.

The first step is to develop a structural base map of the major discontinuities, using mapped faults and worms. A hierarchy of faults can be determined based on strike length (Fig. 1), the inference being that longer faults have commensurate subsurface extent (independent of dip and relative displacement). There is generally good agreement between mapped fault positions and related worms (particularly aeromagnetic data), and this gives a reasonable degree of confidence in the interpretation of these structures under cover. The length and upward continued height persistence (in many instances, a proxy for depth of penetration) of worm edges is a guide for the shape and extent of major bounding surfaces in the model. The relationship of the worms to the imaged seismic data provides a key determinant for the gross geometry of these boundaries in the model.

Inversion modelling of the gravity data, using UBC code, was also performed. The combination of inversion modelling, upward continuations and wavelet processing (worms) is a very useful and informative format (Fig. 2) from which geological cross sections were drawn (according to a standard geological legend).

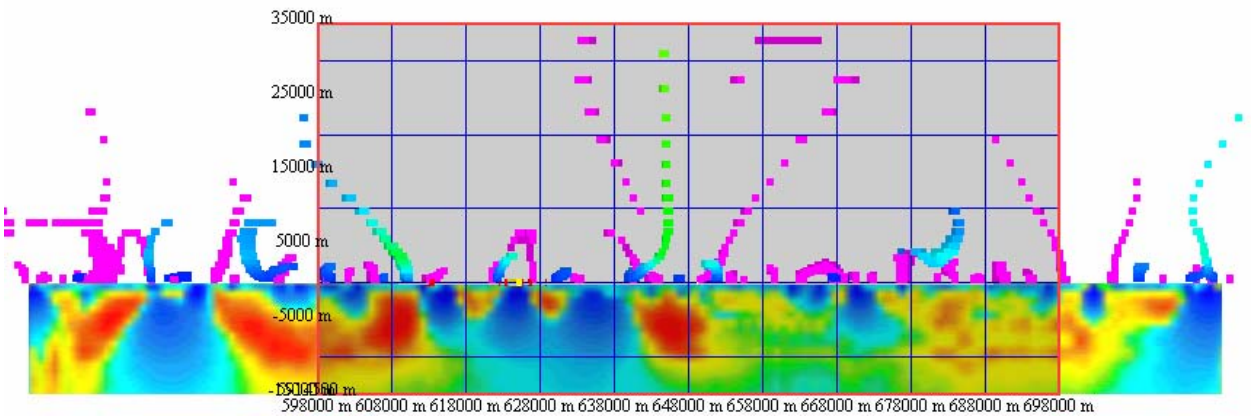

Figure 2. E-W profile of upward continued aeromagnetic worms (blue-green point arrays), gravity worms (magenta point arrays) above ground surface (mid position in profile) and, below surface, gravity inversion model to 15km (pseudocolour image), section 5915000N.

Each geological section was subsequently modelled in the GM-SYS software - using both project specific and generic petrophysical parameters – to create gravity and magnetic profiles for comparison with actual profiles. Once a "best fit" profile was achieved, the revised sections were captured in GoCad from which wireframe surfaces have been generated. The project is currently progressing towards completing the GoCad model, and the model is being imported on an on-going basis to a FracSIS database. A large element of iteration in required to mould the sections into a 3D model, with the FracSIS database being used as a key element of the visualisation and modelling routine.

Once complete, forward modelling of the potential field response of the 3D model will be undertaken as a reality check against the actual potential field.

Numerical fluid flow modelling, using critical aspects of the geometrical model, will be performed with the objective of highlighting potential prospective areas on a regional scale.

Results

The initial results from the modelling are displayed in two perspective views (Fig. 3). While we largely affirm the major boundaries, as determined by the GSV mapping, some changes in fault positions are warranted (e.g. the Moyston Fault, south of Stawell) and there are changes in emphasis regarding the relative dominance of some structures – for example, the Pleasant Creek Fault is modelled as a major break that significantly impacts on the 3D architecture as much as, if not more than, the Moyston Fault.

The Coongee Break, being a locus for gold mineralisation, represents a major steep west dipping boundary, separating low grade from substantially high grade metamorphic rocks to the west. In the model, it appears to have formed as a back-thrust to a major ramp developed in the basal detachment geometry. It has undergone later strike slip sinistral reactivation.

We interpret the overall architecture (Fig. 3) as a series of major east-dipping structures that sole onto a master detachment. This latter boundary separates the Palaeozoic from the inferred Proterozoic basement, and has an elongate doubly plunging dome shaped expression. While the geometry resembles an extensional detachment in a core complex-type model, the geodynamic setting is grossly contractional.

Reference

Miller, J. M., Phillips, D., Wilson, C. J. L. and Dugdale, J. L., submitted. Evolution of a hybrid Orogenic zone in response to changing accretion dynamics: the Delamerian and Lachlan orogens, SE Australia.

a)

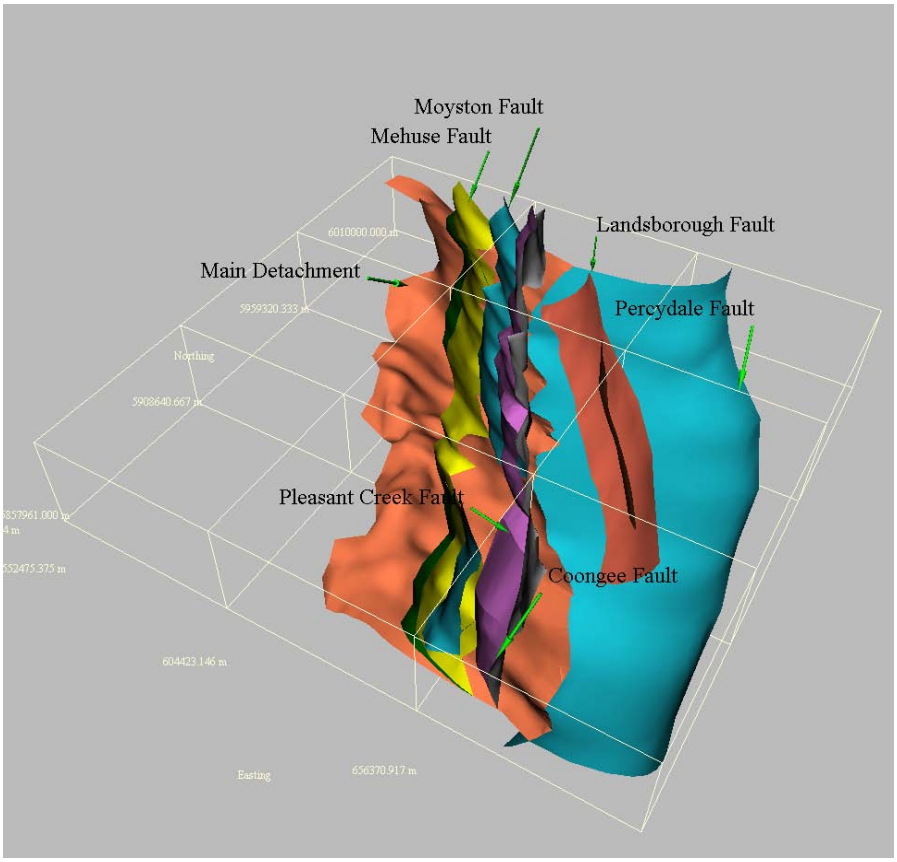

b)

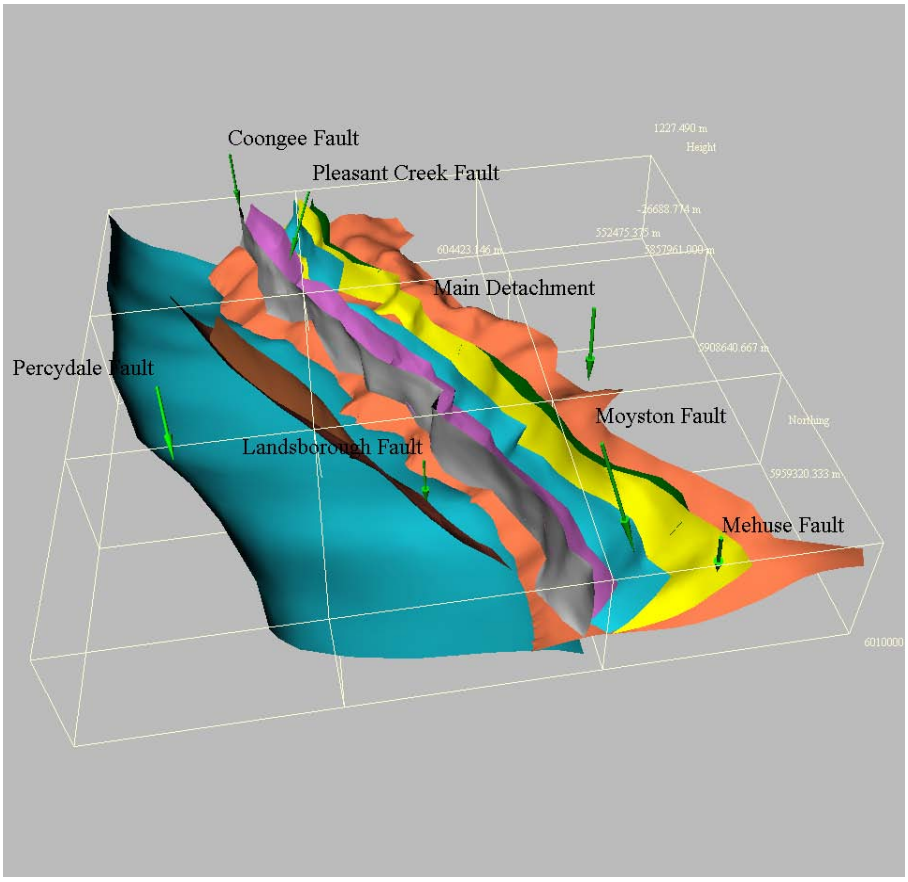

Figure 3: Perspective views of the 3D geological model, a) from the SE and b) from the north, showing major fault structures that have been modelled.

The role of unmixing in magnetite ± copper deposition in Fe-oxide Cu-Au systems

R. Mustard[1], T. Baker[1], P.J. Williams[1], T. Mernagh[2], C.G. Ryan[3],

E. Van Achterbergh[3] and N. Adshead[4]

*[1] pmd*CRC, Economic Geology Research Unit, School of Earth Sciences, James Cook University, Townsville, QLD 4811.*
*[2] pmd*CRC, Geoscience Australia, GPO Box 378, Canberra, ACT 0200*
[3] CSIRO Exploration and Mining, PO Box 136, North Ryde, NSW 1670
[4] Placer Dome Inc. PO Box 49330, Bentall Station, Vancouver, BC, Canada

roger.mustard@jcu.edu.au

Introduction

The process of unmixing appears to play a critical role in the precipitation of magnetite ± copper in Fe-Oxide Cu-Au systems in the Eastern Fold Belt of the Mt Isa Block. Co-existing multi-solid brine and halite-bearing liquid CO_2-rich fluid inclusions that have undergone unmixing have been recognized at Osborne Cu-Au and Starra Au-Cu mines. This process has also been recognized at Lightning Creek prospect, an Fe oxide system that is demonstrably magmatic in origin (Perring et al., 2000).

A combination of microanalytical tools including conventional microthermometry, Laser Raman spectroscopy, and proton induced X-ray emission (PIXE) were utilized to study the composition of fluid inclusions from the Osborne Fe-Oxide Cu-Au deposit. Element concentrations in fluid inclusions were determined using the CSIRO-GEMOC PIXE nuclear microprobe at CSIRO, North Ryde. Gas composition of vapour bubbles was determined using the Laser Raman spectroscope at Geoscience Australia, Canberra.

General Geology

The Osborne deposit is a located 195 km southeast of Mount Isa and is owned by Placer Pacific Limited. In 1996 Osborne had a total measured and indicated mineral resource of 11.3 Mt @ 2.9% Cu, 1.18 g/t Au (Adshead et al., 1998). The deposit is hosted within a multiply deformed sequence of upper amphibolite facies metamorphic rocks, including feldspathic psammites, pelites, metasedimentary gneisses, amphibolites, and pegmatites of the Mount Isa Eastern Sucession. The deposit can be divided into the 'Western' and 'Eastern' domains based on differences in the host rocks and mineralization characteristics. The western domain contains the bulk of the Cu-Au mineralization, occurs at the contact between a banded ironstone formation and feldspathic psammite, and is dominated by a hematite-magnetite-pyrite mineral assemblage. The eastern domain mineralization is not spatially associated with the ironstones, forms a discrete body hosted within strongly silicified rocks, and exhibits a more reduced pyrrhotite-magnetite±pyrite assemblage.

Fluid Inclusion Types

Pre-syn mineralization quartz contains primary to pseudosecondary hypersaline fluid inclusions that are associated with silica flooding. In the western domain these commonly coexist with high density halite-bearing liquid CO_2 inclusions providing clear evidence of fluid unmixing (Figure 1). Two end member fluid inclusion types include multi-solid brine (LVnS, n=4-6) and halite-bearing liquid CO_2 (LCO_2nS, n=3-5; Figure 2). The multi-solid brine inclusions typically consist of liquid,

vapour (5 vol %), halite, sylvite, lesser CaCl solid, one or two ferropyrosmalite phases (Fe-rich and Fe-poor), an unidentified <1µm opaque phase (possibly chalcopyrite), magnetite, and rare calcite. Many liquid CO_2 inclusions contain halite, sylvite, ferropyrosmalite and calcite. The multi-solid brine inclusions have salinities of 33-60 wt % NaCl equivalent and homogenize primarily by ferropyrosmalite dissolution or less commonly vapour disappearance at 260-505°C (Table 1). Total homogenization for liquid CO_2 inclusions occurred between 308 and 375°C. CO_2 homogenisation temperatures ranged from -10 to 29°C.

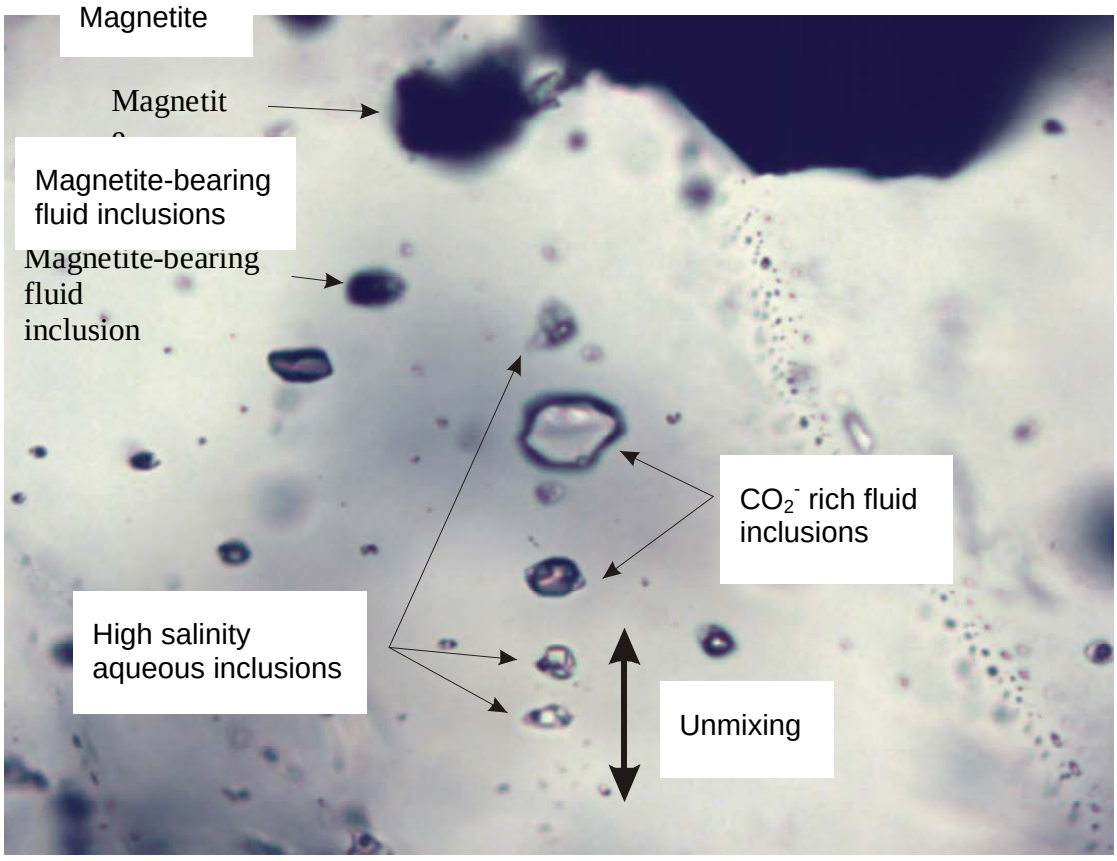

Figure 1. Clear evidence of fluid unmixing into aqueous brine and high density carbonic fluids is observed at the Osborne deposit. Note the presence of a large magnetite phase in one of the inclusions, demonstrating a direct association of unmixing with magnetite precipitation. PIXE analyses of the magnetite-bearing inclusions in this trail indicate the presence of copper in direct association with the magnetite (Refer to Figure 3).

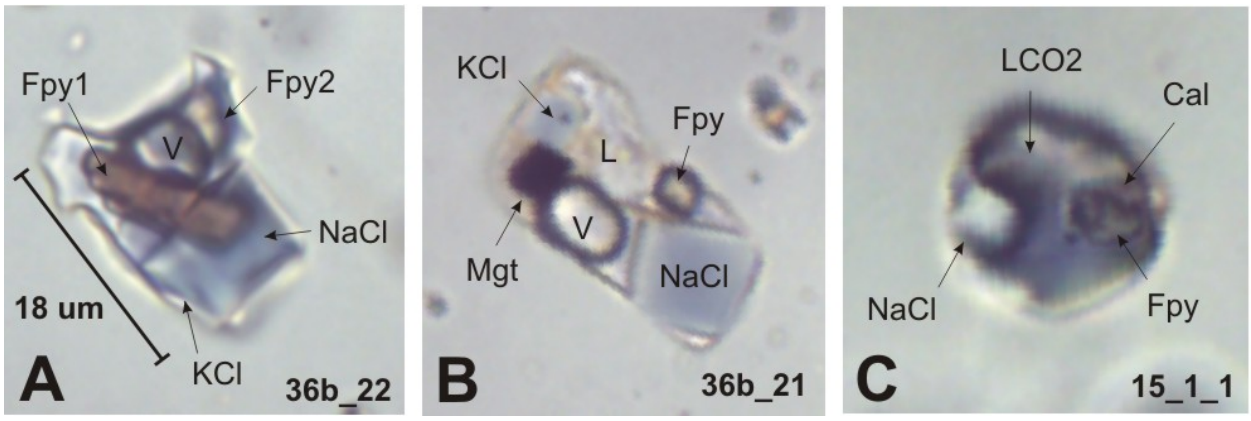

Figure 2. Multi-solid (A & B) and LCO_2-rich (C) fluid inclusion associated with pre to syn-mineralisation unmixing at Osborne Cu-Au deposit. Fpy = ferropyrosmalite, NaCl = Halite, KCl = Sylvite, Cal = Calcite, Mgt = Magnetite.

Laser Raman Results

Laser Raman highlighted the presence of solid phases including: Fe-rich and Fe-poor ferropyrosmalite, calcite, magnetite and up to 3 separate salt phases. This technique also indicated the absence of gases from the brine inclusions. Coexisting liquid CO_2 inclusions were dominantly CO_2 bearing with minor N_2 and CH_4.

PIXE Results

PIXE analyses of the inclusions described above reveal that Cu displays a strong spatial association with a Fe-rich rod-shaped ferropyrosmalite phase and to a lesser degree with magnetite (Figure 3). A second round-shaped Fe-poor ferropyrosmalite phase contains significantly less Cu when present. Multi-solid brine inclusions with higher levels of Cu exhibit a strong spatial association between Fe, Cu, Zn, Pb and Rb. Despite both inclusion types containing similar concentrations of calcium, in the multi-solid brine inclusions Ca is located in the liquid phase. In contrast the liquid CO_2-rich inclusions contain Ca in a calcite solid phase only.

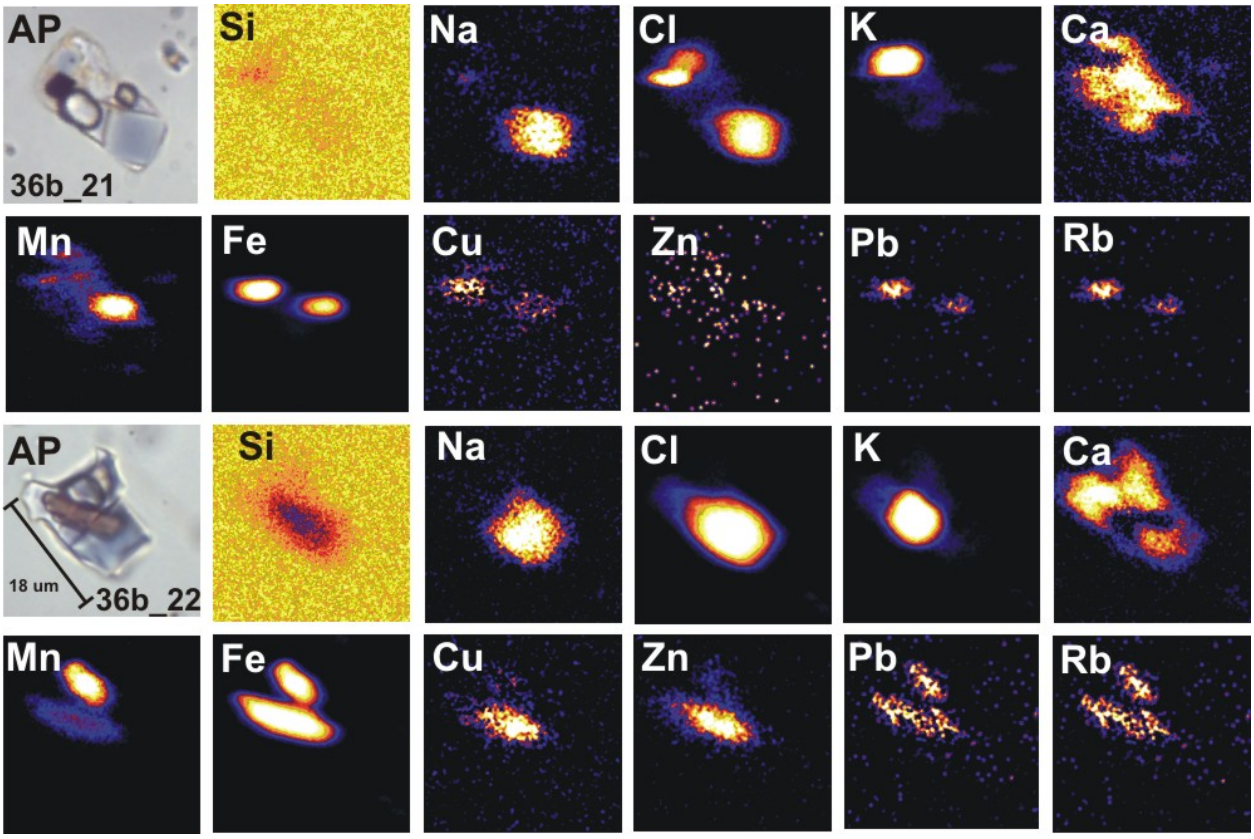

Figure 3. Location of Cu in multi-solid fluid inclusions. Cu is associated with magnetite in sample 36b_21. Cu is associated with a Fe-rich, rod-shaped ferropyrosmalite phase in sample 36b_22.

Discussion

Fluid inclusion studies from Fe-oxide Cu-Au deposits have documented the existence of both hypersaline aqueous and low-salinity CO_2-rich fluids associated with sodic-calcic alteration and mineralisation (Pollard, 2000) and have been interpreted to have formed by unmixing of an original H_2O-CO_2-NaCl-CaCl fluid (Adshead., et al. 1998).These previous studies have revealed both inclusions in the one sample but have not displayed unambiguous coexistence of the two in the same populations. Here we have shown clear examples of co-existing hypersaline aqueous and high salinity CO_2-rich fluid inclusions occurring along single trails from pre-syn-mineralisation quartz associated with both magnetite and minor chalcopyrite (Figure 1). The unmixing occurred under conditions of high P-T of >500°C and ~0.5 GPa when placed on the NaCl,$CaCl_2$-H_2O-CO_2 triplot of Shmulovich and Graham (2004).

Studies of the Starra Au-Cu deposit (Rotherham et al., 1998) reveal the presence of primary multi-solid inclusions (containing liquid, vapour, halite, ferropyrosmalite, calcite, and magnetite) and liquid CO_2 inclusions associated with ironstones. The inclusion types are comparable to those coexisting at Osborne. Furthermore, Perring et al. (2000) noted comparable co-existing primary 'magmatic' fluid inclusions in albite-magnetite-quartz sills. PIXE analysis of the brine inclusions revealed high levels of Cu (1.0-1.9 wt %). Futher studies by Williams et al. (2003) revealed that Ci is in the ferropyrosmalite.

Unmixing is a critical process in early magnetite-rich ± Cu deposition, based on its presence at Osborne Cu-Au mine, Starra Au-Cu mine and Lightning Creek prospect. The source of fluid is debatable but Lightning Creek is demonstrably magmatic and may imply magmatic processes occurring at Starra and Osborne.

Deposit	Starra		Osborne		Lightning Creek	
Reference	Rotherham et al., 1998		Adshead, 1995		Perring et al., 2000	
Inclusion Type	Multisolid	CO_2-rich	Multisolid	CO_2-rich	Multisolid	CO_2-rich
Th (°C)	345 to 615	no data	260 to 520	308 to 375	>420	no data
$ThCO_2$ (°C)	no data	-20.2 to 24	no	-10.6 to 29	no	26.5 to 28.7
Salinity wt % NaCl equiv.	34 to 52	no data	33 to 60	6 to 21	33 to 55	no data
Density g/cm^3	no data	0.72 to 1.0 (0.)	no data	0.63 to 0.94 (0.8)	no data	0.7
Est. Depth	7.5-9km (2.1 to 3.7 kbar)		7km (2.1 kbar)		>6.25km (>1.5->2.5kbar)	

Table 1. Comparison of co-existing multi-solid and CO_2-rich fluid inclusions from Starra Au-Cu mine, Osborne Cu-Au mine and Lightning Creek prospect.

Acknowledgements

We thank Frank Tullemans, Alan Blackburn and Britt Kuhneman (Placer) for their support and cooperation at Osborne Mine. Gregg Morrison (Klondike Exploration Services) is thanked for his guidance with sampling.

References

Adshead, N.D., 1995. Alteration, geochemistry, and parageneisis of the Osborne Cu-Au deposit, NW Queensland: Unpublished PhD thesis, James Cook University, Australia, 382pp.

Adshead, N.D., Voulgaris, P.and Muscio, V.N., 1998. In: Berkman, D.A. and Mackenzie D.H., eds., Geology of Australian and Papua New Guinean Mineral Deposits. Australasian Institute of Mining and Metallurgy, Melbourne, 739-799.

Perring, C.S., Pollard, P.J., Dong, G., Nunn, A.J. and Blake, K.L., 2000. The Lightning Creek Sill Complex, Cloncurry District, Northwest Queensland: A source of fluids for Fe Oxide Cu-Au mineralization and Sodic-Calcic Alteration. Economic Geology, 95, 1067-1089.

Pollard P.J., 2000. Unmixing of H2O-CO2-salt fluids: consequences for alteration in Fe-oxide-Cu-Au systems. In: Roberts, M.D. and Fairclough, M.C., eds., Fe-oxide-Cu-Au Deposits: A discussion of critical issues and current developments. Economic Geology Research Unit, James Cook University, Contribution, 58, 30-35.

Rotherham, J.F., Blake, K.L., Cartwright, I. and Williams, P.J.,,1998. Stable Isotope Evidence for the origin of the Mesoproterozoic Starra Au-Cu Deposit, Cloncurry District, Northwest Queensland. Economic Geology, 93, 1435-1449.

Shmulovich, K.I. and Graham, C.M., 2004. An experimental study of phase equilibria in the systems H_2O-CO_2CaCl_2 and H_2O-CO_2-NaCl at high pressures and temperatures (500-800°C, 0.5-0.9 GPa): Geological and geophysical applications. Contributions to Mineralogy and Petrology, 146, 450-462.

Williams, P.J., Gouyi, D., Pollard, P.J., Broman, C., Martinsson, O., Wanhainen, C., Mark, G., Ryan, C. and Mernagh, T.P., 2003. The nature of iron oxide-copper-gold ore fluids: Fluid inclusion evidence from

Norbotten (Sweden) and the Cloncurry district (Australia). In: Eliopoulos et al., eds., Mineral Exploration and Sustainable Development, 2, 1127-1130.

Statistical evaluation of the spatial relationship of intrusions and faults to Fe-Oxide Cu-Au systems, Cloncurry district

R. Mustard[1], T. Blenkinsop[1], C. McKeagney[1], C. Huddleston-Holmes[1]

and Greg Partington[2]

*[1] pmd*CRC, Economic Geology Research Unit, School of earth Sciences, James Cook University, Townsville, QLD 4811*

[2] Kennex Knowledge Systems Ltd, Eastbourne, Wellington New Zealand

roger.mustard@jcu.edu.au

Introduction

The origin of Fe oxide-(Cu-Au) deposits and the relative role of played by magmas (both felsic and mafic) versus evaporite-rich country rocks as a source of fluids and/or metals remains controversial. A popular model for the formation of IOCG deposits in the Mt Isa Eastern Succession involves fluids derived from the late orogenic granites mixing with a second external fluid source forming Fe- (commonly magnetite-) rich alteration zones that contain vein stockwork, breccia, dissemination or replacement style mineralization (Oliver et al., 2000). This is assumed to be commonly spatially and temporally associated with felsic pluton emplacement and cooling around 1540-1500 Ma. This contrasts with an alternative model in which the fluids are entirely intra-basinal and amagmatic in origin (Barton and Johnson, 1996). Recent dating studies at Osborne have highlighted a potential syn-peak metamorphic timing to mineralization (based on 1595 Ma Re-Os age dates on molybdenite and a 1595 ± 6 Ma U-Pb age date on hydrothermal titanite), with no apparent proximal major intrusion (Gauthier et al., 2001). There is also a potential link between mineralization and widespread mafic intrusive activity that occurs in the Eastern Succession for the entire range of known mineralization ages. Futhermore, at some deposits (276 orebody at Starra) intra-ore mafic intrusives have been recorded.

In this paper we investigate this considerable range of potential geological controls on IOCG mineralization. A prospectivity analysis was undertaken, aimed at evaluating the relative importance of a range of spatial variables including: host rock type, proximity to felsic granites or mafic intrusives, stream geochemistry (Cu and Au), faults, and geophysics (including magnetics, gravity and wavelet-processed potential field data or “worms”). A data driven approach was taken in view of the considerable uncertainty in genetic models for IOCG deposits.

Cloncurry District

The Cloncurry district forms the eastern part of the Mount Isa Inlier in northwest Queensland. The district is largely composed of evaporite-rich cover sequence 2 rocks and siliciclastic-rich cover sequence 3 rocks (ca. 1740 Ma and ca. 1670 Ma, respectively). There are three principal fabric - forming deformation events within the Cloncurry District, although the structural history can be more complex locally (Adshead-Bell, 2000). The first compressional event D_1 formed horizontal S_1 fabrics sub-parallel to bedding. The second deformation produced prominent N-S trending regional fabric and fold axes during east-west shortening. D_3 also involved east-west directed compression, resulting in N-S trending upright folding and faults exhibiting more brittle

behaviour. Many of the principal deposits in the region are spatially associated with reactivated "master faults" where earlier basin forming faults were overprinted by brittle strike-slip, and thrust faults (Sleigh, 2002). The metamorphic grade varies from upper greenschist to upper amphibolite facies, with two apparent metamorphic peaks at ~1584 Ma and ~1530 Ma. The eastern part of the district has been intruded by mafic to felsic, K-rich, magnetite series intrusions of the Williams and Naruku batholiths (ca 1550-1500 Ma).

Methodology

Important data sources used in this study include (1) the Northwest Queensland Mineral Province Report, (2) mineral occurrence data and newly available open file geochemistry available from the Queensland Department of Mines and Energy, and (3) regional magnetics and gravity digital datasets available from Geoscience Australia. The initial study area consisted of six 1:100,000 sheets covering Cloncurry and the area to the south.

Mineral deposit locations for hard rock Cu-Au mineralisation were extracted from the Queensland Geological Survey mineral resource database (MinOcc 2002). A training data set consisting of 567 occurrences was then subset from this database, including the Ernest Henry, Eloise, Osborne, Mt Elliot, and the Selwyn line. Spatial correlations were calculated using the Weights of Evidence technique, using the Spatial Data Modeller extension developed for Mapinfo software. A unit area of 0.25 km^2 was used in these calculations assuming the known deposits have a 0.25 km^2 area of influence. The spatial correlation (prior probability) of a feature can be calculated by using the relationship of the area covered by the data variable being tested and the number of training data points. This produces a W+ result when the feature is present and a W- result when the feature is absent. A contrast value C is then calculated from the difference (Table 1). The standard deviations of W (Ws and Cs) are calculated, from which the Studentised value of the contrast (StudentC) can then be calculated (the ratio of the standard deviation of the contrast Cs to the contrast C). StudentC gives an informal test of the hypothesis that C=0 and as long as the ratio is relatively large, implying the contrast is large compared with the standard deviation, then the contrast value is likely to be real. The StudentC value should be larger. This ratio is best used as a relative indicator of spatial correlation, rather than an absolute sense. In this study a strong correlation is inferred from C values > 2.0, StudentC values >3.0, moderate correlations inferred from C values between 1.0-2.0, StudentC values between 3.0-1.5, weak correlations inferred from C values between 0.5-1.0, StudentC values between 1.5-0.5 and poor correlations inferred from C values between < 0.5, StudentC values <0.5.

Results

Contrast and Student C values for all evidential layers indicates that the host lithology as the most important criterion, followed by geochemistry (Cu and then Au), structure, geophysics, felsic and mafic igneous intrusions. The results enable a list of target criteria to be statistically ranked. A comparison of these results can be made with expert driven predictions. The study area is being expanded to include the entire Eastern Succession, including solid geology maps interpreted through cover.

Evidential Layer	Contrast	StudentC
Host Lithology	2.19	2.23
Cu Stream Geochemistry	1.84	8.45
Au Stream Geochemistry	1.63	4.31
Major N-NNW fault intersections	1.44	4.56
N-NNW trending Faults	1.11	5.45
Gravity	0.77	3.17
Magnetics	0.72	2.98
Felsic Granite Buffer	0.60	2.99
Medium Faults	0.55	2.90
Gravity Worms	0.46	2.21
Magnetics Wmax	0.46	2.21
Mafic Buffers	0.36	1.46
Magnetics Worms	0.36	1.81
Gravity Wmax	0.32	1.58

Table 1. Results of initial prospectivity analysis. Note host lithology, stream geochemistry (Au and Cu) and Major N-NNW fault intersections display moderate correlations with Cu-Au occurrences with Contrast values (C) > 1.

Discussion

An important outcome for ore genetic models is the recognition that intersections of N to NNW structures with other faults have the strongest spatial association with IOCG deposits after host rock and geochemistry. This result implies that fluid pathways are much more important than fluid sources for controlling the distribution of IOCG deposits. This understanding can possibly explain some of the diversity in the range of IOCG deposit types and models. A common mineralizing process could generate deposits in a variety of host rocks depending on the fluid pathways. The dominance of the fluid pathways means that fluid sources cannot be clearly recognized from spatial associations of the deposits alone, and mineralizing fluids may be complex and heterogeneous in view of their possible interactions with a variety of wall rocks. A detailed understanding of fluid pathways and structures at all scales is the most important direction for future research. Mechanical modeling directed at understanding fluid flow in the Mt Isa Eastern Succession based on this structural knowledge will also be an important tool.

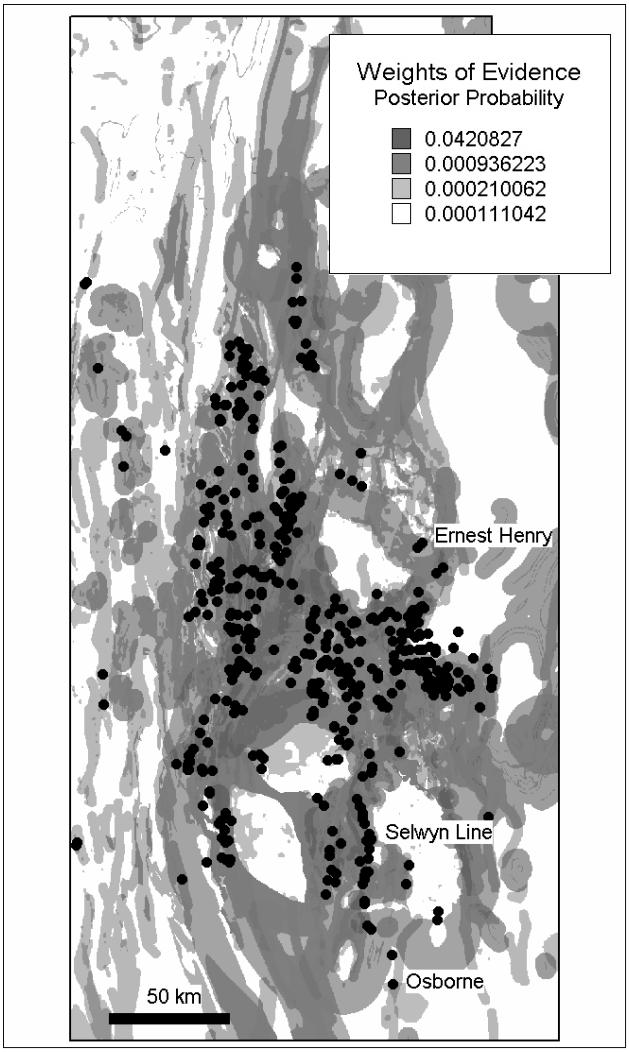

Figure 2. A 5-Layer prospectivity map for the Mt Isa Eastern Succession. Evidential layers include host lithology, N-NNW trending faults, fractionated felsic granites, mafic intrusives and magnetics.

Faults and Fe-Oxide Cu-Au Deposits

All known major deposits have a clear link to fault architecture, with ore localized in dilational jogs generated during broadly E-W compression. The potentially older Osborne deposit is considered to have also formed during a period of E-W compression.

Mt Elliot forms a NE plunging ore-body localized between NNW trending, moderate to steep NE dipping faults. Ore deposition is interpreted to have been controlled by reverse movement along the NNW-trending faults and flat-lying linking faults (Little, 1997; Wang and Williams, 2001) The Selwyn Line which consists of a group of 5 Au-Cu deposits (222, 244, 251, 257 and 276) are localized along the steeply inclined NNE to NS-trending Starra shear zone (Sleigh, 2002). The ribbon like ore shoots extend between 50 to 300m along strike and more than 600m down plunge (commonly 60-80° NNE). They are localized at the intersection of the hanging wall to the main Starra shear zone and NE-trending 'link' structures within the Starra shear zone (Sleigh, 2002).

Ernest Henry forms a SE plunging body constrained between NE-trending, moderate SE dipping shear zones (Williams and Skirrow, 2000). Ore deposition is interpreted to have occurred during reverse fault movement along bounding shear zones forming a pipe-like zone of dilation (Mark et al., 2000). Eloise is located in a steeply-dipping N-trending splay located adjacent to a bend in the regional Levuka shear. Magnetite was deposited at the bend some 500m south of the lodes (Williams and Skirrow, 2000; Baker and Laing, 1998). At the Osborne Mine, ore is localized in areas of anomalous moderate to shallow dipping, NW-trending fabrics.

These sites may have localized dilation during reverse faulting adjacent to the ironstones (Adshead, 1998).

Faults have a stronger spatial association with mineral deposits than mafic and felsic intrusives. This suggests that detailed analysis of faults and their relationship to Fe-oxide Cu-Au deposits will be a potential useful targeting tool. Future prospectivity models should focus on developing an understanding of the fault controls at known deposits and extrapolating these conditions to the Cloncurry District.

Acknowledgements

We would like to thank Martin Higham (Avantra Geosystems) for continual upgrades to his MI-SDM software.

References

Adshead-Bell, N.S., 2000. Structural Constraints of the Ironstone Hosted Au-Cu Starra Deposit and Selwyn Range Region, Eastern Fold Belt, Mt Isa Inlier. Unpublished PhD thesis, James Cook University, Townsville.

Adshead, N.D., Voulgaris, P. and Muscio, V.N., 1998. In: Berkman, D.A. and Mackenzie D.H., eds., Osborne copper-gold deposit. Geology of Australian and Papua New Guinean Mineral Deposits, The Australasian Institute of Mining and Metallurgy, Melbourne, Monograph Series 22, 793-799.

Baker, T. and Laing, W.P., 1998. The Eloise Cu-Au deposit, east Mount Isa Block: structural environment and structural controls on ore. Australian Journal of Earth Sciences, 45, 429-444.

Barton, M.D. and Johnson, D.A., 1996. Evaporitic-source model for igneous-related Fe-oxide-(REE-Cu-Au-U) mineralization. Geology, 24, 259-262.

Gauthier, L., Hall, G., Stein, H. and Schaltegger, U., 2001. The Osborne Deposit, Cloncurry District: A 1595 Ma Cu-Au Skarn Deposit. In: Williams P.J., ed, 2001: A hydrothermal Odyssey Extended Conference Abstracts. Economic Geology Research Unit, James Cook University, Contribution, 59, 58-59.

Little, G.A., 1997. Structural evolution and paragenesis of alteration mineralization at Mt Elliot Cu-Au mine, northwest Queensland. Unpublished BSc (Hons) thesis, James Cook University, Townsville, 131pp.

Oliver, N.H.S., Mark, G., Pollard, P.J., Rubenach, M.J., Williams, P.J., Baker, T. and Nemchin, A. A., 2000. Mass transfer and fluid flow in the Eastern Fold Belt of the Mt Isa Block: searching for local and distal mass sources for ore deposits. In: Roberts, M.D. and Fairclough M.C., eds., Fe-oxide-Cu Deposits: A discussion of critical issues and current developments. Economic Geology Research Unit, James Cook University, Contribution 58, 19-25.

Sleigh, D.W.W., 2002. The Selwyn Line Tabular Iron-copper-gold system, Mount Isa Inlier, NW Queensland, Australia. In: Porter, T.M., ed., Hydrothermal Iron Oxide-Copper-Gold and Related Deposits. A Global Perspective, Volume 1. PGC Publishing, Adelaide, 77-93.

Wang, S. and Williams, P.J., 2001. Geochemistry and origin of Proterzoic skarns at the Mount Elliot Cu-Au-(-Co-Ni) deposit, Cloncurry district, NW Queensland, Australia. Mineralium Deposita, 36, 109-124.

Williams, P.J., 1998. Metalliferous economic geology of the Mt. Isa Eastern Succession, northwest Queensland. Australian Journal of Earth Sciences, 45, 329-341.

Williams, P.J. and Pollard, P.J., 2001. Australian Proterozoic Iron Oxide-Cu-Au Deposits: An Overview with New Metallogenic and Exploration Data from the Cloncurry District, Northwest Queensland. Exploration and Mining Geology, 10, 191-213.

Wyborn, LAI., 1988. Younger ca. 1500Ma granites of the Williams and Naruku Batholiths, Cloncurry district, eastern Mt Isa Inlier: Geochemistry, origin, metallogenic significance and exploration indicators. Australian Journal of Earth Sciences, 45, 397-411.

Williams, P.J. and Skirrow, R.G., 2000. Overview of Iron Oxide-Copper-Gold deposits in the Curnamona Province and Cloncurry District (Eastern Mt Isa Block), Australia. In: Porter, T.M., ed., Hydrothermal Iron Oxide-Copper-Gold and Related Deposits. A Global Perspective, Volume 1. PGC Publishing, Adelaide, 105-122.

Hydrothermal alteration footprints and gold mineralization in the St Ives gold camp

Peter Neumayr[1], John L. Walshe[2], Leo Horn[3], Klaus Petersen[1], Cari Deyell[4], Kate Moran[5], Daniel Howe[6], Karen Connors[6], Ned Stolz[6], Robert S. Morrison[6], Steffen G. Hagemann[1]

*[1]pmd*CRC, Centre for Global Metallogeny, The University of Western Australia*
*[2]pmd*CRC Divison of Exploration and Mining, CSIRO*
[3] CSIRO, Division of Exploration and Mining (Present address: Goldfields Agnew Gold Mining Company Pty Ltd)
[4] CODES, University of Tasmania
[5] Lion Ore Pty Ltd
[6] St. Ives Gold Mining Company Pty Ltd.

Introduction

This research project focuses on delineating hydrothermal alteration patterns in three dimensions and through time as well as at different scales from camp- to deposit-, to ore-shoot scale. The analyses of these hydrothermal "footprints" are primarily guided by the geometry and kinematics of fault zones at all scales and geophysical signatures such as magnetics and gravity that delineate porphyry bodies at depth. Detailed field and petrographical analyses are then complemented by whole rock and trace element analyses of alteration zones, mineral analyses of key hydrothermal alteration minerals as well as fluid inclusion and stable isotope analyses. The spatial distribution of hydrothermal alteration types and their mineralogical and chemical signals are then interpreted with respect to fluid sources, ore transport and depositional processes to provide guides to gold mineralization. The key to unravelling hydrothermal alteration footprints and their use for exploration targeting is to understand the relative timing of alteration types as well as their spatial distribution. In addition, spatial information on the variation of stable isotope compositions is vital to determine metal transport and depositional processes, and in combination with multi-element geochemistry and fluid end-member composition data sets, provide critical input parameter into geochemical modeling of metal transport and depositional processes.

The aim of this paper is to summarize the key results of current studies (some are still on-going) and also discuss potential models to explain the mineralogical and chemical footprints with respect to ore deposition.

Geological setting

The St Ives gold camp is located in the southern part of the Norseman-Wiluna greenstone belt within the Eastern Goldfields Province of the Yilgarn Craton of Western Australia. The St Ives gold camp is hosted in predominantly mafic-ultramafic lavas and intrusions that have been metamorphosed to upper greenschist and lower amphibolite facies. The greenstone sequence has been intruded by felsic to intermediate porphyry stocks which predate, are synchronous with and post-date gold mineralization.

The St Ives gold camp is bounded by two major NNW-trending regional structures: the Boulder-Lefroy fault to the east and the Merougil fault to the west, and has undergone four major Archaean deformation events. The first (D1) produced regional south-over-north thrusts. The second (D2) produced upright, NNW-trending, gently plunging folds, such as the Kambalda anticline. The third event (D3) generated brittle-ductile, NNW-trending, oblique-sinistral strike-slip fault systems that localized major N-trending, reverse, gold-bearing shear zones. During the fourth event (D4), NE-trending, dextral faults offset stratigraphy and earlier fault systems, and

caused dextral±reverse reactivation of these earlier faults. Gold mineralization is mainly controlled by the D3 and D4 deformation events.

Hydrothermal alteration

In the St Ives camp, a range of alteration styles are documented. Oxide and sulphate assemblages are correlated to reduced and oxidized conditions using f_{O2}-a$\sum$S diagrams at 400º C and 2 kbars. Documented styles are: 1) carbonate associated with deformation along transcrustal structure (Lefroy), 2) epidote-calcite-magnetite$_1$-pyrite-chalcopyrite-quartz, 3) magnetite$_2$ halo around gold-bearing structures (interpreted as oxidized hydrothermal fluid), 4) pyrrhotite±pyrite alteration flanking oxidized domains on a camp scale (interpreted as reduced hydrothermal fluid), and 5) Au-associated, zoned chlorite-biotite-feldspar-carbonate-pyrite quartz alteration. Widespread carbonation is typically recorded in ultramafic hostrocks. Its spatial distribution and textural setting is being studied by Heydari (this volume) and is not discussed further.

Epidote-calcite-magnetite$_1$-pyrite-chalcopyrite-quartz alteration is spatially associated with felsic to intermediate porphyries at a camp scale. At a drill core scale, this alteration style is developed typically adjacent to the contact of porphyry intrusions. Epidote and magnetite$_1$ occur in massive bands and replace pre-existing amphibole. Carbonate-pyrite±quartz veins and quartz ±chalcopyrite±magnetite?±carbonate? veins overprint epidote and magnetite$_1$ assemblages. Importantly, epidote dominant alteration pre-dates gold mineralization, but is locally spatially associated with gold-bearing structures.

In the camp, two main domains of hydrothermal alteration are mapped out: 1. Magnetite$_2$ and magnetite$_2$-pyrite assemblages (oxidized), and 2. pyrrhotite and pyrrhotite-pyrite assemblages (reduced). The oxidized assemblage is focused around massive porphyry stocks. This spatial association is well developed around a kilometre-scale gravity low which is interpreted to reflect buried intrusions beneath the Victory-Defiance gold deposits, but also around smaller-scale porphyry stocks at the Revenge deposits. The domains with reduced alteration assemblages flank those of oxidized alteration assemblages on a camp scale. They are well developed to the SW and NE of the Victory-Defiance deposits and the Revenge deposits. Locally, reduced and oxidized alteration assemblages occur intermingled at the Revenge deposits.

At a drill core scale, reduced alteration assemblages are fine-grained and disseminated within mafic host rocks and occupy zones distal to gold mineralization. Reduced assemblages occur also in quartz-pyrrhotite veins which cross cut mafic host rock with disseminated pyrrhotite-pyrite alteration. Outer proximal zones (to gold) are characterized by a broad halo of magnetite$_2$ around gold-bearing structures, whereas inner proximal zones contain magnetite$_2$ and magnetite$_2$-pyrite assemblages. The magnetite$_2$ halo overlaps partially with typically gold-associated distal chlorite-carbonate and intermediate biotite-chlorite-carbonate alteration zones.

At a micro-scale, magnetite$_2$ appears to be in equilibrium with biotite, as indicated by biotite inclusions in the magnetite. Magnetite$_2$ (oxidized assemblage) forms inclusions in the cores of gold-associated pyrite grains and is replaced by hematite inclusions (very oxidized assemblage) in the outer zones of the pyrite grains. Importantly, magnetite$_2$ inclusions in pyrite have locally a thin rim of hematite. Within the proximal (to gold) feldspar-carbonate-pyrite zone, magnetite is least abundant to absent. Locally, clusters of magnetite are present, but texturally in disequilibrium with feldspar-carbonate-pyrite alteration. Magnetic susceptibility readings are high outside the feldspar zones and drop to a minimum within the feldspar zones.

Relative timing of hydrothermal alteration

Spatial relationships indicate that epidote-dominated alteration developed early in the alteration sequence. However, in most places it does not spatially overlap with later magnetite$_2$ and gold-related feldspar alteration. Locally, relict (?) epidote is present in feldspar alteration zones. Most of the magnetite$_2$ halos pre-date gold mineralization. However, the presence of magnetite$_2$ inclusions within gold-associated pyrite indicate that this magnetite was stable during the early phases of gold mineralization. Subsequently, hematite was stabilized over magnetite, as

indicated by hematite inclusions in the rims of gold-associated pyrite. The relative timing of the reduced pyrrhotite-pyrite assemblage is unclear at present. The reduced domains are typically separated from oxidized alteration domains by unaltered or poorly altered wallrock. Within the reduced assemblage, textures indicate that one generation of pyrite pre-dates pyrrhotite. The evolution of the redox state of hydrothermal alteration can only be safely assessed in the oxidized to very oxidized domains. Textural relationships clearly indicate that the very oxidized pyrite-hematite assemblage post-dates the oxidized magnetite$_2$-pyrite assemblage.

Stable isotope variations in the St Ives Camp

Compilation of the significant historic data sets of C, O isotopes in carbonate and S isotopes in sulphates, as well as acquisition of new data, is providing a significant constraint on the variation of fluid temperatures and redox state of hydrothermal fluids in the St Ives gold camp. The variation of δ^{18}O in carbonate is particularly sensitive to temperature with the lightest δ^{18}O values reflecting the highest temperature fluids. In contrast, the variations in δ^{13}C in carbonate and δ^{34}S in pyrite are sensitive to redox changes in the hydrothermal fluid. Redox variations in the carbon and the sulphate systems are interpreted to mirror variations in the CH_4/CO_2 and H_2S/sulfate ratios, respectively. In the Revenge area, the lightest δ^{18}O values occur in the central part of the field west of Revenge (LD7114: 7.5 to 9.5 ‰ δ^{18}O, VSMOW) and are heavier to the east in the vicinity of the Playa Shear (LD70426 and LD70449: 9.3 and 12.5 ‰ δ^{18}O) consistent with carbonate precipitation at progressively cooler temperatures distal to mineralization and also to the main porphyry intrusions. The limited variation in δ^{13}C over this interval (-6.8 and -3.2 ‰ δ^{13}C, PDB) is an indication that the fluid is dominated by CO_2. The inferred δ^{13}C of the CO_2 in the fluid is close to zero suggesting that the dominant (?) reservoir for CO_2 was seawater with little reduction of the CO_2 during recycling within the greenstones.

In the Revenge, Victory- Defiance, Argo and Junction deposits, significant variations of δ^{13}C in carbonate with limited variations of δ^{18}O are indicative of a variation in CH_4/CO_2 in the fluid. The lighter δ^{13}C signal in proximal carbonate in pyrrhotitic (reduced) assemblages is taken to reflect CH_4 in the fluids, which is consistent with CH_4 –rich fluid inclusions in the Junction deposits. In the Victory-Defiance profile across the central corridor, δ^{13}C values are lighter (-8.7 to -7.1 ‰. in the altered Flames Porphyry in the central part of the Victory-Defiance deposit and again Britannia Shear on the eastern side of the central corridor. At both these locations, the reduced and oxidized alteration domains overlap. From available data, δ^{13}C values are heavier (-7.4 to -4.4 ‰) in domains of the oxidized alteration assemblage.

Within in the Victory-Defiance area, the sulphate isotopes also vary with respect to reduced and oxidized mineral domains. Within the oxidized domains, δ^{34}S ranges from -7.9 to -6.8 ‰. However, δ^{34}S ranges from +1.6 ‰ to -6.5 ‰ in reduced domains or in domains where reduced and oxidized domains overlap, which indicates that the gradient in δ^{34}S in pyrite across the Victory-Defiance deposit corresponds with the change in sulphate/oxide mineralogy. Available δ^{34}S values for background pyrite in the Kapai Slate, Black Flag and Merougil beds, west of the Kambalda Dome and in the Tramways area, distant from the St Ives Camp, range from 0.3 to 0.7 ‰. Two samples of least altered carbonaceous, pyritic Kapai Slate from the Central Corridor of the St Ives camp have values of 0.7 and 1.8 ‰ δ^{34}S. In the absence of any evidence that the sulphate isotope values within the camp, either negative or positive, were influenced by the background sulphate in the rock mass, they are interpreted in terms of the chemical processes that operated within the hydrothermal system. The negative signals in sulphate are taken to reflect the presence of sulphate in oxidized fluid(s) and the positive signals are taken to reflect reduction of this sulphate to H_2S in the reduced environments within the gold system. Locally, a heavy δ^{18}O in carbonate, up to 18-25 ‰, with δ^{13}C around -5 to -7 ‰ in the Revenge and Victory deposits could reflect magmatic CO_2. The signal is unconstrained paragenetically.

Discussion

Hydrothermal alteration types show a clear spatial and temporal variation in the St Ives gold camp. Epidote-dominated alteration appears to develop early and is focused around porphyry intrusions. Significant Te anomalies are spatially associated with epidote-dominated alteration and are interpreted to be driven by porphyry intrusion and associated epidote alteration.

Magnetite$_2$ alteration appears to postdate epidote alteration, but is largely predating gold. The spatial distribution of magnetite$_2$ with respect to gravity lows and porphyry distribution in the camp indicates also a close genetic link. Minor magnetite$_2$ inclusions in gold-related pyrite indicate that magnetite$_2$ was stable at the onset of pyrite growth but was replaced by hematite during most of the pyrite growth and gold mineralization. This suggests that the oxidation state of the hydrothermal fluid changed to extremely oxidized conditions during gold mineralization. The relative timing of pyrrhotite and pyrrhotite-pyrite assemblages is unconstrained at present. However, the fact that the reduced assemblage occurs distal to the oxidized assemblage (and gold), and that pyrrhotite does not overprint the oxidized assemblage, indicates that the reduced assemblage either pre-dates or is synchronous with oxidized alteration assemblages.

The textural relationships may be explained either by mixing of two different fluids of grossly different redox state or by sequential precipitation of hydrothermal alteration out of these fluids. In the sequential precipitation model, pulses of fluids with grossly different redox conditions precipitated a sequence of alteration assemblages. Subsequent pulses reacted with previously precipitated alteration assemblages, thus explaining the presence of reduced and oxidized alteration mineral assemblages.

The co-variance of $\delta^{13}C$ and $\delta^{34}S$ with oxidized and reduced assemblages, together with the paragenetic link of $\delta^{13}C$ and $\delta^{34}S$ variations with high grade gold zones, may be explained by the presence of both methane-rich (reduced) and sulphate-rich (oxidized) fluids in the gold zones at about the time of gold deposition. The mixing of fluids of contrasting redox state provides a powerful gold precipitation mechanism and can account for the stable isotope relationships. In the sequential precipitation model, a heavy S isotope source must be inferred to account for co-variation of heavy S and light C isotopes. Other commonly discussed mechanisms such as sulfidation and fluid unmixing (boiling) do not account adequately for the spatial, textural and stable isotope relationships. In order to rigorously test the two competing models, detailed textural, stable isotope, fluid inclusion and geochronological studies are currently being conducted in high-grade gold zones with co-variation of carbon and sulphate isotopes.

The spatial association of oxidized assemblages with porphyry intrusions at the drill core to camp scale strongly suggests that magmatic volatiles were the source of oxidation. This conclusion is supported by similarities in the hydrothermal evolution of deposits in the Central Corridor with the evolution of the Wallaby deposit. Recent detailed mapping of this deposit has identified both close spatial and paragenetic links between gold mineralization and syenite magmatism (Drieberg et al., this volume).

Integration of the stable isotope data with detailed fluid inclusion data (Petersen et al., this volume) provides some clues to the specific fluid-flow events that may be correlated across the St Ives Camp and to the sources of the fluids. Low salinity carbonic-aqueous fluids in carbonate most likely correlate with fluids locally recycling CO_2 within the greenstones, driven by granitic/porphyry heat sources at depth. The more saline aqueous-carbonic fluids, particularly associated with late quartz may represent an injection of a magmatic brine component to a high level in the system during depressurization, heat loss and quartz precipitation. It is suggested that the magmatic volatile phase probably consisted largely of CO_2, as evidenced by the carbonic fluids in albite and for which there is some cryptic C and O isotope evidence. The SO_2 in magmatic volatile phase could have produced the high oxidation conditions seen in the high grade gold zones. Other components in the magmatic volatile phase included tellurium, possibly vanadium species as well as trace Mo, W and As (?) Au (?). The source(s) of the CH_4 –rich

fluids remain problematical. They could be derived from local sedimentary basins, from deeper in the crust or mantle, or from as yet unidentified magmatic source of reduced fluids.

High-grade gold mineralization (>100g/t) is preferentially located in domains where reduced and oxidized alteration assemblages overlap, or close to the border of the domains, but within the oxidized domain. In combination with the fact that oxidation state of the hydrothermal fluid changed to extremely oxidized conditions during mineralization, this suggests that large gradients in redox conditions specifically, and large chemical gradients in general, are powerful gold precipitation mechanisms.

Acknowledgements

During the past two years two postdoctoral fellows, two honours students, and one staff member from the Centre for Global Metallogeny at the University of Western Australia as well as one “embedded” researcher and one staff member from CSIRO have conducted these studies under the auspices of the pmd*CRC Yilgarn 3 project and under a part of the MERIWA 358 project. Two more PhD students from UWA will work on aspects of the Kambalda geology in 2004 and 2005. The various studies have been supported and invaluable information shared by many company geologists from St Ives Gold Mining Company Pty. Ltd.

Invaluable discussions with Placer Dome geologists namely Scott Halley and Greg Hall, as well as with “embedded researchers” Glen Masterman and Susan Drieberg supported this research.

Brittle fracturing at the laboratory to outcrop scale

A. Ord, Y. Zhang, B.E. Hobbs and K. Regenauer-Lieb

*pmd*CRC, CSIRO Exploration and Mining, PO Box 1130, Bentley, WA 6102*
Alison.ord@csiro.au

Introduction

Brittle fracturing is ubiquitous in the upper crust, and is a common feature associated with ore deposits. However, prediction of its initiation, development, and evolution, and of associated properties such as dilatancy, is remarkably difficult. This is a function partly of the variability of rock properties, and partly because we cannot see into specimens to see how they behave during physical deformation experiments. This is where computer experiments can provide such valuable information. In this case we look at the opportunities provided by a particle code for exploring microstructural changes during deformation. We validate the code against physical deformation experiments, use it to improve our understanding of rock behaviour during deformation, and apply it to shear zone evolution and fracture development at outcrop scale.

The development of fracture systems, shear zones, zoned mineral alteration systems (including ore bodies), and fluid percolation networks can all be thought of as emergent phenomena in geomaterials.

Emergence is a property of large dissipative systems driven far from equilibrium (see Kondepudi and Prigogine, 1998). The term refers to the spontaneous development of structure or patterning in a system that previously had been homogeneous. In such systems, intriguing patterning and order can be generated, both in time and space, in systems that otherwise one would expect to behave in uniform manners. This can commonly be represented as a symmetry breaking phase transition (see Sethna, 1992). A characteristic of such systems is that there are first order feedback relationships between a number of processes. Another important characteristic is that the resultant patterning occurs on a number of scales so that something of a fractal nature is developed.

Emergent behaviour is associated with **bifurcation** in the system of differential equations that describes the mechanics of the system. A classical simple example of bifurcation is the behaviour of the solutions to the equation 1 $d\alpha/dt = -\alpha^3 + \lambda\alpha$ where λ is a parameter such as amount of strain. When $\lambda<0$ there is only one real stationary state, $\alpha=0$; when $\lambda>0$ two real stationary states exist, $\alpha=\pm\sqrt{\lambda}$. $\lambda=0$ is a bifurcation point (see Figure 1a). The typical stress strain curve for a rock is an example of bifurcation behaviour (see Figure 1b). Here the material behaviour departs from homogeneous deformation to localised deformation at a bifurcation point determined by the amount of strain.

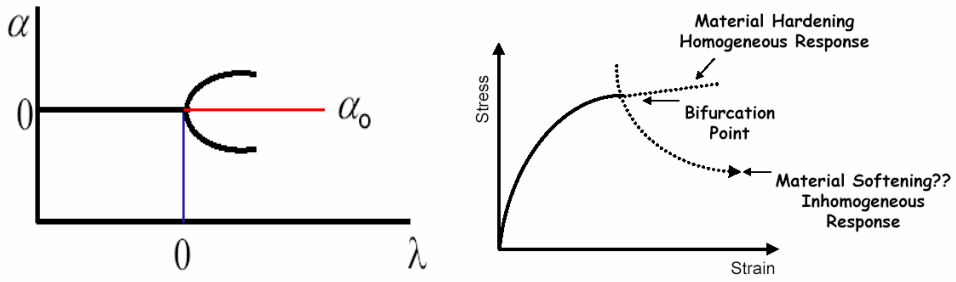

Figure 1. Bifurcation behaviour. (a) Behaviour of equation (1). (b) A typical stress strain curve showing the departure from homogeneous to localised deformation at a bifurcation point determined by the amount of strain.

The classical (engineering) description of materials is restricted to the detection of such bifurcation points in a linear stability analysis. In geology we are interested in the post failure evolution which we do by trading energy fluxes in a self-consistent particle simulation.

Fracture development at laboratory scale

In laboratory experiments, it is well known that homogeneous loading of a homogeneous specimen does not continue for ever. At some stage in the process, as noted above, the system bifurcates, and localisation of the deformation occurs. This phenomenon has been noted for various materials and environmental conditions, being observed as buckling, shearing, and the 'elephant's foot' instability. These represent emergent phenomena; which arise spontaneously from a material and loading conditions with no a priori similar structures. How can we duplicate this phenomenon *ab initio* in virtual rock experiments?

We initiated a suite of experiments for validating a particle flow code (PFC, Cundall, 2000; Cundall, 2001; ITASCA, 2003) against physical deformation experiments, in this case the triaxial experiments of Edmond and Paterson (1972), for various materials, including Gosford sandstone. The initial experiments were sufficiently encouraging for us to attempt validation of the code in a plane strain biaxial experiment against the experiments of Ord (1991). The same phenomenon, localisation of the deformation into a shear zone, emerged from a numerical specimen undergoing uniform loading (Figure 2). This behaviour is not promoted in any way through special conditions within the experiments; no notches were cut, there were no seeds of particularly weak zones.

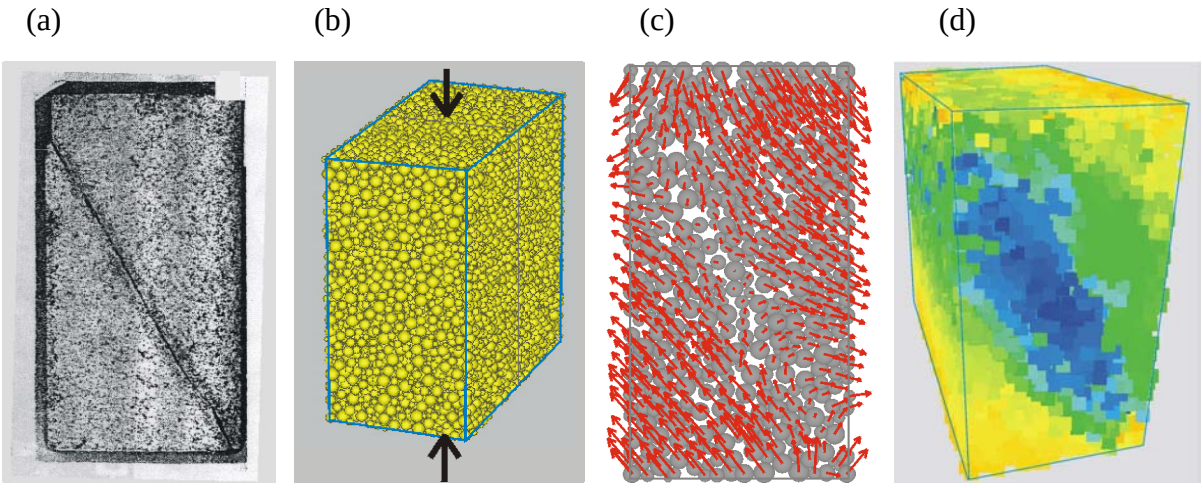

Figure 2. (a) End result of localization of deformation and failure in Gosford sandstone (Ord 1991). Dark areas either side of fracture represent dilated zone, now filled with epoxy. (b) Equivalent numerical experiments using PFC3D. (c) Displacement vectors displayed for plane in centre of the numerical models, highlighting the location of a shear zone. (d) Square root of the horizontal displacement contour (blue – minimum; yellow to orange – maximum).

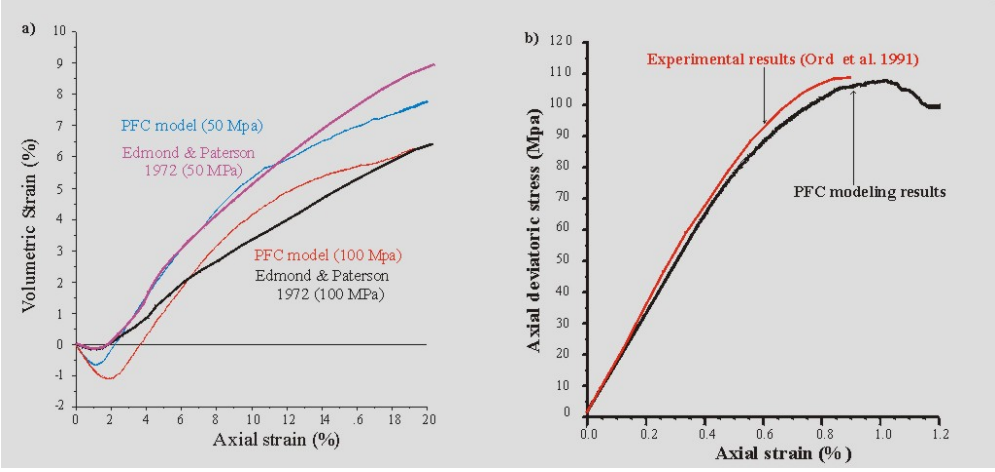

Figure 3. Comparison of numerical results with physical experimental results. (a)Volumetric strain versus axial strain. (b) Axial differential stress versus axial strain.

In geological situations, we are interested in the post-localisation behaviour of the rock. For example in a situation where a fracture, once initiated, continues to develop within the rock mass (rather than breaking it in two as shown in Figure 3a), how does the associated dilatancy evolve? How does the evolution of this system affect, and be affected by, any existing and/or developing flow regime?

The numerical particle model is a collection of rigid spheres with a distribution of sizes and contact strengths. The contacts between individual particles are described by elastic and by Coulomb style interaction laws, including Newton's Laws of Motion. In contrast, the continuum descriptions of such behaviours require non-intuitive variables in order to fit the results. The potential of particle flow codes to simulate this rich emergent behaviour of natural systems has been noted recently by Cundall (2001). We explore this potential further here for the patterning of shear zones. In addition, we spell out clearly the merits in exploring the multiscale physics and evolution of dilatancy of shear zones. In Figure 4, we see the result for shear band formation of loading the material to about 10% shortening, far beyond localization at about 0.6%. This is an excellent example of the emergence of patterned shear zones. Conjugate sets of shear bands are well developed.

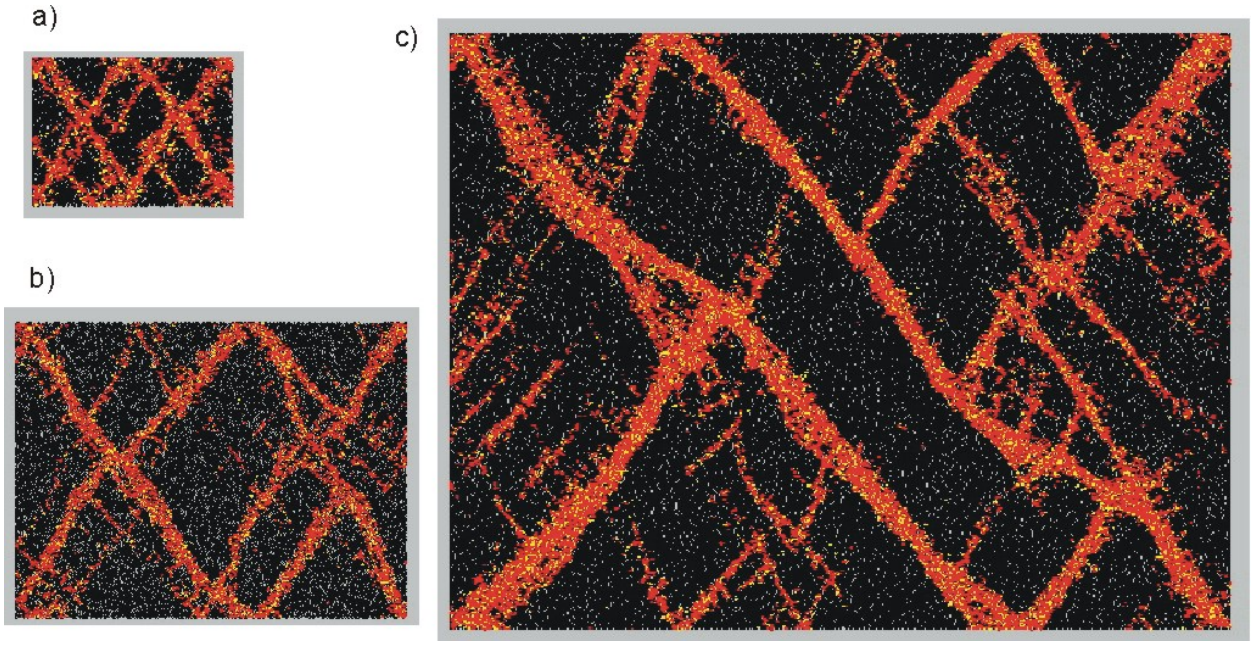

Figure 4. Development of shear bands in three numerical rock samples with different initial size (experimental scales); a) 5 x 5 cm; b) 10 x 10 cm; c) 20 x 20 cm. Shortening is in the vertical direction and confining mechanical pressure is 10 MPa. Bulk shortening of the models is about 10%.

Fracture development at an outcrop scale

Fracture development around pre-existing faults has attracted extensive attention (e.g. Reches, 1988; Zhang et al., 2003). Our outcrop scale PFC2D model examines fracture development around short isolated faults. These models are 20 metres long and 10 metres wide, containing one or two short faults, and are subject to dextral shearing. Fracture formation is represented by breakage of bonds between particles and is illustrated in red (Fig. 5a, b and c). It is noted that wing-crack type fractures developed in all the three models, in the tensile domain of shearing near the tips of pre-existing faults. It is interesting to note that in the models with two short faults, the overlapped portion is both fractured, as a result of either dilation (Fig. 5b) or contraction (Fig. 5c). These models show that a particle code can simulate fracture development consistent with observed natural fracture patterns (Fig. 5d).

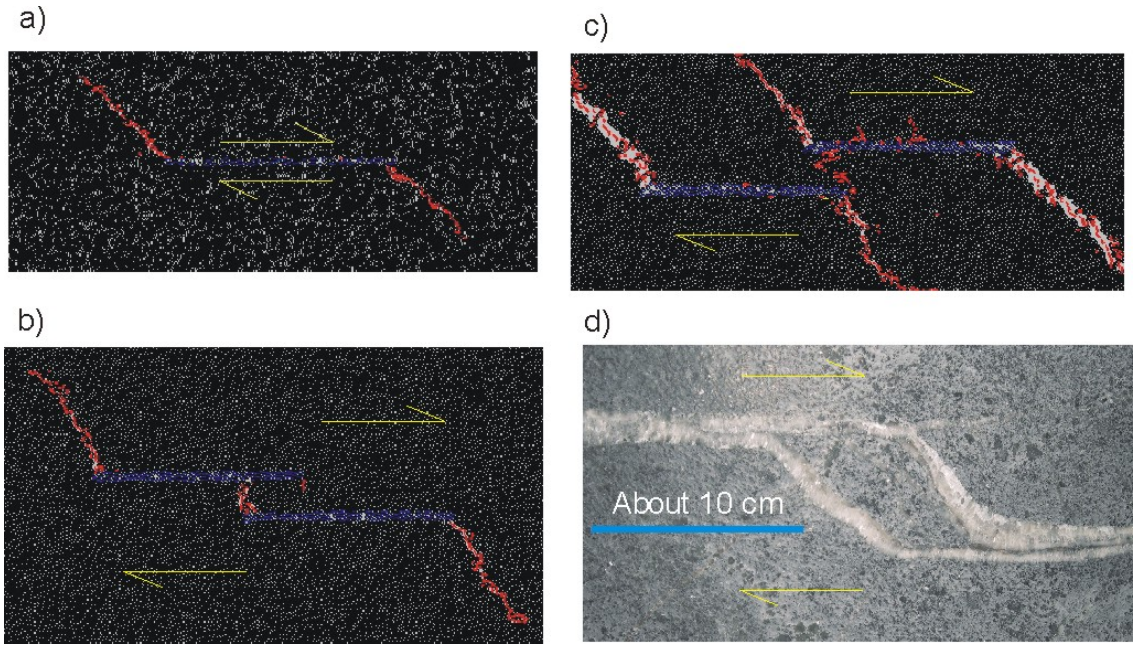

Figure 5. Wing-crack fractures (red) developed in PFC2D models with one pre-existing short fault (a); two short faults (b, dilation); and two short faults (c – contraction). Only the central part of the models around the pre-existing faults are shown. (d) A natural dilatant jog.

Conclusions

These virtual rock experiments are remarkable in their simulation of the dilatancy of rock during deformation. Such experiments offer a unique opportunity to explore a physical space scale not available through physical experiments.

References

Cundall, P. A., 2000. Numerical experiments on rough joints in shear using a bounded particle model. In: Lehner, F.K. and Urai, J.L., eds., Aspects of Tectonic Faulting. Springer, Berlin, 1-9.

Cundall, P. A., 2001. A discontinuous future for numerical modelling in geomechanics? Proceeding of the Institution of Civil Engineers, Geotechnical Engineering, 149, 41-47.

Edmond, J. M. and Paterson, M. S. 1972. Volume changes during the deformation of rocks at high pressures. International Journal of Rock Mechanics and Mining Science, 9, 161-182.

Itasca Consulting Group, 2003. PFC3D and PFC2D – Particle Flow Code, User's Guide. Minneapolis, Minnesota, USA.

Kondepudi, D. and Prigogine, L., 1998 Modern Thermodynamics: From Heat Engines to Dissipative Structures, John Wiley and Sons, Chichester.

Ord, A., 1991. Deformation of rock: a pressure-sensitive, dilatant material: Pure and Applied Geophysics, 137, 337-366.

Reches, Z. 1988. Evolution of fault patterns in clay experiments. Tectonophysics, 145, 141-156.

Sethna, J.P., 1992. Order parameters, broken symmetry, and topology. In: Nadel, L. and Stein, D., eds., Lectures in the Sciences of Complexity. Addison-Wesley, New York., 243-288.

Zhang, Y., Hobbs, B.E., Ord, A., Barnicoat, A., Zhao, C., Walshe, J.L. and Ge Lin 2003. The influence of faulting on host-rock permeability, fluid flow and mineral precipitation: a conceptual 2D numerical model. Journal of Geochemical Exploration, 78-79, 279-284.

P-T-x-fO_2-t of hydrothermal end-member fluids and fluid evolution in the St. Ives gold camp

Klaus Petersen, Peter Neumayr and Steffen G. Hagemann
*Pmd*CRC, Centre for Global Metallogeny, The University of Western Australia*
kjpeters@segs.uwa.edu.au

Introduction

The Y3 project focuses on the spatial extent and chemical characterization of hydrothermal alteration through time on a camp to deposit scale which is then interpreted, in combination with structural controls and their temporal evolution, to provide vectors to gold mineralization. In order to produce a sound interpretation of its evolution, the hydrothermal alteration has to be characterized at a range of scales from camp- to drill core- and even to micro-scale. Importantly, the detailed characterization of the fluid chemistry and its evolution through time allows the reconstruction of the composition of end-member fluids and their inflow paths into, and outflow paths from, sites of deposition. These data are critical input parameters into any chemical model attempting to study and model numerically transport and depositional processes.

In the St Ives gold camp, detailed mapping and core logging has identified a range of alteration styles through time. The fluid compositions and evolution of two of these styles, namely the epidote-magnetite$_1$-carbonate-amphibole alteration, the gold-associated feldspar-carbonate-pyrite $_1$ and the overprinting quartz-pyrite $_2$ alterations have been studied in greater detail so far. The aim here is to document patterns at the hand sample to micro-scale: paragenetic relations and characteristics of fluid inclusions. Hydrothermal fluid data on the other alteration styles present in the camp will be reported at a later date.

Geological and structural setting

The St Ives gold camp is located in the southern part of the Norseman-Wiluna greenstone belt within the Eastern Goldfields Province of the Yilgarn Craton of Western Australia. The St Ives gold camp is hosted in predominantly mafic-ultramafic lavas and intrusions that have been metamorphosed to upper greenschist and lower amphibolite facies. The greenstone sequence has been intruded by felsic to intermediate porphyry stocks which predate, are synchronous with and post-date gold mineralization.

The St Ives gold camp is bounded by two major NNW-trending regional structures (Lefroy and Merougil faults) and has undergone four major Archaean deformation events. The first (D1) produced regional south-over-north thrusts. The second (D2) produced upright, NNW-trending, gently plunging folds, such as the Kambalda anticline. The third event (D3) generated brittle-ductile, NNW-trending, oblique-sinistral strike-slip fault systems that localized major N-trending, reverse, gold bearing shear zones. During the fourth event (D4), NE-trending, dextral faults offset stratigraphy and earlier fault systems, and caused dextral±reverse reactivation of these earlier faults. Gold mineralization is mainly controlled by the D3 and D4 deformation events.

Alteration petrography

In the St Ives camp, a range of alteration styles can be documented:

1. carbonatization associated with deformation along transcrustal structure (Lefroy);
2. epidote-calcite-magnetite$_1$-pyrite$_1$ (?)-chalcopyrite-quartz alteration of mafic rocks spatially associated with porphyry stocks (contact aureole?);
3. magnetite$_2$ halo around gold-bearing structures;
4. pyrrhotite±pyrite alteration (reduced hydrothermal fluid);
5. distal (to Au) chlorite-carbonate and intermediate (to Au) biotite-carbonate;

6. proximal (to Au) feldspar-carbonate (Fe-rich dolomite to ankerite)-pyrite$_1$-Au±magnetite$_2$±hematite (very oxidized hydrothermal fluid), related to fault zones in micro and macro scale and postdate alteration (2);
7. quartz vein system (+Au?) with pyrite$_2$, documented to overprint alteration (2) and (6).

Epidote alteration could be recognized, at the drill core scale, where epidote-calcite-quartz-magnetite$_1$-pyrit $_1$-chalcopyrite alteration occurs in mafic rocks immediately adjacent (up to several metres) to intermediate porphyry intrusions. Importantly, this style of alteration is unmineralized with respect to gold. Based on macro- and microtextures the relative timing of this style of alteration is (Fig. 1):

1. amphibole;
2. epidote-calcite-magnetite$_1$±pyrite$_1$;
3. carbonate-pyrite$_1$ (?)±quartz veins;
4. quartz vein±chalcopyrite±magnetite$_1$±carbonate.

Feldspar-carbonate-pyrite$_1$ alteration forms part of the gold-associated hydrothermal system. Mafic host-rocks are completely replaced by feldspar-carbonate alteration, which hosts the majority of pyrite$_1$. The latter contains abundant visible gold as well as magnetite$_2$ and hematite inclusions. Quartz veins intruded and partially replace the feldspar alteration which is documented by dissolution textures and quartz pseudomorphs of feldspar. Where quartz veins accessed pre-existing pyrite$_1$, a thin overgrowth of clean pyrite$_2$ formed. However, the majority of quartz veins do not contain pyrite. Based on the macro- and microtextures the relative sequence of this alteration is (Fig. 1):

1. actinolitic hornblende/actinolite;
2. total replacement of wallrock by feldspar-Fe-rich dolomite/ankerite-pyrite$_1$;
3. quartz vein±pyrite$_2$.

Both alteration styles are spatially associated, but appear to be separate events. Consequently fluid inclusions within the two styles are discussed separately.

Fluid inclusion petrography

Within each alteration sequence, primary and pseudosecondary fluid inclusions were examined in different host minerals such as quartz, carbonate, feldspar and epidote. This allows us to reconstruct the fluid(s) evolution through time for each style.

Fluids associated with epidote-magnetite $_1$-carbonate system

In the epidote-calcite-magnetite$_1$-pyrite$_1$ (?)-chalcopyrite-quartz alteration style, fluids evolved from aqueous to aqueous-carbonic (e.g., samples LD7113A/42.3m and LD7113A/42.8m):

1. aqueous inclusion with low salinity in epidote;
2. carbonate veins contain very small, possibly aqueous, fluid inclusions which could not be analyzed;
3. aqueous-carbonic inclusions locally with carbonate (?) and halite daughter minerals.

Fluid inclusions in epidote are primary and do not show any evidence of post-entrapment modifications. Fluid inclusions in the epidote are aqueous without any sign of visible CO_2 and show a small gas bubble (liquid-vapor ratio: 0.9) at room temperature. Eutectic temperatures (T_e) vary between -35.0 to -49.1 ^oC (n=10), suggesting the presence of Ca and/or Mg cations and salinities vary from 0.2 – 7.0 wt% equiv. NaCl. The total homogenization temperature to liquid ($T_{H(l)}$) varies between 219 to 276^oC (average 251^oC, n=16) and the density is about 0.8 g/cm^3.

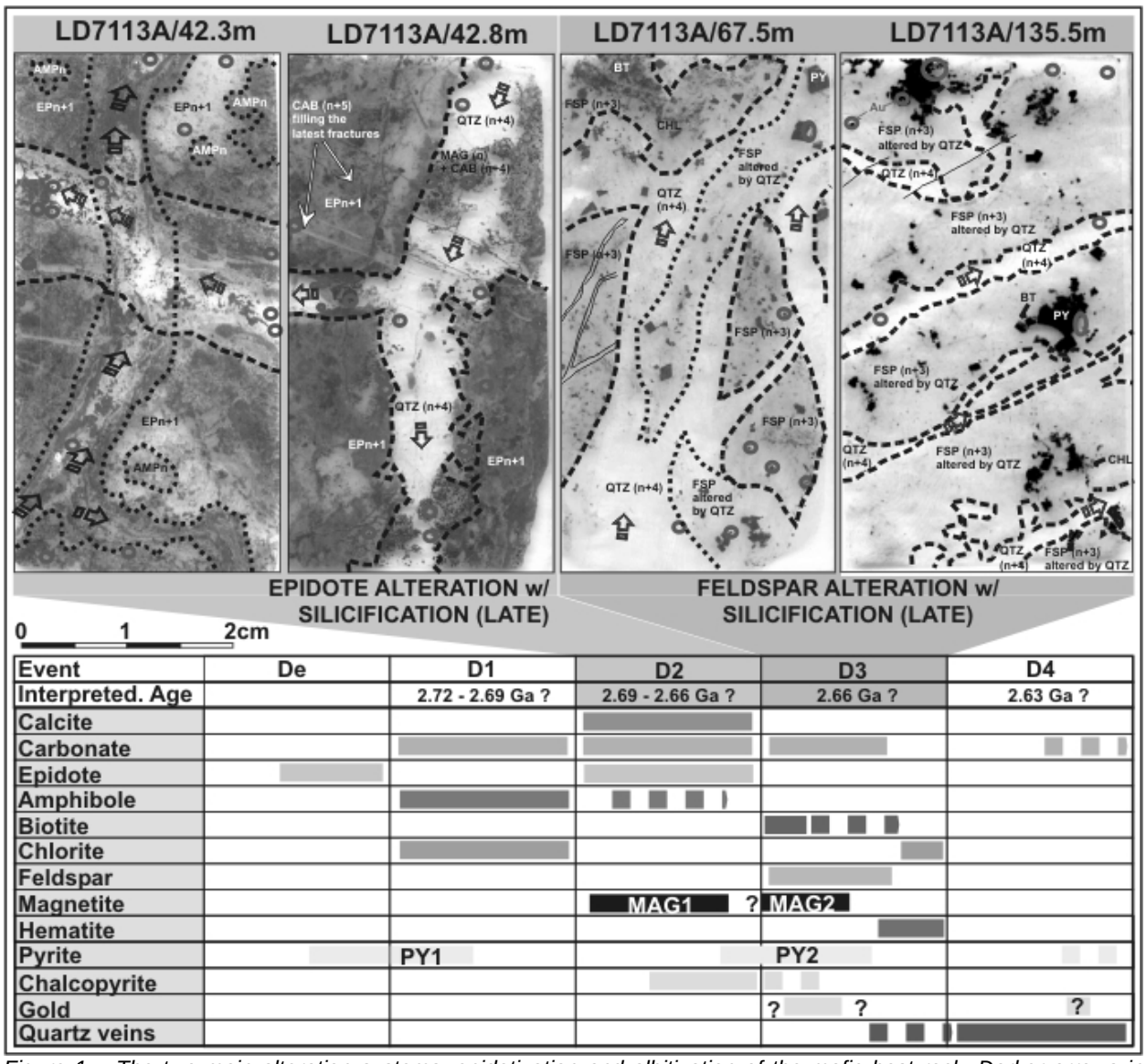

Figure 1 – The two main alteration systems, epidotization and albitization of the mafic host rock. Darker arrows in LD7113A/42.3 show the fluids associated with epidote alteration, grey arrows mark the late quartz fluids. Small circles represent the selected areas for fluid inclusion study. Chart below the pictures shows the relative timing and interpreted absolute timing of hydrothermal alteration systems. Abbreviations: AMP: amphibole, BT: biotite, CAB: carbonate, CHL: clorite, EP: epidote, FSP: feldspar, MAG: magnetite, PY: pyrite, QTZ: quartz.

However, in the quartz vein system that overprints the epidotization, ratios of the aqueous to the carbonic phase are highly variable. Locally, the carbonic phase is missing and the fluid inclusions are aqueous only. Fluid inclusions from the quartz veins contain locally daughter minerals (carbonate and/or halite), variable gas ratios, and Te varies from -31.9 to -52.3 ^{o}C (n=20). If CO_2 is present, Tm_{CO2} from -56.6 to -56.8 (n=2) indicate high purity CO_2. In aqueous fluid inclusions without daughter minerals, salinities vary between 0.99 and 6.67 wt% equiv. NaCl and average densities of 0.7 g/cm^3. The $T_{H(l)}$ vary from 90 to 371 ^{o}C (n=40).

Fluids associated with feldspar-carbonate-pyrite$_1$-gold system

In this alteration style fluid(s) evolved from carbonic (±water) to saline aqueous-carbonic (e.g., samples LD7113A/67.5m and LD7113A/135.5m):

1. carbonic fluid inclusions in feldspar and carbonic with traces of H_2O in carbonate;
2. aqueous-carbonic fluid inclusions with carbonate and halite daughter minerals.

Feldspar contains primary fluid inclusions that seem to be pure CO_2, but due to the small sizes (<5µm), traces of H_2O may be present as indicated by carbonic inclusions with visible traces of H_2O in carbonate. The carbonic fluid inclusions in feldspar do not contain any other gases than

CO_2 with Tm_{CO2} from -56.7 to -56.8 °C (n=11), T_e from -36.4 to -37.4 (n=2), and have an average density of 0.50 g/cm^3. In the associated carbonate, the carbonic-aqueous fluid inclusions show Tm_{CO2} from -56.6 to -57.0 °C (n=20), T_e from -38.4 to -53.5 (n=11), have low salinities of 1.06 wt% equiv. NaCl and an average density of 0.69 g/cm^3. $T_{H(l)}$ vary from 151.2 to 310 °C.

Fluid inclusion in the quartz veins, which overprint the feldspar alteration, show very similar characteristics to the quartz veins that overprint the epidote alteration. If CO_2 is present, Tm_{CO2} varies from -56.6 to -57.0 °C (n=46), T_e from -32.0 to -58.2 (n=45), salinities from 0 to 7.54 wt% equiv. NaCl and average densities of 0.95 g/cm^3. The $T_{H(l)}$ vary from 53.4 to 371 °C (n=50) and if halite is present, they dissolve at temperatures between 139.2 to 286.9 °C (n=8).

Discussion

The key to understanding fluid evolution in complexly overprinted systems is detailed mineral and fluid inclusion petrography. Most importantly, the analysis of fluid inclusions in a range of alteration minerals (e.g., carbonate, epidote, feldspar, quartz) and not only in quartz, as done in traditional fluid inclusion studies, allows reconstruction of the fluid evolution in greater detail.

The fluid evolution in the epidote-dominated alteration assemblage is distinct from that in the feldspar-dominated alteration. The former has an early phase of low salinity aqueous fluids with epidote. The latter has a dominantly carbonic fluid with feldspar and carbonate. Both systems are crosscut by later quartz veins which resulted in brecciation of the feldspar alteration. Fluids in the overprinting quartz veins are similar in both systems with large variations in the aqueous/carbonic ratios, high salinities and local saturation with respect to salt and carbonate. Detailed fluid inclusion analysis at the contact of quartz to feldspar indicates an increasing variation in fluid chemistry, whereas compositions of fluid inclusions from cores of the veins are more homogeneous. The large variation in the fluid chemistry in the quartz vein system can be explained by three mechanisms: 1. phase separation and trapping in situ, 2. mixing of two or more fluids, and 3. contamination of the incoming fluid due to dissolution of pre-existing alteration and metamorphic minerals. At least for the quartz veins in the feldspar alteration type, the third model is preferred, because of increasing variation in fluid inclusion chemical composition proximal to quartz-feldspar contacts and clear textural evidence for feldspar replacement by quartz. This indicates that fluid inclusions at the margins of these quartz veins do not provide reliable compositional data for the incoming fluid. Fluid inclusions in the core of these quartz veins are a better proxy for the fluid initial composition.

We are currently testing whether both overprinting quartz vein systems are part of the same event. Furthermore, detailed laser ICP-MS analyses are planned to determine whether the quartz veins also contain gold mineralization, possibly in thin $pyrite_2$ overgrowths on $pyrite_1$.

Conclusions

Detailed petrographic and fluid inclusion studies of epidote-calcite-quartz-$magnetite_1$-$pyrite_1$-chalcopyrite assemblages and feldspar-carbonate-$pyrite_1$-Au ± $magnetite_2$ ± hematite assemblages in an E-W profile across the Revenge deposits have demonstrated that:

1. the fluid evolution and fluid chemical composition is different in epidote- and feldspar-dominated alteration as also indicated by macro- and micro-textures;
2. the CO_2 dominated system in gold-associated feldspar contrasts with “traditional” H_2O-CO_2-NaCl gold fluids;
3. late quartz vein fluids are similar in both epidote and feldspar alteration styles;
4. modification of initial fluid compositions in fluid inclusions at the margins of quartz veins are likely modified due to feldspar dissolution.

The similarity of fluid inclusion types at the quartz stage in the Revenge section with some of the fluid inclusion types in the quartz stage(s) in the Junction deposit hint to the possibility of correlating specific fluid-flow events across the St Ives Camp.

Application of template-based generic numerical modelling to exploration at all scales

Warren Potma, Peter Schaubs and Thomas Poulet

*pmd*CRC, CSIRO Exploration and Mining, PO Box 1130, Bentley, WA 6102*

warren.potma@csiro.au

Introduction

Template-based generic numerical modelling provides a powerful tool for exploring the influence of geometric variability on modelling scenario results in the short time-frames required by exploration schedules.

Historically, model geometries have either been constructed manually or derived from complex adaptations of 3D geological wire frames. Both of these processes are time consuming with up to 1-2 weeks required to generate some numerical meshes. Manually created meshes tend to consist of planar surfaces or only simple curves, and wire frame derived meshes, while significantly more complex, are very time consuming to create. In both cases the meshes, once created, are very difficult to edit, precluding any systematic exploration of the portion of parameter space which relates to the geometry of the geological model.

By describing all surfaces within the 3D models using mathematical equations, we are now able to generate multi-variant 3D model geometries (and the corresponding meshes) based on descriptive geological nomenclature, in minutes rather than days. Fault and/or lithology strike, dip and curvature (both along strike and down dip) can be described mathematically and the resultant complex curved surface intersections can be calculated and used as the basis for the construction of detailed numerical modelling meshes.

This functionality allows for systematic exploration of geometric parameter space in “generic” geometry scenarios where the orientation, asymmetry, thickness or surface intersection characteristics of a model are thought to impact on ore forming processes.

This template-based generic numerical process can be applied at all scales and phases of the exploration process from simple fault intersection models in greenfields exploration projects to plane of the vein grade distribution modelling of lodes in a mining environment. Template-based generic modelling of up to 30 variants of a base geometric scenario can be completed in as little as two weeks, and fed immediately back into the exploration process. This is a similar turn-around time to exploration sample assays.

At this stage the application of these templates has been limited to 2D and 3D deformation and fluid flow modelling such as the examples described below.

Examples

Greenfields-Brownfields fault intersection models: Eastern Goldfields Kundana Example

Placer Dome is currently actively exploring its Kundana tenements. Targeting within the mineralised trend is predominantly driven by a mineralization model based on empirical observations related to fault intersection architecture, backed up by pathfinder geochemical analysis.

While the correlation between mineralization and the two intersecting fault sets (D2 and D4) is clear, not all intersections contain economic mineralization. The challenge is to understand what controls economic grade mineralization in the system using numerical modelling, and then apply this knowledge to ranking the remaining unexplored targets within the belt.

Here we explore the impact of varying fault intersection geometries (strike and dip), far-field stresses, juxtaposition of key lithologies and thickness changes in those lithologies in order to understand the geometric, deformation and fluid flow parameters which control the focusing of ore-bearing fluids.

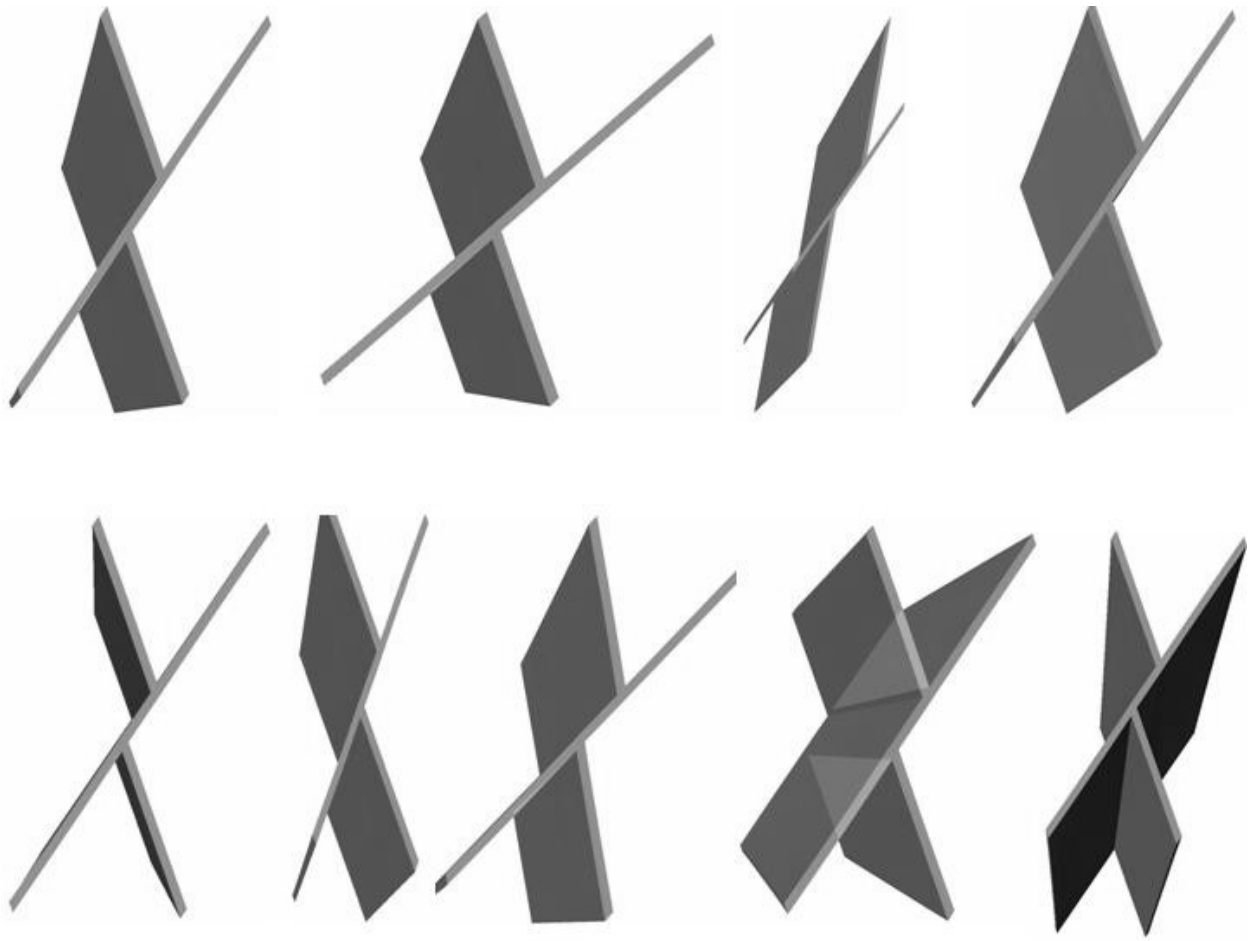

Figure 1. A representative range of the fault geometries used in the initial phase of generic modelling of the Kundana Camp.

Brownfields Curved Fault Models: Kanowna Belle Example

The Kanowna Belle (KB) deposit is located on the apex of a folded D1 thrust near its intersection with the Kanowna Shear Zone. We explore the use of generic modelling template which allows for fault curvature of varying wavelengths and amplitudes and varied far-field stress orientations. Generic 3D deformation and fluid flow modelling of the Kanowna Belle geometry produced significant dilation and fluid focusing within the model at the location the deposit. It also indicated that the orientation of σ_1 with respect to the fault curvature had a significant impact on dilation in the vicinity of the ore body. A series of models were run with a much tighter and more asymmetric curvature of the D1 structure. These resulted in a much smaller volume of rock affected by dilation, although the maximum intensity of dilation was similar in both models.

A similar structural setting exists in another prospect to the north of KB, however, this prospect contains a large body of porphyry in the footwall to the D1 structure (which is not present at KB). This lithological competency contrast was also modelled in the context of the models described above. In all cases, the presence of the competent body in the footwall of the D1 structure magnified the dilation in the hanging-wall of the structure. This competency contrast also triggered significant dilation west of the Kanowna Shear Zone (an area not previously considered a high priority target).

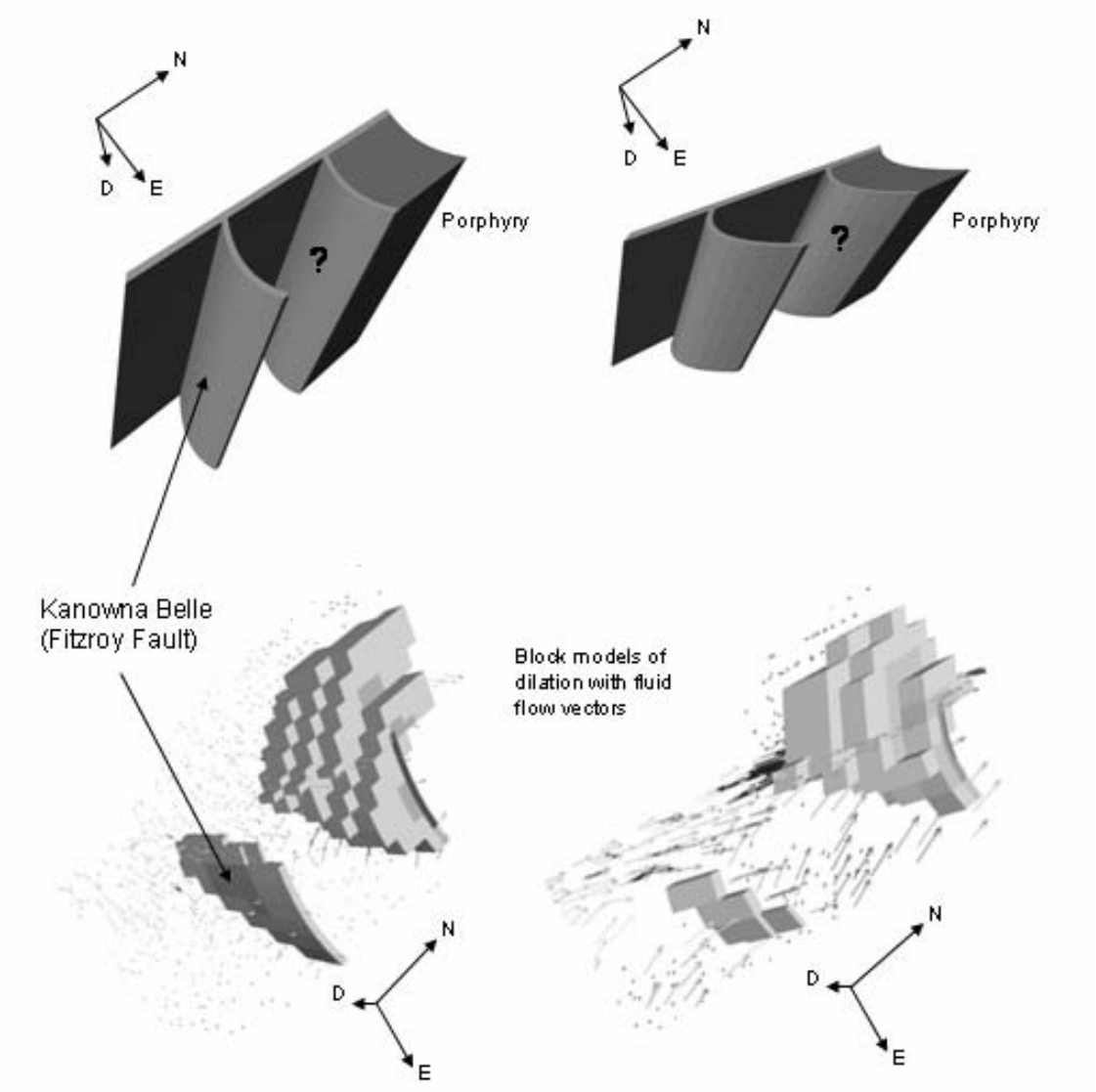

Figure 2. Kanowna Belle curved F1 fault generic models: Two models illustrating how varying fault curvature and footwall rheology can impact on dilation within the system.

Plane of the Vein Grade Distribution Modelling: Wallaby Example

Preliminary models of a generic ramp-flat geometry (presented at the pmd*CRC review in November 2003) indicate that in undulating shallow ore-bearing structures it is not simply the flats within the structure that are the focus for dilation. The Models indicate that the main focus for dilation are the points and/or lines of inflection within the surface where the dip and/or strike of the surface changes. The concave side of the inflection is most prone to dilation and the foot-wall generally has greater magnitudes of dilation than the hanging-wall. Dilation along these lines of inflection tends to produce plunging shoots of higher dilation which is a reasonable explanation for high grade shoots within the plane of the vein/structure. Thus it may be possible to predict (in structurally controlled lode systems) the preferred orientation (and perhaps even the location) of high grade/tonnage shoots within the main mineralised structures.

Recent work by Susan Drieberg (pers. comm.) on the Wallaby orebodies has indicated that this relationship is observed within the Wallaby flat lodes, where both the maximum grade and grade-thickness values are influenced by inflections in the mineralised structure.

Acknowledgements

Thanks to Placer Dome Asia Pacific Exploration & Mining teams for access to data and personnel during the course of these projects. The Kundana example is the result of a co-funded one-on-one numerical modelling project with Placer Dome.

Science and modelling at all scales

Klaus Regenauer-Lieb, Alison Ord, Yanhua Zhang, Heather Sheldon and Chris Wijns

*pmd*CRC, CSIRO Exploration and Mining, PO Box 1130, Bentley, WA 6102*

klaus.regenauer-lieb@csiro.au

Introduction

A good metaphor for the science of modelling at all scales is a Russian nesting doll figuring a portly mother of a big family stackable up to a variable level < 30, commonly known as the "Babushka" (grandmother), probably an aberration of "Matryoshka" (from the Latin "mater").

Figure 1. Crossing the scales from brittle microprocesses to planetary-scale convection. The red lines delineate boundaries where new constitutive laws emerge out of spatial averaging of discontinuous processes. Inspired by Kubin's (2003) unpublished manuscript on electronic to crystal scale processes, which, of course, incorporates a smaller series of Babushkas with its scale dependent physics and mechanical transitions.

While the physics of multi-scaling is reasonably well understood from dislocation to crystallographic level (Moriarty et al., 2002), and for isolated cracks (Abraham et al., 2000), there is a dearth of information crossing the scales from multiple interacting cracks through to the dynamics of fault groups, from the behaviour of plate boundaries to styles of planetary convection. Therefore, up to now, it is common practice to model geological processes by useful phenomenological approaches such as the Coulomb failure criterion, or rate and state variable friction. While this simplification enables a quantitative description of tectonics, the main shortcoming is, perhaps, that it does not lend itself to (or is difficult to implement in) a unified approach coupling chemistry and mechanics. Another criticism is that the phenomenological approach is blind to the scale transitions marked in Figure 1, i.e., it essentially relies on an uncritical extrapolation of laboratory laws to plate tectonic behaviour.

Yet numerical models at local scale need (and are severely influenced by) far field boundary conditions. In the sections to come we briefly describe how we implement a thermodynamic description of the chemical-fluid-mechanical problems. We begin by deriving a self-consistent energy based framework for mechanical porosity by discrete modelling of microcracks. We derive smeared volumes of microcracks to be used at geological terrane scale. Here, we show how scale variant modelling can be simplified at pre-set scales.

Multiscale-modelling Framework

At the brittle level, we begin with the smallest scale (micron-decimetre scale), and start by compiling results of dilatant rock mechanics laboratory experiments for basic rock types, and reproduce these “ab initio” by particle code (micron - meter scale) (PFC2/3D) calculations. The particle code solves the Helmholtz free energy evolution in a direct way (see Appendix), tracking the local cracking and its self-organization into a shear band. It is subsequently scaled up beyond classical laboratory scale to mining scale observation. At this scale, the discreteness of the individual crack is lost, and crack populations are handed over into their smeared continuum calculations. The smeared continuum calculations are done with classical finite element (FE) methods tracking the Helmholtz free energy fluxes from hundreds of meters - 100 km scale. This part of the project is done in cooperation with Vladimir Lyakhovsky at the University of Jerusalem and is illustrated in Figure 2.

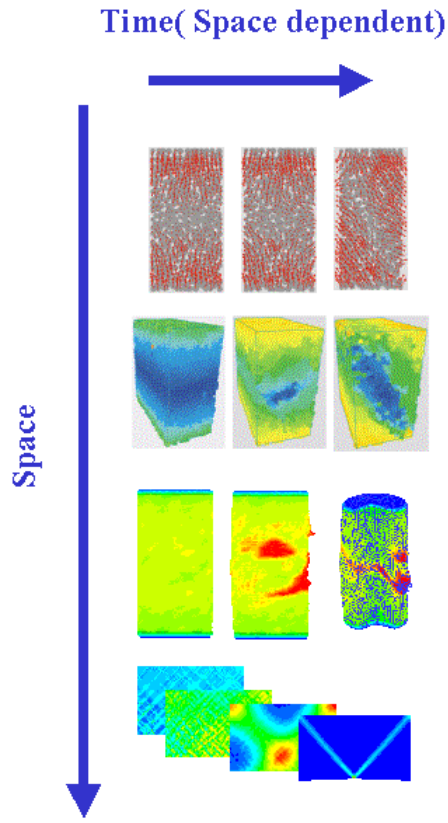

Figure 2 *Top panel: displacement vectors of a particle code simulation of an evolving shear band in a virtual biaxial rock experiment calibrated by a laboratory experiment (see Ord et al., this volume, Fig. 1 and 2, on Gosford sandstone,* ***Time < 1 hour, Space < 1 m****). Second panel: magnitude of displacement vectors of the same particle code calculation as a spatial average of damage (****Time < 1 hour, Space < 1 m****). Third panel: finite element (FE) damage mechanics calculation of a triaxial rock experiment based on Helmholtz free energy evolution, by V. Lyakhovsky (University of Jerusalem). The dilatancy pattern (damage) mimics the crack evolution of the discrete particle code simulation in a smeared continuum. The FE approach can be applied to the brittle crust scale, while the particle code calculation will be useful to verify the upscaling from laboratory to geological scale. The method is useful for modelling self-consistent dilatancy on shear bands in the brittle part of the lithosphere (****Time < 1 day, Space < 10 km)****. Bottom panel: lithosphere-scale, ductile faulting controls the large-scale tectonics. The dissipation contours of lithosphere-scale ductile damage evolving by self-organization of interacting small-scale ductile faults. The birth of this new plate boundary takes less than 100 k years and only occurs if there is an elevated flux of water into the lithosphere. In this calculation, the feedback with the brittle crust has been ignored (****Time < 1 Ma , Space < 100 km****).*

At the lithosphere to mantle scale (100 km – 1000 km), fully coupled solid-fluid interaction of lithosphere and mantle is implemented by embedding the FE domain into a boundary element domain for the larger scales. In the future, this model will be coupled to the particle code, thereby obtaining a self-consistent multi-scale geological modeling framework where the different spatial solution routines can in principle be called, based on critical local dissipation. In a first step, we will use a simplified approach and formulate a specific region of interest based on a particle code simulation. We will embed this region within a coupled FEM-BEM method, thus supplying the full feedback between large-scale geodynamic boundary conditions and processes in the local regions of interest.

Simplified Modelling at Preset Scales

Prior to the completion of this software framework, we can use the first results in intermediate solutions and show how modelling can be simplified at preset scales for the purpose of hypothesis testing. The multi-scale framework is useful to add rigour to simplified approaches by exploring the limits of these approaches. If we consider, for example, the crustal scale, we can feed the results from multi-scale modelling back into a simplified phenomenological description. We devise a rheology that satisfies aspects of fault nucleation and weakening. Such a rheology has recently been used to model the genesis of metamorphic core complexes, and is also reproduced in the fully self-consistent energy approach, allowing faulting and core complex exposure to occur through thermodynamic feedback (Wijns et al., work in progress). The fully self-consistent, numerically more expensive simulation is in good agreement with the simplified laws, i.e., it reproduces the same geometric features. The complete approach therefore provides a better base for the simplifying assumptions used. In another example for modelling the Carlin gold trend in northern Nevada, U.S.A. (Wijns et al., this volume), we show how this simplified rheology can be used to test folding/thrusting hypotheses at a local scale. Similarly, at the yet smaller upper crustal scale, we use a simplified reactive transport equation as a proxy for the transfer, dissolution, and precipitation of silica (Sheldon and Ord, this volume). Another simplified approach is presented for the reactive transport modelling of the Mount Isa Copper mineralized system (Kühn et al., this volume).

Discussion and the Future

Understanding and explaining emergent constitutive laws in the multi-scale evolution from grain size to plate tectonic scales is making steady progress. Owing to increasing computer power, there have been significant breakthroughs in large-scale geodynamic modelling, which are still awaiting implementation to constrain regional geological modelling. For instance, large-scale convection models have significantly improved to the point of reproducing basic modes of planetary tectonics as self-consistent features of the same physical planetary heat transfer problem (Moresi and Solomatov, 1998; Mulhaus and Regenauer-Lieb, 2004; Stein et al., 2004). The Earth appears to be the only planet known to have developed stable plate tectonics as a means to get rid of its heat. The emergence of plate tectonics out of mantle convection relies intrinsically on the capacity to form extremely weak faults in the top 100 km of the planet, which, in turn, can be related to the critical quantity of water available for thermodynamic rheological feedback mechanisms (Regenauer-Lieb et al., 2004). This explains cycles of co-located resurgence of plate generation and consumption, but also allows a new perspective of lithosphere-scale faults, which in the future shall be used to constrain terrane scale models of massive transfer of mantle volatiles, including reactive transport modelling with upper crustal fluids.

Appendix: A Common Thermodynamic Framework for Chemistry and Mechanics

We summarize the four basic thermodynamic potentials and their interrelation Schroeder, 2000. The thermodynamic potentials are useful in the chemical thermodynamics of reactions and non-cyclic processes, as well as in mechanical modelling. They are the internal energy, the enthalpy, the Helmholtz free energy, and the Gibbs free energy. The four thermodynamic potentials are

related by offsets of the "energy from the environment" term TS (S being the entropy, a state variable defining the amount of “disorder” of the system, see second law of thermodynamics) and the "expansion work" term PV. A mnemonic diagram suggested by Schroeder 2000 can help keep track of the relationships between the four thermodynamic potentials and their state variables: S, temperature T, pressure P, and volume V.

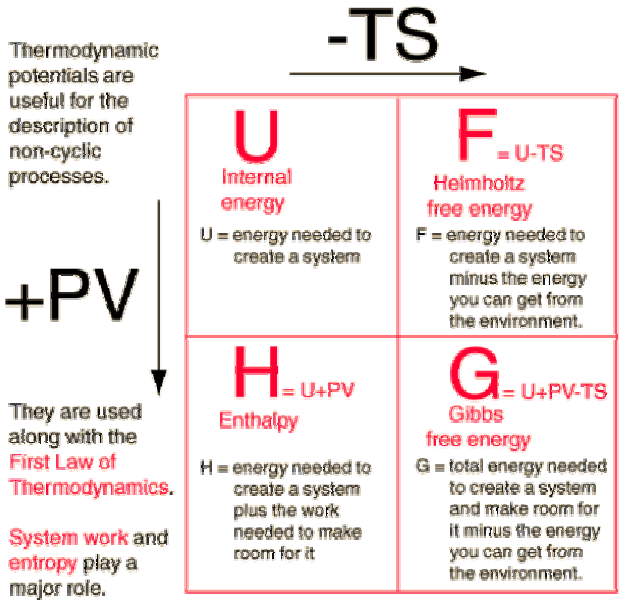

Figure 3. *Schroeder’s mnemonic thermodynamic diagram can be found as an active graphic on http://hyperphysics.phy-astr.gsu.edu/hbase/thermo/thepot.html .*

In reactive transport, we minimize Gibbs free energy (for example, HCh or Perplex software), and in mechanical modelling, we describe the fluxes of Helmholtz free energy. Both are related through a transformation (the PV term). The trend in future modelling will go towards predicting mechanical and thermal properties of materials from thermodynamics. A common framework is already available for water (Wagner and Pruss, 2002). It has been implemented for upper crustal convection (Hornby et al., work in progress).

References:

Abraham, F.F., Bernstein, N., Broughton, J.Q. and Hess, D., 2000. Dynamic fracture of silicon: Concurrent simulation of quantum electrons, classical atoms, and the continuum solid. Materials Research Society Bulletin, 25 (5), 27-32.

Kühn, M., Alt-Epping, P., Gessner, K. and Wilde, A. 2004. Application of reactive transport modelling to the Mount Isa Copper mineralised system. This volume.

Moresi, L. and Solomatov, V., 1998. Mantle convection with a brittle lithosphere: thoughts on the global tectonic styles of the Earth and Venus. Geophysical Journal International, 133 (3), 669-682.

Moriarty, J.A., Vitek, V., Bulatov, V.V. and Yip, S., 2002. Atomistic simulations of dislocations and defects. Journal of Computer-Aided Materials Design, 9 (2), 99-132.

Mulhaus, H. and Regenauer-Lieb, K., 2004. Non Newtonian Effects in Simple Shear and Natural Visco-elastic Convection. Physics of Earth and Planetary Interiors, in preparation.

Regenauer-Lieb, K., Hobbs, B., Mulhaus, H., Ord, A., Yuen, D.A. and van der Lee, S., 2004. Lithosphere Fault Zones Rejuvenated. Tectonophysics.

Schroeder, D.V., 2000. An Introduction to Thermal Physics, Addison Wesley, New York.

Sheldon, H.A. and Ord, A., 2004. Coupled processes in faulted environments. This volume.

Stein, C.A., Schmalzl, J. and Hansen, U., 2004. The effect of rheological parameters on plate behaviour in a self-consistent model of mantle convection. Physics of the Earth and Planetary Interiors, in press.

Wagner, W. and Pruss, A., 2002. The IAPWS formulation 1995 for the thermodynamic properties of ordinary water substance for general and scientific use. Journal of Physical and Chemical Reference Data, 31 (2), 387-535.

Wijns, C., Hall, G. and Groves, D. 2004. Compressional tectonics of the Carlin Gold Trend. This volume.

Tectonothermal evolution, metasomatism and mineralisation, Eastern Fold Belt, Mt Isa Inlier

Mike Rubenach and Mohammad Sayab

*pmd*CRC, School of Earth Sciences, James Cook University, Townsville, QLD 4811*
michael.rubenach@jcu.edu.au

Evolution of the Snake Creek Anticline

The Snake Creek Anticline, although poorly mineralised, is a key area in understanding the tectonothermal and metasomatic evolution of the Eastern Fold Belt. A SHRIMP zircon age of 1686Ma for a tonalite, which shows mixing relationships with dolerite and gabbro, indicates that the Llewellyn Creek Formation which they intrude is older than other units of the Soldiers Cap Group (1654-1677 Ma; Page and Sun, 1998). The first major orogenic episode (O_{NS}) following deposition of the Soldiers Cap Group produced a number of events, including D_1 (E-W folds with shallowly dipping axial plane foliation) and D_2 (steep EW folds and foliations) of Rubenach and Lewthwaite (2002). This was followed by E-W compression (O_{EW}) that produced at least two steep events (D_3, D_5) and a shallowly-dipping event, D_4 (Rubenach and Lewthwaite, 2002). The peak of metamorphism occurred late D_3 (D_2 of previous authors) or syn-D_4, around 1595 Ma.

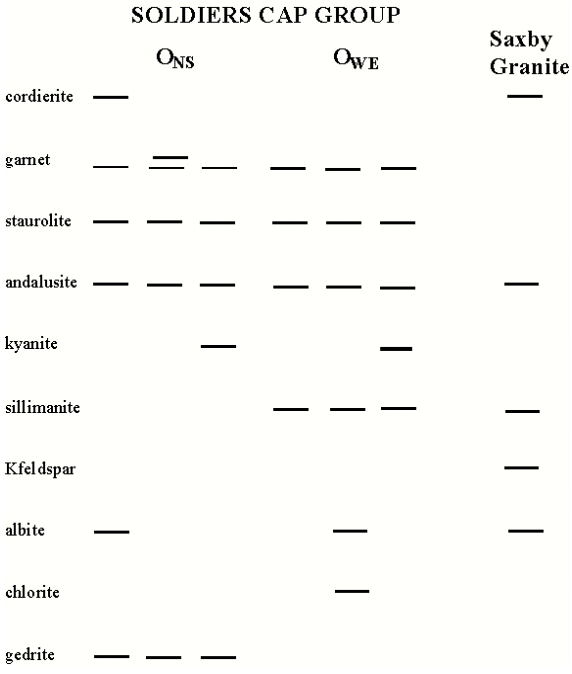

Figure 1. Timing of growth, Soldiers Cap Group, Snake Creek Anticline.

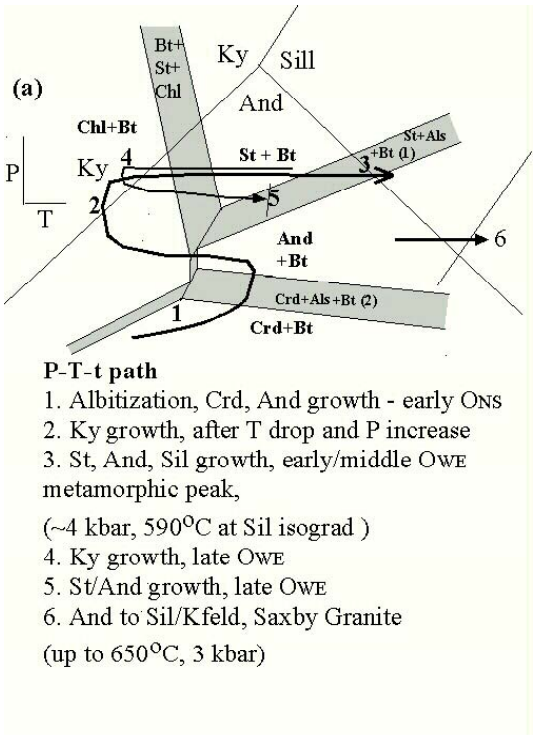

Figure 2. P-T-t path, Snake Creek Anticline.

The timing of metamorphic and metasomatic minerals is summarized in Figure 1, while Figure 2 is a revised version of the P-T-t path for the Soldiers Cap Group, Snake Creek Anticline. A significant change from earlier work (e.g., Rubenach and Lewthwaite, 2002) concerns the timing of the main albitisation event in the Soldiers Cap Group as syn-D_1, not syn-D_3. Critical observations included finding albitites parallel to the axial planes of F1 folds, and albite inclusions in early cordierite and andalusite. The extensive albitisation at the Osborne Mine is

also prior to the metamorphic peak, probably also syn-D_1. Significant enrichment of chlorine in biotite is probably associated with albitisation, but the precise relationship is complex (Rubenach, in press).

To the west of the Snake Creek Anticline the stratigraphically older Corella beds have been juxtaposed against the Soldiers Cap Group by the Cloncurry Fault. The fault is probably an early structure, but lower metamorphic grades in the Corella beds indicate late additional movement on the fault subsequent to the metamorphic peak. Numerous intrusions of felsic granite (generally albitised) and dolerites occurred along the fault, and significant brecciation and Na-Ca alteration occurred synchronously with the intrusions (probably late in the history, around 1520-30 Ma). Figure 3 summarizes the peak assemblages and later metasomatic assemblages in the Corella beds.

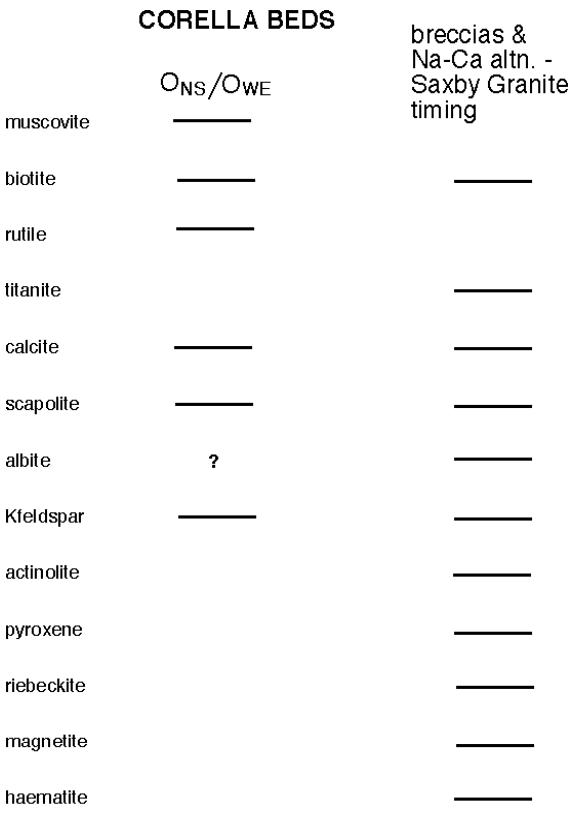

Figure 3. Timing of metamorphic and metasomatic phases, Corella beds adjacent to Cloncurry Fault, Snake Creek Anticline.

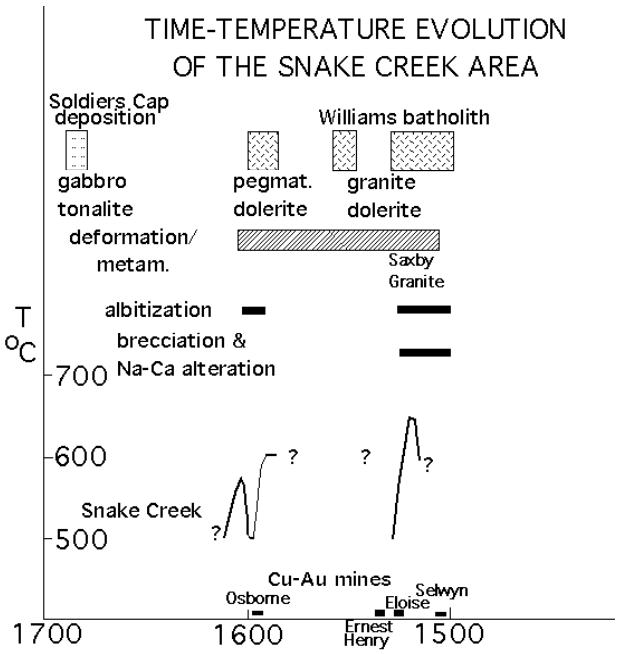

Figure 4. Evolution of the Eastern Fold Belt, with particular reference to the Snake Creek Anticline.

Cu-Au mineralisation in relation to the metasomatic evolution

Figure 4 summarizes the magmatic, thermal, metasomatic and mineralisation history of the Eastern Fold-Belt. Although most of the Cu-Au deposits overlap with the emplacement of the Williams/Naraku batholiths and related brecciation and Na-Ca alteration, Osborne is a significant exception. The extensive albitisation, biotite alteration and localized Na-Ca alteration at Osborne are prior to the metamorphic peak, and are not obviously related to igneous intrusions.

Acknowledgements

The following are gratefully acknowledged: Nick Oliver, Tim Bell, Tom Blenkinsop and Kris Butera. The dating of the tonalite was done in collaboration with Mark Fanning.

References

Page, R.W. and Sun, S-s.1998. Aspects of geochronology and crustal evolution in the Eastern Fold Belt, Mount Isa Inlier. Australian Journal of Earth Science 45, 343-361.

Rubenach, M.J. and Lewthwaite, K., 2002. Metasomatic albitites and related biotite-rich schists from a low-pressure polymetamorphic terrane, Snake Creek Anticline, Mount Isa Inlier, north-eastern Australia: microstructures and P-T-d paths. Journal of Metamorphic Geology, 20, 191-202.

Rubenach, M. J. Inclusion trails in andalusite and the relative timing of albitization and chlorine enrichment in biotite, Snake Creek Anticline, north-eastern Australia. Canadian Mineralogist, in press.

^{187}Re - ^{188}Os isotopes in metallogenesis: an overview

Bruce F. Schaefer

*pmd*CRC, School of Geosciences, Monash University, VIC 3800*
BSchaefer@earth.monash.edu.au

Introduction

Advances in Negative Thermal Ionisation Mass Spectrometry (N-TIMS) over the past decade have allowed the application of the Re-Os isotopic system to many geological problems which were previously not amenable to radiogenic isotopic analysis. Central amongst these have been the investigation of sulphide bearing systems due to the highly siderophile and chalcophile nature of Re and Os, and also to highly reducing situations, such as organic rich sediments, due to complex redox chemistry of Re and Os and their "organophilic" nature.

Such a combination of chemically favorable attributes has led to immediate insights into the genesis of mineralized systems and the generation of geochronological information from phases which were not amenable to lithophile isotope investigation. However, experience has illustrated that whilst the Re-Os isotopic system is a powerful tool for investigating mineralized systems, it is not a universal panacea for sulphide geochronology and metallogenesis. This contribution aims to summarise the state of play of Os isotope geochemistry with respect to mineralized systems, and highlight some of the applications and limitations of the system with existing technology levels.

The Re-Os isotopic system

^{187}Re decays to product ^{187}Os with a decay constant of 1.666×10^{-11} a^{-1}, which corresponds to a half life of ~42 Gyr. Such a slow rate of decay in the comparatively rare elements (typical abundances in the silicate earth of less than 1 part per billion) would severely limit the applications of this isotopic system within the earth sciences except for one feature: Re is comparatively incompatible with respect to Os, allowing for significant fractionation of parent from daughter. Such chemical fractionation allows for a substantial range in ^{187}Os/^{188}Os isotopic ratios within the earth, and particularly between silicate and sulphide materials.

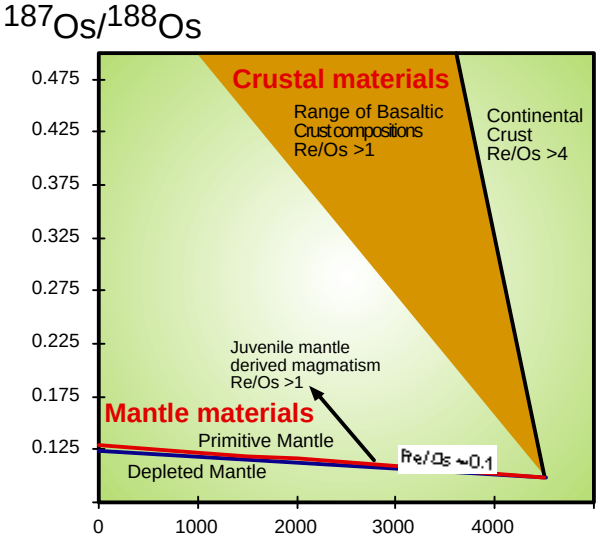

Figure 1: ^{187}Os/^{188}Os isotopic signatures of major geochemical reservoirs on the silicate earth since the formation of the Earth. Partial melts and crustal materials have high Re/Os and hence very rapidly develop radiogenic ^{187}Os/^{188}Os.

Because Re is *relatively* incompatible with respect to Os (both elements are highly compatible in silicate melting situations however), Re is enriched in the crust (typically occurring at concentrations of ~50 ppt (parts per trillion, or pgg^{-1}) compared to Os which is typically <5 ppt in crustal materials. Therefore, crustal materials have highly radiogenic ^{187}Os/^{188}Os isotopic signatures, with values >1 and typically greater than 4 (Figure 1). In contrast, mantle materials such as MORB, OIB and the SCLM have ^{187}Os/^{188}Os ratios which are close to or below chondritic (i.e., <0.13). Such a

fundamental dichotomy in radiogenic isotope signatures (i.e., greater than an order of magnitude) in the key terrestrial reservoirs offers a means to track the source of Highly Siderophile Elements (HSE) within geological materials. Such extreme parent-daughter fractionation is uncommon in the commonly applied lithophile radiogenic isotope systems.

Os isotopes as a geochronometer

Os isotopes can be applied to geochronology in three basic ways: 1) Direct dating of molybdenite, 2) Whole rock isochron geochronology of appropriate lithologies such as basalts or organic rich sediments, and 3) mineral isochrons of cogenetic sulphide phases.

Os in molybdenite

Molybdenite (MoS_2) preferentially incorporates Re into its mineral lattice, and typically contains > 1 ppm levels of Re. In contrast, it incorporates virtually no Os upon crystallizing, meaning that effectively all Os measured in a sample is radiogenic ^{187}Os formed by in situ decay of ^{187}Re. Since molybdenites typically contain ratios of $Re/^{192}Os$ (ie, rhenium to common Os) > 10^6, the age of the sample can be calculated directly from measurement of ^{187}Os, assuming that it is all derived from *in situ* decay. This effectively represents a modified form of the decay equation, such that $^{187}Os = {}^{187}Re\ (e^{\lambda t}-1)$, where both ^{187}Os and ^{187}Re can be measured directly via ID-NTIMS. The greatest source of error in closed systems investigated by this approach is that introduced by uncertainty in the decay constant (λ), which is of the order of 0.3%, and of the calibration of the spike solutions used to conduct the isotope dilution (ID) analysis. Continuing advances in calibration of gravimetric standards and repeat analyses at increasing precisions have reduced the source of this error to substantially below that introduced by uncertainty introduced by the decay constant, limiting the precision on the molybdenite chronometer to that of the decay constant, or ~0.3%.

However, successful radiogenic geochronology requires that the isotopic system has remained closed, with neither parent nor daughter entering or leaving the system through alteration, metamorphism, metasomatism or any other open system behaviour. Additionally, the grain size of molybdenite exerts a major control over the distribution of Re. Small grain sizes tend to have homogeneous Re (and hence radiogenic Os) distributions, whereas coarse grains often exhibit heterogeneous Re distribution and diffusive Re (and Os) loss from grain margins. Therefore, reproducible molybdenite analyses require careful sample homogenization and removal of crystal edges, through either abrasion or physical removal. Such within grain heterogeneity is the source of scatter commonly observed by *in situ* microbeam molybdenite analysis, such as laser ICP-MS studies. Duplicate dissolution analyses on decreasing volumes of well-characterised fine-grained molybdenites suggest that even in well-homogenised samples that Re and ^{187}Os decoupling takes place on sample volume of <~50mg, suggesting a critical sampling scale necessary to produce geologically meaningful and analytically reproducible results (eg, Stein et al., 2001). Whilst direct model ages are commonly calculated for molybdenites, a more robust approach is to plot multiple cogenetic molybdenite analyses on a modified isochron diagram, whereby a number of duplicate analyses define a linear array passing through the origin with a slope directly proportional to the age of the sample. Such an approach provides an inbuilt check for closed system behaviour, as significant disturbance will produce arrays that do not pass through the origin of the plot. However, while a useful geochronometer, the molybdenite system contains no information pertaining to the source of PGE and hence has no application in tracking metal paragenesis.

Whole rock isochrons

In addition to mineral specific applications, such as molybenite, the Re-Os chronometer can be applied to generate whole rock isochrons in a manner analogous to Rb-Sr or Sm-Nd. While Re and Os are present in very low concentrations in the vast majority of crustal materials, they do preserve a wide range in Re/Os (and hence spread on the x-axis of an isotope plot) on the

whole rock scale for samples within close physical proximity. Two types of material are commonly investigated using this approach; mafic magmatic products (particularly cumulates) and highly reducing organic rich sediments (Figure 2). Both systems typically contain appreciable levels of Re and Os (>100 ppt), and whereas mafic magmatic rocks preserve the $^{187}Os/^{188}Os$ initial isotopic ratio of the parental magma, organic rich sediments preserve the $^{187}Os/^{188}Os$ isotopic ratio of the water column that the sediments were deposited in. This latter situation is appropriate for situations where there is no appreciable detrital Re or Os, and the bulk (>95%) of the PGE budget is scavenged and concentrated from the water column and hence is hydrogenous in origin.

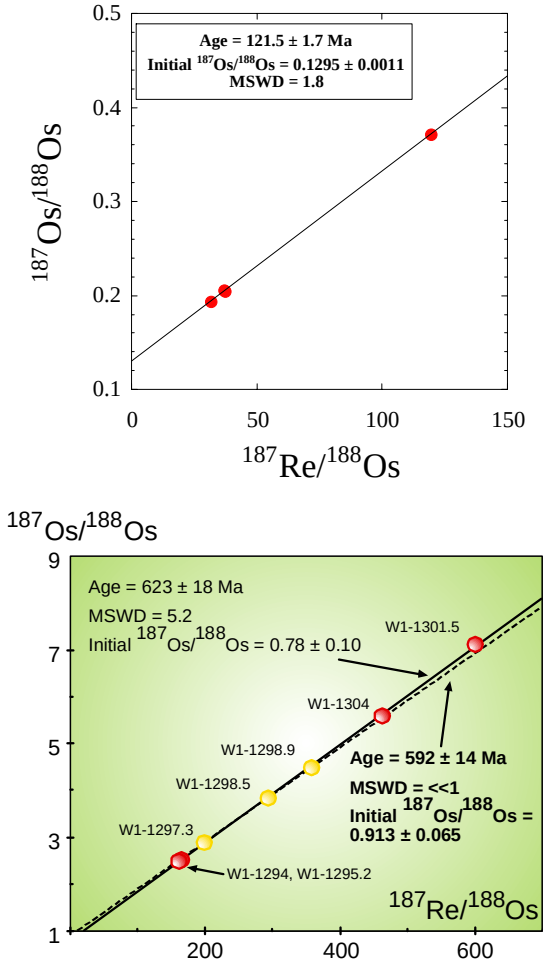

Figure 2: Re-Os whole rock isochron diagrams. TOP: Four point isochron for picrites from the Ontong Java Plateau. BOTTOM: Isochrons for organic rich sediments from the Amadeus Basin, central Australia. Data from Parkinson et al. (2004) and Schaefer and Burgess (2003) respectively.

Such an approach not only yields potentially high resolution geochronological data, but the initial ratio of such systems is a powerful piece of information in elucidating the source of PGE. Unradiogenic initial ratios (i.e., $^{187}Os/^{188}Os$ < ~0.130) are generally indicative of mantle input, whereas radiogenic $^{187}Os/^{188}Os$ values (i.e., > 0.5) suggest interactions with or input from continental crustal materials (e.g., Schaefer et al., 2000). This is of immense use not only in unraveling the paragenesis of basaltic systems in constraining the amount of potential crustal assimilation, but also in sedimentary systems for tracking whether the oceanic water column is dominated by metal input from mid ocean ridge magmatism, or by dissolution from continental runoff.

The ultimate source of metals in mineralized systems is central to assessing the prospectivity of a given terrain. Increasingly, it is becoming clear that large scale mineralized systems generally require mantle input, either as a source of heat, or of metals, or both (see Keays et al., this volume). Thus, the isochron approach offers a level of information beyond basic geochronology.

Mineral isochrons of cogenetic sulphides

A variant on the whole rock approach outlined above has been to extract cogenetic sulphides (and more rarely, oxides such as magnetite) from mineralized systems in an attempt to directly date the age of mineralization. This approach has many advantages, not least that Re and Os are both highly chalcophile, however it is also subject to critical limitations. These can be summarized as: 1) accurately knowing whether different mineral phases are truly cogenetic within the mineralized systems, 2) avoiding potential overprinting or resetting in highly complex systems, 3) dramatic variations in Re and Os concentrations within certain minerals due to their varying modal abundance within a given ore deposit, and 4) being able to demonstrate closed system behaviour for Re and Os during the varying redox conditions commonly associated with mineralization.

Each of these issues is becoming less significant as increasing data become available for different situations, allowing sampling and sample preparation strategies to take this into account.

Indeed, one of the outstanding issues is still that whereby the presence of sulphides does not necessarily correspond to appreciable levels of Re and Os- on the contrary, large volumes of sulphide mineralization often distribute a limited budget of PGE amongst a large volume, resulting in analytical difficulties due to low levels of Re and Os in mineral separates. However, despite these caveats, significant advances have been made in routine solution analysis of common sulphide phases such as pyrite, arsenopyrite, pyrrhotite and to a lesser extent pentlandite and galena.

One advantage of sulphide mineral isochron geochronology is that in situations where it is appropriate to be used and applied effectively, the initial isotopic ratio reflects the source of the PGEs within the mineralized system. Further discussion regarding this aspect can be found in Keays et al. (2004). Hence it is possible to place first order constraints on the mass balance necessary to produce the mineralised system in question. Therefore, initial ratio tracing of sulphides offer the potential to act as a first pass filter on the relative prospectivity of a given terrain.

Acknowledgements

This contribution constitutes a distillation of many people's efforts over a number of years, and I am particularly grateful to the group at the Open University who first introduced me to the intricacies of Re-Os. Ian Parkinson and Anthony Cohen have been particularly good sounding boards, as has Reid Keays since my return to Australia.

References

Keays, R., Gregory, M., Murphy, T., Wilde, A., and Schaefer, B., 2004 Insights into the Age and Genesis of Mt Isa Cu-Pb-Zn sulfide ores from Re-Os Isotopes, this volume, 2004.

Parkinson, I.J., Schaefer, B.F. and Arculus, R.J., 2004. A high precision Os isotope isochron from OJP: A lower mantle origin for the world's biggest LIP?. Geological Society of Australia, Abstracts, 73, 282.

Schaefer, B.F., Turner, S.P., Rogers, N.W., Hawkesworth, C.J., Williams, H.M., Pearson, D.G. and Nowell, G.M., 2000. Re-Os isotope characteristics of post-orogenic lavas: implications for the nature of young lithospheric mantle and its contribution to basaltic magmas. Geology, 28, 563-566.

Schaefer, B.F. and Burgess, J.M., 2003. Re-Os isotopic constraints on deposition in the Neoproterozoic Amadeus Basin: Implications for the "Snowball Earth". Journal of the Geological Society of London, 160, 825-828.

Stein, H.J., Markey, R.J., Morgan, J.W., Hannah, J.L. and Schersten, A. 2001. The remarkable Re-Os chronometer in molybdenite: how and why it works. Terra Nova, 13(6), 479-486.

Using 3D modelling and numerical deformation - fluid flow simulations to target gold mineralisation around basalt domes in the Stawell Zone, Central Victoria

Peter Schaubs[1], Tim Rawling[2], Jon Dugdale[3], Chris Wilson[2]

*[1] pmd*CRC, CSIRO Exploration and Mining, PB Box 1130, Bentley, WA 6102*
*[2] pmd*CRC, School of Earth Sciences, University of Melbourne, VIC 3010*
[3] MPIMines, Stawell, Victoria

peter.schaubs@csiro.au

Expensive 'drill-centric' exploration programs typically have unpredictable outcomes. In the Victorian goldfields, over the last few decades, they have been spectacularly unsuccessful at finding any significant new gold deposits. At Stawell, in western Victoria, new cost effective exploration tools are being developed and tested. These techniques use 3D modelling and numerical deformation-fluid flow simulations to discriminate the potential fertility of prospect regions based on limited (but reliable) field data. The strategy adopted to facilitate this predictive modelling is to develop strong understanding of a 'type model' through research. This provides the deformation, alteration and metamorphic history, and the geometry of critical units, plus the petrophysical properties of those units are defined. Numerical simulations are carried out on this well defined model and results of the simulations can be compared with known deposit geometries and grades. Data sets are acquired to constrain the geometries of similar geological features in identified target areas (by field mapping, potential field data, geochemical drilling, inversion modelling). Realistic 2D and 3D models can be constructed which may include various alternative interpretations. Numerical simulations are applied to the 'target models' using the (now tested) 'type model' parameters. Predicted targets are tested with strongly spatially constrained drilling programs.

At Stawell, type models have been developed at both ore shoot scale (Dukes Nose locality) and at the dome scale (Magdala Dome). Using extensive drillcore, underground mapping and sampling databases, initial 3D models were constructed in gOCAD. These geometries were used in deformation - fluid flow numerical simulations. Critical variables, such as the orientation of stress fields during deformation, were well established from previous research. Initial results show a strong correlation between the location and geometry of zones of predicted high fluid flow and actual ore shoot geometries in the Magdala system, both at shoot and dome scale. This indicates that at the dome-shoot scale the geometry of the dome and its geometrical relationship to the syn-mineralisation stress fields is absolutely critical to the localisation of mineralisation within the deposit. The same modelling techniques and philosophies were applied to identified exploration targets within the same structural belt (Kewell and Wildwood Domes). 3D models were constructed using a combination of aircore drill data, potential field data and geophysical inversion modelling.

Geological background to numerical models

During the model definition process three critical elements were identified. These were: 1) the geometry of the model elements, 2) the rock types involved, and 3) the orientation of the stress field during gold mineralisation.

The geometry for the Dukes Nose model was defined by a combination of drilling, underground mapping and, to a lesser extent, geophysical interpretation. The Kewell and Wildwood model geometries were defined by air core drilling, minor diamond drilling and detailed magnetics and gravity inversion modelling. The three dimensional model at Dukes Nose was originally built in MineSight by the mine geologists at MPI and was then imported into gOCAD where it was pre-processed for FLAC modelling. The Kewell and Wildwood models were both built in gOCAD.

Three major rock types were considered to be critical to the modelling. These were the basalt (domes), volcanogenics (altered and deformed? volcanogenic sediments) and the mine schist. The petrophysical data used for each rock type in the modelling was taken from geotechnical data supplied by MPI but better data is currently being acquired and the models will be reassessed in light of these data once they become available.

The deformation history at the Magdala mine has been well documented by Miller and Wilson (2002). Three early ductile deformation events predated the gold mineralisation and produced a variably developed layer parallel schistosity, upright folds with a strong axial planar fabric, and a differentiated crenulation cleavage and refolding, respectively. Gold mineralisation was coeval with two subsequent brittle deformation events. The first (D4) resulted in the development of NE striking reverse faults due to dominantly ENE-WSW directed compression. The second event (D5) marked a switch to a sinistral shearing environment characterised by tension gashes near the basalt that formed during NW-SE oriented shortening. The deposit was subsequently dismembered by several later brittle faulting events, the effects of which were removed for the purposes of this modelling exercise.

Numerical modelling results

In all models, areas of high fluid flow rate occur within the volcanogenics because of the high permeability assigned to them, but within this unit high fluid flow is controlled by the proximity of areas of contraction and dilation. Areas of contraction on the flanks of the basalt dome occur where the dip is steep and at a high angle to the shortening direction. Towards the top of the domes the volcanogenics become areas of dilation. This causes fluid flow rates to be highest close to the top of the dome where both volume strain and pore pressure gradients are highest.

Dukes Nose, Magdala Dome - Ore-shoot scale

Models of the Dukes Nose show that, on the ore/-/shoot scale, areas of high fluid flow and dilation are in part controlled by variations in thickness of the volcanogenics unit along strike. Rotating the far-field stress field causes areas of high fluid flow to be shifted down plunge.

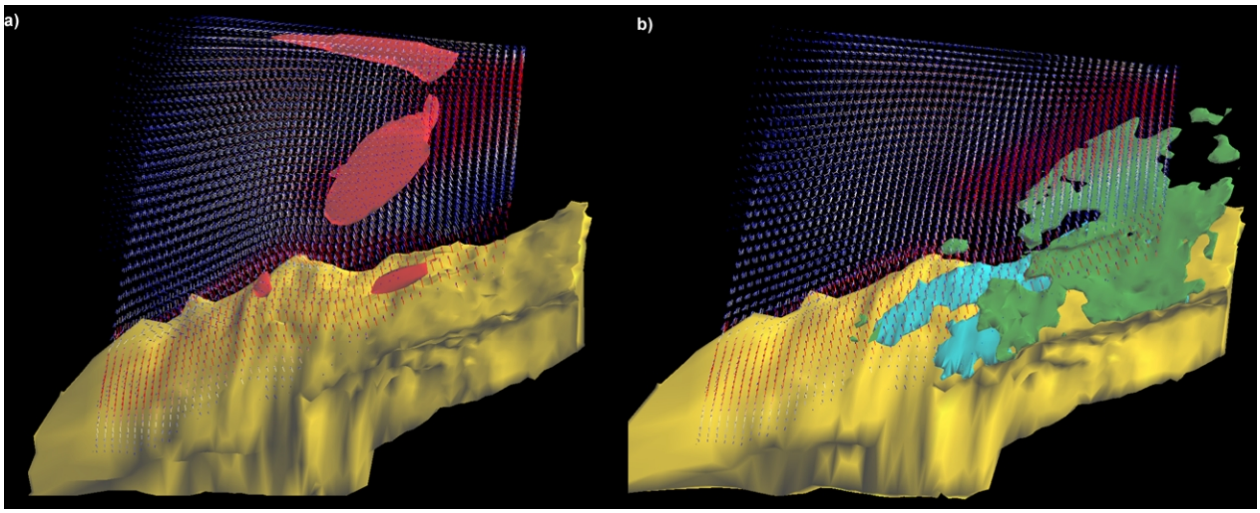

Figure 1. Dukes Nose numerical simulation results. (a) Minesight model of Dukes Nose and Extended Basalt with Darcy Flow vectors (red – highest flow rate, blue – low flow rate) and shear strain contour, (b) basalt surfaces with flow vectors and grade envelopes (aqua – Dukes Grade 4g/t, green – Central Lode Grade 4g/t).

In both ore-shoot and dome scale models, areas of high fluid flow are concentrated at the top of basalt lobes on the flanks of the dome. This occurs because the volcanogenics separating the basalt bodies are contracting and are areas of higher fluid pressure. Fluid is forced up this thin unit towards the area of dilation, which occurs near the top of basalt lobe. Areas of maximum dilation still occur near the top of the main basalt dome but the fact that the intervening volcanogenics are contracting and have high permeability causes high fluid flow rates to be localised above the minor lobe.

Magdala Dome

Areas of maximum fluid flow in models of the entire Magdala Dome shortened from the NE-SW are located near the top of the dome on both flanks. When the stress field is rotated to E-W, it causes the maximum fluid flow rate to be shifted towards regions near the Dukes Nose on the SW flank – an area of known mineralisation. High values of fluid flow on the flanks of the dome appear to be coincident with disseminated mineralisation, while areas of dilation are closer to the crest of the dome and are coincident with areas of vein hosted mineralisation. Areas of maximum dilation occur where the plunge is relatively shallow and changes in the plunge are gradual.

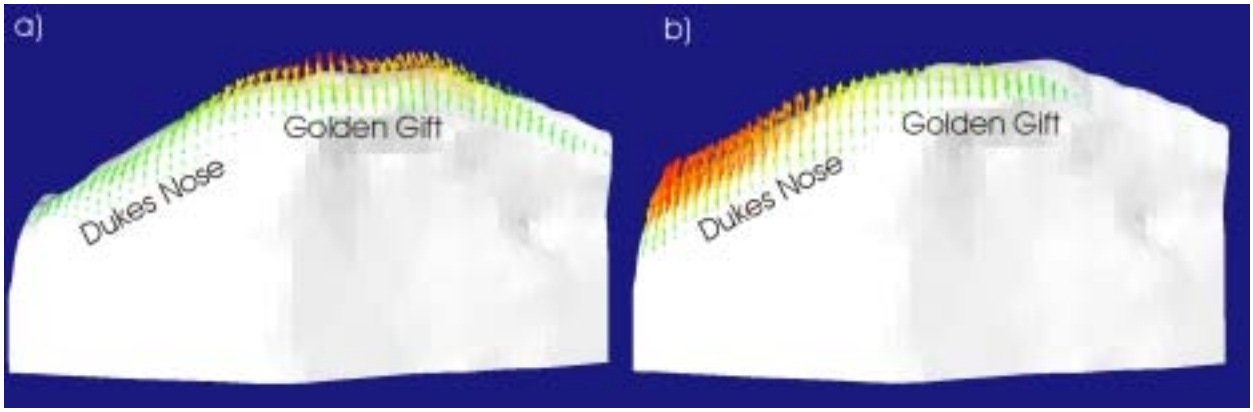

Figure 2. Fluid flow vectors from models of the Magdala dome. b) NE-SW shortening b) E-W shortening after NE-SW shortening.

Kewell Dome

In the Kewell Dome models, the presence of thin basalt lobes on the flanks of the domes cause the region above the basalt lobes, within the intervening volcanogenics, to become the region with the highest fluid flow rates. This occurs because this unit separating the basalt bodies is contracting and is an area of high fluid pressure. Fluid is forced up this thin unit towards the area of dilation which occurs above the top of basalt lobe. Areas of maximum dilation still occur near the top of the main basalt dome but the fact that the intervening volcanogenics are contracting and have high permeability cause high fluid flow rates to be localised above the minor lobe.

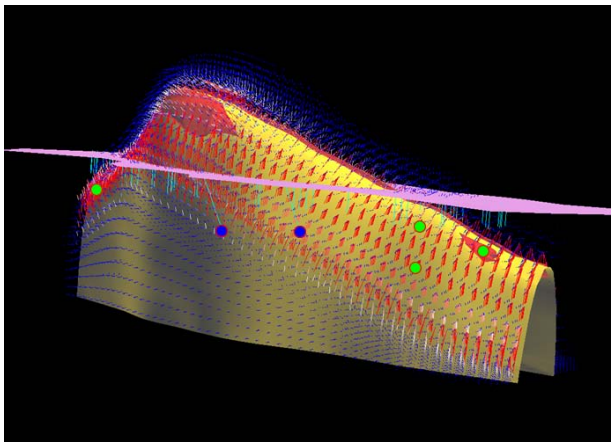

Figure 3. Kewell Dome numerical simulation results. Yellow surface – basalt, red surface – shear strain contour, mauve surface – ground level, fluid flow vectors. Existing diamond holes KD1 and KD2 are marked (blue circles) as are the proposed diamond hole locations (green circles). Dome is 3.5km in length and view is to the north.

Wildwood Dome

In the Wildwood model, areas of maximum dilation occur on the NNW end of the dome where the plunge is relatively shallow and changes in the plunge are gradual. At the SSE end of the dome where the plunge is more variable, dilation is lower. This is consistent with the Kewell model where areas of maximum dilation coincide with the gentle plunge of the dome on the SSE side.

Summary

Numerical modelling has placed constraints on some of the factors which may be important for the location of gold mineralisation on the flanks of these basalt domes. In all models, areas of high fluid flow rate correlate well with areas of known mineralisation. Areas of high fluid flow rates are controlled by the shape of the basalt domes and the far-field stress direction. Areas of dilation do not necessarily coincide with these same areas. The presence of the volcanogenics (which are given weaker mechanical properties than the matrix or the basalt) causes the absolute values of dilation and fluid flow to increase; however, the relative position of areas of dilation and high fluid fluxes with respect to the position of the domes does not vary greatly.

The volcanogenics are areas of contraction on the flanks of the basalt dome where the dip is steep and at a high angle to the compression direction. Towards the top of the domes the volcanogenics become areas of dilation. This causes fluid flow rates to be highest close to the top of the dome where areas of contraction and maximum dilation are in close proximity.

The presence of thin basalt lobes on the flanks of the domes cause the region above the basalt lobes, within the intervening volcanogenics, to become the region with the highest fluid flow rates. This occurs because the volcanogenics separating the basalt bodies is contracting and is an area of high fluid pressure. Fluid is forced up this thin unit towards the area of dilation which occurs within the volcanogenics near the top of basalt lobe. Areas of maximum dilation still occur near the top of the main basalt dome but the fact that the intervening volcanogenics are contracting and have high permeability cause high fluid flow rates to be localised above the minor lobe.

In the Magdala Dome models, the rotation of the compression direction from NE-SW directed to E-W directed causes the locus of maximum dilation to be located within the upper portions of the volcanogenics high above the Dukes Nose. The region of highest fluid flow also changes position; down plunge along the top of the Dukes Nose. This is caused by the higher fluid pressure gradient within the Dukes Nose towards the NNW end of the model.

The numerical simulations run on these models predicted zones of high fluid flow (high mineralisation potential) that matched very closely the existing drilling and assay data. More importantly, the analysis of these results immediately changed the targeting criteria that will be used to assess basalt domes in the region, as well as providing an excellent template for developing explorative drilling programs within these prospect regions. Drilling on the south end of the Kewell Dome where the models predicted areas of high fluid flow and significant dilation, has yielded encouraging results.

Reference

Miller, J.McL. and Wilson, C.J.L. 2002. The Magdala Lode System, Stawell, Southeastern Australia: Structural Style and Relationship to Gold Mineralization across the Western Lachlan Fold Belt. Economic Geology, 97, 325-349

Coupled processes in faulted environments

Heather A. Sheldon and Alison Ord

*pmd*CRC, CSIRO Exploration and Mining, PO Box 1130, Bentley WA 6102*
Heather.Sheldon@csiro.au

Introduction

Many hydrothermal ore deposits occur within fault zones, suggesting a relationship between mineralisation and faulting. However, not all faults are mineralised. In order to predict whether a given fault will be ore-bearing, we must improve our understanding of processes that occur within fault zones, focussing in particular on the coupling between such processes, and their relationship to mineralisation. A particular aim of the pmd*CRC is to develop earth process software that is capable of fully-coupled simulation of all relevant processes, to enable identification of particular sets of conditions that favour mineralisation. Such a fully-coupled model does not yet exist, but significant progress has been made in coupling subsets of the relevant processes within numerical models. Here we present results of numerical simulations that illustrate progress in this field.

Fault zone processes

Processes associated with fault zones can be broadly classified into deformation (mechanical processes), fluid flow, heat transport (conduction and advection), and chemical processes (reactions and solute transport). These processes are coupled in many ways, and there are complex feedbacks between them. For example, fault slip events are generally accompanied by an increase in porosity and permeability. This leads to focusing of the regional fluid flow field, such that fluid is drawn into the fault and flows along it much faster than it does in the country rock. If the fault crosses a thermal gradient, transport of heat by the fluid may result in significant perturbation of the regional thermal field. Convection cells may develop within and around faults under certain conditions, particularly if the permeability is high for a long period of time. The fluid will also transport chemical components, and these components will react with the wall rocks to achieve a new equilibrium state determined by the local pressure and temperature conditions. Over time, a combination of mechanical and chemical processes will reduce the porosity and permeability of the fault zone (fault sealing), thus restricting further fluid flow and in some cases leading to development of overpressured compartments within the fault. Overpressure itself feeds back into the mechanical process, making it easier for the fault to slip again.

A key question in the context of mineral exploration is, how do these processes transport metals to the fault, and what causes them to precipitate when they reach the fault? The results presented below may provide some clues.

Model results 1: Fluid flow in dilatant faults

In this section, we focus on the evolution of porosity and permeability following a fault slip event, and the consequences for fluid flow. The numerical model represents a steep fault cutting across a horizontal seal, which separates an overpressured region below from a hydrostatic region above. Failure of the fault is accompanied by an abrupt increase in porosity, with a corresponding increase in permeability and a drop in fluid pressure. The drop in fluid pressure causes fluid to be drawn into the fault from all directions, both above and below the seal, until the pressure has recovered (Fig. 1A). Fluid subsequently moves up the fault, escaping from the

overpressured region below the seal (Fig. 1B). The fault is acting like a “valve”, as implied by the fault valve model of Sibson (1992). Following the failure event, the porosity decreases exponentially over time, at a rate consistent with fault sealing by pressure solution and cementation (Renard et al., 2000; Gratier et al., 2003). This has two interesting consequences: Firstly, it gradually reduces permeability and thus inhibits further flow through the fault. Secondly, it eventually results in development of overpressure within the fault zone. A fully-coupled, deformation and fluid flow model would enable us to investigate the feedback between overpressure development and subsequent fault slip events. However, there is much to be learnt from the relatively simple model that we present here, in which failure and sealing of the fault is represented by a prescribed porosity evolution. For example, the model shows that the volume of fluid that passes through a fault after a single failure event is insufficient to account for the volume of vein quartz that is present in many fault zones. This is consistent with petrographic observations and isotopic data which indicate that a significant proportion of the vein quartz in some faults is sourced locally, from dissolution along stylolites (e.g. Gratier et al. 2003, and references therein). In other cases, the observed quartz may be accounted for by precipitation from externally derived fluids during multiple fault-slip events (e.g. Cox 1995).

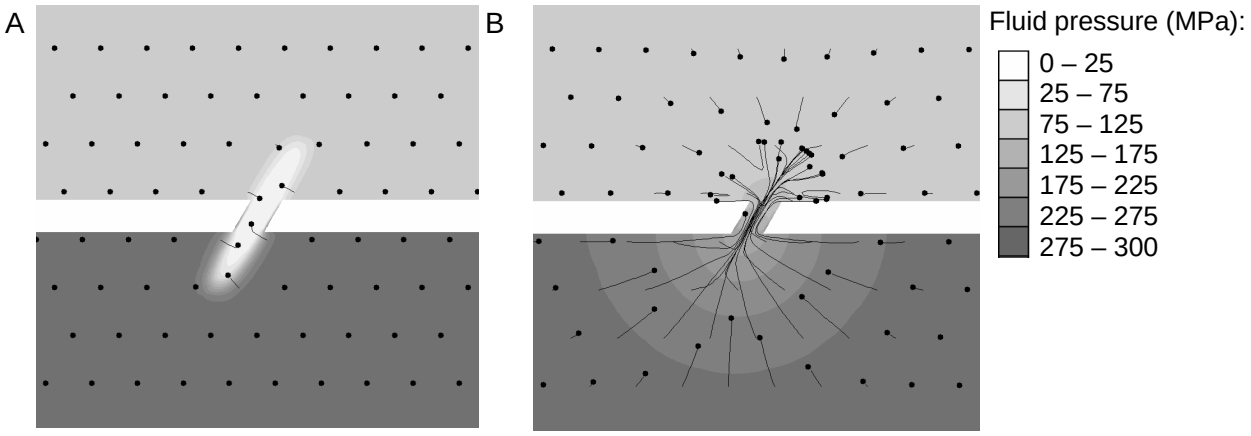

Figure 1. Fluid flow through a dilatant fault cutting across an impermeable seal. Height of model = 1.5km, depth to seal = 10km. Contours show fluid pressure; black dots and lines indicate movement of passive markers in the pore fluid. (A) 10 years after failure. (B) 1000 years after failure.

A further interesting result obtained from this model is the potential for downward flow in dilatant faults. This occurs when the wall rocks below the seal have a lower permeability than the wall rocks above. In this situation, it is easier for fluids to be drawn into the fault from above the seal; hence fluids get drawn down across the seal to infill the newly created porosity in the fault below the seal. Downward flow occurs *despite* the regional driving force for upward flow. This result may have relevance for unconformity-related uranium deposits, which occur in brecciated fault zones, at or just below an unconformity between relatively impermeable, crystalline basement, and overlying, more permeable sedimentary rocks. Mixing of oxidised, basin-derived brines with more reducing fluids is often cited as a cause of uranium and gold deposition; our model results suggest a mechanism by which such mixing could be achieved (Fig. 2).

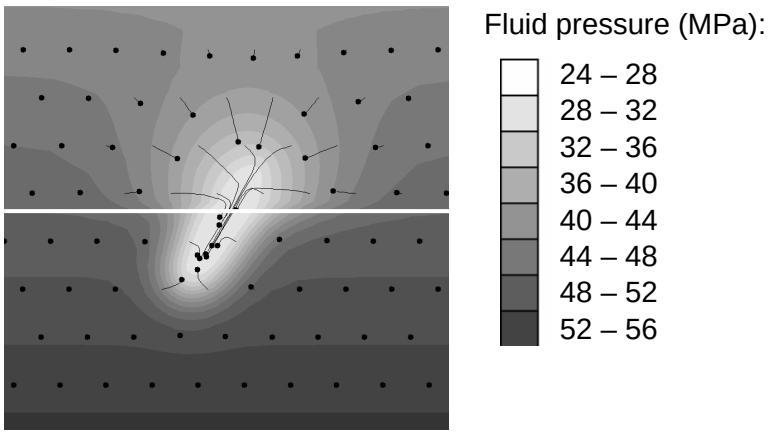

Figure 2. Fluid flow through a dilatant fault cutting across an unconformity (indicated by white line), separating relatively impermeable basement from overlying sedimentary rocks. Height of model = 1.5km, depth to unconformity = 5km. Plot shows fluid pressure contours and pathways of passive markers, 1000 years after failure of the fault.

Model results 2: Convection and mineralisation

We now consider the interaction between thermal convection and reactive transport. The numerical model represents an overpressured compartment separated from the hydrostatic upper crust by an impermeable seal, underlain by impermeable basement. The basement contains a small intrusion, which is initially hotter than the surrounding rocks. This heat source initiates convection in the sealed compartment. We investigate the consequences of convection for dissolution and precipitation of quartz, using the following equation as a proxy for reactive transport of dissolved silica:

$$R = u \cdot \nabla T \frac{\partial C}{\partial T} + u \cdot \nabla P \frac{\partial C}{\partial P} \qquad (1)$$

(1991), where *R* is the reaction rate, *u* is the Darcy flux, *T* is temperature, *P* is pressure, and *C* is the equilibrium concentration of silica in the pore fluid, which in turn is a function of *T* and *P*. In simple terms, this equation shows that flow down a gradient in pressure or temperature will result in precipitation, whereas flow up temperature or pressure gradients results in dissolution, because the solubility of silica increases with *T* and *P*. In the model, precipitation and dissolution are coupled to changes in porosity and permeability; hence there is feedback between reaction and fluid flow. Figure 3 shows the porosity distribution after 1 million years of convection.

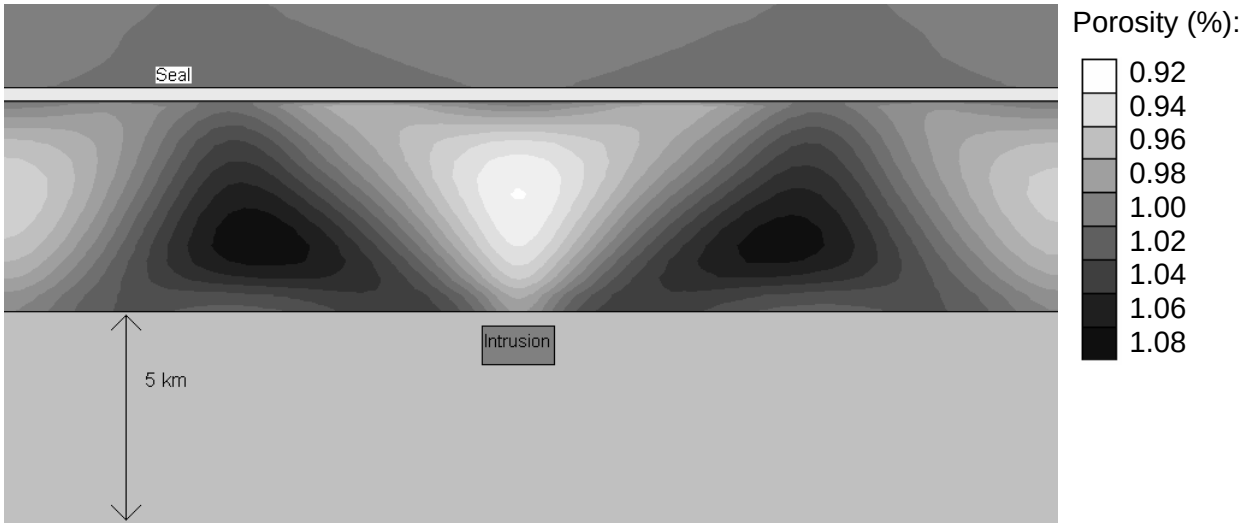

Figure 3. Porosity distribution after 1 million years of convection, initiated by intrusion in impermeable basement. Initial porosity = 1% throughout the model. Note the slight reduction in porosity above the intrusion, which is an area of upwelling, and slight increase in porosity in areas of downwelling (dark areas).

Some time after the convection cells have become established, a permeable fault is created to allow transport of fluid across the seal. The fluid flux through the fault is ~2 orders of magnitude larger than the Darcy flux due to convection alone, hence the rate of quartz precipitation is relatively high within the fault. However, the results show that it would take many 10's of thousands of years to completely seal the fault in this way.

This simple approach to reactive transport is computationally much easier and faster than implementing a full reactive transport algorithm within the model. However, it cannot be applied to reactive transport of trace metals, because it does not conserve mass. For example, Equation 1 might predict dissolution of gold, but it does not take account of whether there is any gold to dissolve. Consequently, the model can predict negative amounts of trace metals in some areas, and very high concentrations in other areas. The pattern of dissolution and precipitation in these cases is purely qualitative, whereas the pattern for quartz is quantitative because (in this case) the quartz is never completely dissolved. A further limitation in applying this method to trace metals may be that other mechanisms, such as fluid mixing, are more important in controlling precipitation of these materials, than flow along P-T gradients.

Concluding remarks

The results presented here illustrate the importance of coupled models in understanding mineralisation within fault zones. Each model described here represents a subset of processes operating within the system, and provides insights into possible mechanisms for mineralisation. Future work will focus on development of more complete, fully coupled models, in particular coupling deformation (including a realistic representation of discrete, seismic slip events on faults) with reactive transport.

References

Cox, S.F. 1995. Faulting processes at high fluid pressures - an example of fault valve behavior from the Wattle Gully Fault, Victoria, Australia. Journal of Geophysical Research, 100, 12841-12859.

Gratier, J.P., Favreau, P. and Renard, F., 2003 Modeling fluid transfer along California faults when integrating pressure solution crack sealing and compaction processes. Journal of Geophysical Research, 108, 2104-2129.

Phillips, O.M., 1991. Flow and reactions in permeable rocks. Cambridge University Press, Cambridge, UK.

Renard, F., Gratier, J.P. and Jamtveit, B., 2000. Kinetics of crack-sealing, intergranular pressure solution, and compaction around active faults. Journal of Structural Geology, 22, 1395-1407.

Sibson, R.H., 1992. Fault-valve behavior and the hydrostatic lithostatic fluid pressure interface. Earth-Science Reviews, 32, 141-144.

Deformation zone architecture, reactivation and mineralisation processes in the Eastern Succession of the Mount Isa Inlier

Michelle Stark and Thomas G. Blenkinsop

*pmd*CRC, School of Earth Sciences,James Cook University, Townsville, QLD 4811*

michelle.stark@jcu.edu.au

Introduction

This project aims to integrate each separate stage of regional scale faulting in the Eastern Succession of the Mt Isa Inlier, in order to form a complete history of localised deformation, and to regard the role of the deformation zones in fluid flow and mineralization in IOCG deposits.

IOCG deposits are currently considered to be closely related to the intrusion of a suite of syn- to late-tectonic granitoids. However, this association has been challenged by new age data, and a preliminary analysis of the spatial distribution of these deposits shows a stronger relationship between deposits and moderate to large S to SE trending faults than to granites. Every large, discovered ore deposit in the Eastern Succession possesses evidence that clearly indicates formation was influenced or dominated by fluid flow along deformation zones.

The research will focus on key areas of dilation and irregularity along major faults (which may control the sites of important deposits e.g. Ernest Henry Cu-Au deposit) and fault junctions and intersections of major fault systems of the same and of different ages. This method will allow the use of a large body of pre-existing fault data, recorded during the exploration of now well established orebodies. The distinction in geometry, kinematics and fluid conduit properties of the major faulting events will be investigated.

Questions

This research addresses three of the five fundamental questions posed by the pmd*CRC in the context of IOCG deposits in the Eastern Succession, and applies this evaluation to realistic deformation architecture problems specific to the Eastern Succession.

- What is the architecture of the system?
- What are the fluid flow drivers and pathways?
- What are the metal transport and depositional processes?

These questions will be addressed through the investigation of the major regional deformation zones, which will allow them to be applied directly to circumstances specific to the Eastern Succession. This in turn will generate site and region specific solutions to fault history problems. This project will also investigate the individual geometries of the faults, fault jogs and bends, and fault intersections which make up this architecture, and the fluid systems in place pre- during and post-mineralisation, which utilise these structural scale fluid conduits and fluid traps.

Study Areas

The first study area targeted by this project is the Cloncurry Fault. This is a major regional fault system and long lived fluid conduit. The Cloncurry Fault has been recognised as having a long and complex history of movement, involving multiple reactivation episodes, potentially spanning

entirely separate deformation events. It is this long, recorded history of activity which makes the Cloncurry Fault a valuable asset to the field research campaign.

The input of structural information from currently mined orebodies affected by multiple phases of deformation, such as Ernest Henry, Eloise, Osborne, Cannington and Selwyn, will be achieved by mine site work including data collaboration and mine site observation

The second major target area for field research is the major structural junction created between the Fountain Range Fault and the Pilgrim Fault/Ballara-Corella River Fault Zone. Crosscutting smaller late- to post-tectonic faults complete a picture of a substantial period of faulting in this locality. The field investigation of this “series” of faults should create a relatively comprehensive faulting history for the area, which will in turn lend itself to correlation over the entire inlier.

Mechanical Modelling

The long and complex history of faulting of the Eastern Succession was created by structural activity during multiple, style-distinct deformation events. This has produced a regional architecture which shows a massive variation in fault geometry over time. Far field stresses applied to geometrically distinct brittle structures and brittle structural regimes, show a wide variation in effects with regard to resultant fault geometry and reactivated fault geometry, crustal composition and fluid migration pathways. This project will apply mechanical models to regional architecture within the Eastern Succession in order to simulate mechanical processes over time and document and evaluate the geological results of these processes.

Conclusion

This project will involve some exciting mechanical modeling, fluid flow modeling and, in turn, ore-formation locality prediction. The evaluation of the stratigraphic perturbation caused by faulting over the history of mineralised rocks in the Eastern Succession should provide a fundamental building block for the formation of the overall evaluation of the geology of the Eastern Succession.

Remote sensing and spectral investigations in the Western Succession, Mount Isa Inlier: Implications for exploration

Simon van der Wielen, Simon Oliver and Aleks Kalinowski

*pmd*CRC, Geoscience Australia, GPO Box 378, Canberra, ACT 2601*
Simon.vanderWielen@ga.gov.au

Introduction

Detailed stratigraphic, structural and mineralogical investigations carried out in the northern part of the Leichhardt River Fault Trough (Bull Creek) as part of a Predictive Minerals Discovery Cooperative Research Centre study have identified several areas of intense hydrothermal alteration. These investigations demonstrate the utility of satellite imagery in identifying and discriminating mineral signatures formed through hydrothermal processes.

Satellite data complement geological and geophysical datasets to assist in better target selection in areas of exploration interest. Landsat Thematic Mapper, Advanced Spaceborne Thermal Emission and Reflection Radiometer (ASTER) and Hyperion imaging spectrometer data covering the Bull Creek area of the Mount Isa Block have been used to test the ability of remote sensing methods to map regional geological units and alteration patterns (hydrothermal footprints). ASTER and Landsat investigations were expanded to cover the Termite Range Fault adjacent to the Century Mine. Band ratios and spectral unmixing techniques show promise in being able to discriminate between different mineralogies and lithologies, and can be a useful guide to understanding regional fluid movements when examined in conjunction with structural data. These data also have the potential to improve the spatial accuracy of mapping. Hyperion provides the opportunity to evaluate the capabilities of short-wave-infrared spaceborne hyperspectral data in the Mount Isa Terrain. This capability is especially valuable in remote areas where available geological and other ground truth information is limited.

The use of remotely sensed alteration maps enables exploration companies to gain a good understanding of the distribution of spectrally like materials on a regional scale. This can be important for highlighting areas prospective for mineralisation.

Methodology

Satellite/Sensor	Processing Level	Path Row/Area of Interest	Date of acquisition
Landsat 5	Ortho-corrected	99/73	23/09/89
Landsat 5	Ortho-corrected	100/73	14/09/89
Landsat 7 ETM+	Ortho-corrected	99/73	30/5/2002
Landsat 7 ETM+	Ortho-corrected	100/73	21/5/2002
ASTER	Path oriented	Bull Creek	13/9/2000
ASTER	Path oriented	Termite Range	23/11/2000
Hyperion	Raw image oriented	Bull Creek	21/9/2003

Table 1. A table and description of remote sensing data used in the orientation study.

Various data sets were acquired for the study (table 1). Preprocessing was required to enable the generation of spectral products from satellite image data. The Landsat and ASTER were

radiometrically calibrated by converting the image digital number values to top of atmosphere radiance and atmospherically corrected using the dark pixel subtraction method.

The Hyperion preprocessing steps included the replacement of bad lines, elimination of bad bands, illumination correction, and local destreaking (treating VNIR and SWIR bands separately) to remove artifacts associated with the pushbroom sensor. The FLAASH module in ENVI was used to generate a surface reflectance product from the Hyperion data. Spectral polishing was then used to smooth the data.

Techniques

The generation of alteration and geologically relevant products utilized three main techniques including: 1. band ratios to isolate significant spectral absorption features for a target mineral from ASTER and Landsat data to highlight clay, iron and silica rich lithologies (figure 1), 2. Decorrelation techniques to highlight spectral variability and reduce data dimensionality, and 3. Spectral unmixing techniques to isolate and identify specific spectral targets.

Band ratios and Relative absorption-Band Depth (RBD, Crowley et al., 1989) images are generated through simple band arithmetic given knowledge of the absorption features of a target mineral. Band ratios provide a good quick pass of possible mineralogy in a given scene. RBD images have the numerator as the sum of the bands representing the shoulders and the denominator as the band located nearest the absorption feature minimum (Crowley et al., 1989).

The decorrelation technique stretches the principal components of an image to display inter-band variance. This method highlights spectral variability and can be a simple way to discriminate lithologies.

Hyperion required the application of spectral unmixing techniques, including 1. Minimum Noise Fraction generation to separate signal from noise (Hyperion has a fairly low signal to noise ratio of around 80:1 in SWIR; Datt et al., 2003), 2. Pixel purity index to highlight areas of spectrally pure pixels, 3. N-dimensional visualiser to select end members, 4. Spectral analysis to identify end members with reference to the USGS mineral spectral library and the Bull Creek PIMA spectral library (figure 2), and 5. Full or partial unmixing functions to map end members back to the data for the production of mineral maps.

Samples were collected over areas of mineral alteration and specific lithologies within the study area. Geological descriptions and spectral signatures, using Portable Infrared Mineral Analyser (PIMA) were compiled for both fresh and weathered surfaces in order to establish a spectral library. The spectral library helped differentiate particular lithological units and alteration mineralogy.

Preliminary Results

Landsat Thematic Mapper data in the Bull Creek area were processed to broadly highlight clay, iron and silica rich units (figure 1). The processing was able to distinguish areas of gossans and silification. ASTER data, with heightened spectral resolution were used to break the broad mineralogical groupings of the Landsat ratio images into smaller more precise groupings. ASTER was able to discriminate between alunite, phengite, kaolinite, and carbonate with varying degrees of success. Phengite was restricted to zones within Leichhardt Metamorphics, basement granites as well as two areas at crystal creek. Alunite showed localized concentration along faults and in preferred stratigraphic horizons. Hyperion data were used to map specific mineralogical targets.

In the Termite Range area, ASTER data were used to map phengite, carbonate and kaolinite mineral occurrences (figure 3). The Kamarga Dome showed diffuse kaolinite alteration that highlighted northeast-southwest trending faults, possibly due to increase weathering of feldspar minerals. The Termite Range Formation showed distinct zoning of phengite-kaolinite mineralogy in areas with little vegetation. No significant alteration was observed along the Termite Range Fault itself.

It is important to note that several factors complicate the ability of remotely sensed data to generate reliable mineral index images. These include vegetation cover and greenness, time of year, weathering, soil moisture and particle size, target size and material brightness (highly reflective materials are more reliably extracted). Producing accurate alteration maps requires a good understanding of the limitations of satellite data as well as knowledge of alteration and geochemical processes.

Figure 1. Bull Creek Target - At left, clay, iron and silica RGB Landsat TM band ratio image. At centre, ASTER Phengite, Muscovite and Alunite RGB thresholded to highlight likely occurrence. At right, Hyperion derived Minimum Noise Fraction image representing MNFs 3,4 and 5 as RGB.

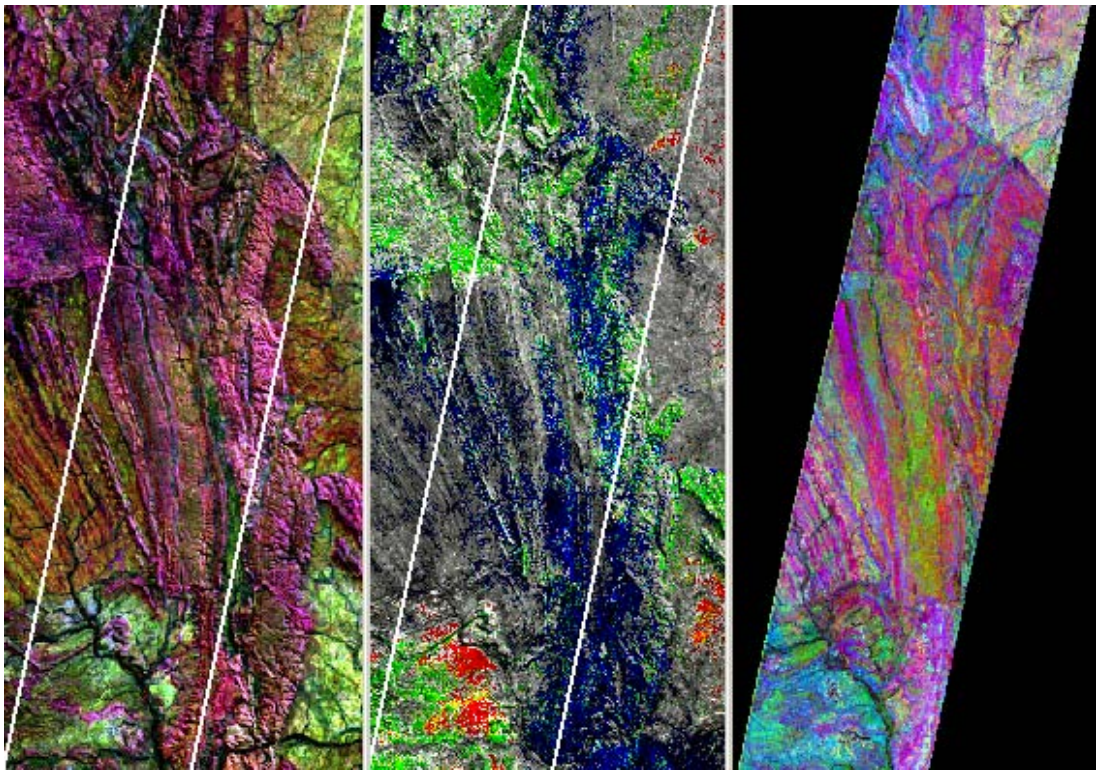

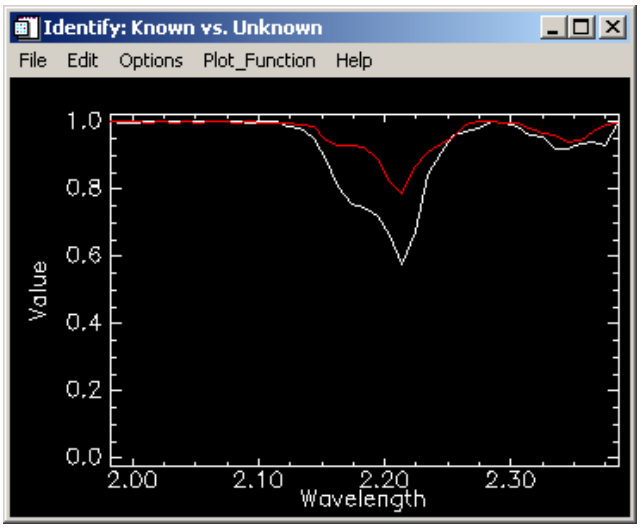

Figure 2. Hyperion end-member compared to PIMA sample 030603J1 (Halloysite) PIMA spectrum white, Hyperion red.

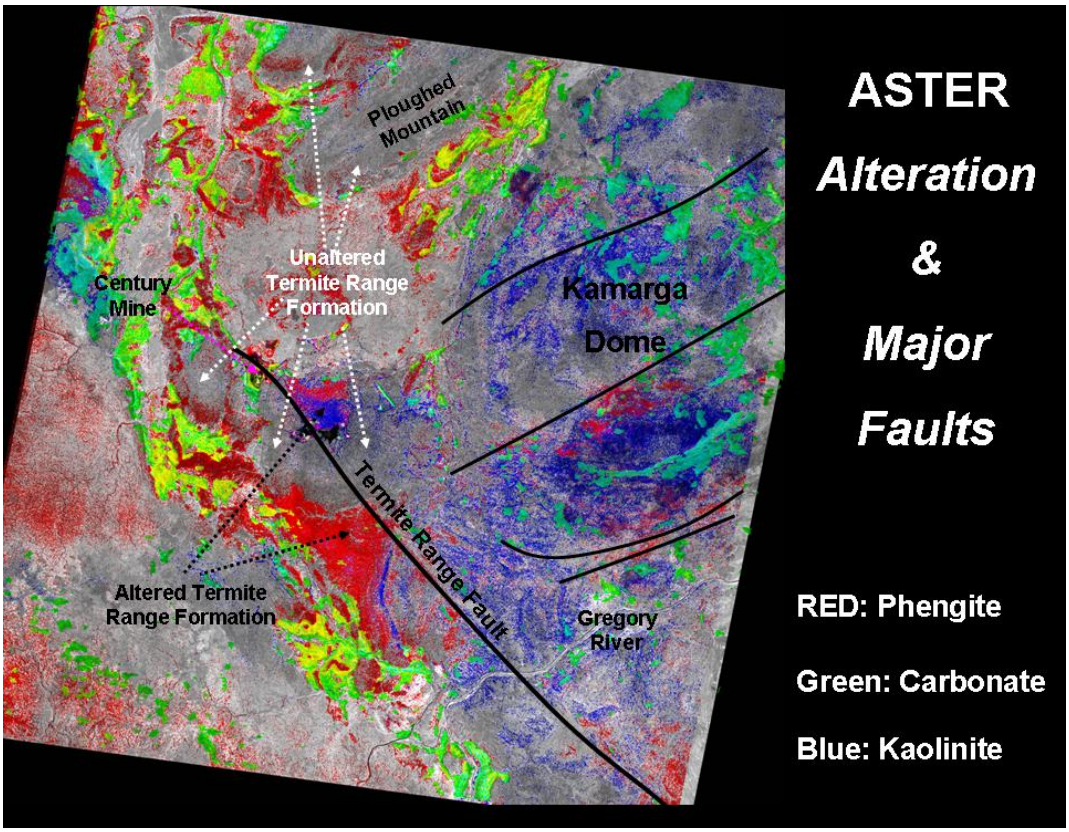

Figure 3. An ASTER derived phengite-carbonate-kaolinite map showing the major structural and alteration features.

Future Work

The next phase of the satellite image investigations will involve field validation of spectral processing methodology used in this study. Investigations will also focus on improving Hyperion data pre-processing. It is anticipated that field validation will be completed during the next 12 months. Successful acquisitions of Hyperion and Advanced Land Imager (ALI) data have been made over the Mount Gordon Fault and are yet to be processed to extract geological information.

The preliminary results have highlighted the usefulness of remote sensing in the production of alteration maps. As there is very good coverage of ASTER data, future work is needed to expand the alteration maps on a regional scale to cover the entire Mount Isa Inlier.

Acknowledgements

The authors would like to thank George Gibson, John Creasey and Craig Smith for their valued input into the project.

References

Datt, B., McVicar, T.R., Van Neil, T.G., Jupp, D.L.B. and Pearlman, J.S., 2003. Preprocessing EO-1 Hyperion Hyperspectral Data to Support the Application of Agricultural Indexes. IEEE Transactions on Geoscience and Remote Sensing, 41(6), 1246 – 1259.

Crowley, J.K., Brockely, D.W. and Rowan, L.C., 1989. Airborne imaging spectrometer data of the Ruby Mountains, Montana: mineral discrimination using relative absorption band-depth images. Remote Sensing of Environment, 29, 121-134.

The mineral potential of major fault systems: case studies from northeastern Queensland, Australia

Ivo Vos[1], Frank Bierlein[1], Barry Murphy[2] and Mike Barlow[3]

*[1] pmd*CRC, School of Geosciences, Monash University, PO Box 28e, Victoria 3800*
*[2] pmd*CRC, School of Earth Sciences, University of Melbourne, Victoria 3010*
*[3]pmd*CRC, Geoscience Australia, GPO Box 378, Canberra, ACT 2601*
ivovos@earth.monash.edu.au

Introduction

The pmd*CRC-funded Architecture ('A1') project "What are the fundamental characteristics of mineralised (trans-lithospheric) fault systems?" adapts a multi-disciplinary approach to predicting the mineral potential of major fault systems in a number of regions within Australia. Major fault systems that penetrate deep into the crust are important, but poorly understood, elements of the Earth. Conceptually, such structures provide pathways and foci for mineralising fluids and magmatism into the upper crust. Why some of these fault systems are metallogenically well-endowed, whereas other seemingly analogous systems remain barren, is a critical question. This study focuses on fault systems and their endowment in low data-density regions of the Broken River and Hodgkinson provinces in northeastern Queensland (Figure 1). Three case studies are presented where the integration of existing and reinterpreted geological, geophysical and geochemical datasets illustrate the strength of multi-disciplinary research. Insights into the nature of fault systems and their mineral potential are also developed, not only in northeastern Queensland, but also in analogous regions elsewhere.

Methods

Field studies have been carried out in a number of localities within the Hodgkinson and Broken River provinces. These studies aim at ground-tracking the existence and nature of poorly constrained major fault structures, and unravelling the metallogenic evolution of gold deposits associated with some of the major structures. For the latter aspect, petrographic, geochemical, SEM and fluid inclusion analyses of mineralised quartz vein samples have been carried out. Regional geophysical datasets (200m line airborne magnetics, 10km spaced gravity and limited petrophysics) have been interpreted, and using multi-scale edge analysis ('worming') and forward modelling, the subsurface expression of the major fault systems has been assessed.

Case Study I: The Amanda Bel Goldfield – challenging exploration in a low-data density area

The Amanda Bel Goldfield (Teale et al., 1989) is situated in the Camel Creek Subprovince (CCSP) of the Broken River Province (Figure 1). The CCSP displays overall eastward younging from Ordovician to Early Devonian with internally westward younging imbricate stacks of thrust sheets (Withnall et al., 1997). The CCSP is suggested to represent an accretionary wedge, oversteepened by ramping and or later shortening (e.g. Henderson, 1987). Gold and antimony mineralisation in the Amanda Bel Goldfield occurs in lower greenschist facies, folded sediments of the Silurian Greenvale Formation and the Early Devonian Kangaroo Hills Formation. To the east and northeast, Middle Carboniferous intrusions, mainly of the Almaden Supersuite, intrude the sediments (Withnall et al., 1997). The area has undergone three periods of deformation before deposition of the Clarke River Formation in the Early Carboniferous.

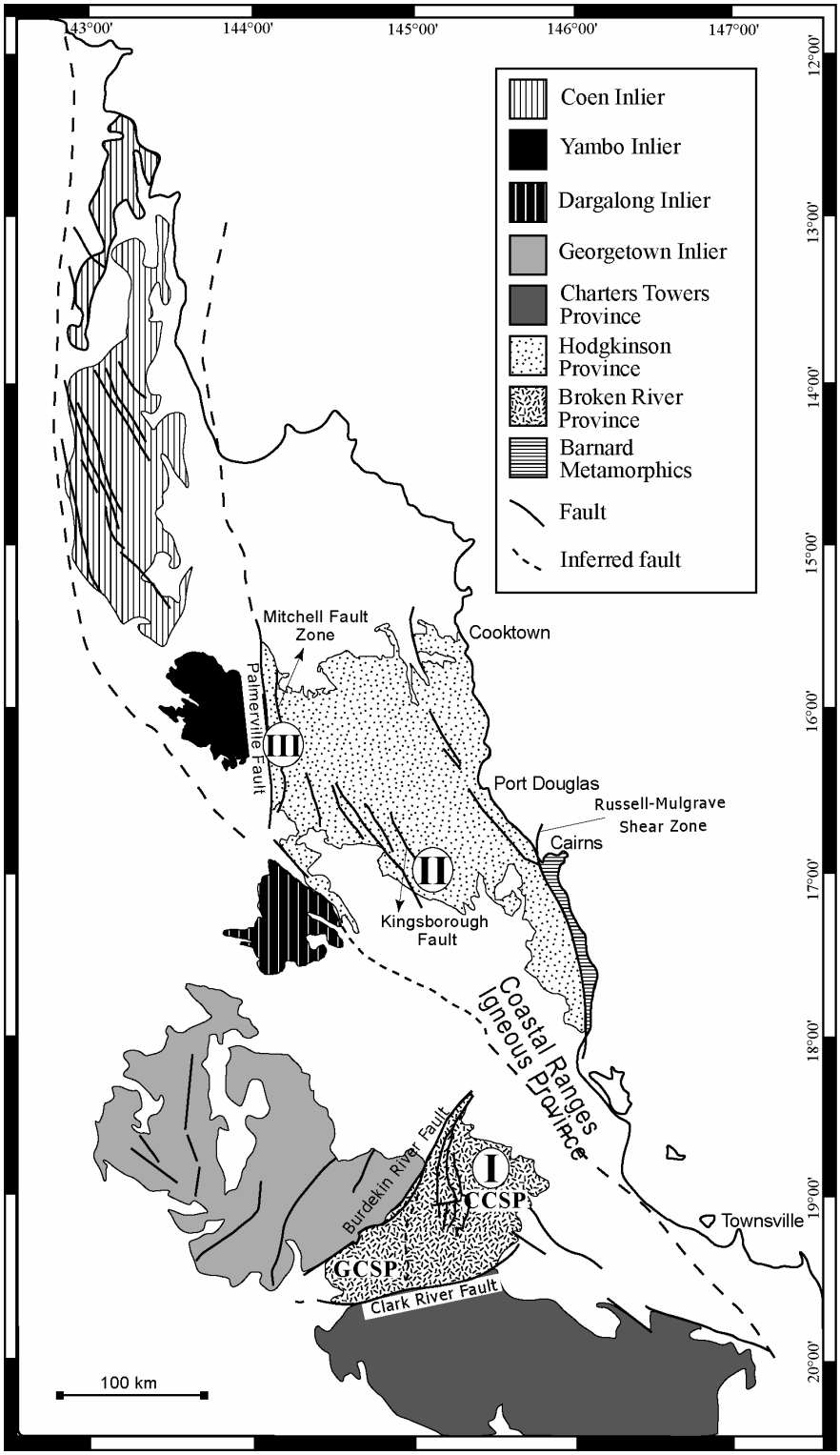

Figure 1: Geological framework of north-eastern Queensland with case study areas indicated in Roman capitals. GCSP = Graveyard Creek Subprovince, CCSP = Camel Creek Subprovince.

Results

A clear relationship between deformation and mineralisation can be demonstrated in the Amanda Bel Goldfield on the basis of field relationships. Petrographic, SEM and fluid inclusion studies of mineralised quartz samples indicate that gold deposits in the Amanda Bel Goldfield can be classified as 'orogenic' (Vos et al., 2004). In spite of the absence of recognised fault structures in geological and GIS databases of the study area, the nature of the gold deposits and their classification as orogenic gold deposits implies that there is also a strong structural control on gold mineralisation. Based on our findings we suggest that previously unrecognised fault structures do exist in the study area, obscured by lack of surface exposure and reduced geophysical control as a result of poor lithological contrasts.

Case Study II: The Hodgkinson Goldfield (Northcote District) – an example of orogenic gold mineralisation in a low-data density area

The Northcote District is situated in the southern part of the Hodgkinson Goldfield located in the central portion of the Hodgkinson Province (e.g. Peters et al., 1990). Gold mineralisation is predominantly located within shear zones and associated quartz veins that are hosted in lower greenschist facies meta-sedimentary rocks of the Hodgkinson Formation. The setting of the Hodgkinson Province is similar to that described in case study I, in that a series of thrust slices internally young westward, while overall younging eastward, which may indicate the presence of an accretionary prism (Bultitude et al., 1993). Gold and antimony are the primary commodities in the Northcote District and are commonly associated with high strain anastomosing quartz veins, faults and shears. Mineralised shear zones are commonly parallel to bedding planes and are associated with axial planes of folds that developed during the second of four deformation phases recognised in the Hodgkinson Province.

Results

The Northcote District is located in a region dominated by large fault structures such as the Kingsborough Fault (Figure 1). Results from this and previous studies confirm the 'orogenic' nature of the gold deposits in the Hodgkinson Goldfield. Gold-quartz veins are typically anastomosing and mineralisation is localised in dilational sites at cross-fracture intersections and zones of rheological contrast. Here, the model of Cox (1999) would be applicable, implying that the Kingsborough Fault might form a primary feeder structure, possibly linking into the deeper lithosphere or connected to a flat-lying continuation of the Palmerville Fault. Even though this is a low-data density area (as for instance compared to the Yilgarn Province), integration of field observations and available data can lead to important inferences for exploration.

Case Study III: The Palmerville Fault – a long-lived and barren 1st-order fault?

The Palmerville Fault is at least 400 km long and marks a major discontinuity in North Queensland, separating the Palaeozoic Hodgkinson Province in the east from Proterozoic domains in the west. The repeatedly reactivated Palmerville Fault forms an example of a first-order (potentially trans-lithospheric) fault that has remained ('seemingly') unmineralised along most of its strike. Although relatively poorly understood, previous interpretations of regional gravity data (Shaw et al., 1987) implied that the fault is an upper-crustal feature and originally dipped shallowly to the west (and possibly still does at depth) despite the steep easterly dips at the surface.

Results

A more 'elegant' model of opening of the Hodgkinson Province controlled by normal movement along an easterly dipping Palmerville Fault, as supported by field observations and forward modelling of magnetic and gravity data, has been applied here. The modelling shows the regional significance of the Palmerville Fault and highlights the tectonic importance of other structures like the Mitchell Fault Zone (Figure 1). A more detailed discussion of these findings can be found in Barlow et al. (this volume).

Inferences and applications of this research

Our research investigations showcase how multi-disciplinary studies in low-data density areas can provide important insights into exploration possibilities within such areas. Low-data density areas will always present a challenge to mineral exploration, but careful consideration of the data at hand as demonstrated can invariably increase the success rate for exploration in these areas. The Amanda Bel Goldfield provides a particularly good example. The dominant occurrence of the gold deposits along a distinct northeasterly trend and the orogenic nature of the deposits almost necessitate the presence of previously unrecognised, deep-seated fault structures that provided conduits for the ore-bearing fluids. Our results indicate the strength of multi-disciplinary research for exploration in areas of low exposure and limited availability of geophysical data.

The regional significance of first-order structures such as the Palmerville Fault has long been considered, but remains poorly understood. Understanding of 1st-order structures through integrating available data and forward modelling can provide clues about the importance of these structures in mineral exploration that may be applied elsewhere. In addition, when compared to other significantly mineralised structures of

the same order (for instance in the Yilgarn craton – see Murphy et al., this volume), a better understanding of the factors that control mineralisation of such structures may be gained.

In this multi-disciplinary investigation, we focus on metallogenesis and its relationship with large-scale fault structures in low-data density key areas in northeastern Queensland. The metallogenic data supplemented by geochemical and geochronological data as part of our study has enabled a better understanding of the geodynamic framework and overall tectonic evolution of the (northern part of the) Tasman Fold Belt System. In turn, the knowledge generated will prove valuable for future exploration in northeastern Queensland and analogous regions elsewhere.

Acknowledgements

We would like to thank Graham Teale and Lynch Mining for their support in the Amanda Bel Goldfield, Jackson Gold for their support in the Northcote District, and Richard Blewett for discussions on the Palmerville Fault.

References

Bultitude, R.J., Donchak, P.J., Domagala, J. and Fordham, B.G., 1993. The Pre-Mesozoic stratigraphy and structure of the western Hodgkinson Province and environs. Department of Minerals and Energy, Queensland, Geological Record, 29, 259.

Cox, S.F., 1999. Deformational controls on the dynamics of fluid flow in mesothermal gold systems. In: McCaffrey, K. J. W., Lonergan, L. and Wilkinson, J., eds., Fractures, fluid flow and mineralisation. Geological Society of London, Special Publication, 155, 123-140.

Henderson, R.A. 1987. An oblique subduction and transform faulting model for the evolution of the Broken River Province, northern Tasman Orogenic System. Australian Journal of Earth Sciences, 34, 237-249.

Peters, S.G., Golding, S.D. and Dowling, K. 1990. Melange- and sediment-hosted gold-bearing quartz veins, Hodgkinson Gold Field, Queensland, Australia. Economic Geology 85, 312-327.

Shaw, R.D., Fawckner, J.F. and Bultitude, R.J., 1987. The Palmerville Fault System: a major imbricate thrust system in the northern Tasmanides, North Queensland. Australian Journal of Earth Sciences, 34, 69-93.

Teale, G.S, Plumridge, C.L., Lynch, J.E. and Forrest, R.J., 1989 The Amanda Bel Goldfield: a significant new gold province. Proceedings North Queensland Gold '89 Conference, Australasian Institute of Mining and Metallurgy, 103-109.

Vos, I.M.A., Bierlein, F.P. and Teale, G.S. 2004. Timing, nature and characteristics of orogenic gold deposits in the Broken River Province, NE Queensland, Australia. Geological Society of Australia, Abstracts, 73, 133.

Withnall, I.W., Lang, S.C., Lam, J.S., Draper, J.J., Knutson, J., Grimes, K.G. and Wellman, P., 1997. Clarke River Region. In: Bain, J.H.C. and Draper, J.J., eds., North Queensland Geology. AGSO Bulletin, 240, 327-364.

Comparative Camp-scale studies in the Eastern Yilgarn Craton

John Walshe[1], Peter Neumayr[2], Glen Masterman[3], Scott Halley[4], Susan Drieberg[2], Ned Stolz[5], Karen Connors[5], Leo Horn[6], Phung Nguyen[6]

*[1] pmd*CRC, CSIRO Exploration and Mining, PO Box 1130 Bentley, WA, 6102.*

*[2] pmd*CRC, Centre for Global Metallogeny, School of Earth and Geographical Sciences, University of Western Australia, Crawley, WA 6009*

*[3] pmd*CRC, School of Earth Sciences, University of Melbourne, VIC, 3010.*
[4] Placer Dome Asia Pacific
[5] St. Ives Gold Mining Company Pty Ltd.
[6] Agnew Gold Mining Company Pty Ltd.
john.walshe@csiro.au

Introduction

The emphasis within the AGCRC and more recently within the ***pmd****CRC* on "where is the deposit" led inevitably to a restating of the "source", "transport" and "trap" paradigm of mineral systems. The "5 Question" description of the mineral system explicitly highlights the problem of understanding the system in time and space.

The "where" question is inherently a scale independent question. It may be asked at an ore shoot-scale or at a terrane scale. Hence there is a need to build models that are scale integrated, that is, models that are consistent with the data sets at all scales.

As part of the scientific drive to build scale-integrated models, we are developing camp-scale comparative studies. The work is focused on properties of Placer Dome Asia Pacific in the Kalgoorlie and Laverton districts and the St Ives property of GoldFields of South Africa and supported by MERIWA within the framework of the ***pmd****CRC* Yilgarn terranes (Y) project. Future work is planned for the Agnew property of Goldfields of South Africa.

The comparative study of camps is designed in part to understand the influence of district-scale factors, such as bulk composition of host sequences, regional metamorphic grade, proximity to granites and porphyries, on the types of alteration assemblages and the compositions of the fluids that produced those alteration assemblages. Another goal is to establish the diversity of processes leading to the formation of high grade gold deposits. Inter-camp comparisons may help to elucidate lithological and structural controls on seals, aquicludes and aquifers in the system and the size and geometry of large-scale hydrothermal cells.

Here we comment on learnings that are emerging from inter-camp comparison of lithostratigraphic settings of the deposits, styles of alteration associated with gold and on some future research directions.

Comparative Lithostratigraphic Setting and Regional-scale Seals

In the eastern Yilgarn, gold deposits occur in all the major rock units of the Kalgoorlie Group and correlates as well as in the conglomerates of the late basins. Relative and increasing absolute age constraints overlap the timing of gold deposition with emplacement of the mafic to syenitic granites that peaked circa 2665 to 2650 Ma and with Black Flag and late-basin sedimentation.

In the St Ives camp, deposits are hosted in predominantly mafic-ultramafic lavas and dolerite intrusions. In the Central Corridor, of the camp, deposits are hosted by units stratigraphically below the Blag Flag Beds (Kambalda Komatiite, Kapai Slate, Paringa Basalt, Defiance Dolerite) and along porphyry-ultramafic rock contacts. Deposits on the southwestern side of the camp (Argo and Junction) are hosted by the Junction and Condenser Dolerites that intruded the Black Flag Beds. Theses dolerites are correlates of the Golden Mile Dolerite and the overall lithostratigraphic setting is similar to that of the Golden Mile.

In the Kanowna district, northeast of Kalgoorlie the upper sequence of the Kalgoorlie Group (Paringa Basalt, Blag Flag Beds) is absent and the lower sequence of mafic, ultramafic and intermediate volcanic rocks is unconformably overlain by coarse, clast-supported polymict conglomerate and felsic, crystal-rich volcaniclastic units (re-sedimented pryoclastic mass flow deposits) that are correlated with the late basin stratigraphy. Mineralization in the Kanowna Belle deposit straddles this boundary, defined locally by the Fitzroy Fault. The major portion of the deposit is hosted by the Kanowna Porphyry, which is part of the mafic granite suite. By contrast, the Wallaby gold deposit, located 25km southwest of Laverton, occurs within late-basin conglomerates. The deposit is hosted by a >1500m thick, polymict, matrix-supported conglomerate that has been intruded by a differentiated alkali syenite suite of dykes. The dykes range in composition from relatively early monzonite and carbonatite through younger syenite and porphyritic syenite. Both pre-ore and post-ore lamprophyre dykes are also present.

Again in the Agnew Camp the equivalent of the upper sequence of the Kalgoorlie Group is absent and the lower sequence correlates (Lawlers Basalt, Agnew Ultramafic) are overlain by conglomerates rich in mafic and ultramafic clasts and sandstones. Deposits occur in all rock types but within 100s of metres stratigraphically of the mafic or ultamafic conglomerates.

The proximity of deposits to either the footwall of the Black Flag Group or the late basins hint that these units of the lithological architecture may have acted as regional aquicludes at the time of gold mineralization, such that fluid pressures were sustained in compartments beneath these units. The formation of deposits above these seals reflected localized rupturing of the seal. It may be that the ultramafic units also acted as aquicludes within camps hosted in the lower sequence of the Kalgoorlie Group and correlates. The occurrence of ultramafic units subjacent to deposits, at Kanowna Belle and in the St Ives camp hints that more competent rocks such as the porphyries were the aquifers and the ultramafic rocks were aquicludes.

Comparative Camp-scale Alteration Studies

The study of the St Ives Camp has shown that high-grade gold mineralization is localized in zones where reduced, pyrrhotite-bearing assemblages overlap with oxidized, magnetite-bearing assemblages (Neumayr et al., this volume) which indicates that large differences in the redox state of hydrothermal fluids facilitated gold deposition. Do such spatial as well as temporal zonations in oxidized and reduced assemblages occur in all camps proximal to mineralization or are there gradients in other parameters such as pH or H_2S activity? Is the mineralogical and/or geochemical expression of such gradients always the same?

The Kanowna Belle deposit and environs is dominated by pyrite, with little known magnetite or pyrrhotite. However, sulfur isotopes variations in pyrite at the deposit- to district-scale at Kanowna Belle are similar to those documented in the St Ives camp and may be related to changes in redox state. Variations in the abundance of phengite relative to muscovite and the trace metal contents of the alteration zones across the Kanowna Belle deposit demonstrate that it is possible to finger print the redox gradient in different environments using different mineralogical indicators and by correlating trace element suites with mineralogical assemblages. It remains to be determined if all the observed variations reflect changes in the redox state of the fluids or sympathetic changes in other chemical parameters such as pH, etc.

A feature of the Agnew Camp is the S to N zoning over about 8 km from Au-pyrite mineralization (Sonvang deposit) with marginal magnetite and distal pyrrhotite, features typical of deposits in the Central Corridor of the St Ives camp, to Au-magnetite mineralization (Crusader deposit) to Au-biotite-amphibole mineralization (Redeemer deposit), the latter two lacking in sulfide or magnetite. These last styles of mineralization occur in an equivalent stratigraphic setting to deposits in the Central Corridor, St Ives and in the Kanowna district. So, clearly the mineralogical differences do not reflect a host-rock control. The mineralogy of the Crusader and Redeemer deposits is consistent with higher temperature fluids, and/or more reduced fluids and/or sulfur poor fluids compared to inferred temperatures and fluid compositions from other camps. However mineralogical zoning equivalent to Agnew camp-scale pattern is observed at the drill-core and hand-specimen scale in the Revenge and Wallaby deposits. It may be that study of the Agnew camp will provide insights into a significant fluid end-member not easily deciphered in the other camps.

Summary Comments on Future Directions: Architecture, Chemical Gradients and Targeting

The work on both the St Ives camp and the Kanowna area has elucidated mineralogical zoning patterns that may be mapped at the camp scale that reflect chemical gradients at the time of gold mineralization. High grade gold zones occur on these gradients. The task is to identify the optimum places for finding **high grade-large tonnage** deposits on these gradients. Paragenetic and sulfur isotope studies in the Revenge and Kanowna Belle deposits indicate that these will be places of maximum oxidation: hematite stable, negative sulfur isotope signal in pyrite. They may well be places of minimum oxidation also and combined C and S isotope studies are being directed to resolve this question.

In the St Ives camp, the spatial association of oxidized assemblages with porphyry intrusions at the drill core to camp scale strongly suggests that magmatic volatiles drove the oxidation. Recent detailed mapping of the Wallaby deposit has identified both close spatial and paragenetic links between gold mineralization and syenite magmatism (Drieberg et al., this volume). In the Kanowna Belle District, a series of transitional TTG and mafic-granite porphyry intrusions have intruded the Kanowna stratigraphy before, during and after deposition of the sedimentary and felsic volcanic facies into the late basins. A better understanding of the geodynamic setting and the prediction of the location of these magmatic suites emerges cleary as a critical goal in the quest of predictive mineral discovery.

One task is to geochemically finger print the porphyries to identify the precise chemical characteristics that correlate with the occurrence of highly oxidized fluids in each of the camps. Another task is to establish the whole-rock geochemical characteristics of the most reduced and oxidized fluids in the system, correlating these characteristics with fluid inclusion and stable isotope data and identify the pathways of these fluids. These characteristics may well change with depth in the system. Successfully correlating these constraints across camps should provide some powerful insights into the structures that controlled flux of the most chemically contrasting fluids in the system at various scales, aiding the effort to build robust, scale-integrated models and the targeting process. The integration of the architecture of these critical faults with the chemical composition of the hydrothermal fluids in 3D-4D at and beyond camp scale will be critical to improve our predictive capability in the targeting process in brown fields to greenfields exploration.

Airborne gravity gradiometry of Broken Hill: Strengths and weaknesses

Roberto Weinberg, Laurent Ailleres and Terry Lees

*pmd*CRC, Australian Crustal Research Centre*
School of Geosciences, Monash University, Clayton VIC 3800

Introduction

The Airborne Gravity Gradiometry (AGG) survey covered over 1000 km^2 of the Broken Hill Block, roughly centered around the Line of Lode at Broken Hill. This type of data has the potential to greatly increase the efficiency of exploration for dense ore bodies, particularly in remote, poorly known parts of the world. This paper explores the usefulness of the AGG survey in constraining 3D geological models of this well-known terrane and in defining targets for Broken Hill-type deposits and other massive sulfide deposits.

Three-Dimensional Geology of the Broken Hill Area: Pitfalls for Gravity Survey

The geology of the area covered by the AGG survey consists of the Willyama Supergroup, a sequence of ca. 1.7 Ga pelites, psammo-pelites and psammites interlayered with volcanic rocks and intruded by dykes and sills. Intrusive and extrusive magmatism is bi-modal, characterized by granitic and basaltic rocks (e.g. Gibson and Nutman, 2004). The entire sequence underwent high-grade metamorphism and multiple deformation phases during the 1.6-1.59 Ga Olarian Orogen and later events.

The stratigraphic sequence of the Curnamona Block is well established. Less well established, however, is the assignment of a particular outcrop or series of outcrops to particular stratigraphic units, particularly in regions of intense deformation where rock packages are considerably thinned and possibly disrupted. By contrast to the well-established stratigraphy, the nature of the deformation history and its effects in re-arranging strata remains controversial. The deformation history is characterized by multiple phases of deformation, including several phases of crustal shortening and possibly an early extensional phase (e.g. Gibson and Nutman, 2004) associated with faulting. Deformation and high grade metamorphism, including partial melting events have profoundly reorganized the rock pile, with much of the original stratigraphy now inverted (younging downwards). Despite its clear map expression, and unambiguous evidence for the existence of faults, the role of faulting in disrupting and repeating the sequence (Noble 2000, White et al. 1995) remains highly controversial (e.g. Stevens 1996, comments on the White et al. paper).

In this project, a 3D geological model of the area covered by the AGG is being developed in order to integrate it with the AGG survey through forward and inverse modeling. In the building of the 3D geological model, we were confronted with two major difficulties, one that reveals the deficiencies in the geological understanding of the Curnamona terrane, and the other that reveals the difficulty in using gravity surveys to constrain the 3D geometry of the Broken Hill block.

The first difficulty is that it is not possible to reliably reconstruct the 3D geometry of the survey area based on the NSWDMR 1:25 000 maps. Historical reasons have led to lithological mapping of the block being carried out separately from structural mapping. This dichotomy in approach has inevitably led to deficiencies in the understanding of the geometry and evolution of the block, as recognized by the recent Gap Analysis (T. McConachy, pers. comm., 2004). It has also led to fundamentally different interpretations of the exposed rocks and their

geometrical relationships, as revealed by the published discussion between White and Stevens. The reason why it is not possible to reliably build a 3D geological model at the 1:25 000 scale using the survey maps is that there are a number of possible, equally valid ways to interpret the maps in the third dimension, given the lack of structural data, and the ambiguity in assignment of outcrops and rock sequences to the broader stratigraphic units. We found that cross-sections based on the geological maps were not reproducible, as different researchers in the team derived equally valid but significantly different cross sections by taking different assumptions.

The second difficulty is that gravity-based interpretation of the regional geology must take into account the distribution of the most and least dense rocks in the area, which are typically amphibolites (densities of ~3200 kg/m^3), and granitic or quartz-feldspathic alteration rocks (~ 2700 kg/m^3). This compares with densities around 2800 kg/m^3 for the high-grade rock sequences in the area (R. Lane pers. comm.). A visual comparison between the AGG image and geological maps reveals that there is a direct correlation between gradiometry highs and lows and the 2D distribution of these most and least dense rocks, indicating their influence on the gravity signal. Unfortunately, however, both these rock groups have unpredictable distributions, as they commonly form discontinuous layers and their distribution changes along strike. Their unpredictable distribution is a combined result of their primary distribution (e.g. magmatic intrusions or local alteration processes) and later folding, disruption and transposition.

This implies that, in addition to the natural spread in density values within any rock package, the density variation within that package will be increased due to the influence of those most/least dense intrusive rocks. The spread of density values within each unit causes an overlap between unit densities. If rock packages cannot be unambiguously characterized by a given density, it becomes impossible to then ascertain rock geometries based on density. Thus, by taking into account the likely range of densities in each unit, a significant degree of freedom is added to any forward or inverse modeling, making such approaches relatively insensitive to the geometry of rock distribution. The consequence is that any reasonable, but not particularly well-constrained, 3D geological model can be successfully matched (at least for the long wave length anomalies) by forward modeling to a gravity survey by varying the density values within each rock package. Conversely, any gravity image can be successfully matched through inversion to an acceptable but poorly constrained 3D geological model if again densities are allowed to vary widely within the same package.

In this paper, we will demonstrate how much the AGG image is controlled by the distribution of these most and least dense rocks and also how a wide number of ill-constrained 3D geological models can be matched by inverse modeling the AGG image by playing with densities and density distributions.

Discussion and Conclusions

This study focuses on a well-known part of the world. The combination of uncertainties in the 3D geological interpretations based on available geological maps, and the nature of the density variation in this area, with numerous bodies of most and least dense rock types irregularly distributed, is such that it makes constraining the 3D geometry by means of gravity survey singularly inefficient. Simply stated, the large degrees of freedom are such that infinite solutions can be derived. Thus, constraining the 3D geometry of the Broken Hill Block is best done by integrating careful structural analysis with stratigraphical studies, as suggested by Gap Analysis, (T. McConachy, pers. comm., 2004) and combining that with both aeromagnetic and seismic interpretations.

The AGG image is very sensitive to the distribution of rocks of end-member densities and so it clearly delineates high density potential targets close to the surface. However, the existence in Broken Hill of a large number of amphibolite bodies gives rise to a similar number of uninteresting potential targets. As any explorer knows, targets must be further constrained by geological considerations and other geophysical surveys.

Would similar surveys help define targets in poorly known terranes? Yes, absolutely. Firstly, the AGG image defines relatively well the broad geological shapes and trends, even in Broken Hill, with its complex density distribution. Secondly, AGG surveys may be much more efficient in defining targets in terranes with better defined density structures and less plagued by the noise related to dense amphibolites.

References

Gibson, G. M. and Nutman, A. P., 2004. Detachment faulting and bimodal magmatism in the Palaeoproterozoic Willyama Supergroup, south-central Australia: keys to recognition of a multiply deformed Precambrian metamorphic core complex. Journal of the Geological Society, London, 161 55-66.

Noble, M. 2000. Geology of the Broken Hill Synform, N.S.W. Australian Crustal Research Centre, Department of Earth Sciences, Monash University (unpublished M.Sc. thesis).

White, S. H., Rothery, E., Lips, A. L. W., and Barclay, T. J. R., 1995. Broken Hill area, Australia, as a Proterozoic fold and thrust belt: implications for the Broken Hill base-metal deposit. Transactions of the Institution of Mining and Metallurgy (Section B: Applied Earth Sciences), 104, 1-17.

Stevens, B.P.J., White, S.H., Rothery, E., Lips, A.L.W., and Barclay, T.J.R., 1996. Broken Hill area, Australia, as a Proterozoic fold and thrust belt; implications for the Broken Hill base-metal deposit; discussion and reply. Transactions of the Institution of Mining and Metallurgy, (Section B: Applied Earth Sciences), 105, B89-B98.

Compressional Tectonics of the Carlin Gold Trend

C. Wijns[1,2], G. Hall[3], and D. Groves[1]

[1] *pmd*CRC, Centre for Global Metallogeny, University of Western Australia, Crawley, WA 6009, Australia*

[2] *pmd*CRC, CSIRO Exploration and Mining, PO Box 1130, Bentley, WA 6102, Australia*

[3] *Placer Dome Asia Pacific Ltd., PO Box 1907, West Perth, WA 6872, Australia*

cwijns@cgm.uwa.edu.au

Introduction

Pre-existing crustal structures are important in localising strain related to the large-scale evolution of an orogeny. Rheological contrasts between basement blocks will also influence the degree and location of faulting and relative uplift. In northern Nevada, U.S.A., basement architecture in the form of early rifted continental margins, formed during Proterozoic extension, may dictate the subsequent structural geometry of overlying sedimentary sequences during large-scale compression (Figure 1a). Within the region of the Carlin gold trend, specific anticlinal fold and thrust geometries in the sedimentary rocks, involved in various orogenies up until the Laramide, may focus fluid movement and provide effective traps to the system, resulting in the unique gold endowment of the area. Most mineralisation is situated less than 100 m below the Roberts Mountain thrust, which defines the lower boundary of the sequence of deep-water sedimentary rocks that has ridden over both the basement and younger sedimentary layers.

Muntean et al. (2003) argue that the Carlin and Battle Mountain–Eureka (BME) gold trends (Figure 1b) correspond to reactivated normal faults that likely had their origins in Proterozoic rifting. Numerical modelling offers a way to test the basic hypothesis by which “steps”, relics of continental rifting, control the subsequent location of upper crustal faults and anticlinal structures during compression.

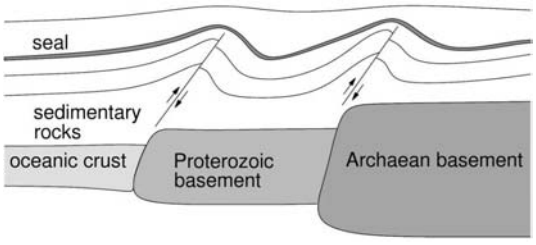

a

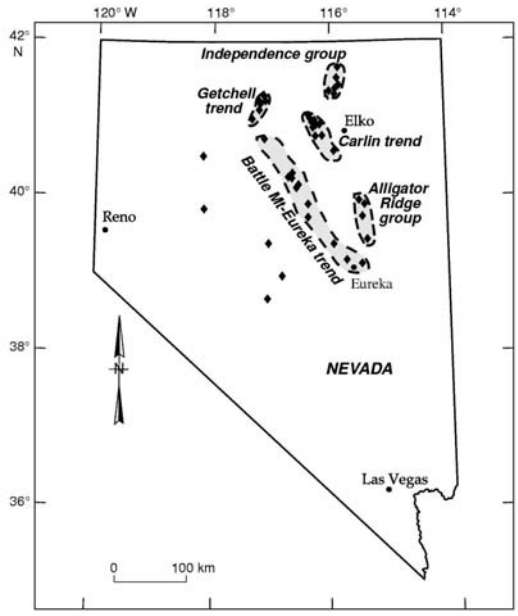

b

Figure 1: (a) Schematic conceptual model for the structural setting of the Carlin trend above a basement normal fault that is reactivated during compression. Three crustal blocks represent the product of a rifted continental margin. (b) Gold deposit trends in northern Nevada, U.S.A. Image from Wooden et al. (1998).

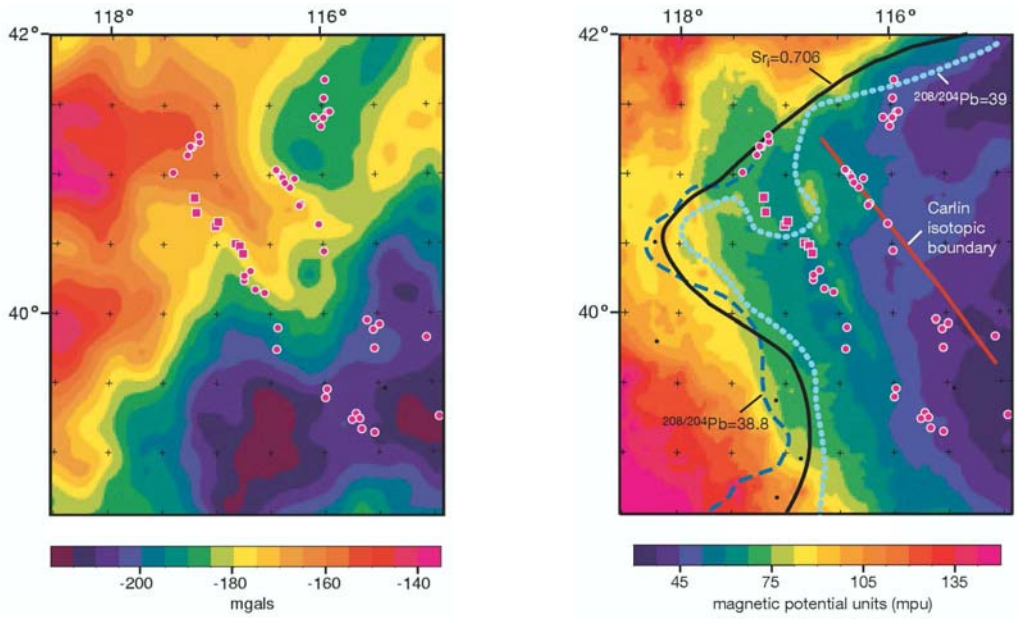

Figure 2: Gold deposits (circles and squares) on top of (a) 5 km upward continued Bouguer gravity anomaly with basin effects removed, and (b) magnetic potential with Pb and Sr isotope ratio boundaries. Images from Grauch et al. (2003).

Geological Setting

Following continental rifting in the Proterozoic through to Devonian, present-day northern Nevada has been subject to a number of compressional episodes of varying duration. These range from the Antler orogeny, approximately 340 Ma ago, through to the Laramide orogeny, which ended with the onset of Basin and Range extension about 50 Ma ago (Miller et al., 1992). The Roberts Mountain thrust, which defines a regional cap to the mineralisation, and probably acted as a permeability seal, occurred during the Antler orogeny. Subsequent events thrust more sedimentary sequences over the Roberts Mountain allochthon.

The linear arrangements of gold deposits along the BME and Carlin trends (Figure 1b) have prompted many researchers to look for evidence of large-scale structural controls, especially in geophysical data (e.g., Rodriguez, 1998; Grauch et al., 2003). The demarcation between ancient continental crust and younger oceanic crust is well established through Pb and Sr isotope ratios (Wooden et al., 1998; Grauch et al., 2003), but this boundary, although close, is not coincident with the major mineral trends. Processing of gravity and magnetic data by Grauch et al. (2003) has revealed features that align with mineral occurences; these are more persuasive for the BME than the Carlin trend (Figure 2). A 2D inversion of magnetotelluric data also shows narrow, vertically extensive, electrically conductive zones under the two trends, which Rodriguez (1998) interprets as crustal faults.

If the geophysical data are highlighting major crustal faults that control the locations of the mineral trends, these may be expressions of the reactivation of early normal rift faults at even deeper levels (Figure 1a). The relative offsets between reactivated normal faults and their propagated thrusts in overlying sedimentary rocks are likely to be complicated by multiple orogenies, gravitational slumping, and widespread extension in the Eocene and later.

Numerical Modelling

The numerical approach has been developed explicitly to deal with unlimited strain, and can simulate the spontaneous localisation of shear structures (Moresi et al., 2001, 2002). The 2D section model follows an approximate ENE–WSW transect running from Archaean cratonic crust in present day Utah,

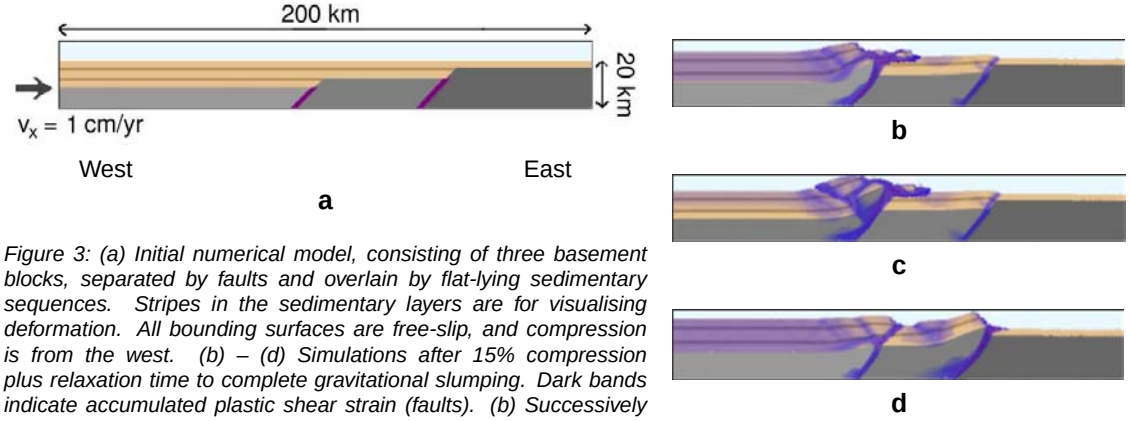

Figure 3: (a) Initial numerical model, consisting of three basement blocks, separated by faults and overlain by flat-lying sedimentary sequences. Stripes in the sedimentary layers are for visualising deformation. All bounding surfaces are free-slip, and compression is from the west. (b) – (d) Simulations after 15% compression plus relaxation time to complete gravitational slumping. Dark bands indicate accumulated plastic shear strain (faults). (b) Successively less competent blocks from east to west, (c) equally competent oceanic and transitional blocks, and (d) stronger western fault.

U.S.A, to the oceanic crust along the protomargin of western North America. The numerical model represents three basement crustal blocks – Archaean, transitional or Proterozoic, and oceanic – that are the product of continental rifting during the Proterozoic through Devonian (Figure 3a). These blocks are separated by normal faults that provide zones of weakness that will reactivate. The strengths of the different crustal blocks and the weakness of the faults vary, in order to determine the importance of fault reactivation versus rheological contrast in controlling the structural development in the overlying layers.

In the case of successively weaker basement blocks from east to west, and equally weak basement faults (Figure 3b), most slip occurs along the first fault, and the eastern fault is barely reactivated. The oceanic crust is thrust up against the transitional crust, providing the elevation for thrusting of western sedimentary rocks over eastern ones, mostly by gravitational slumping. Eastern sedimentary layers are isolated from deformation.

A lack of rheological contrast between oceanic and transitional basement (Figure 3c) does not affect the outcome in terms of strain partioning between basement faults. However, the more competent oceanic crust undergoes faulting rather than homogeneous thickening, which provides locally greater elevation for the sedimentary rocks in the vicinity of the basement thrust.

When the western fault is stronger, the eastern fault is not protected from reactivation (Figure 3d). Strain is equally partioned between both basement faults, with the result that neither area experiences the elevation of previous cases, and the sedimentary sequences are not thrust very far to the east.

Discussion

The structural evolution of the sedimentary sequences that host Carlin-type deposits depends less on rheological differences between basement blocks (Archaean, transitional, oceanic) than the ability to reactivate deep faults, which then propagate into the overlying sedimentary rocks. The upper plate motion across the lower plate is largely a product of gravitational slumping rather than thrusting due to far-field stress, but this may be due in part to the steeper (45°) angle of thrusting that is an outcome of the constitutive model in the numerical code. Uplift is important for promoting slumping over great distances, and depends on basement rheology. Weaker blocks undergo greater thickening overall, but more competent blocks may experience localised uplift as a result of pop-up structures (Figure 3c).

Field evidence shows that anticlines are important for hosting Carlin-type gold deposits, and these would act as natural fluid ponding sites if seals are present. A ramp anticline often develops when there is compression across existing faults (e.g., Cooke and Pollard, 1997), or, as in the model, against a ramp between two basement blocks. The ramp is effective in localising an anticline in the sedimentary rocks above basement topography. The fluid ponding potential of such structures is enhanced if they remain unbroken by thrusting.

Another ubiquitous feature of the model is the nature of the first fault that forms in the sedimentary cover: a backthrust formed off the basement asperity (Figures 3b to d). The implication is that an early backthrust should exist in such a field situation, and it will reach the basement and thus be a candidate for tapping deep fluids. This feature of the model also explains anomalous west-vergent deformation associated with a geanticline that is locally, but not everywhere, subparallel to the Sr 0.706 line – the inferred edge of the continent (Madden-McGuire and Marsh, 1991; Saucier, 1997).

Elevated pore pressure is one of the most effective ways to change the stress regime and promote failure and fracturing where it would not otherwise occur. A low-permeability cap in the sedimentary layers, perhaps in the form of the Roberts Mountain thrust, would lead to elevated pore pressures in the rock column below as more material is thrust above (e.g., Hubbert and Rubey, 1959). This has the immediate effect of extending the depth of faulting towards the basement, possibly reaching more deeply sourced fluids and enhancing the control that basement features exert on fault locations. If a permeability seal can be kept contiguous, deeper faulting will be allied to an effective fluid trap until a significant change in the stress regime allows venting and mineral precipitation.

References

Cooke, M. and Pollard, D., 1997. Bedding-plane slip in initial stages of fault-related folding. Journal of Structural Geology, 19, 567–581.

Grauch, V., Rodriguez, B. and Wooden, J., 2003. Geophysical and isotopic constraints on crustal structure related to mineral trends in north-central Nevada and implications for tectonic history. Economic Geology, 98, 269–286.

Hubbert, M. and Rubey, W., 1959. Role of fluid pressure in mechanics of overthrust faulting. Geological Society of America Bulletin, 70, 115–166.

Madden-McGuire, D. J. and Marsh, S. P., 1991. Lower Paleozoic host rocks in the Getchell gold belt: Several distinct allochthons or a sequence of continuous sedimentation? Geology, 19, 489–492.

Miller, E., Miller, M., Stevens, C., Wright, J. and Madrid, R., 1992. Late Paleozoic paleogeographic and tectonic evolution of the western U.S. Cordillera. In: Burchfiel, B., Lipman, P. and Zoback, M. (eds.), The Cordilleran Orogen: Conterminous U.S. The Geology of North America, Vol. G-3, Geological Society of America, Boulder, Colorado, 57–106.

Moresi, L., Dufour, F. and Mühlhaus, H.-B., 2002. Mantle convection modeling with viscoelastic/brittle lithosphere: Numerical methodology and plate tectonic modeling. Pure and Applied Geophysics, 159, 2335–2356.

Moresi, L., Mühlhaus, H.-B. and Dufour, F., 2001. Viscoelastic formulation for modelling of plate tectonics. In: Mühlhaus, H.-B., Dyskin and A., Pasternak, E. (eds.), Bifurcation and Localization in Soils and Rocks. Balkema, Rotterdam, 337–344.

Muntean, J., Coward, M. and Tarnocai, C., 2003. Paleozoic normal faults in north-central Nevada: deep crustal conduits for Carlin-type gold deposits. Unpublished paper presented at Marco T. Einaudi Symposium, April 3, 2003, Colorado School of Mines, 20 pp.

Rodriguez, B., 1998. Regional crustal structure beneath the Carlin trend, Nevada based on deep electrical geophysical measurements. In: Tosdal, R. (ed.), Contributions to the Gold Metallogeny of Northern Nevada. U.S. Geological Survey Open-File Report 98-338, Denver, Colorado, 15–19.

Saucier, A., 1997. The Antler thrust system in northern Nevada. In: Perry, A. and Abbot, E. (eds.), The Roberts Mountains Thrust, Elko and Eureka Counties, Nevada. 1997 Spring Field Trip Guidebook, Nevada Petroleum Society, 1–16.

Wooden, J., Kistler, R. and Tosdal, R., 1998. Pb isotopic mapping of crustal structure in the northen Great Basin and relationships to Au deposit trends. In: Tosdal, R. (ed.), Contributions to the Gold Metallogeny of Northern Nevada. U.S. Geological Survey Open-File Report 98-338, Denver, Colorado, 20–33.

Reducing exploration risk through research: Project I4 - Predictive discovery of Mt Isa style copper

Andy Wilde[1], Klaus Gessner[2], Peter Jones[3], Melissa Gregory[1], Rob Duncan[1]

*[1] pmd*CRC, MORE, School of Geosciences, Monash University, Clayton, VIC 3800*
*[2]pmd*CRC, CSIRO Exploration and Mining, PO Box 1130, Bentley, WA 6102*
*3 pmd*CRC, School of Earth Sciences, James Cook University, Townsville, QLD 4811*
Wilde@earth.monash.edu.au

Introduction

Even though a massive volume of data has been accumulated in Mount Isa's 80 year mining history, there are many aspects of ore deposition that remain controversial or uncertain. The main aim of the I4 project was to reduce exploration risk through developing a process model of copper ore formation and to produce 3D geometric models of the Mount Isa western succession at different scales. Here, we summarise key scientific results in the light of the "five questions", as defined by the Australian Geodynamics CRC.

Architecture of the Mineralizing System

The abundant information from surface and underground drilling and from underground workings has been compiled into a mine-scale 3D geometric model of the orebodies, their host-rocks and structures, using the software GOCAD. This model architecture provided the base for mesh-generation in numerical simulations and was viewed using virtual reality facilities. Among the insights that this generated was that the copper orebodies contain a number of finger-like protuberances which extend from the highest ore grade region close to the Paroo Fault, upward into the Urquhart Shale. This suggests that the ore deposition process involved vertical fluid flow rather than the horizontal flow implied by previous research (Waring et al., 1998). This inference has been supported by numerical modelling discussed below.

A second, regional scale model consists of lithological boundaries and faults to a depth of 10 km for a 50 km radius about Mount Isa. This model has been used to estimate the location of an inferred unconformity surface above the Mount Isa Group during the copper event, based on regional constraints such as post Isan orogeny basins and metamorphic grade distribution. The significance of this unconformity surface for copper ore formation stems from the likelihood that the oxidised copper and sulphur-rich brines were derived from syn- to post-metamorphic cover rocks (see below).

Fluids and Reservoirs

Previous fluid inclusion studies suggested that the ore-forming solutions at Mount Isa were brines at temperatures of 100˚C or higher. The true temperatures of formation cannot be accurately determined from fluid inclusion studies, however, because the depth of formation and fluid pressure at entrapment are unknown. Fluid salinity varies from pure water to halite-saturated brines, with an average of about 14 wt% NaCl equiv. This suggests chloride complexing of copper. Preliminary XANES & EXAFS analysis of fluid inclusions has found $Cu(H_2O)_6^{2+}$ at ambient temperature. In a similar study of fluid inclusions from the Mole granite, $Cu(H_2O)_6^{2+}$ at ambient temperature was replaced by a chloride ($CuCl_2^-$) after heating to over 300˚C (Mavrogenes et al., 2002).

Nuclear microprobe and laser ablation ICP-MS analysis of fluid inclusions in quartz confirm earlier indications that fluid compositions are extremely variable (with respect to total salinity,

cation ratios and ore metal contents) and indicate variability within individual fluid inclusion assemblages trapped at more or less the same time. We cannot discount post-depositional change given that there is plentiful evidence (including new cathodo-luminesence data) that quartz at Mount Isa has been deformed. Thus we attribute this variability to a combination of rapidly changing fluid composition with respect to the speed of quartz precipitation as well as post-entrapment modification. The variability of hydrothermal fluid composition appears to be consistent with the predicted variability of flow patterns using mechanical-fluid flow coupled numerical modelling.

The main aquifers for oxidised copper-rich brines are believed to be within an overlying "phantom basin" correlative of the Quamby Conglomerate and/or Roper Group and/or Nathan Group. Analysis of fluid inclusions in the Roper Group by Dutkiewicz et al. (2003), however, has revealed the presence of brines generally more saline than those present at Mount Isa.

Tourmaline veins west of Mount Isa have been implicated in Pb-Zn ore formation by the presence of extremely metal-rich fluid inclusions and presence of sphalerite. Pb-Pb step-leaching of tourmaline will be used to date tourmaline and assessing its relationship to base-metal formation (Duncan and Wilde, 2004).

We have also reviewed the extraordinary database of stable isotopic determinations (over one thousand oxygen and carbon isotope determinations of metasediments and carbonate veins). The oxygen isotopic pattern around Mount Isa has previously been suggested as an effective tracer of hydrothermal fluid flow (Waring et al., 1998). 3D visualisation and spatial analysis revealed, however, that the isotopic patterns are more complex than originally thought and that the $\delta^{18}O$ values correlate better with faults than they do with economic copper (Fig. 1).

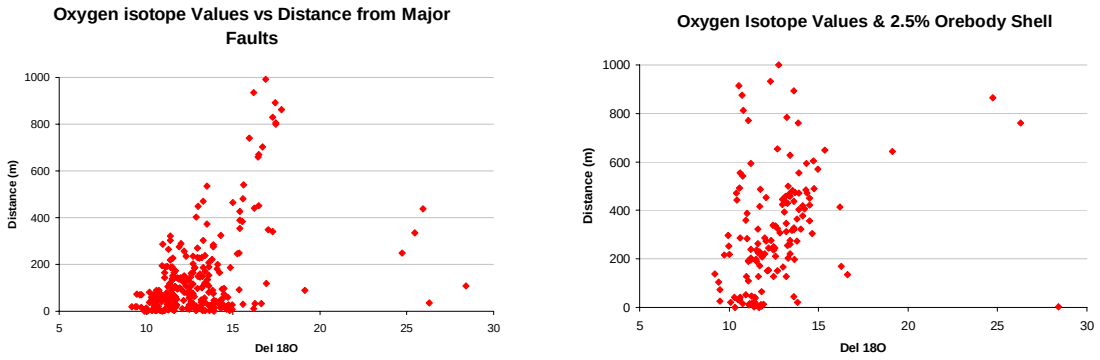

Figure 1: Oxygen isotope values versus distance to faults (left) and 2% Copper outline (right)

Driving Forces for Fluid Flow

At least two major fluid flow events have been recognised in the copper orebodies. Textural and paragenetic studies point to an early fluid flow event with quartz deposited by a cooling (upwards flowing) basement-derived fluid. We interpret this to be the result of convection and/or contraction, probably during the Isan orogeny (D2). Numerical simulation (FLAC3D) of deformation-driven fluid-flow in a mine-scale model has demonstrated that upward fluid flow patterns dominate in contraction, while mixed flow patterns are much more likely to occur in extension and strike-slip. Coupled thermal and fluid-flow numerical simulation (SHEMAT) suggests that advective heat transport is a potential driver for the fluid flow during silica deposition, without need for deformation. Since hydrothermal convection in porous media is highly dependent on permeability, the flow patterns are strongly affected by the distribution of permeable rock units. In the case of a fractured and therefore relatively permeable Urquhart Shale, precipitation of quartz due to flow across negative temperature and pressure gradients is

predicted in a pattern comparable to the distribution of the silica-rich portion of the silica-dolomite body (see Kühn et al., 2004).

Structural mapping has recognised the relationship between ore formation and spatially restricted zones of D3-dilation, which was caused by dextral transpression. Pre-D3 silicification is inferred to have played an important role in making the host-rocks at Mount Isa brittle and susceptible to fracturing and brecciation during the D3 event. In the copper orebodies quartz was overprinted by dolomite and eventually chalcopyrite suggesting that the flow field had reversed during ore deposition. This is consistent with the need to introduce relatively oxidised and therefore copper-rich fluids into the depositional site from an overlying source. Prolonged circulation of oxidised fluids through the reduced rocks of the Eastern Creek Volcanics and Mount Isa Group is likely to have rendered them incapable of transporting substantial amount of copper, which may explain the widespread occurrence of (sub-economic) copper-enrichment within these rocks. Numerical modelling cited above shows that the change from contractional to transpressional deformation would produce such a change in flow pattern.

Pressure, Temperature and Deformation Histories of the Rocks

The I4 project has contributed to the understanding of P-T-t history by reviewing all available absolute age data and working with pmd*CRC history projects to generate new dates for ore and host-rocks. The latter work is in progress. New Re-Os isotopic data for various ore and host-rock samples have been obtained in collaboration with project H1 (see Keays et al., and Gregory et al, 2004). A preliminary isochron age of 1370 ± 80 Ma has been obtained (MSWD of 49) by pooling all the available samples. Additional data gathering is in process and new isochrons will be prepared from paragenetically similar rocks and phases.

A series of numerical simulations of conductive heat transport have pointed to the significance of the thermal history of the Mount Isa inlier to its metal endowment. The thermal structure at 1.5 Ga has been reconstructed using present-day heat-flow measurements at Mount Isa and seismic data on current crustal structure. A significant finding is the likelihood of a weak lithosphere, with felsic rocks close to melting. This has been attributed to continuing mantle plume activity from the Barramundi to the Isan Orogeny that drove magmatic accretion and fractionation of the lithosphere This resulted in significant metal transfer from the mantle to the crust, while at the same time considerably weakening the lithosphere.

While most of the Mount Isa inlier appears to contain a high heat producing felsic mid-crustal layer, the position of the Sybella Batholith appears to be insignificant for the thermal history of the copper system. This is, because after D2 contraction, the Sybella was at a shallow crustal level, similar in depth to the Urquhart shale, therefore its radiogenic heat production would have primarily influenced younger, overlying units.

Thermal modelling further suggests that exhumation of metamorphic rocks in the hanging wall of the Mount Isa Fault at geologically reasonable fault slip rates would have been too slow to generate a thermal anomaly capable of driving hydrothermal convection in the manner proposed by Matthäi et al., (2004).

Fluid Transport and Copper Depositional Processes

An important contribution of this project has been a systematic documentation of various hydrothermal alteration types and grouping them into three “suites”. This includes the expression of each alteration type in exploration datasets (including hyperspectral mapping data). Geochemical modelling has been used to explain the significance of the alteration assemblages with respect to copper depositional processes. All of this information has been assembled as an alteration “guide” that will form a valuable reference for exploration geologists.

Depositional mechanisms have been investigated using a variety of numerical models (Geochemists’ Workbench & HCh). The contact between Urquhart Shale and metabasalt of the Eastern Creek Volcanics is commonly assumed to be a redox interface. Our geochemical

modelling suggests that this is not the case. The models show clearly that the presence of pre-existing sulphide would promote high copper grades. There is, however, a lack of textural evidence for wholesale pyrite consumption during copper deposition. The question is then whether sulphur was introduced with copper in the same fluid or in a separate fluid, requiring fluid mixing for ore deposition. Modelling suggests that copper and high levels of sulphate could have been co-transported provided that the fluid had a relatively high Na/Ca ratio, such that anhydrite precipitation was inhibited. Thus deposition could have been in response to influx of an oxidised Na- and SO_4-rich fluid or mixing of discrete oxidised Cu-rich and reduced S-bearing fluids. The available data do not yet allow discrimination between these possibilites.

Putting it all Together – The Exploration Toolkit

The delivery of research results in a form that is relevant and usable by exploration geoscientists is a critical issue. We have chosen to synthesise our results in the form of the "exploration toolkit", a concept attributed to Douglas Haynes. Each toolkit is a set of mutually independent criteria that can be applied to exploration datasets. The need to couch research outcomes in terms of available exploration data is therefore paramount and a useful discipline for researchers. The requirement for the criteria to be mutually independent stems from the use of these criteria for ranking. For example visual recognition of hydrothermal dolomite cannot be combined with the presence of gravity anomalies that result from high dolomite concentration.

We have provided three toolkits, one for terrane selection and ranking, one for tenement or camp-scale selection and ranking and the third for prospect selection and ranking. The terrane-scale toolkit allows ranking and definition of key terranes. It is important that the absence of data does not lead to downgrading of a terrane, so in the case of poor quality or absent data a neutral weighting is applied. This further emphasizes the need to acquire key data in certain areas of interest.

The tenement and prospect-scale toolkits contain criteria that are to be used to create a series of GIS data layers (these can be in 2D or in 3D). The layers can then be combined, either using a simple intersection process or using a more complex system of weighting in order to generate a prospectivity map. This approach is clearly distinct from the weights of evidence or similar approaches which seek to explain a known distribution of deposits statistically. In the toolkit approach, process thinking is applied without any need for the presence of mineral deposits to guide the selection process. Furthermore, the process is not impaired by the absence of data, a common problem in the exploration environment.

Acknowledgements

The research presented above has benefited from discussions with numerous geologists including Dave A-Izzedin, James Cleverley, Melanie Coward, Bruce Hobbs, Dan Johnson, Gordon Lister, Mark McGeogh, Alison Ord, Bill Perkins, Paul Roberts, Justin Tolman and Chris Waring. We would also like to thank Dugi Wilson and Paul Gow of Xstrata Copper for their support, and Rick Valenta and John Anderson for dreaming up the project in the first place.

References

Dutkiewicz A., Volk, H., Ridley J., and George, S., 2003. Biomarkers, brines and oil in the Mesoproterozoic Roper Superbasin, Australia. Geology, 31, 981-984.

Matthäi, S.K., Heinrich, C.A., and Driesner, T., 2004. Is the Mount Isa copper deposit the product of forced brine convection in the footwall of a major reverse fault? Geology, 32, 357–360.

Mavrogenes, J.A., Berry A.J., Newville M., and Sutton, S.R., 2002. Copper speciation in vapor-phase fluid inclusions from the Mole granite, Australia. American Mineralogist, 87, 360-1364.

Waring, C.L., 1990. Genesis of the Mt Isa Cu Ore System. Unpublished PhD Thesis, Monash University, 296 p.

Waring, C.L., Andrew, A.S., and Ewers, G.R., 1998. Use of O, C and S stable isotopes in regional mineral exploration: Australian Geological Survey Organisation Journal, 17, 301-313.

Fluid inclusion microanalysis: Advances and future challenges

P.J. Williams[1], T.Baker[1], T. Ulrich[2] and C.G.Ryan[3]

*[1]pmd*CRC, Economic Geology Research Unit, School of Earth Sciences, James Cook University, Townsville, QLG 4811*
[2]Department of Geology, Australian National University
*[3]pmd*CRC, CSIRO Exploration and Mining, School of Geosciences, Monash University*
Patrick.Williams@jcu.edu.au

Introduction

The analysis of fluid inclusion contents is one of the main keys to predictive mineral discovery. For terrain selection it may characterize vital ingredients that lead to the formation of problematical ore types (e.g. the sources of salinity in iron oxide-copper-gold (IOCG) deposits). Within terrains it provides essential constraints for geochemical models of ore deposition in so much that in the absence of such constraints the models have no demonstrated connection to reality. Fluid inclusion analysis has therefore formed a cornerstone of research within the pmd*CRC, particularly through the enabling technologies F3 project: Micrometallogeny of Hydrothermal Fluids. Here we highlight advances in fluid inclusion microanalysis research both within the pmd*CRC and elsewhere, and we discuss some of the challenges that lie ahead in a rapidly developing research field.

Progress within pmd*CRC

Prior to the commencement of the pmd*CRC, Australian researchers led the world in economic geology applications of one relevant microanalytical technology, namely Proton Induced X-ray Emission (PIXE; Heinrich et al., 1992; Heinrich et al., 1999; Ryan et al., 2001; Ryan et al., 1993). Elsewhere, laser ablation inductively coupled mass spectrometry (LAICPMS) techniques have been developed and through the application of an internal standard and the use of a short wavelength laser now allow absolute quantification of single fluid inclusions (Günther et al., 1998; Heinrich et al., 2003).

The major achievements of F3 and other recent work in Australia outside the scope of the CRC have been (a) the development here of complementary LAICPMS methods and the first demonstrations anywhere, of reproducibility of results from these two leading technologies in a variety of datasets; and (b) the application of these datasets in CRC terrain-based projects (Fu et al., 2004; Gillen et al., 2004; Mark et al., 2004; Mustard et al., 2004). A particularly challenging outcome has been the common discovery that ostensibly homogeneous fluid inclusion populations display substantial chemical variations (Figures 1 and 2). While this complicates the application of data in modelling it also offers an unexpected insight into the geochemical processes at the time of fluid entrapment.

Limitations, challenges and opportunities

Some imperfections in the combined technology reproducibility referred to above, combined with outcomes from new PIXE imaging technology, have revealed a number of issues that require modifications to existing experimental and data-reduction procedures (Figure 2). Modified LAICPMS software also needs to be written to replace the current procedures, which are overly labour intensive, prone to human error, and non-conducive to scientific rigour. The number of samples investigated to date is small and it is evident that analytical datasets from

some systems of interest are dominated by fluids that were highly evolved prior to entrapment (i.e. “input fluids” not sampled). This represents a major challenge particularly for geochemical modelling and requires careful examination of the geological context of the fluid inclusion to constrain the suitability of the microanalytical data to the modelling issue being addressed.

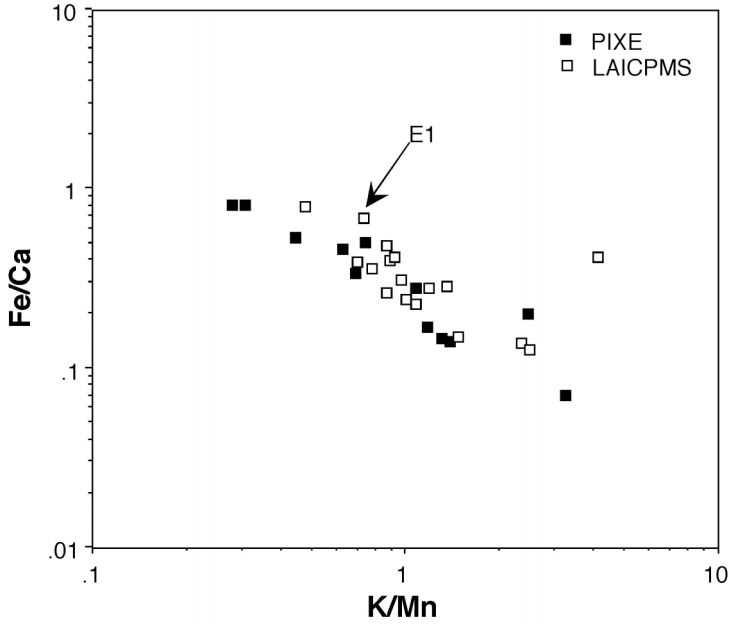

Figure 1: The plot of Fe/Ca versus K/Mn illustrates the range in fluid compositions from petrographically similar brine inclusions. Both PIXE and LAICPMS techniques display this variation independently confirming that the wide compositional ranges is a real phenomenon and demonstrating the reproducibility of the techniques.

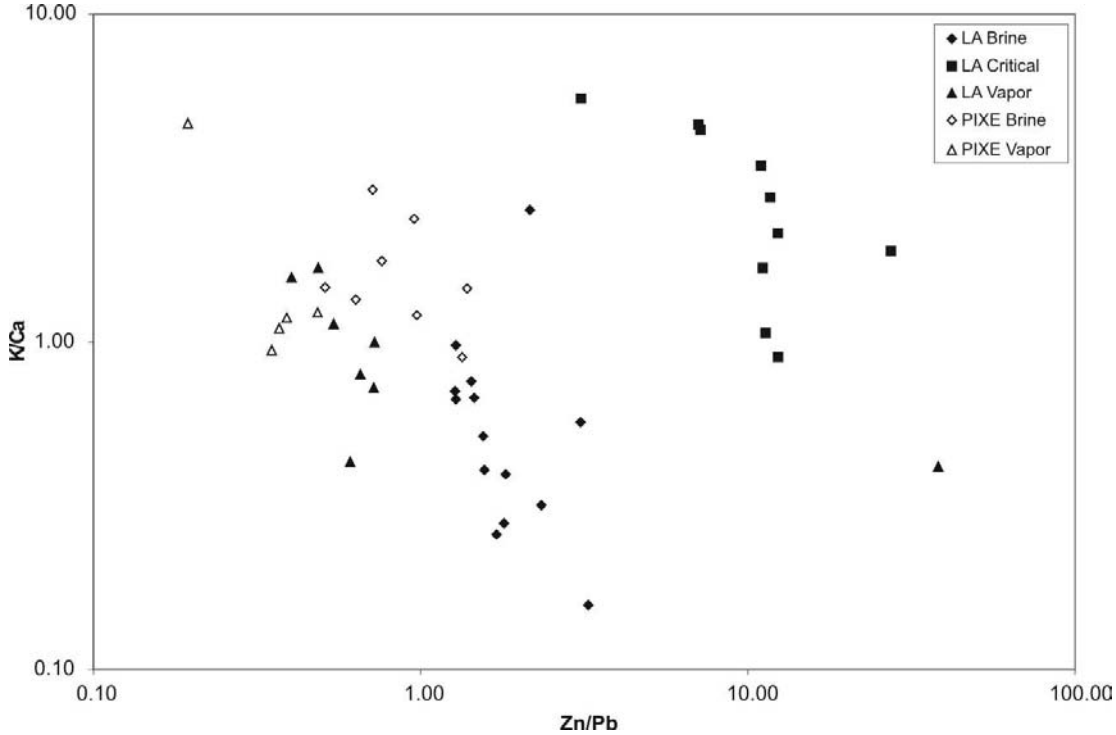

Figure 2: The plot of K/Ca versus Zn/Pb further illustrates the use of combined PIXE and LAICPMS on fluid inclusion populations. Three different inclusion types have been analysed from the Bismark skarn deposit (Baker and Lang, 2003; Baker et al., 2004) including brine inclusions (halite and sylvite bearing), low salinity vapor-rich inclusions and low to moderate salinity critical inclusions (liquid:vapor ratio approximately equal). PIXE and LAICPMS analyses of the vapor-rich inclusions have reasonably consistent K/Ca and Zn/Pb ratios whereas there are distinct differences in the K/Ca ratios in the brine inclusions. The explanation for this has yet to be fully resolved but may reflect a combination of depth estimate and X-ray absorption issues from PIXE, and/or elemental ablation (e.g. Ca in the liquid versus K in sylvite) and surface contamination issues in LAICPMS. Critical inclusions have similar K/Ca ratios between the two methods, however, Pb is below detection in all PIXE analysis (therefore no PIXE data are shown on the plot for critical inclusions). LAICPMS has lower detection limits for Pb than PIXE and has provided new insights into the Zn/Pb ratios of this key ore stage fluid (Bertelli et al., 2004).

Bertelli et al. (2004) describe the application of fluid inclusion microanalytical data to geochemical modelling. This test case study highlights several important features of the combined microanalysis and modelling approach. Firstly, the techniques were applied to a geologically well understood ore deposit that possessed a well constrained fluid inclusion history (Baker and Lang, 2003; Baker et al., 2004). Secondly, the application of LAICPMS analysis to ore stage fluids enabled accurate estimates on Pb contents of ore stage fluids that had previously been poorly constrained through PIXE (due to high detection limits; Figure 2). Finally, the salinity and P-T conditions of the ore stage fluids were well defined through microthermometry and can be constrained by known thermodynamic datasets (Bertelli et al., this volume). This represents another significant challenge in the interface between fluid inclusion microanalysis and geochemical modeling, because many of the ore systems of interest have fluid inclusion P-T-X histories that are unconstrained by current thermodynamic datasets. An excellent example of this is highlighted by Mustard et al. (2004) at the Osborne deposit that exhibits high pressure, high temperature unmixing between multi-solid brine inclusions and halite-bearing liquid CO_2 inclusions.

A major deficiency at the present time is the inability of the existing technologies to determine geologically-relevant concentrations of sulphur, except in extreme circumstances such as in examples of copper and sulphur-rich magmatic vapour inclusions. This needs to be addressed though a combination of technique development and the establishment of routines to constrain sulphur abundance and speciation from independent measurements. While the determination of halogen ratios may provide the solution to several major ore genetic problems, there is currently no method for halogen ratio (e.g., Br/Cl) determination by LAICPMS in Australia, whereas PIXE has inherent limitations. Evaluation of LAICPMS data from brine inclusions at Cannington suggest that halogen analysis is achievable, provided that appropriate standards are obtained and specialized methodologies applied to generate consistent data (Figure 3). Heinrich et al. (2003) have also shown that such analysis is achievable by LAICPMS techniques.

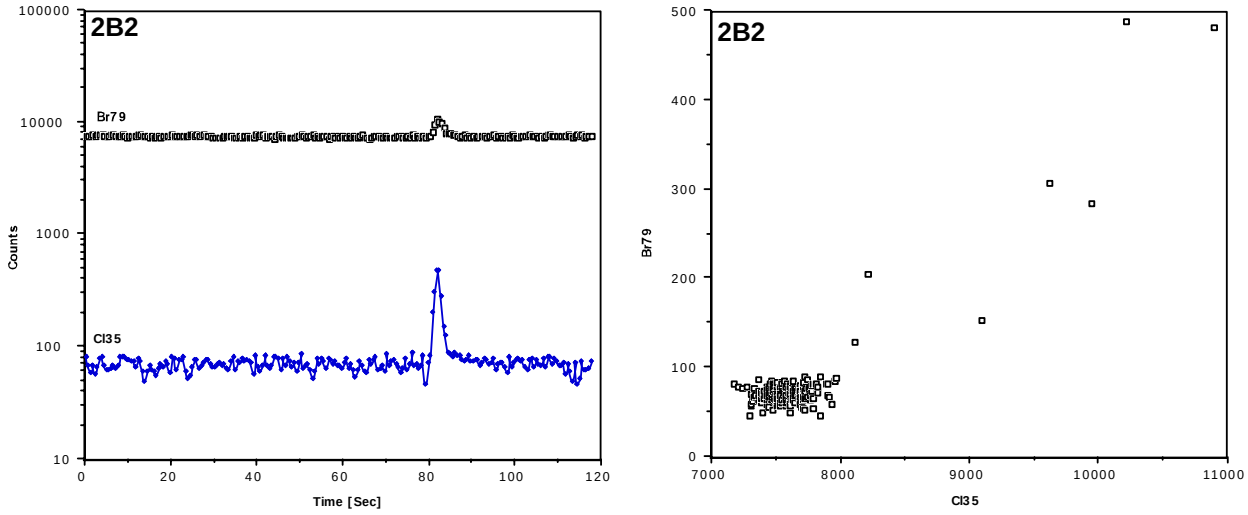

Figure 3: LAICPMS analysis of Cannington brine inclusions showing distinct count signals for Br and Cl. Current internal standards used at ANU do not contain Br and the signals can not be quantified. Many inclusions analyzed in the same batch gave much weaker Br signals suggesting that specialized analytical routines in which a limited number of mass numbers are recorded will be needed to generate useful halogen ratio data.

While work is evidently needed to enhance the value of our existing data and methodologies it is equally clear that there are exciting new possibilities ahead for the next few years. These include integration of single inclusion halogen data from modified LAICMPS procedures with halogen and noble gas data from in vacuo extraction-MS analysis of irradiated fluid inclusion populations, dating of fluid inclusions using the $^{40}Ar/^{39}Ar$ method, determination of Pb isotope ratios, and the application of synchrotron techniques in areas such as the characterization of ore metal speciation in natural and synthetic fluid inclusions.

Acknowlegements

Funding for this research was from the pmd*CRC F3 project and an ARC discovery grant to Williams.

References

Baker, T. and Lang, J.R., 2003. Reconciling fluid inclusion types, fluid processes and fluid sources in skarns: an example from the Bismark deposit, Mexico. Mineralium Deposita, 38,474-495.

Baker, T., Van Achterberg, E., Ryan, C.G. and Lang, J.R., 2004. The composition and evolution of ore fluids in a magmatic-hydrothermal skarn deposit, Geology, 32,117-120.

Bertelli, M., Baker, T. and Cleverly, J.S., 2004. Controls on ore deposition in Zn-Pb skarns: geochemical modelling and fluid inclusion constraints. This volume.

Fu, B., Baker, T., Oliver, N.H.S., Williams, P.J., Ulrich, T., Mernagh, T.P., van Achterberg, E., Ryan, C.G., Marshall, L.J., Rubenach, M.J., Mark, G. and Yardley, B.W.D., 2004. Regional fluid compositions of the Mount Isa Eastern Succession, NW Queensland, Australia.

Gillen, D., Baker, T., Hunt, J.A., Ryan, C.G. and Win, T.T., 2004. PIXE analysis of hydrothermal fluids in the Wernecke Mountains, Canada. This volume.

Günther, D., Audétat, A., Frischknecht, R. and Heinrich, C.A., 1998. Quantitative analysis of major, minor and trace elements in fluid inclusions using Laser Ablation-Inductively Coupled Plasma-Mass Spectrometry (LA-ICP-MS). Journal of Analytical Atomic Spectroscopy, 13, 263-270.

Heinrich, C.A., Ryan, C.G., Mernagh, T.P. and Eadington, P.J., 1992. Segregation of ore metals between magmatic brine and vapor: A fluid inclusion study using PIXE microanalysis. Economic Geology, 87, 1566-1583

Heinrich, C.A., Günther, D., Audétat, A., Ulrich, T. and Frischknecht, R., 1999. Metal fractionation between magmatic brine and vapor, determined by micro-analysis of fluid inclusions. Geology, 27, 755-758.

Heinrich, C.A. et al., 2003. Quantitative multi-element analysis of minerals fluid and melt inclusions by laser ablation inductively-coupled-plasma mass-spectrometry. Geochimica et Cosmochimica Acta, 67, 3473-3496.

Mark, G., Baker,T., Williams, P.J., Ryan, C.G.and Mernagh, T.P., 2004. The geochemistry of magmatic fluids, Cloncurry district, Australia: relations to IOCG systems. This volume.

Mustard, R., Baker, T., Williams, P.J., Mernagh, T., Ryan, C.G., van Achterberg, E.and Adshead, N., 2004. The role of unmixing in magnetite±copper deposition in Fe-oxide Cu-Au systems. This volume.

Ryan, C.G., Heinrich, C.A. and Mernagh, T.P., 1993. PIXE Microanalysis of fluid inclusions and its aqpplication to study ore metal segregation between magmatic brine and vapor: Nuclear Instruments and Methods in Physics Research, B77, 463-471.

Ryan, C.G., Jamieson, D.N., Griffin, W.L., Cripps, G. and Szymanski, R., 2001. The new CSIRO-GEMOC Nuclear Microprobe: First results, performance and recent applications: Nuclear Instruments and Methods in Physics Research, B181, 12-19.

Modelling Software Framework (M1) and Knowledge Management and Data Integration (M4)

Robert Woodcock[1], Lesley Wyborn[2] and Paul Roberts[1] and Stuart Girvan

*[1]pmd*CRC, CSIRO Exploration and Mining, PO Box 1130, Bentley, WA 6102*
*[2]pmd*CRC, Geoscience Australia, GPO Box 378, ACT 2601*

robert.woodcock@csiro.au

The pmd*CRC modelling program uses scientific knowledge along with sophisticated earth process numerical modelling to aid in ore targeting. The process is embodied in a Modelling Workflow consisting of nine stages:

1. Determine the scale and type of the investigation:

a. Does it involve a specific ore deposit (Wallaby) or a larger scale mineralised system (e.g. Laverton)?

OR

b. Are the models "generic" and may apply to a number of mineralised systems?

2. Using the "Five Questions", identify what information we know and do not know about the target mineralising system? Where can numerical modelling be used to investigate the "what-ifs" and fill in some of the gaps or reduce the possibilities? What information needs to be obtained to create better models and obtain parameter values? How sophisticated must the modelling be? (cost benefit analysis).

3. Determine what questions you want to answer with the modelling. What is required to prove or disprove an hypothesis?

4. Build the geometry for the model or family of models. What model information is already available and how do we obtain it? Is it compatible with the numerical modelling software?

5. Choose properties of the model appropriate for model sophistication - all or only part of mechanical, fluid flow, thermal, chemical rock properties? Determine where can we obtain this information in a compatible format (see below)?

6. Choose the boundary conditions for the model - fluid flow, deformation, thermal, chemical etc. Assume boundary conditions based on local information or from multiscale simulations?

7. Run the model(s) - manual or automatic (there may be a lot of scenarios)? Distribute jobs across multiple PCs or a HPC facility remote from local computation? Many of these models may need to be run in an inversion-style process in order to help identify viable hypotheses for ore formation in the target mineralised system. On some occasions, a second round of forward modelling (generally involving fewer models) will then take place in order to predict directly either the likely location of ore bodies or to direct drilling at higher grade parts of known mineralised systems.

8. Visualise the results.

9. Interpret the results. There may be a LOT of data to sift through; how do we do this?

The use of numerical modelling and the investigation of many scenarios provides insight into the possible scenarios leading to (or not to) mineralisation and the key indicators that would be present. Most importantly, the approach builds a predictive picture of what might be there along with key indicators which can be used to guide the selection and use of detection technologies and or to directly predict the location of ore. Thus the aim is reduce ore discovery costs by improving both the efficiency of the detection process and the quality of targets tested. The approach has clearly demonstrated success at the Kewell prospect in the Stawell district by helping direct drilling of ore grade and width gold mineralised intersections.

The M1 Software Framework project is concerned with the software requirements and computational demands of the Modelling Workflow. This presentation will identify, within the context of the modelling workflow, the primary software requirements and computational needs and how the Software Framework architecture and technologies are meeting them.

The focus in M4 for 2003-2004 has been to ensure that data relevant to rock properties and thermodynamics can be delivered in real time from distributed data sources to the M1 Software Engineering Framework.

In recent years, with increasing computational capacity, modelling has become much more flexible. Run times have been significantly reduced, resulting in modelling becoming a much more iterative process, so that more differing scenarios can be run. As time goes on, it will be possible to run more and more of these scenarios simultaneously. Storage costs have also significantly reduced, so that in any modelling scenario, all of the input data and the associated pedigree and metadata can be stored.

These expanded capabilities in modelling have put significant pressure on how the data are accessed, in particular real world data. It is now a real requirement for M1 that the latest data is accessed in real time from the original custodian, and that as part of the pedigree, the lineage of the original data be accessible. Further, any fundamental processing done to these data should be standardised where ever possible.

In order to achieve these requirements, the M4 project has been making a step change in how the relevant geoscientific data for M1 are stored and processed. At a high level, data storage architectures are being developed with ISO/OGC standards for interoperability in mind. The use of OGC standards and reference implementations will allow the M1 software framework to harvest data in real time from the source databases within Geoscience Australia (GA). However, there are other relevant data sources external to Geoscience Australia that are of interest to the pmd*CRC. Additional funding has been obtained from AUSIndustry, the Minerals Council of Australia, GA and all State and Territory Geological Surveys in an effort to assist all relevant Government agencies to deliver data interoperably in real time, using international standards for interoperability.

With the thermodynamic data modelling in F1/F2, it is clearly more appropriate if the data used to model the fluid-rock interactions are real world data collected as part of the F3 project. Hence a ‘Virtual Centre for Geofluids and Thermodynamic data’ has been established at GA (http://www.ga.gov.au/rural/projects/geofluids.jsp). Projects in F3 can now enter fluid inclusion data into this database. To standardise processing, Prof Phil Brown of the University of Wisconsin, has contributed his internationally acclaimed MACFLINCOR fluid inclusion programs that calculate salinity and other fluid parameters. These programs have been included as wrappers to the database and allow consistent calculation of fluid parameters from a chosen real world scenario (e.g., the trap site or a regional alteration system). Creating machine readable, OGC compliant interfaces into the fluid inclusion database will allow both primary and derived data to be imported in real time into the coupled fluid modelling systems of M1. This

step change will ensure that the parameters used in fluid-rock modelling are based on up to date, real world examples collected as either part of the pmd*CRC or other similar projects.

The development of a comparable rock property database is being planned for 2004-2005. As with the fluid inclusion and thermodynamic databases, care will be taken to develop the database with OGC standards such as SensorML in mind and to ensure that data pedigree and other appropriate metadata are captured.

The fluid inclusion and thermodynamic databases have structures that are designed to help ensure that any processing applied to data is transparent and, if required, an end user can trace the pedigree of the original data and make their own judgments about how appropriate that data is for their purposes. The same design concepts could equally well apply to age determination data sets collected by the H program. It should be possible to collect all data direct from the recording instruments via the Internet, including calibration and correction factors and standards used. As with the fluid inclusion data system the common programs used to process the data could also be stored as wrappers that are loosely coupled to the database. As these processing programs are upgraded, then data already processed by earlier versions of the software could also be updated. This would ensure greater standardization of results and transparency of processing. A data system, such as this would also ensure that when individual results are compared, it would be possible to ascertain if differences between results are geologically meaningful, or are simply an artifact of initial variance in laboratory techniques and/or processing. For the pmd*CRC, this approach may be significant, particularly for the experimental dating techniques in the H program such as $^{40}Ar/^{39}Ar$, Pb-Pb step leaching and Re/Os, where data collection and processing techniques are not as yet fully standardised.